

EUCARYOTIC AND PROKARYOTIC
BIOMIMETIC CELL MEMBRANES:
structure and its relation
to environmental conditions



Emilia Ewa Krok

Cover design and artwork: Jolanta Ewa Krok
Digitalized version of the cover: Damian Rakowski

Eukaryotic and prokaryotic biomimetic cell membranes: structure and its relation to environmental conditions

author: M. Eng. Emilia Ewa Krok

supervisor: Dr. habil. Eng. Łukasz Piątkowski, Prof. PUT



Poznan University of Technology
Faculty of Materials Engineering and Technical Physics
Institute of Physics
February 2024

A thesis submitted in partial fulfillment of the requirements for the degree
of Doctor of Philosophy

To my mother, for her constant fight for me, especially when everyone else was telling her to give up.

Contents

Abstract	7
Streszczenie	9
Funding	11
Abbreviations	13
1 Introduction	17
1.1 Motivation	17
1.2 Outline	21
2 Cell membrane	25
2.1 Lipid bilayer	25
2.2 Diversity of membrane lipids	28
2.3 Differences between eukaryotic and prokaryotic cell membranes	30
3 Model membrane systems	35
3.1 Giant unilamellar vesicles	35
3.2 Small unilamellar vesicles	38
3.3 Supported lipid bilayers	39
4 Experimental techniques	43
4.1 Fluorescence microscopy	43
4.1.1 Fluorescence	44
4.1.2 Confocal microscopy	46
4.2 Fluorescent probes	47
4.2.1 Phase-specific probes	48
4.2.2 Solvatochromic probes	50
4.3 Atomic force microscopy	52
4.3.1 Imaging modes	53
4.3.2 AFM as a tool for line tension determination	54
4.4 Fluorescence recovery after photobleaching	56
4.5 Dynamic light scattering	59
4.6 Zeta potential measurements	61
5 Lateral organization of biomimetic cell membranes in varying pH conditions	65

6	Nanoscale structural response of biomimetic cell membranes to controlled dehydration	81
7	Tunable biomimetic bacterial membranes from binary and ternary lipid mixtures and their application in antimicrobial testing	105
8	The most important results of the thesis and future outlook	129
8.1	Summary of results	129
8.2	Outlook	131
9	Scientific achievements	135
9.1	Education	135
9.2	Internships	135
9.3	Publications	136
9.4	Published conference abstracts	137
9.5	Participation in conferences	138
9.6	Patents/Patent applications	140
9.7	Scientific grants	140
9.8	Scholarships/Awards	142
9.9	Courses	143
9.10	Reviewing activity	143
	Bibliography	143
	Declarations of co-authors	161
	Acknowledgments	169

Abstract

Cell membranes play a crucial role as the basic building blocks of cells across various organisms, ranging from simple bacteria to more intricate plants and mammals. The primary purpose of lipid membranes is to maintain the structural integrity and functionality of the cell, which is accomplished by ensuring a stable state of homeostasis within the cell, regardless of alterations in the intracellular space or the surrounding environment. Cell membranes are not homogeneous matrices composed of evenly distributed lipids and proteins, but they are rather characterized by the presence of local heterogeneities made of saturated lipids, cholesterol and very often enriched in proteins. The idea of lateral segregation of membrane components, driven by phase separation, is a widely embraced concept in our current understanding of membrane structural organization, encapsulated within the framework of the "fluid mosaic" model of the cell membrane. Lipid domains, composed of saturated lipids and different sterol analogs remain conserved across relatively different organisms such as eukaryotes, prokaryotes, yeast, or plants. These highly ordered regions play a crucial role in the arrangement of specific membrane elements, including proteins. By mediating proper protein folding, membrane domains are involved in a variety of processes such as enzymatic reactions, viral binding, and entry, or penetration of bacterial toxins to the cell interior. The indisputable importance of raft-like regions in cell activity has led to studies on recreating the local membrane heterogeneities in model membrane systems, determining factors that are driving the phase separation, and finally unraveling the basic requirements that need to be fulfilled to effectively manipulate the shape, size, and density of lipid domains. In the following thesis, I endeavored to elucidate the intricate mechanisms underlying phase separation and the emergence of local membrane heterogeneities in model prokaryotic and eukaryotic cell membranes. The preparation of phase-separated biomimetic cell membranes under conditions of varying environmental pH revealed that by changing the concentration of H^+ and OH^- ions it is possible to precisely control the size and density of liquid ordered (L_o) phase domains. The size of ordered domains increased with the increase of the buffer pH in the whole tested range 1.7-9.0. Importantly, the lipid membranes exhibited high lateral lipid mobility regardless of the changes in the pH of the hydrating buffer, implying that the alterations in the membrane organization did not have any influence on the dynamic properties of the membrane constituents. Understanding the impact of the ionic composition of the buffer hydrating the lipid bilayer on its lateral organization, I focused my attention on exploring the hydration layer itself and its influence on the structural properties of model cell membranes. The reduction of the membrane's hydration state caused increased mixing of the lipids characteristic for liquid disordered (L_d) phase, with those forming L_o phase. Atomic force microscopy (AFM) measurements revealed that this admixing effect was associated with a 2-fold decrease in the hydrophobic mismatch between the L_d and L_o lipid

phases, accompanied by a 3-fold decrease in line tension for the fully desiccated membrane. Finally, this thesis also focuses on the structural organization of membranes found in bacteria, which, despite being relatively simple organisms, have developed very sophisticated cell envelopes. By concentrating specifically on the manipulation of membrane lipid composition, I undertook the challenge of inducing phase separation, replicating the membrane domains within model bacterial cell membranes, and characterizing their structural properties. Overall, the studies presented here shine new light on our understanding of the formation of local membrane heterogeneities, provide us with novel methods for manipulating the size, shape, curvature and distribution of membrane domains, and help us to explain the fascinating mechanisms behind the phenomenon of phase separation in both eukaryotic and prokaryotic cell membranes.

Streszczenie

Błony komórkowe odgrywają kluczową rolę jako podstawowy element tworzący komórki różnych organizmów; od prostych bakterii po bardziej skomplikowane rośliny i ssaki. Głównym celem błon lipidowych jest utrzymanie integralności strukturalnej i funkcjonalności komórki, co osiągnięte jest poprzez zapewnienie stabilnego stanu homeostazy we wnętrzu komórki, niezależnie od zmian w przestrzeni wewnątrzkomórkowej czy w otaczającym środowisku. Błony komórkowe nie są jednorodnymi matrycami złożonymi z równomiernie rozmieszczonych lipidów i białek, lecz charakteryzują się obecnością lokalnych heterogeniczności, które zbudowane są z nasyconych lipidów, cholesterolu i bardzo często wzbogacone w białka błonowe. Idea lateralnej segregacji składników błony, napędzanej przez proces separacji fazowej, jest szeroko przyjętą koncepcją w naszym obecnym rozumieniu organizacji strukturalnej błony, zamkniętą w ramach powszechnie akceptowanego modelu „płynnej mozaiki” błony komórkowej. Domeny lipidowe, złożone z nasyconych lipidów i szeregu pochodnych steroli, są obecne w błonach stosunkowo różnych organizmów, takich jak eukarionty, prokarioty, drożdże czy rośliny. Te wysoce uporządkowane regiony odgrywają kluczową rolę w ustrukturyzowaniu określonych elementów błonowych, w tym białek, zapewniając ich prawidłowe zwijanie w określoną konformację. Ponadto są zaangażowane w różnorodne procesy, takie jak reakcje enzymatyczne, przyłączanie i wnikanie wirusów lub przenikanie toksyn bakteryjnych do wnętrza komórki. Niekwestionowane znaczenie tratw lipidowych w utrzymaniu prawidłowej aktywności komórek doprowadziło do szeregu badań nad odtworzeniem lokalnych heterogeniczności błon w modelowych układach membranowych, określeniem czynników modulujących separację fazową, a wreszcie nad zdefiniowaniem podstawowych wymagań, które muszą być spełnione, aby skutecznie manipulować kształtem, rozmiarem i gęstością domen lipidowych. W poniższej rozprawie starałam się wyjaśnić skomplikowane mechanizmy leżące u podstaw separacji fazowej i powstawania lokalnych heterogeniczności w modelowych prokariotycznych i eukariotycznych błonach komórkowych. Przygotowanie biomimetycznych błon komórkowych wykazujących separację fazową w warunkach zmiennego pH środowiska ujawniło, że poprzez zmianę stężenia jonów H^+ oraz OH^- można precyzyjnie kontrolować rozmiar i gęstość domen uporządkowanej fazy (z ang. *liquid disordered*, L_o). Rozmiar domen wzrastał wraz ze wzrostem pH buforu w całym badanym zakresie 1,7-9,0. Co ważne, błony lipidowe wykazywały wysoką mobilność lateralną lipidów niezależnie od zmian pH buforu, co oznacza, że strukturalna reorganizacja błony nie miała żadnego wpływu na właściwości dynamiczne tworzących ją elementów. Znając wpływ składu jonowego buforu nawadniającego dwuwarstwę lipidową na jej lateralną organizację, skupiłam swoją uwagę na badaniu samej warstwy hydratacyjnej i jej wpływu na właściwości strukturalne modelowych błon komórkowych. Obniżenie stanu nawodnienia błony spowodowało zwiększone mieszanie się lipidów charakterystycznych dla fazy nieuporządkowanej (z ang. *liq-*

uid disordered, L_d), z tymi, które tworzą fazę uporządkowaną. Pomiary przy pomocy mikroskopu sił atomowych (z ang. *atomic force microscopy*, AFM) wykazały natomiast, że efekt wzajemnego przenikania się faz był związany z 2-krotnym zmniejszeniem niedopasowania hydrofobowego między lipidami z fazy L_d i L_o , któremu towarzyszył 3-krotny spadek napięcia na granicy faz dla w pełni wysuszonej membrany. Wreszcie, niniejsza rozprawa koncentruje się również na organizacji strukturalnej błon występujących u bakterii, które, choć są stosunkowo prostymi organizmami, rozwinęły bardzo skomplikowane otoczki komórkowe. Skupiając się w szczególności na zmianie składu lipidów błonowych, podjęłam się wyzwania odtworzenia separacji fazowej, replikacji domen błonowych i ich strukturalnej charakteryzacji. Podsumowując, przedstawione tutaj badania rzucają nowe światło na zrozumienie formowania się lokalnych heterogeniczności w błonach, dostarczają nam nowych metod manipulacji rozmiarem, kształtem, krzywizną i rozmieszczeniem domen błonowych oraz wyjaśniają fascynujące mechanizmy stojące za zjawiskiem separacji faz zarówno w eukariotycznych, jak i prokariotycznych błonach komórkowych.

Funding

The research presented in this thesis was funded by:

First Team, Foundation for Polish Science, *HYDRA – Elucidating the role of hydration heterogeneity and hydrophobic mismatch in biomimetic cell membranes organization*, grant number: POIR.04.04.00-00-5D32/18-00, principal investigator: Dr. habil. Eng. Łukasz Piątkowski, Prof. PUT.



EMBO Young Investigator Small Grant, European Molecular Biology Organization, *How do transmembrane proteins deal with the hydrophobic mismatch?*, principal investigator: Dr. habil. Eng. Łukasz Piątkowski, Prof. PUT.



EMBO Installation Grant, European Molecular Biology Organization, *Biological water: the role of hydration in cell membrane organization*, grant number: IG 4147, principal investigator: Dr. habil. Eng. Łukasz Piątkowski, Prof. PUT.



Abbreviations

AC Alternating current

AFM Atomic force microscopy

BODIPY 4,4-difluoro-4-bora-3a,4a-diaza-s-indacene

D Diffusion coefficient

DLS Dynamic Light Scattering

DOPC 1,2-dioleoyl-sn-glycero-3-phosphocholine

DOPE 1,2-dioleoyl-sn-glycero-3-phosphoethanolamine

DOPS 1,2-dioleoyl-sn-glycero-3-phospho-L-serine

DOTAP 1,2-dioleoyl-3-trimethylammonium-propane

DPPE 1,2-dipalmitoyl-sn-glycero-3-phosphorylethanolamine

ER Endoplasmic reticulum

FCS Fluorescence correlation spectroscopy

FRAP Fluorescence recovery after photobleaching

GPI Glycophosphatidylinositol

GFP Green fluorescent protein

GP Generalized polarization

GPMV Giant plasma membrane vesicle

GUV Giant unilamellar vesicle

HIV Human immunodeficiency virus

IM Inner membrane

IMF Immobile fraction

ITO Indium tin oxide

ABBREVIATIONS

LCH	Long-chain hydrocarbon
L_d	Liquid disordered
L_o	Liquid ordered
LUV	Large unilamellar vesicle
MF	Mobile fraction
MLV	Multilamellar vesicle
MVV	Multivesicular vesicle
NBD	Nitrobenzoxadiazole
NA	Numerical aperture
OM	Outer membrane
PAH	Polycyclic aromatic hydrocarbons
PC	Phosphatidylcholine
PDI	Polydispersity index
PE	Phosphatidylethanolamine
PI	Phosphatidylinositol
PEG	Polyethylene glycol
PG	Phosphatidylglycerol
POPC	1-palmitoyl-2-oleoylphosphatidylcholine
POPG	1-hexadecanoyl-2-(9Z-octadecenoyl)-sn-glycero-3-phospho-(1'-rac-glycerol)
PS	Phosphatidylserine
PVA	Polyvinyl alcohol
QCM	Quartz crystal microbalance
ROI	Region of interest
SCFA	Short-chain fatty acid
SLB	Supported lipid bilayer
SM	Sphingomyelin
STED	Stimulated emission depletion
STM	Scanning tunneling microscopy

SUV Small unilamellar vesicle

SPT Single particle tracking

TIRF Total internal reflection

T_m Transition temperature

UV Ultraviolet

Chapter 1

Introduction

Cell membranes serve as the fundamental structural components of cells in a wide range of organisms, spanning from very simple bacteria to much more complex plants and mammals. The main function of lipid membrane is to maintain the integrity and functionality of the cell. This is achieved by preserving a stable state of homeostasis within the cell's interior, irrespective of the changes in the extracellular space or the surrounding environment. In 1972, S. J. Singer and G. L. Nicolson introduced the fluid mosaic model, a groundbreaking concept that laid the foundation for our current understanding of the structural organization of cell membranes [1]. Initially, a lipid membrane was conceptualized as a simple lipid bilayer consisting of myriad lipid species meticulously organized to orient their hydrophilic headgroups toward the aqueous environment, while securely protecting their hydrophobic tails within the core of the bilayer. The term "mosaic" underscored the existence of diverse proteins clustered together to form well-organized islands embedded in the sea of lipids. Merely four years after introducing the revolutionary fluid mosaic model, Nicolson proposed an enhanced version that incorporated additional membrane complexities [2]. This updated model now accounted for observed heterogeneities, in particular the lateral organization of various lipid species within the membrane structure. Extensive studies of model cell membranes have shown that their structure can be divided into two fractions: detergent-labile and detergent-resistant [3]. The preferential interactions between saturated and glycosylated lipids and cholesterol lead to the formation of the so-called *domains* or *lipid rafts* [4]. These regions, characterized by a more ordered and tightly packed structure, play a pivotal role in recruiting molecules like proteins, facilitating their integration into the membrane, and establishing an environment conducive to proper protein folding and hence their activity. These heterogeneous and highly dynamic domains, in terms of lateral mobility, are present in both leaflets of the membrane and are considered to be the platforms responsible for the regulation of various cellular processes [5, 6].

1.1 Motivation

Although the concept of liquid-liquid phase separation and the emergence of membrane heterogeneities such as lipid rafts is generally gaining increasing acceptance, the existence, function, and biological significance of these membrane structures in biological cells are still the subject of an ongoing debate [3]. Skepticism surrounding the raft hypothesis arises

primarily from the absence of direct observations of these membrane heterogeneities. This is attributed to the limitations of current microscopy tools, whose spatial resolution is insufficient to offer unequivocal proof of their existence in living systems. The current constraints of optical microscopy are dictated by the diffraction limit, which is set at approximately 250 nm. Consequently, rafts or nanoscopic domains with sizes fluctuating below 200 nm elude detection with currently available optical tools [7]. Nevertheless, as biochemical and biophysical methods continuously evolve, we are gaining increasingly robust evidence affirming that membrane rafts not only exist within cells but also remain conserved across all organisms within the phylogenetic tree of life [8]. Recent publications unequivocally show that bacterial cell membranes undergo phase separation and that the formation of lipid domains takes place in both gram-positive [9] and gram-negative strains [10]. The application of the cardiolipin-specific fluorescent dye 10-N-nonyl-acridine orange unveiled lateral heterogeneities in the form of distinct lipid phases within *E. coli* membranes [11]. Furthermore, the identification of phosphatidylethanolamine (PE)-rich domains in *B. subtilis* cells was achieved through the utilization of a cyclic peptide probe designed to bind selectively to PE [9]. Domains composed of glycosphingolipids and ergosterol were found in membranes of yeasts *S. cerevisiae*, which not only, analogously to rafts in mammalian cell membranes, serve as functional centers for protein binding [12] but also participate in growth and apoptosis of the yeast cell [13]. The greater diversity of sterols in plant membranes is mirrored in the composition of their rafts, which, apart from cholesterol, contain stigmasterol, sitosterol, and 24-methylcholesterol [14]. Notably, the sphingolipid content in plant rafts is diverse across species, encompassing more than just sphingomyelin (SM); lipid domains in plants are enriched in cerebroside sphingolipid (glucosylceramide) and glycosyl inositol phosphorylceramides, among others [15, 16]. Recent advances in the development of microscopy tools, including super-resolution microscopy, stimulated emission depletion (STED) microscopy, and the emergence of techniques based on particle dynamics measurements such as single particle tracking (SPT) [17], fluorescence correlation spectroscopy (FCS), STED-FCS [18] or spot variation FCS [19], all together provide solid evidence for the existence of lipid rafts in mammalian cell membranes. The fact that membrane heterogeneities remain conserved among membranes of very different organisms underscores their importance in the structural organization of the membrane components and in maintaining the proper functioning of the cell.

The main function of the membrane raft domains is the organization of specific membrane elements, which allows their interactions with other membrane components (Figure 1.1 A). Proteins known for selective binding to ordered domains, undergo conformational changes upon interactions with typical raft-forming lipids such as cholesterol or sphingolipids, [20]. This raft-driven structural organization of proteins supports their proper folding and consequently ensures the maintenance of their activity (Figure 1.1 B). The affinity of various regulatory components such as e.g. specific enzymes to raft-like domains is higher than that for non-raft regions, leading to an increased concentration of these molecules in rafts [3]. The local accumulation of mutually interacting molecules generates a higher probability of their encounter and beginning of the reaction (Figure 1.1 C). Recent studies indicate that membrane rafts initiate and modulate interactions between host organisms and pathogen (see Figure 1.1 D). The characterized by high line tension boundaries between L_o domains and the surrounding L_d phase serve as preferential binding regions for human immunodeficiency virus (HIV) fusion peptides [21]. SM and

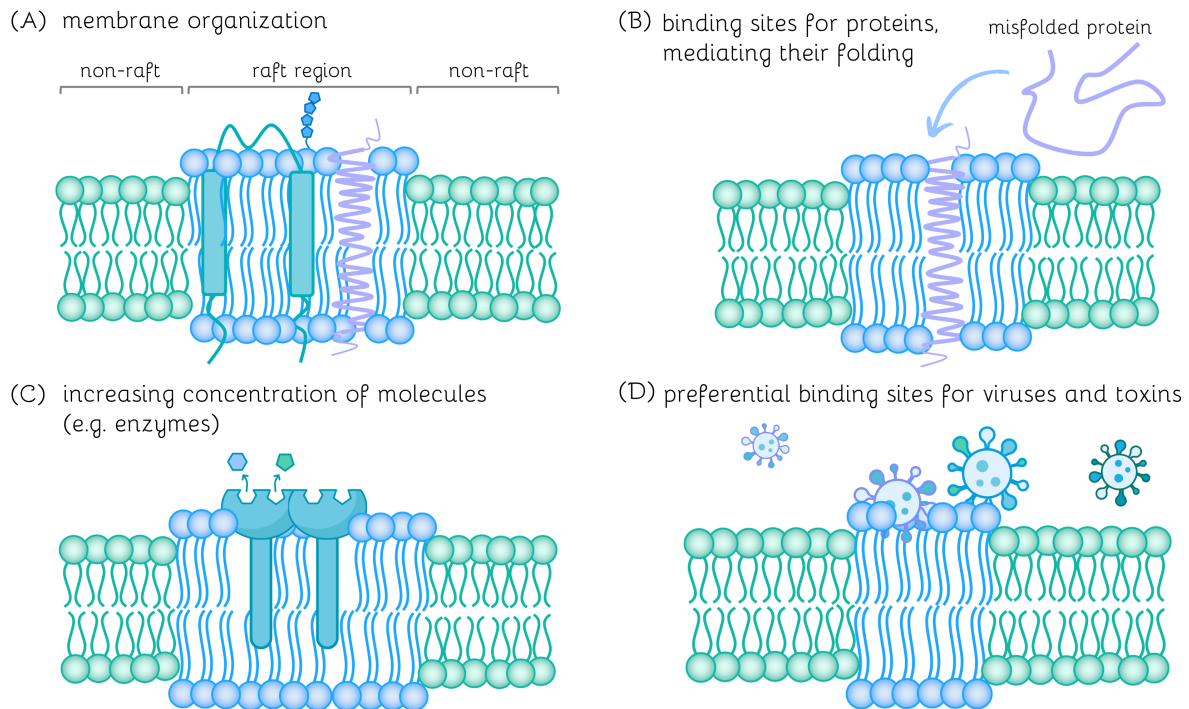


Figure 1.1: Biological significance of membrane rafts: (A) Raft-like domains organize the membrane components, effectively segregating domain-binding molecules, regulating their functioning, and facilitating controlled mutual interactions. (B) Lipid rafts play a pivotal role in promoting appropriate protein folding and regulating their activity. (C) Certain molecules and complexes exhibit a distinct preference for binding to raft regions. Domains containing a higher concentration of molecules, such as enzymes, increase the probability of their encounter and consequently trigger the reaction. (D) Pathogens, including viruses or bacteria, as well as various toxins, exhibit a selective affinity for the more organized membrane regions. They specifically target these raft areas as points of interaction, facilitating their entry into the cellular interior.

cholesterol-enriched rafts are also binding sites for various bacterial products, including toxins, which through these raft-like domains penetrate into the cell [22]. As shown in [23] rafts are potentially involved in the development and progression of cancer. The mucin 1 (MUC1), which induces the development of various cancer forms [24], urokinase plasminogen activator surface receptor (uPAR), which is responsible for the invasion and spreading of cancerous cells [25] or mutated RAS proteins [26] are abundantly found in raft regions. Furthermore, cancer stem cells, pivotal in cancer initiation and progression, exhibit a preference for localizing within membrane rafts [27]. The increased presence of various oncogenic factors within the ordered domains of the membrane led to the development of drugs such as edelfosine, miltefosine, or perifosine, whose anticancer mechanisms are based on the disruption of raft-like regions [28]. Surprisingly, rafts are also associated with the development of several cardiovascular diseases. Atherosclerosis is a consequence of the accumulation of cholesterol-laden macrophages in arterial walls. As these macrophages evolve into foam cells, they trigger the development of congestion in the blood vessels, a process that serves as a direct precursor to conditions such as stroke, heart attacks, and

other vascular diseases [29]. The receptors responsible for this macrophage transition are confined to the raft areas within the membranes [30]. We are constantly unveiling the impact of ordered domains on the proper functioning of membrane proteins, the development of diseases, or the presence of abnormalities in cell activity. Although the exact impact of lipid rafts on cellular function remains elusive, the development of advanced tools and technologies holds the promise of unlocking the full potential of these membrane heterogeneities.

The formation of phase separation and the size of the domains are driven by an interplay between different external and internal factors such as temperature, lipid composition (especially the degree of lipid saturation), hydrophobic mismatch resulting from differences in chain length of lipids and proteins, and a variety of lipid-lipid and lipid-protein interactions [3]. The formation of regions enriched in saturated lipids originates from the stronger affinity of cholesterol to sphingolipids, and gangliosides than to phospholipids [31]. This preferential interaction is most likely caused by the presence of the amide group in sphingolipids, which makes them not only acceptors but also donors of hydrogen bonds [32]. It is well established that proteins featuring lipid-binding motifs strategically position themselves in cholesterol and SM-rich domains. However, this increased affinity does not only cause the recruitment of proteins into domains. It is a mutual interaction in which also proteins, such as palmitoylated scaffold protein PSD-95, can induce the nucleation of ordered microdomains by recruiting saturated lipids to specific membrane regions [33]. Despite the molecular interactions between membrane constituents, membrane organization is also driven by external factors, among which water seems to play the most crucial role. When lipids with different lengths of hydrophobic tails form a bilayer, the longer ones may get their acyl chains exposed to the aqueous solution. As shown in [34] mixture of d18:1 SM, cholesterol and 16:1 phosphatidylcholine (PC) leads to the height mismatch of 1.33 nm, which is sufficient for water molecules to interact with the exposed tails of SM. To minimize this unfavorable exposure of the hydrophobic tails, lipids self-organize according to the length of their acyl chains. The higher is this height mismatch between phases the larger is the average size of the formed ordered domain. Domains, while locally accumulating more lipids of similar length, tend to minimize the boundary at the interface between phases [34]. Phase separation can also be modulated by the actin cytoskeleton, which acts bidirectionally to stabilize or destabilize membrane domains *in vitro* [35, 36]. In living cells, actomyosin undergoes self-organization into asters, structures with easily distinguishable nucleation centers and radially oriented actin strands [37]. Asters bind to the charged phosphatidylserine (PS) lipids and cause their immobilization in the inner leaflet of the membrane [38]. The as-formed PS-rich domains interact with the glycosylphosphatidylinositol (GPI)-anchored proteins located in the outer leaflet, forming transbilayer raft-like regions [6]. It should be emphasized that although the organization of the cell membrane and the segregation of specific lipid species through actin-driven processes have been demonstrated both *in vitro* and in model lipid membranes, the exact molecular mechanism behind this membrane remodeling still remains not fully understood.

Undoubtedly, the phase separation and the development of local membrane heterogeneities are crucial for ensuring the proper functioning of the cell and the activity of its constituent components. Ongoing research reveals that numerous well-known cellular processes, such as immune signaling [39], enzymatic reactions [40], or toxin binding

[41], are intricately dependent on the presence of membrane rafts. The fact that membrane domains have remained evolutionarily conserved among various organisms points out towards the biological significance of phase separation and lateral segregation of specific components within the membrane structure. Since the fluid mosaic model was first presented, our understanding of membrane heterogeneity has advanced tremendously, however, we still have multiple knowledge gaps in our understanding of the mechanisms driving phase separation, the physical properties of membrane rafts, and the biological significance of these structures. Certainly, the structural organization of cell membranes holds immense potential for further interdisciplinary research. The ongoing development of novel tools and the improvement of the current imaging techniques may cast a fresh perspective on the properties and function of ordered membrane subcompartments.

1.2 Outline

Many studies have been devoted to the study of phase separation in lipid membranes and the formation of lipid domains, which play a crucial role in processes such as protein sorting [42], membrane trafficking [43], organization of the cytoskeleton [44], and pathogen entry [45]. A variety of factors influence the presence (or absence) of lipid domains, their density, size, and shape. Among them, we can distinguish internal factors that refer to the membrane properties such as lipid composition, leaflet asymmetry and curvature, and external factors, encompassing diverse properties of the local environment [46]. In the following sections, I undertook the challenge of unraveling the mechanisms driving phase separation and formation of local membrane heterogeneities in model prokaryotic and eukaryotic cell membranes (see Figure 1.2). Throughout my PhD studies, I particularly focused on the following areas:

- Evaluation of changes in the architecture of biomimetic cell membranes in response to diverse environmental conditions, including variation in pH and temperature (**publication 1**).
- Characterization of membrane dynamics upon exposure to a wide range of environmental pH (**publication 1**).
- Determination of the role of water in membrane organization into compartments (**publication 2**).
- A comprehensive description of the interactions between the membrane and its direct hydration layer on both micro- and nanoscale (**publication 2**).
- Characterization of the hydrophobic mismatch zone in biomimetic cell membranes with particular emphasis on the changes in the height mismatch and line tension at the boundary of lipid phases (**publication 2**).
- Correlation between the composition of prokaryotic cell membranes and their structural organization, manifested in the form of phase separation, local membrane curvature, and leaflets asymmetry (**publication 3**).
- Impact of the antimicrobial peptide daptomycin on biomimetic prokaryotic cell membranes and its interaction with negatively charged lipid species (**publication 3**).

In this thesis, chapters 2-4 introduce the reader to the diversity of cell membrane components, different approaches and models used to reconstruct membrane complexity, and finally a variety of experimental techniques indispensable for characterizing membrane structure, dynamics, and molecular properties. Chapters 5-7 comprise experimental work on the structural organization of eukaryotic and prokaryotic biomimetic cell membranes, presented in the form of three, peer-reviewed scientific publications, published in journals indexed in Journal Citation Reports (JCR):

1. **Emilia Krok***, Agnieszka Batura, Madhurima Chattopadhyay, Hanna Orlikowska, Lukasz Piatkowski*,
Lateral organization of biomimetic cell membranes in varying pH conditions,
Journal of Molecular Liquids, 2022, volume 345, number 117907
doi: 10.1016/j.molliq.2021.117907, **IF: 6.0**
2. **Emilia Krok***, Henri G. Franquelim, Madhurima Chattopadhyay, Hanna Orlikowska, Petra Schwillle, Lukasz Piatkowski*,
Nanoscale structural response of biomimetic cell membranes to controlled dehydration,
Nanoscale, 2023, volume 16, issue 1, 72-84,
doi: 10.1039/D3NR03078D, **IF: 6.7**
3. **Emilia Krok***, Mareike Stephan, Rumiana Dimova*, Lukasz Piatkowski,
Tunable biomimetic bacterial membranes from binary and ternary lipid mixtures and their application in antimicrobial testing,
Biochimica et Biophysica Acta (BBA) - Biomembranes, 2023, volume 1865, issue 7,
doi: 10.1016/j.bbamem.2023.184194, **IF: 3.4**

*corresponding author(s)

In **publication 1** (chapter 5), I presented a comprehensive study of how the environmental pH influences the formation, dynamics, stability, and lateral organization of phase-separated biomimetic cell membranes. A delicate balance between H^+ and OH^- ion concentrations that occurs outside and inside the cell is crucial for orchestrating cellular functions, regulating the mobility of membrane components, and influencing cell deformation. Internally, the intracellular pH fluctuations contribute to the signaling mechanisms that govern numerous cellular processes, including the regulation of the cell cycle, proliferation, differentiation, and apoptosis. The nuanced pH patterning within the cell plays a critical role in organizing the cytoskeleton and regulating the migration of its components. As shown in publication 1, exposure of the biomimetic cell membranes to the varying pH of the buffer hydrating lipid membrane can drastically change its structural organization. The lipid membranes formed under a wide pH range of 1.7-9.0, exhibited a substantial increase in domain size corresponding to the rise in pH of the medium hydrating the lipid membrane. The tunable lateral organization of the membrane with specific density, size, and shape of liquid ordered (L_o) domains formed at the specific pH remained stable for up to 3 days upon replacement of the aqueous medium with the buffer of neutral pH. At the same time, the diffusion coefficient for both L_o and liquid disordered (L_d) phases was insensitive to the changes in pH and remained constant in the whole range of the tested pH values. The presented in this publication novel approach of pre-defining shape and

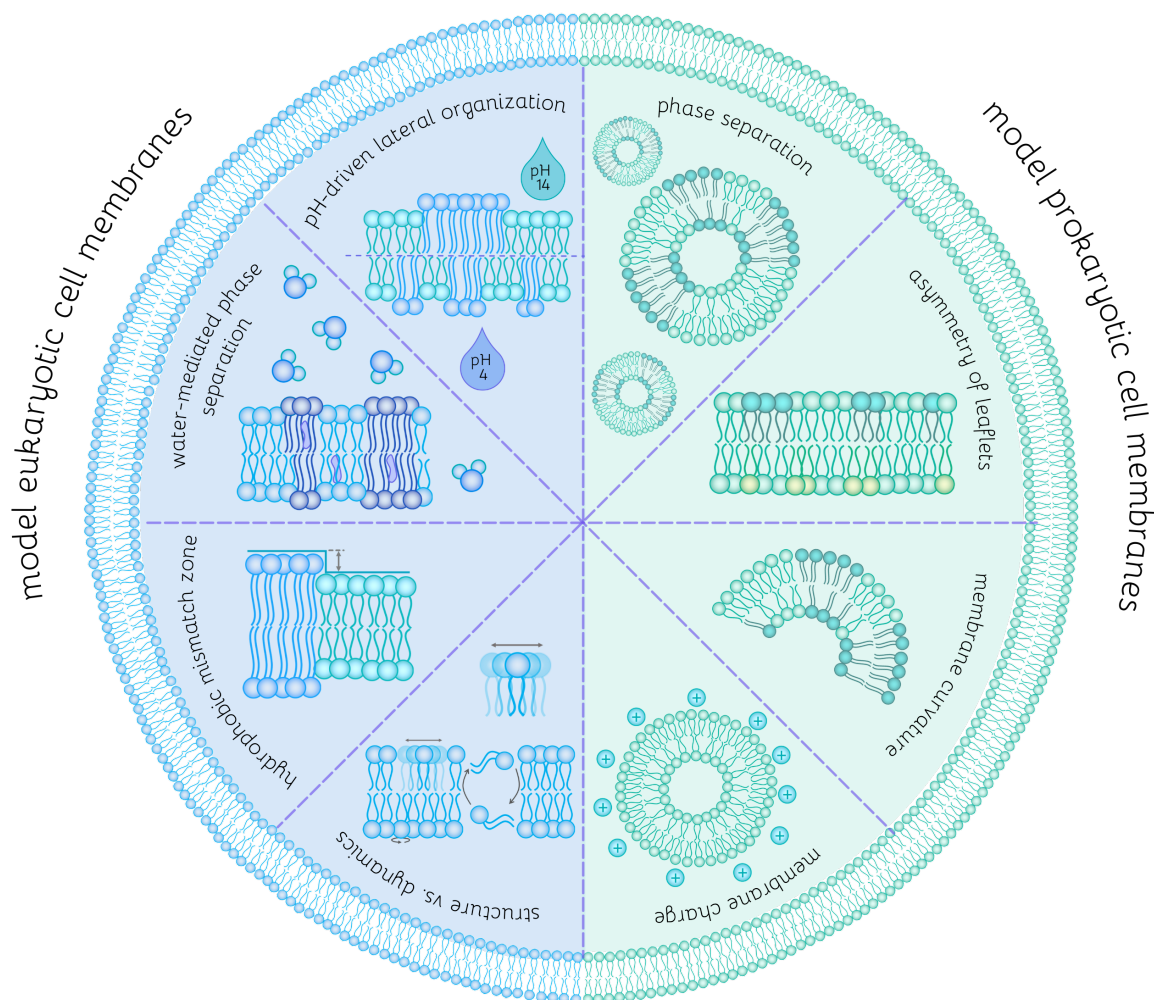


Figure 1.2: Outline of the thesis in graphical representation: the following work focuses on unraveling the internal (membrane composition) and external (properties of the environment) factors that are driving phase separation and formation of local membrane heterogeneities in model prokaryotic and eukaryotic cell membranes.

size of L_o phase domains can be successfully utilized for studying molecules that show preferential binding to more ordered membrane regions such as transmembrane proteins and membrane channels as well as observation of their mutual interactions.

In **publication 2** (chapter 6) I focused on the changes in the structural organization of membranes under varying hydration conditions. It is commonly accepted that water is an indispensable factor responsible for the formation of phase separation, the spatial arrangement of membrane proteins, and the overall cell membrane organization, all of which govern the proper functioning and activity of various biochemical processes that occur within and between cell membranes. My goal was to elucidate the micro- and nanoscale structural reorganization of membranes exposed to the varying hydration states (from fully hydrated membrane to completely desiccated) and to provide a comprehensive molecular-level picture of the membranes response to the decreasing water content. I observed that the process of dehydration led to a prominent nanoscale structural reorganization manifested as: (i) admixing of lipids forming L_d and L_o phases; (ii) an

extensive formation of nanoscopic domains of the L_d phase within the L_o phase domains; and (iii) formation of the jagged perimeter of the L_o domains. This enhanced admixing of lipids was associated with a 2-fold decrease in the hydrophobic mismatch between the L_o and L_d phases and a 3-fold decrease in the line tension between the phases for the fully dehydrated membrane. The results presented here bring new insights into the structural adaptation of lipid membranes to dehydration conditions, which is an essential intermediate step in all fusion events involving the merging of two cell membranes.

In **publication 3** (chapter 7) I focused on the modeling of the bacterial cell membranes, which although derived from less complex organisms, are still characterized by a high degree of complexity in lipid composition and structural organization. The commonly used models of bacterial cell membranes are usually very simple and composed of one or two types of lipids. In many cases, the lipids characteristic for bacterial cell membranes are replaced by their mammalian analogues, which on the one hand are easier to incorporate into the membrane structure, but on the other hand they are not naturally synthesized by bacterial cells and therefore cannot be considered as typical bacterial lipids. Due to differences in the lipid profile as well as structural and organizational features, these models fail in portraying the characteristics of bacterial membranes. In this research, I took up the challenge of reconstructing and characterizing model bacterial cell membranes with increasing level of complexity developed from binary and ternary lipid mixtures. I showed that even small changes in the lipid profile of the formed giant unilamellar vesicles (GUVs) can have a tremendous impact on the fundamental membrane properties such as membrane phase state, curvature, size, and leaflets asymmetry. The proposed bottom-up approach of reconstituting cellular membranes by mixing the desired ratio of lipids gives the possibility to reproduce, and most importantly tune, the lipid composition as well as structural and organizational characteristics for both gram-negative and gram-positive bacterial cell membranes. Finally, to validate the bio-application of the reconstructed model gram-positive bacterial membranes, I exposed them to the commonly used lipopeptide antibiotic daptomycin and quantified the daptomycin binding efficiency as a function of the amount of negatively charged lipid species in the membrane.

Chapter 2

Cell membrane

The life and death of all cells are inextricably dependent on the presence and functioning of their cell membranes. The plasma membrane defines the boundaries of the cell, separating its internal fluid – cytosol and embedded organelles from the surrounding environment [47]. It is responsible for maintaining homeostasis inside the cell, which is the steady physical and chemical state of the cell interior regardless of the changes occurring in the extracellular space. The plasma membrane allows cell compartmentalization, it surrounds the cell nucleus, mitochondria, endoplasmic reticulum, Golgi apparatus, and other organelles, which enable different biochemical reactions to occur simultaneously within the cell. The cell membrane contains various receptors and channels, that are responsible for the selective transport of water, ions, nutrients, biomolecules, and metabolic products inside and outside of the cell in the processes of endo- and exocytosis. The embedded in its structure signaling proteins act as sensors, responding to the physical (e.g. pressure, sheer stress, light) or chemical (such as molecules or ions), external stimuli [48]. These membrane receptors participate in signal transduction, where the extracellular messenger binding to the surface receptor, causes changes in cell biochemistry, triggering the specific cellular response to the received external stimuli. The variety of performed functions, together with their biological significance, require cell membranes to be not only diverse in terms of their constituents but also be able to quickly adapt to the constantly changing environment.

2.1 Lipid bilayer

"Life needs a membrane to contain itself so it can replicate and mutate."

Frans Lanting¹

Lipids, which constitute up to 50% of the cell membrane mass, form a fluid matrix embedded with proteins. A lipid bilayer of the area 1 um^2 is composed of approximately 5×10^6 lipid molecules [49]. The structure of each lipid molecule can be divided into two parts: hydrophilic (“*water-loving*”) or polar head group and hydrophobic (“*water-fearing*”) or non-polar hydrocarbon tail/tails. The amphiphilic character of lipids determines their spatial organization and tendency to form bilayer in a polar medium such as water. The

¹Frans Lanting (born July 13, 1951) – Dutch National Geographic photographer.

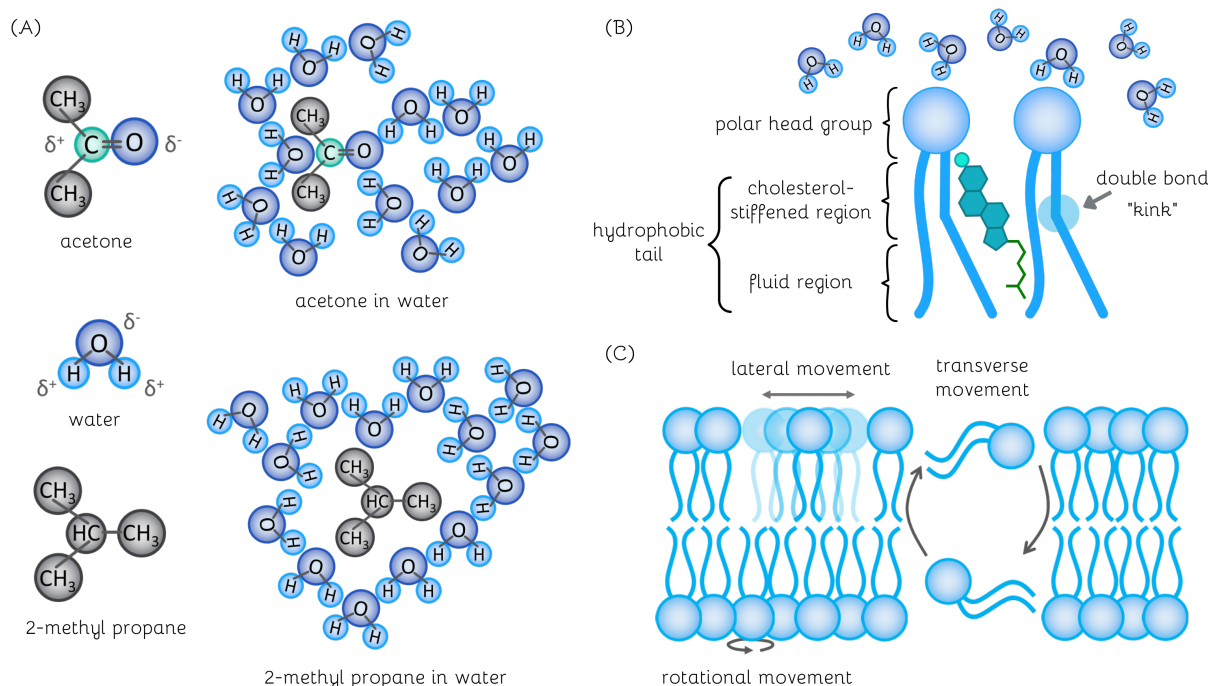


Figure 2.1: Hydrophobic effect drives lipids assembly and formation of a lipid bilayer: (A) Hydrophilic and hydrophobic molecules interact differently with water. Acetone which is a polar molecule can form favorable electrostatic interactions with water molecules. 2-methyl propane cannot form electrostatic interactions with water, it forces water molecules to reorganize into a cage-like structure, decreasing their entropy and leading to a more energetically unfavorable state. (B) Structure of lipid molecules with marked polar and non-polar regions. Cholesterol (in green) intercalates between lipid molecules. (C) Movement of lipids within bilayer: lateral diffusion along the plane of the bilayer, movement of single lipid molecule around its axis, and translocation between the monolayers (transverse movement or "flip-flop").

high solubility of hydrophilic molecules results from the presence of charged or uncharged polar groups, that easily form hydrogen bonds or undergo electrostatic interactions with the surrounding water molecules (see Figure 2.1 A). Contrary, hydrophobic molecules are characterized by insolubility in a water medium, due to the uncharged and nonpolar character of all of their atoms (or functional groups), resulting in an inability to form energetically favorable interactions with polar water molecules. When a hydrophobic molecule (or the hydrophobic part of the amphiphilic molecule) is dispersed in water, it disrupts the hydrogen bonding network formed by water molecules. To minimize this disruption, the hydrogen bonds orient tangentially with respect to the solute, forming a cage-like (clathrate) water structure around the non-polar moiety [50]. This formation of the clathrate structure diminishes the translational and rotational entropy of the water molecules, making the system more energetically unfavorable. To reduce this increase in free energy, the hydrophobic molecules tend to cluster together to minimize the number of affected water molecules [51].

Due to their amphiphilic structure, lipid molecules spontaneously arrange themselves in a specific manner when exposed to the aqueous solution; the non-polar, hydrophobic

hydrocarbon chains are repelled by water (see Figure 2.1 B), which leads to their congregation inside the lipid bilayer. Consequently, the polar, hydrophilic lipid head groups are directly exposed to the aqueous environment, altogether forming a symmetrically organized lipid bilayer. The hydrophobic effect is not only responsible for the structural arrangement of lipids into double-layered sheets but also drives the self-healing properties of lipid bilayers. Any perturbation in the bilayer structure creates access for water molecules to come in contact with the hydrophobic parts of the membrane. To eliminate these free edges exposed to the aqueous medium, lipids from the already existing membrane rearrange themselves, or additional lipids from external sources are added e.g. in eukaryotic plasma membranes this process is done by fusion of intracellular vesicles to close the membrane discontinuity [52].

Due to the hydrophobic effect, lipids tend to keep a well-defined structural organization, adopting the bilayer type of arrangement. However, regardless of these specific orientational constraints lipids remain in constant movement within the upper and lower leaflets of the cell membrane. As shown in Figure 2.1 C, the free movement of lipids is expressed in the form of lateral diffusion along the plane of the bilayer, rotational movement around their axis, or as occasional translocation between the monolayers (also known as a flip-flop) [53, 54]. The freedom of lipids movement, expressed as membrane fluidity, is affected by the degree of lipids tails saturation, temperature, the amount of cholesterol intercalating between lipids [55] and the membrane's hydration level [56]. Phospholipids undergo a transition from a liquid state to a rigid crystalline or gel phase at a specific temperature called phase transition temperature (T_m), which is lower for lipids with shorter acyl chains or those with one or more double bonds. Shorter hydrocarbon tails have a reduced ability to interact with the adjacent lipids, while double bonds create the so-called "kink", that leads to looser packing of lipid molecules within the bilayer. The temperature rise allows lipids to acquire additional thermal energy, which increases their Brownian motion and causes random rearrangement of the lipid molecules. At lower temperatures (below the phase transition) lipids movement is restricted, because of the denser packing of lipid molecules and the higher order of the membrane. The third factor allowing for the control of membrane fluidity is cholesterol, which works bidirectionally; at high temperatures (above phase-transition temperature), it stabilizes the membrane by raising the melting point of lipid molecules, while at lower temperatures it prevents lipids from stiffening and clustering. Moreover, by altering the membrane fluidity, cholesterol changes the ionic transfer across the membrane, by decreasing the membrane permeability to small water-soluble molecules. Maintaining membrane fluidity is crucial for the proper functioning of embedded membrane proteins, it helps in the regulation of selective membrane transport and is inherent in processes such as phagocytosis and cell signaling. Disruptions in membrane fluidity have been associated with several disorders, including Huntington's disease [57], Crohn's disease [58], Niemann–Pick's disease [59], or Alzheimer's disease [60]. The significance of maintaining membrane fluidity underscores the diverse strategies employed by nature to control this parameter in membranes.

2.2 Diversity of membrane lipids

"Still I had a lurking question. Would it not be better if one could really 'see' whether molecules as complicated as the sterols or strychnine were just as experiment suggested?"

Dorothy Hodgkin²

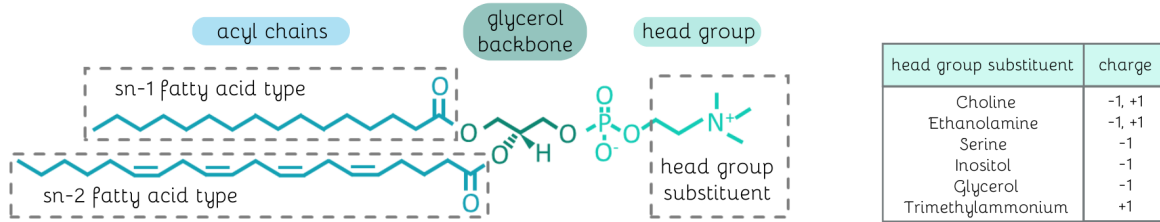
Membrane lipids can be classified into three main groups: phospholipids, sphingolipids, and sterols [61, 62]. Each phospholipid molecule is amphiphilic, featuring a three-carbon glycerol backbone, which connects two hydrophobic tails with the phosphate group, which is further linked to the hydrophilic head. As shown in Figure 2.2 A, the chemical diversity of phospholipids arises from the combination of fatty acid chains, type of sn-1 position linkage, the number of double bonds, their position, and hydroxylation. The fatty acid at the sn-1 position is usually saturated (no double bonds) or monounsaturated (single double bond). In contrast, sn-2 fatty acid tends to be monounsaturated or polyunsaturated (2 and more double bonds) [63]. The length and degree of saturation in fatty acid tails drive the phospholipids packing and lead to changes in membrane fluidity. The type of lipid head group determines whether the lipid molecule is negatively (e.g. 1,2-dioleoyl-sn-glycero-3-phospho-L-serine, DOPS) or positively (e.g. 1,2-dioleoyl-3-trimethylammonium-propane, DOTAP) charged or has a zwitterionic character (e.g. 1,2-Dioleoyl-sn-glycero-3-phosphocholine, DOPC) (see table in Figure 2.2 A). As presented in Figure 2.2 B, instead of glycerol backbone, sphingolipids contain sphingosine, which is a long acyl chain, with two hydroxyl (-OH) and one amino (-NH₂) group. The sphingosine is O-linked to the head group (typical types of head groups are summarized in the table in Figure 2.2 B) and amide-linked to the fatty acid chain [64]. The free hydroxyl group can interact via hydrogen bonds with the head group of neighboring lipids, adjacent membrane proteins, or water molecules.

The names of the fatty acids are generated using omega (ω -) or delta (Δ -) nomenclature as shown in Figure 2.2 C. Both of them require information about the number of carbon atoms (also referred as chain length) and number of saturated bonds within the fatty acid (e.g. 18:1 PC is a phospholipid with 18 carbon atoms and 1 double bond in the acyl chain, where the head group is composed of choline). In the case of ω -nomenclature, the position of the double bond is defined as the number of carbons from the methyl end to the first carbon forming the double bond, that is closest to the methyl end (indicated as n - or ω -). Δ -nomenclature defines the double bond placement as the number of carbons from the carboxylic acid end to the first carbon in the double bond (indicated as Δ).

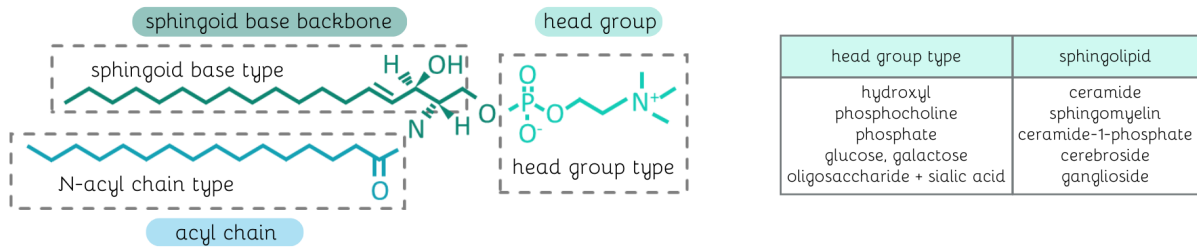
As shown in Figure 2.2 C, the diversity of fatty acids is achieved by differences in their chain length, degree of saturation, and even or odd number of carbons. Fatty acids typically contain between 14-24 carbon atoms, although aliphatic tails with five or fewer carbon atoms, known as short-chain fatty acids (SCFA), can also be synthesized (they are produced in the bacterial fermentation process of fiber) [65]. Fatty acids can be classified based on the number of carbon double bonds; saturated fatty acids do not have double bonds, monosaturated contain one double bond, while polyunsaturated have two or more double bonds. Furthermore, unsaturated fatty acids can adopt cis or trans conformation. In the cis configuration, two hydrogen atoms bound to the carbons forming

²Dorothy Hodgkin (May 12, 1910 – July 29, 1994) – English chemist, the third woman to win the Nobel Prize in Chemistry (1964).

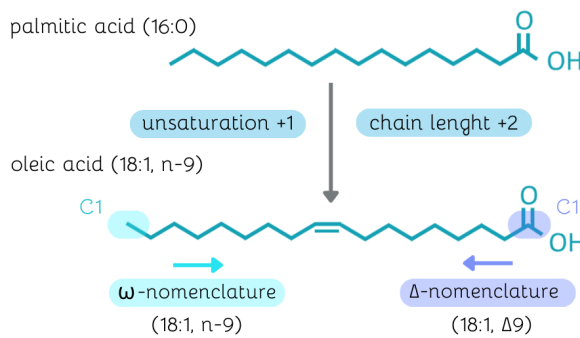
(A) phospholipids diversity



(B) sphingolipids diversity



(C) fatty acids diversity



(D) cholesterol

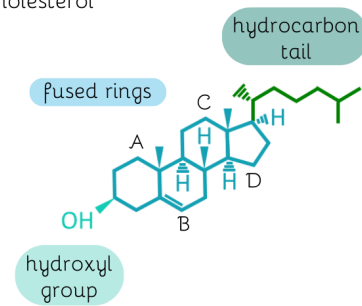


Figure 2.2: Chemical diversity of membrane lipids: (A) In phospholipids the diversity is achieved by length and degree of saturation of fatty acids at sn-1 and sn-2 positions, which are connected via glycerol backbone to the phosphate group with linked hydrophilic head. The type of head group substituent (see table on the right) determines the overall charge of the lipid molecule. (B) Sphingolipids consist of a sphingoid base, which plays the role of both backbone and hydrophilic tail. The sphingoid base and N-acyl chain can vary in the number of carbon atoms, and consequently the fatty acid chain length. Different head group types determine the sphingolipid name. (C) The diversity in fatty acids is achieved by differences in chain length (number of carbon atoms), degree of saturation (unsaturated, saturated), and even or odd number of carbons. The naming of fatty acids is done using ω or Δ nomenclature. (D) Structure of a cholesterol molecule; core rings are labeled A-D.

double bonds stick out on the same side of the chain, while in the trans configuration the adjacent hydrogens lie on the opposite side of the chain. Cis double bonds limit the dense packing of the lipids, due to the bending of the fatty acid chain (formation of a “kink”) and increase the membrane fluidity. Contrary, the trans configuration makes unsaturated chains similar to saturated fatty acids and leads to the denser packing of lipid molecules within the bilayer. Overall, the length and degree of saturation in fatty acid tails determine the phospholipids packing and membrane fluidity.

In addition to phospholipids and sphingolipids, all mammalian cells contain cholesterol, which is a sterol, containing a rigid ring-like structure, connected on one end with a polar hydroxyl group and on the other with a short hydrocarbon chain (see Figure 2.2 D). The structure of cholesterol determines its spatial orientation within the lipid membrane, where the hydroxyl group tends to come closer to polar headgroups of the neighboring lipids, while its hydrophobic tail prefers localization between the fatty acid chains of the lipid molecules [66]. However, the group of sterols is not limited only to one representative - cholesterol, as this class of molecules is present among a variety of species in kingdoms of animals, fungi, prokaryotes, and plants [67]. Fungi synthesize ergosterol, which structurally resembles eukaryotic cholesterol, differing by the additional double bonds on the B-ring and on the acyl chain and the presence of the methyl group at position C24. In the case of prokaryotic organisms, cholesterol can be found in cell membranes of specific strains such as *Chlamydia* [68] or *Mycoplasma* [69], although in general bacteria are unable to intrinsically synthesize it. These strains are considered obligate parasites, which acquire cholesterol, among other molecules, to synthesize their cell membranes. In other types of bacteria, the control of membrane fluidity is accomplished by hopanoids [70]. These sterol analogues have additional pentacyclic ring structure with 4 hydroxyl groups (characteristic for bacteriohopanetetrol [71]) or 3 hydroxyl groups and one -NH₂ group (bacteriohopaneaminotriol [72]) and lack the -OH group on A ring, which is present at the end of the aliphatic tail. Surprisingly, an even greater diversity of sterol molecules can be found in plants. Phytosterols such as stigmasterol, sitosterol or campestanol are responsible for the regulation of plant growth, its development and play a crucial role in signal transduction [73]. As discussed, the presence of sterols in the membranes is conserved among all living organisms, where their main function is the regulation of membrane fluidity, permeability, and dynamics.

2.3 Differences between eukaryotic and prokaryotic cell membranes

"Look closely at nature. Every species is a masterpiece, exquisitely adapted to the particular environment in which it has survived. Who are we to destroy or even diminish biodiversity?"

Edward Osborne Wilson³

The first evidence that the mammalian cell membranes consist of a lipid bilayer, rather than a single layer of lipids, was provided in 1925 by two Dutch scientists Evert Gorter and François Grendel. They collected erythrocytes (red blood cells) from different organisms, among them human, dog, sheep, and guinea pig, and extracted lipids from the known number of cells. Knowing the dimensions of a single erythrocyte, they were able to determine the total surface area of the surrounding plasma membrane. This theoretical estimation was compared with the results obtained from the Langmuir-Blodgett film experiments, now a commonly used technique for compression of various molecules and preparation of lipid films. The surface area occupied by lipids at the air-water interface turned out to be

³Edward Osborne Wilson (June 10, 1929 – December 26, 2021) – American biologist, naturalist, ecologist, and entomologist.

two-fold bigger than the area calculated based on the erythrocyte dimensions. This led to the conclusion that the cell membrane is not formed by a single but rather a double layer of lipids, in which lipid headgroups are exposed to the aqueous environment, while tails are facing the bilayer's interior. The experimental procedure used by Gorter and Grendel had two major drawbacks; first of all, the equation used to determine the cell surface area, significantly underestimated the real values, and secondly the extraction technique was insufficient to isolate all the lipids from erythrocytes. Fortunately for these scientists, both errors largely compensated each other, leading to the absolutely correct conclusion, and the lipid bilayer hypothesis proposed at that time remains valid to this day, not only for eukaryotic cell membranes, but also for lipid membranes of prokaryotes, plants, yeasts, and even viruses.

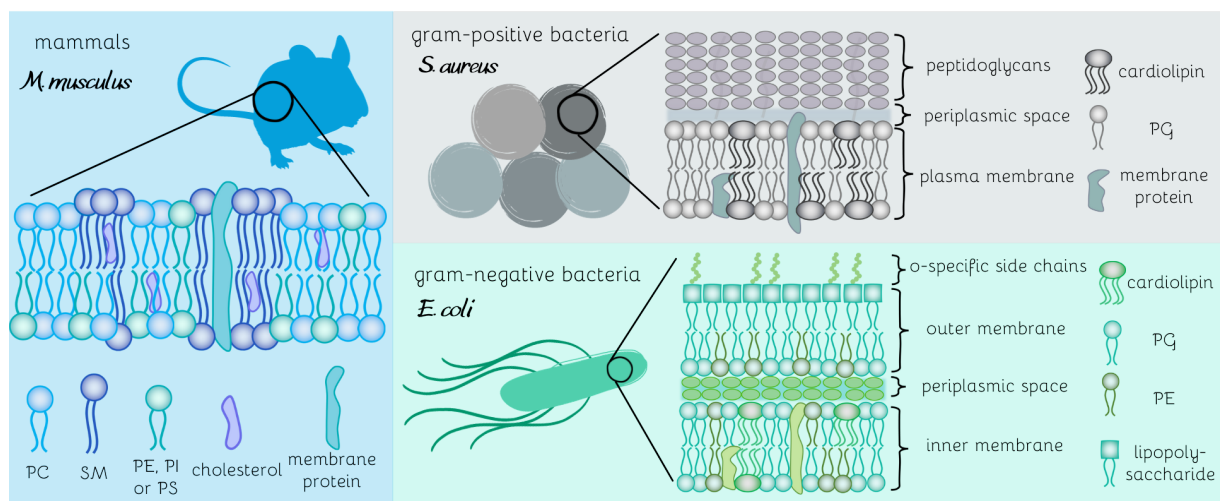


Figure 2.3: Structural differences between eukaryotic (mammals) and prokaryotic (gram-positive and gram-negative bacteria) cell membranes.

The plasma membrane in eukaryotic cells consists of five major phospholipids: PC, PE, PS, phosphatidylinositol (PI), and SM, among which PC constitutes approximately half of the lipid composition within cellular membranes (see Figure 2.3). A common property of the plasma membrane in all eukaryotic membranes is the asymmetric distribution of lipids in the two leaflets, which gives rise to distinct physical properties of each leaflet. The outer leaflet, also defined as the non-cytosolic or luminal side, is predominantly composed of PC and SM, while the inner leaflet, known as cytosolic, contains mainly negatively charged lipids PE, PS, and PI. The perturbations in the asymmetric distribution of lipids, especially the extended flip-flop of PS and PE from inner to outer leaflet, are connected with various biological processes such as coagulation of blood, cell division, myotube formation, cell apoptosis, or vesicle fusion. The membrane fluidity and permeability is controlled by cholesterol, which preferentially occupies the inner membrane (IM) leaflet.

Bacteria are categorized based on the structure of their cell envelope, which is a membrane protecting the interior of the bacterial cell from the surrounding environment. Unlike cells of more complex organisms, bacteria are directly exposed to the unpredictable environment and constantly changing external parameters that can influence the homeostasis of the cytoplasm. Thus, to survive, bacteria developed very sophisticated cell

Table 2.1: Major lipid components in the membranes of the most common gram-positive and gram-negative bacteria. Values are expressed as a percentage of the overall membrane lipid content.

Bacterial strain	PG	lysyl-PG	PE	cardiolipin	source
gram-positive					
<i>Bacillus cereus</i>	40	-	43	17	[74]
<i>Bacillus subtilis</i>	70	-	12	4	[75]
<i>Listeria monocytogenes</i>	29	23	9	22	[76]
<i>Staphylococcus aureus</i>	43	30	-	22	[77]
<i>Streptococcus pneumoniae</i>	50	-	-	50	[78]
gram-negative					
<i>Escherichia coli</i>	23	-	67	10	[79]
<i>Methylomonas methanica</i>	17	-	77	-	[80]
<i>Proteus mirabilis</i>	15	-	80	5	[81]
<i>Pseudomonas aeruginosa</i>	21	-	60	11	[82]

envelopes that protect them from rapid changes of external factors, and at the same time allow selective transport of ions, nutrients, and other macromolecules inside and outside the cell.

In 1884 Christian Gram developed the procedure based on the crystal violet staining of the bacterial cell membranes that till this day allows researchers to classify all bacteria into two groups: gram-positive and gram-negative; a classification that directly reflects the architecture and composition of the membrane [83]. The initial step involves the application of crystal violet, a purple dye, to the bacterial smear. This is followed by addition of iodine solution, known as Gram's iodine, which forms bigger, water insoluble complexes with crystal violet dye. The rinsing with ethanol or acetone changes the color of cell membrane depending on its chemical composition and degree of permeability; the membrane of gram-positive bacteria is impermeable and retains the violet staining. Contrary, the washing solution can easily penetrate the membranes of gram-negative bacteria, leaving them destained. To visualize strains belonging to gram-negative bacteria, an additional counterstain such as safranin or fuchsin is applied, which stains their membranes with characteristic pink color. The structure of the bacterial cell membrane is not only an indicator of their belonging to one of the groups but also determines their resistance to antibiotics [84], ultraviolet (UV) radiation [85], heat [86], and dehydration [87].

The composition of bacterial cell membranes differs significantly from mammalian cell membranes (see Figure 2.3). While mammalian cytoplasmic membranes are composed of different phospholipids such as PC, PS, PE, SM, and cholesterol [62], bacterial membranes contain mostly PE, PG, and cardiolipin and they lack cholesterol (see Table 2.1) [88]. However, some strains, for example, cyanobacteria contain hopanoids that are considered to be bacterial sterol surrogates [70]. The function of hopanoids is similar to cholesterol, it intercalates between lipids, and maintains membrane fluidity and rigidity. Divergent lipid composition makes bacterial cell membranes distinct from their mammalian counterparts, which is expressed by the different structural organization, packing density, surface charge, and membrane curvature.

In terms of the structural arrangement, the cell envelope of gram-negative bacteria is composed of two membranes, that are separated by the periplasm, which is a gel-like

Table 2.2: The composition of main head groups in the membranes of chosen mammalian liver cells, erythrocytes, and nerve cells. Values are expressed in weight percent. Adapted from: [95].

Membrane	PC	PE	PS	PI	SM	cardiolipin	cholesterol
Erythrocyte (human)	20	18	7	3	18	–	20
Plasma (rat liver)	18	12	7	3	12	–	19
ER	48	19	4	8	5	–	6
Golgi	25	9	3	5	7	–	8
Nuclear membrane	44	17	4	6	3	1	10
Mitochondria	38	29	0	3	0	14	3
Neurons	48	21	5	7	4	–	11
Myelin	11	17	9	1	8	–	28

substance containing a thin layer of peptidoglycans [89]. The outer membrane (OM) is composed of phospholipids, lipoproteins, and glycolipids, among them the most common are lipopolysaccharides and various OM proteins such as porins, that form channels for selective transport. The inner membrane is composed of phospholipids – PE, PG, and cardiolipin [90]. In contrary, the cell envelope of gram-positive bacteria is simpler and does not contain the OM. However, this group of bacteria is still able to survive harsh conditions such as e.g. strongly acidic environment in the animal gut. To withstand the potentially dangerous conditions their cell membranes are surrounded by a much thicker layer of peptidoglycans than those present in gram-negative bacteria. Moreover, the composition of the IM differs significantly, it contains mostly PG, lyso-PG, and a much higher amount of cardiolipin than in gram-negative bacteria [91].

It is important to highlight that both eukaryotic and prokaryotic cell membranes display significant diversity in the composition of their constituent lipids. These differences are observed between various organisms, cells, and even between the organelles within the same cell (see Table 2.2). For example, the plasma membranes of human erythrocytes and rat liver contain 20% by weight of cholesterol, whereas in rat liver mitochondria the cholesterol content is reduced to 3% by weight. Phosphatidylcholine constitutes 48% of the total weight in endoplasmic reticulum (ER) of liver cells, whereas it comprises only 11 weight% of nerve myelin [92]. Cardiolipin, a negatively charged lipid primarily found in bacterial cell envelopes, has a unique presence in mammalian membranes, as it is exclusively localized in mitochondrial membranes where it represents approximately 14% of the total lipid content. It should be noted that the underlying causes behind variations in membrane lipid composition among distinct cell types, or even within different organelles of the same cell still remain elusive. Similarly, the ratio of lipids characteristic of bacterial membranes differs not only between gram-positive and gram-negative strains, but also remarkably between strains belonging to the same group (see Table 2.1) or even between bacteria of the same strain grown under different conditions such as nutrient-rich versus nutrient-low agar, varying growth temperature [93] or in medium with addition of solvents (e.g. acetone or aniline [94]). The compositional differences should be taken into account especially when modeling cell membranes for cell-specific drugs, antibiotics, and other active molecules that target cell membranes by recognizing specific lipids or proteins within them.

Chapter 3

Model membrane systems

The study of cellular membranes in their native form is challenging due to their high compositional and structural complexity. Membranes extracted from different types of cells even within the same organism can differ drastically in their chemical composition and resulting from it molecular properties such as fluidity, tension, curvature or phase transition temperature. Additionally, the process of membrane isolation directly from cells is characterized by high complexity and the presence of multiple preparation steps, which have to be performed in laboratories specialized in handling of cell lines. Overall, we observe that the development of simplified model cell membranes and the reconstruction of minimal cell systems are constantly evolving branches of synthetic biology. In this chapter, I will discuss various model membranes, encompassing structures such as planar lipid bilayers or spherical vesicles, which are invariably applied for studying basic biological processes and mechanisms standing behind them.

3.1 Giant unilamellar vesicles

"A drop of water or sucrose solution was then placed on the glass slide and seemed to seep in between the phospholipid lamellae. The swollen phospholipid membranes formed long fingerlike projections attached at one end to the glass slide. Eventually, these membranous structures became detached and rounded up to form vesicles."

John P. Reeves, Robert M. Dowben¹

The development of liposomology had its beginning in the mid-1960s when Alec D. Bangham, a hematologist from Cambridge Babraham Institute described his findings on the formation of large and small "spherulites" [96]. Using electron microscopy, he was able to image small lamellar structures composed of PC (lecithin) and cholesterol. These "spherulites" were produced by dispersing lipids in an aqueous buffer and gentle hand shaking or sonication. In the year 1969 Reeves and Dowben reported the first direct observation of the liposomes growth by applying the gentle hydration of phosphocholine lipids with an aqueous solution (buffer containing ions or sucrose solution) [97]. They proposed how to control the spontaneous swelling by changing the growth conditions of

¹The first observation of gentle swelling of PC bilayer reported in: J.P Reeves, and Robert M. Dowben, *Formation and properties of thin-walled phospholipid vesicles*, Journal of Cellular Physiology **73**, 49–60 (1969).

the dry lipid films. Their findings opened a new path towards the fully tunable and controllable formation of liposomes with pre-defined size and single or multilayer structure. 10 years after the publication of Reeves and Dowben, Adil E. Shamoo and Thomas J. Murphy in the abstract for a Biophysical Society meeting for the first time used the term "giant vesicles", which is the name used up to now [98]. Nowadays, giant unilamellar vesicles (GUVs) are commonly used cell membrane models that have found their applications in studying basic physical and biological processes [99]. GUVs are single lipid bilayer assemblies with a spherical shape and dimensions close to the size of cells (1-100 μm) [100]. Importantly, in GUVs lipids are allowed to move more freely than in models which require immobilization on the solid support, where the movement of one of the leaflets may be impaired due to the contact with the substrate [101]. This similarity between GUVs and native cell membranes explains their wide use in studying biological processes such as cell division [102], deformation [103], lipids diffusion, cell-cell fusion [104], or transport and release of ions and biomolecules across the cellular membrane as the basic models of endo- and exocytosis [105].

GUVs formation methods can be divided into two main groups: techniques based on lipids swelling and those that rely on lipids assembly from the fluid interfaces. In the first group, we can distinguish gentle hydration, gel-assisted swelling, and electroformation (Figure 3.1). All of these methods start with a very similar preparation steps, where the desired composition of lipids, mixed in an organic solvent (typically chloroform or chloroform-methanol mixture), is spread onto a solid surface (e.g. glass) and dried to obtain a desiccated lipid film. The swelling procedure is performed in an aqueous buffer at an elevated temperature above the phase transition temperature ($T > T_m$) of the lipids, which ensures that the lipid species are in fluid state. Regardless of the used method we distinguish three factors that lead to vesicle growth: osmotic pressure, electrostatic interactions, and hydrophobic effect [106].

The most straightforward method for the preparation of GUVs is gentle hydration, alternatively called spontaneous swelling (see Figure 3.1 A), which was also the first technique reported by Reeves and Dowben [97]. Lipids stock solution in chloroform or in a chloroform-methanol mixture is deposited into the glass or Teflon vial and dried to remove residual traces of organic solvent. The aqueous solution is gently added into the vial to hydrate the desiccated lipid film. The type and properties of the swelling solution (pH, presence of divalent ions or sugars, temperature etc.) depend primarily on the charge (positive, negative, or zwitterionic) and phase transition temperature of the used amphiphiles. The spontaneous swelling method can be performed under physiological conditions, which makes it especially useful during the preparation of GUVs from charged lipids. The presence of divalent cations such as Ca^{2+} or Mg^{2+} promotes the swelling of charged amphiphiles [107]. The formation of GUVs composed of zwitterionic lipids such as PC can be improved by adding sugars directly to the stock solution of lipids in chloroform to form sugar-containing dry lipid films [106]. The presence of sugars such as sucrose helps in the separation of stacked PC bilayers by increasing their spacing, and consequently leads to a faster and more efficient swelling. The main advantage of the gentle hydration method is its simplicity, however, the preparation is very time-consuming, taking even one day, and the quality as well as the homogeneity of the formed vesicles is relatively poor compared to other formation methods [108].

A derivative of the gentle hydration method is a gel-assisted swelling technique (see

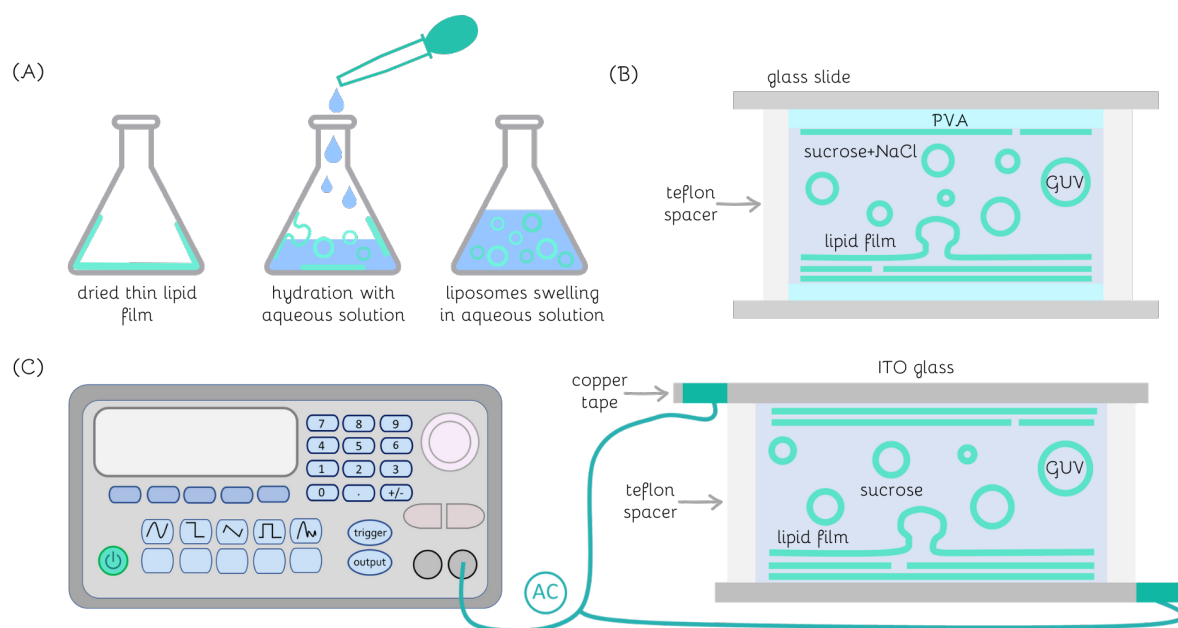


Figure 3.1: Schematic drawings of different formation methods of GUVs: (A) spontaneous swelling/gentle hydration of lipid film, (B) PVA gel assisted swelling, (C) electroformation/electroswelling.

Figure 3.1 B), where bare glass or Teflon substrate is additionally covered with a layer of agarose or polyvinyl alcohol (PVA). The swelling of lipids is more efficient and faster than in spontaneous swelling technique due to the buffer influx between the bilayer and porous polymer substrate. Remarkably, gel-assisted swelling can be performed in buffers containing a high concentration of ions, that is in an environment close to the physiological conditions and can be successfully used for the incorporation of proteins [109] or encapsulation of biomolecules [110]. Although this method leads to the high production of defect-free vesicles, they are prone to residual agarose contamination. Due to the autofluorescence of agarose, it can influence optical detection in fluorescence microscopy measurements. Similar problems may occur when agarose is replaced with a PVA layer, which may become encapsulated within the vesicles, leading to changes in their mechanical and physical properties.

Electroformation (also called electroswelling) was developed in 1986 by Angelova and Dimitrov and it very quickly became the most widely used method for preparing GUVs [111]. In this technique, a thin layer of the desired lipid mixture is deposited onto a conductive surface such as glass coated with indium tin oxide (ITO) or onto two metal wires made of platinum (alternatively titanium or stainless steel can be used). The ITO or metal wires are mounted in a home-built chamber and the lipid film is then hydrated with the sucrose buffer of specific osmolarity (see Figure 3.1 C). The lipids swelling in this method is very fast due to the applied alternating current (AC). The exact mechanism behind GUVs formation in electroswelling method remains not fully understood. Nevertheless, it is speculated that the electric field applied during the GUVs formation generates dielectrophoretic and electroosmotic stress, which are the electromechanical ef-

fects responsible for the membrane deformation [112]. The flow of the current leads to charge deposition on the membrane surface. The dielectrophoretic stress arises from the charge asymmetry between two membrane leaflets, which leads to increased membrane curvature and deformation [113]. The impact of electroosmotic stress on the vesiculation process is relatively low, however, it provides additional energy perturbations needed to control the deformation barriers such as membrane-substrate adhesion [114]. To overcome these attractive interactions between lipid membrane and solid support and induce vesicles swelling, budding, and finally detachment, both of these effects work synergistically. The electroformation technique requires precise adjustment of many parameters such as the duration of the formation procedure, electrical parameters (values of frequency, or peak-to-peak voltage) [115], or temperature [116], which should be tuned depending on the used composition of lipids. It should also be noted that electroformation cannot be applied for GUVs swelling in ionic buffers. This technique is therefore not suitable for lipid mixtures containing charged lipids, which require the presence of ions for successful liposome formation. Despite the more complicated procedure, electrosweeling leads to the formation of very high quality of GUVs and eliminates the risk of residual contamination coming from agarose substrate or oil, which are inherent in other formation techniques.

3.2 Small unilamellar vesicles

"Vigorous mechanical shaking of phosphatidylcholine suspensions produced smooth-edged particles of varying sizes, mostly within the 500 Å range. (...) Swelling in the presence of phosphomolybdate allowed greater penetration of the negative stain and sonication decreased the size range of the particles."

Demetrios Papahadjopoulos, Nigel Miller²

Because of their relatively large size, which is compatible with diffraction-limited imaging techniques, GUVs have attracted much interest from researchers working on biomimetic cell membrane systems. However, models such as liposomes go beyond just the giant vesicles. The classification of liposomes is based on two factors: size and structural arrangement (see Figure 3.2). Small unilamellar vesicles (SUVs) are liposomes with sizes varying between 20 to 100 nm, large unilamellar vesicles (LUV) range between 100 to 1000 nm, while GUVs greatly exceed 1000 nm (their size can reach even up to 200 μm). Multivesicular vesicles (MVVs), also called vesosomes, have a similar size to GUVs, however, they significantly differ in terms of the structural organization of their lumen. MVVs consist of the mother vesicle, which encapsulates the non-concentrically arranged SUVs trapped inside their lumen [117]. Vesosomes have been widely used as very basic models of primitive cells, where the SUVs mimic the intracellular compartmentalization [118]. Finally, structures consisting of many concentric lipid bilayers, organized in a similar manner to layers of an onion, are called multilamellar vesicles (MLVs). Like GUVs, SUVs consist of a single lipid bilayer arranged in a spherical shape. SUVs can be prepared using the sonication or extrusion method. In both techniques, lipids are mixed in the desired molar ratio in chloroform, dried to obtain a thin desiccated lipid film without

²Text published in: *Phospholipid model membranes. I. Structural characteristics of hydrated liquid crystals*, BBA Biomembranes, **382**, 265-275 (1975).

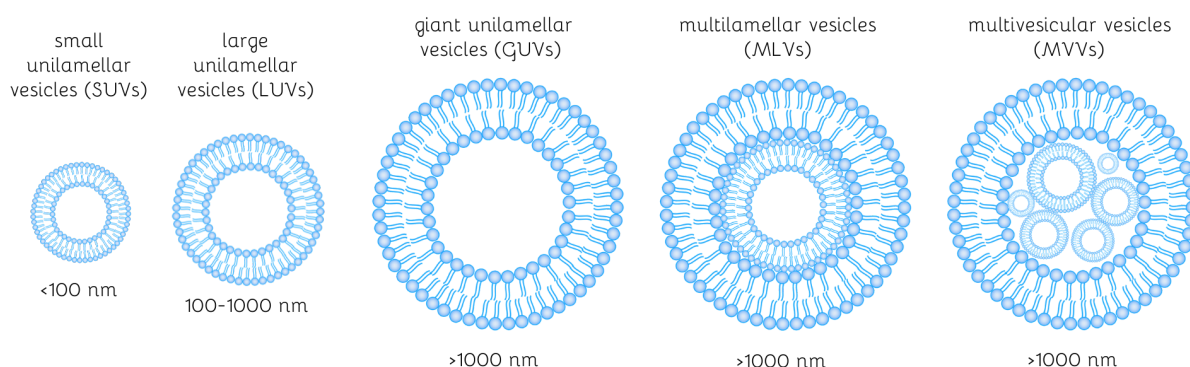


Figure 3.2: Schematic drawing of different types of vesicles.

traces of organic solvent, and rehydrated with the buffer (e.g., HEPES buffer or sucrose solution). Sonication is based on the use of acoustic energy, where ultrasonic waves are applied to break up MLVs, vesosomes, and aggregates into SUVs [119]. It is a very simple and fast procedure, requiring only the use of an ultrasonic bath. The size of the vesicles, in general, decreases with the increase of the sonication time [120]. It should be noted that the application of high-energy waves may significantly increase the temperature of the sample and of the water bath, causing changes in the membrane fluidity or leading to the degradation of proteins and other heat-sensitive molecules incorporated within the lipid membrane. Moreover, sonicated vesicles are characterized by a relatively broad size distribution [121]. In the extrusion method lipid suspension containing MLVs is passed through a polycarbonate membrane with a defined pore size (e.g. 100 nm). This method is more time-consuming and requires additional equipment such as extruder, syringes, and filtering membranes with specific size of pores [122]. It gives better control over the size and polydispersity of the final vesicles, however, recent cryogenic electron microscopy images revealed that they may not be as perfectly monodispersed as initially assumed [123]. Thus, the approach to obtain more homogeneous in size and truly unilamellar vesicles is to combine the two methods. In general, sonication is recommended as a first step, which breaks down the population of bigger vesicles, while the application of extrusion ensures a higher monodispersity of the vesicles.

3.3 Supported lipid bilayers

"At length being at Clapham where there is, on the common, a large pond, which I observed to be one day very rough with the wind, I fetched out a cruet of oil, and dropt a little of it on the water. I saw it spread itself with surprising swiftness upon the surface. (...) and there the oil, though not more than a teaspoonful, produced an instant calm over a space several yards square, which spread amazingly, and extending itself gradually till it reached the leeside."

Benjamin Franklin³

³Benjamin Franklin (January 17, 1706 – April 17, 1790) – an American polymath, a leading writer, scientist, inventor, diplomat, newspaper editor and printer, and political philosopher. In the scientific community Benjamin Franklin is well known for his kite experiment.

Supported lipid bilayers (SLBs), obtained by the spreading of small vesicles on a solid substrate and their subsequent rupture, were pioneered by McConnell et al. [124] in the early 1980s and have since then emerged as versatile membrane platforms for studying a wide range of biologically relevant processes. The mechanism of SLBs formation can be divided into two steps: (i) the adhesion of SUVs on an atomically flat solid substrate, their deformation and rupture, and (ii) the lateral reorganization of the bilayer patches (Figure 3.3) [125]. The vesicles bursting on the solid support can only occur at a very specific concentration of the liposomes, which is called the critical vesicular coverage [126]. When the vesicle is in close contact with the substrate, it undergoes support-induced stress, which is then enhanced by the neighboring vesicles. Upon bursting, the bilayer exposes its edges to an aqueous environment, which is an energetically unfavorable state. Consequently, the formed patches interact with the vesicles, either placed in close vicinity or from the surrounding solution, leading to their rupture and incorporation within the already formed bilayer. When the concentration of vesicles exceeds the critical vesicular coverage, this process can propagate, causing the sequence of rupturing events and the formation of bigger bilayer patches until the moment when the substrate is fully covered with the lipid bilayer [125]. The excess, unruptured vesicles usually deposit on top of the bilayer and require flushing out with the buffer solution in order to obtain a homogenous single bilayer.

SLB formation is driven by the interplay of interbilayer (between the edges of the formed planar bilayer and the neighboring vesicles), intrabilayer (between lipids), and bilayer-support interactions (between the membrane and solid support) [125]. With this

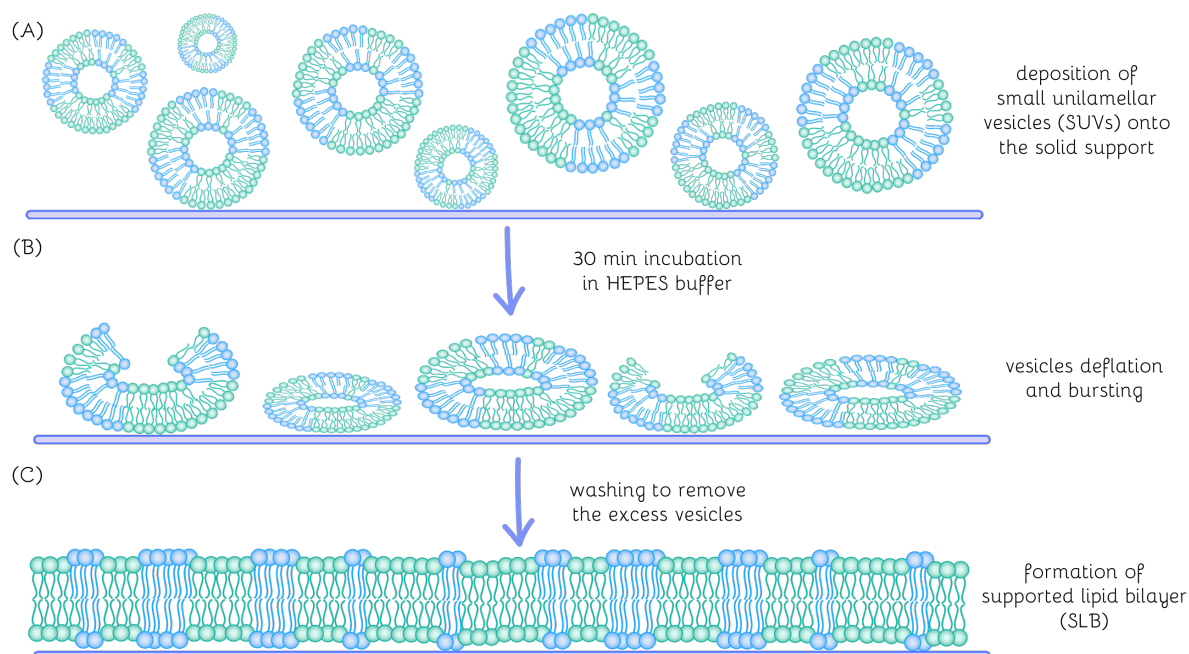


Figure 3.3: Schematic drawing of vesicle fusion method for preparation of SLBs: (A) SUVs are deposited on an atomically flat solid support (e.g. surface of mica), (B) upon contact with the substrate vesicles deflate and burst, (C) lipids diffuse and form a continuous bilayer.

regard, several experimental parameters have to be taken into account during the preparation of SLBs. The formation process of SLBs is mainly driven by the electrostatic interactions between the solid support and deposited SUVs. Charged, hydrophilic surfaces such as mica promote attachment of vesicles. Divalent cations (e.g. Ca^{2+}) are known to increase vesicle-surface interactions, their deformation, and finally rupture [127]. Finally, the ionic strength and pH of the aqueous solution have a strong impact on the vesicles attachment. By varying the nature of the used lipids (e.g. replacing zwitterionic lipids with negatively or positively charged ones), the type of substrate, or the ionic composition of hydrating buffer, it is possible to optimize the SLBs formation protocol to obtain homogeneous and defect-free bilayers.

SLBs possess analogous physical and structural properties to cell membranes but at the same time, they can be simplified to focus on specific biophysical features. Thus, the surface-confined membrane models have been widely applied to study different cellular processes such as adsorption or fusion of membrane proteins, pore formation, intermembrane interactions (e.g. vesicles fusion), lipid diffusion or lateral reorganization of lipid membranes under varying physiological conditions. SLBs have gained a lot of interest due to their unique intrinsic properties such as long-term stability and compatibility with many experimental techniques, for instance, atomic force microscopy (AFM) [128], total internal reflection fluorescence (TIRF) microscopy [129], fluorescence microscopy [130], or quartz crystal microbalance (QCM) [131]. SLBs can remain intact for up to a few days, even when exposed to high flow rates of the surrounding solution [132] or after induction of holes in their structure [133], but more importantly in the context of the presented thesis, they are the only model system allowing for studying lipid membranes under dehydration conditions [56]. The presence of substrate, which makes SLBs so robust is also their biggest disadvantage, especially with respect to lipid mobility. It has been shown that the lipids diffusion in GUVs is more than 2-fold higher than in SLBs due to the lipids' interactions with the solid support [101]. However, the mobility-inhibiting effect of the substrate can be reduced by applying polymer cushions (e.g. layer of polyethylene glycol (PEG) [134], poly(amino acid methacrylate) [135], or hydrogel [136]) as an interlayer between the solid support and the lower leaflet of SLB. Moreover, this approach is especially beneficial for SLBs containing membrane proteins; it not only mitigates the impact of the solid support on their lateral diffusion but also prevents proteins from substrate-induced unfolding and denaturation [137].

Chapter 4

Experimental techniques

Comprehensive characterization of model membranes requires the integration of multiple experimental techniques. Only through their parallel application we are able to attain a thorough understanding of the intricate micro- and nanoscale features inherent to these complex structures. This chapter delves into the fundamental principles of the most widely used experimental techniques to study model cell membranes biophysics. When employed collectively, these methods not only aid in visualizing the structural intricacies of model cell membranes but also facilitate the determination of their topography, charge, or the mobility of constituent lipids.

4.1 Fluorescence microscopy

"Nothing, I believe, is so full of life under the microscope as a drop of water from a stagnant pool."

Agatha Christie¹

The spatial resolution of the human eye is around 200 μm , which means that we are unable to distinguish objects smaller than 200 μm [138]. The size of the typical bacterial cell is around 1 μm [139], while viruses attacking the human body have a diameter between 20 and 200 nm [140]. The existence of these potentially harmful pathogens, as well as other microbes undetected by the human eye, was denied for centuries. The development of microscopy ushered in a whole new era in which scientists discovered a fascinating novel world that exists below the resolution limit of the human eye. The inventions of scientists such as Hans and Zacharias Janssen, Robert Hooke, and Antonie Philips van Leeuwenhoek laid the foundation for modern microscopy techniques. Fields such as biophysics, biology, and microbiology would not exist without light, fluorescence, and confocal microscopy, which provide information about microorganisms, and tissues, down to cells and organelles, all of them undetectable by the naked human eye. In this chapter, I introduce the basics of imaging techniques that are based on the process of fluorescence and I discuss the most common labeling techniques used for the visualization of live and model cell membranes.

¹Agatha Christie (September 15, 1890 – January 12, 1976) – an English writer of crime books, detective stories and thrillers.

4.1.1 Fluorescence

Luminescence is a broad class of processes, in which a molecule emits radiation in the form of photons upon absorption of energy [141]. Imaging of the biological specimens, among them lipid membranes, is possible because of the phenomenon called fluorescence, in which atoms and molecules upon absorption of light of a specific wavelength, tend to emit light of a longer wavelength. The labeling of cells with fluorophores emitting in different wavelengths enables selective, background free visualization of specific parts of the tissues, cells, organelles, cell compartments, and even single molecules.

The infusion of a wood *Lignum nephriticum* was the first reported example of substance emitting fluorescence, which was presented in 1565 by the Spanish botanist Nicolás Monardes [142, 143]. Monardes suggested that the observed blue color of the wood suspension could be used for the detection of falsified infusions, which at that time were used as a costly medicine to treat urinary diseases. Although Monardes and many other scientists such as the mineralogist René-Just Haüy or the physicist Sir David Brewster observed the phenomenon of fluorescence, they were unable to explain the physical mechanism behind this process, mistakenly taking it as a form of light scattering or internal dispersion [141]. The breakthrough in our understanding of fluorescence came in 1852 when Sir George Gabriel Stokes published his paper “On the Change of Refrangibility of Light” [144]. He examined a variety of organic and inorganic substances and concluded that the emission from the excited molecule always occurs at longer wavelengths than the wavelength used to excite it. This spectral shift between absorption and emission is nowadays commonly known as Stokes shift.

Aleksander Jabłoński in 1933 proposed an intuitive way of illustrating the distribution of electronic and vibrational states of a molecule, including a description of the radiative and non-radiative transitions that occur between various states, as well as graphically explaining the origin of Stokes’ observations [145]. This schematic visualization of the energy states of a molecule with the possible energy loss pathways characteristic for an excited molecule is nowadays commonly known as the Jabłoński diagram (Figure 4.1). The horizontal lines on the diagram represent the energy levels that can be occupied by a molecule; the energy increases vertically, with the higher states localized on the top and the lower at the bottom. As the energy increases along the vertical axis, the subsequent energy levels are positioned more closely until they become a quasi-continuum. The thicker lines correspond to the lowest vibrational levels characteristic for each electronic state. Each electronic state is denoted by S (singlet state) or T (triplet state). This naming is based on the configuration of the spin angular momentum, where singlet states are characterized by zero total spin angular momentum, while triplet states have a total spin angular momentum of one:

- S_0 – singlet ground state,
- S_1 – the first excited singlet state,
- S_2 – the second excited singlet state,
- S_n – the n^{th} excited singlet state,
- T_1 – the first excited triplet state,
- T_n – the n^{th} excited triplet state.

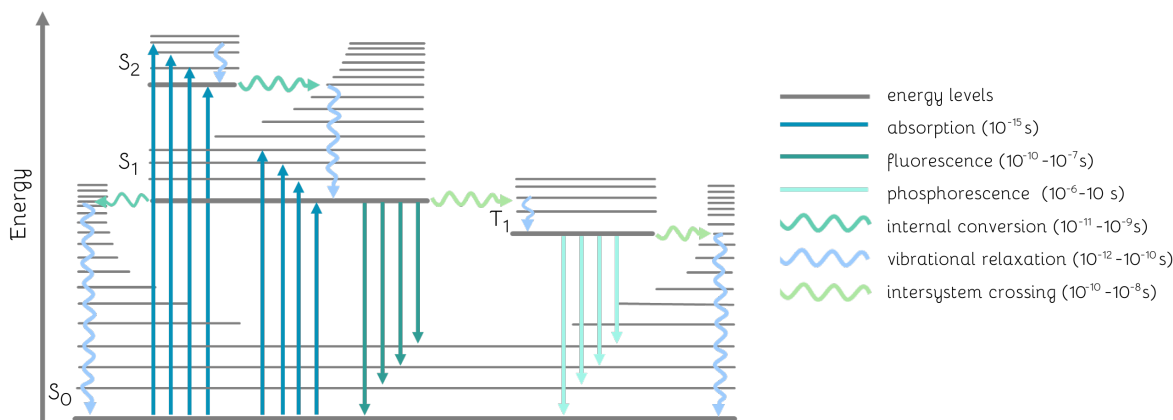


Figure 4.1: Jabłoński diagram of electronic and vibrational energy states of an excited molecule; S_0 is a singlet ground state, S_1 is the first excited singlet state, S_2 is the second excited singlet state, T_1 is the first excited triplet state.

Two different types of arrows represent radiative (straight arrow) and non-radiative (undulating arrow) transitions. A transition is called radiative whenever it involves absorption or emission of photon(s). Analogously, the non-radiative transition between two molecular states occurs when neither absorption nor emission of photons is observed.

When a molecule absorbs a photon of a particular energy (typically in the near UV or VIS range) it can be promoted to the higher electronic state, e.g. from S_0 to one of the singlet excited states (S_1, \dots, S_n). The absorption process is the fastest transition and lasts on the order of only 10^{-15} s. The molecule cannot be directly promoted from the ground singlet state S_0 to one of the triplet excited states (T_1, \dots, T_n) due to the conservation of angular momentum [146]. The excited state is a non-equilibrium state, that cannot last forever, the molecule tends to dissipate the energy gained during absorption and eventually return to the ground state. Firstly, the energy can be given away in the form of kinetic energy, the process known as vibrational relaxation. This energy process occurs rapidly on a time scale ranging from 10^{-12} to 10^{-10} s [147]. The vibrational energy can be transferred to the molecules surrounding the excited molecule (intermolecular) or stay within it (intramolecular). Alternatively, a molecule can transfer from one vibrational level to another, lower vibrational level in a process called internal conversion. The time scale of this process for transitions observed between higher singlet states ($S_3 \rightarrow S_2, S_2 \rightarrow S_1$, etc.) is nearly the same as vibrational relaxation ($10^{-11} \rightarrow 10^{-9}$ s). However, the large energy gap between the ground state S_0 and the first excited state S_1 makes this process relatively slow (less probable), opening the possibility for other processes such as fluorescence and intersystem crossing to compete with the internal conversion. Fluorescence is a photon emission process, which occurs on a time scale ranging from 10^{-10} to 10^{-7} s. Fluorescence occurs when the molecule passes from the lowest vibrational level of the first excited singlet state (S_1) to the singlet ground state (S_0). According to Kasha's rule, the probability of fluorescence taking place from higher excited singlet states (e.g. transition from S_2) has a very low amplitude [148]. The weakly allowed transition from S_1 to ground vibrational T_1 state is called the intersystem crossing, which remains in most cases forbidden due to the conservation of spin angular momentum. The intersystem crossing can be facilitated by the incorporation of heavy atoms in the molecule, which leads to the increased strength of

spin-orbit coupling. Apart from fluorescence, photons can also be emitted in the process known as phosphorescence, which is a transition taking place from the excited triplet state T_1 to the singlet ground state S_0 . This process, similarly to the preceding intersystem crossing has very low probability of occurring, consequently characterized by a very long time scale in the 10^{-6} to even 10 s range. The likelihood that a specific process will happen depends on its probability; the higher the probability of an event to occur, the faster is the transition.

4.1.2 Confocal microscopy

The widefield fluorescence microscope can be considered the protoplast of the more advanced confocal microscopy. In a widefield microscope, light emitted from a light source (e.g. mercury lamp or laser) goes through the excitation filter (see Figure 4.2 A). This filter (shortpass or bandpass) selects light of a specific wavelength from the whole spectrum of the light source. The objective lens directs and concentrates the incoming light onto the imaged specimen within the entire field of view of the objective lens. Upon excitation, the specimen emits fluorescence light, which is then captured by the same objective lens. On its way to the detector or eyepiece, light encounters the dichroic mirror, which allows only specific wavelengths to pass through. Light emitted from the objective lens travels in a precisely focused, parallel (collimated) manner, evenly illuminating the entire sample within the field of view. The emitted fluorescence signal from multiple focal planes of the measured specimen makes widefield microscopy an excellent tool for capturing 2D images of the entire cell or for detecting specific molecules, proteins, or structures within the cell. However, the need to overcome the limitations in imaging thick samples such as tissues or vesicles led to the development of another tool - the confocal microscope.

In 1957 Marvin Lee Minsky patented the basic principle of the confocal microscope, in which any light that was not coming from the focal plane was obstructed by the pinhole aperture [149]. The structure of the confocal microscope, the light path, and its basic elements are similar to those of the widefield microscope (see Figure 4.2 B). It consists of a laser light source, excitation, and emission filters, objective, dichroic mirror, and detector. Additionally, confocal microscopes are equipped with pinholes that are responsible for blocking any out-of-focus light coming from the specimen, thus creating sharp images of a single plane without any background signal.

The spatial resolution of the fluorescence microscope is restricted by the diffraction limit, defined as the minimum distance between two Airy disks or patterns formed when light passes through the aperture. According to Rayleigh's criterion, the minimum separation d between two neighboring points that allows them to be resolved is defined by the equation (4.1) [151]:

$$d = \frac{0.61\lambda}{n\sin\theta} = \frac{0.61\lambda}{NA} \quad (4.1)$$

where λ is the wavelength of light, θ is the half-angle subtended by the pupil of the objective at the specimen, n is the refractive index of the used imaging medium, placed between the objective and the specimen, and NA is defined as the lens numerical aperture.

It can be easily calculated that when using the air objective, the limit for NA is around 0.95, which when imaging at 550 nm (visible light) gives a lateral resolution of $d = 350$ nm. In order to increase the resolution it is recommended to apply immersion

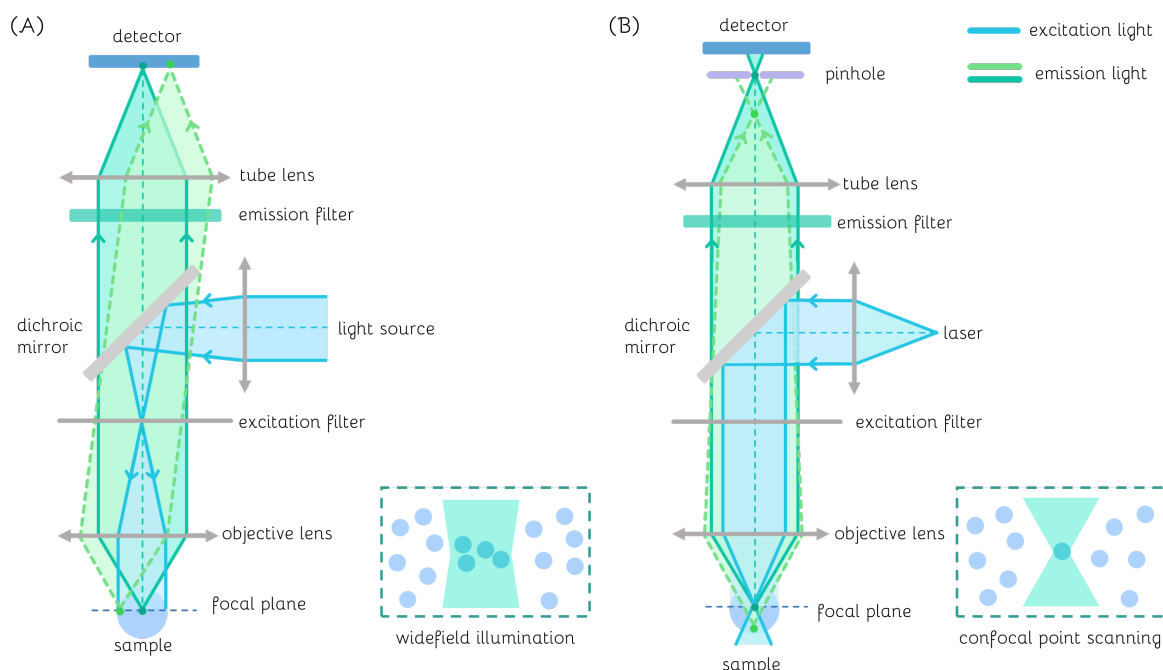


Figure 4.2: Schematic illustration of the basic optical components and light path in (A) widefield and (B) confocal microscope. Adapted from [150].

oil with a refractive index of 1.52 as the imaging medium between the objective and the specimen. The immersion oil replaces the air gap between the immersion objective lens and the cover glass with a medium of high refractive index, causing the reduction of the light refraction and partial loss of signal. Imaging with immersion oil can lead to an improvement of the lateral resolution to approximately $d = 200$ nm. Alternatively, water ($n = 1.33$) and glycerol ($n = 1.47$) can be used as optional imaging media.

4.2 Fluorescent probes

"Nothing can dim the light that shines from within."

Maya Angelou²

Fluorescent probes are compounds commonly used for visualization of biological samples including tissues, cells, or model cell membranes. Probes absorb photons of a specific wavelength upon illumination and emit light of a typically longer wavelength in a process called fluorescence. Fluorophores are characterized by several parameters that should be considered when selecting a probe for specific purposes:

- *Excitation and emission wavelengths* – values corresponding to the peaks and widths in the excitation and emission spectra. Both parameters play a crucial role in imaging the samples labeled with 2 or more fluorescent probes to eliminate the possibility of fluorescence crosstalk (overlapping of fluorophores excitation or emission spectra).

²Maya Angelou (April 4, 1928 – May 28, 2014) – an American writer, poet, and civil rights activist. Her books focus on topics such as racism, identity, family, and travel.

- *Stokes shift* – the difference between absorption and emission maxima. It allows the separation of the excitation light from the collected emission light. The large Stokes shift diminishes the possibility of self-absorption, in which emitted fluorescence is partially reabsorbed by the emitting molecules, causing a substantial reduction of the detected fluorescence intensity and alteration of the emission spectrum.
- *Fluorescence lifetime* – the average time fluorophore stays in the excited state before it emits a photon and returns to the ground state. The time range of this process varies from picoseconds to nanoseconds for different fluorophores. In case of overlapping emission spectra of two or more fluorophores, a fluorescent lifetime can be used for their distinguishing.
- *Quantum yield* – describes the efficiency of conversion of excitation light into fluorescence signal. It is defined as the ratio of the total number of emitted photons to the total number of absorbed photons. Probes characterized by a high quantum yield generate stronger emission signal while applying less excitation light. The use of lower laser power reduces the risk of fluorophore photobleaching. Moreover, samples labeled with high quantum yield fluorophores are typically sharper with easily distinguishable features, even when the exposure time is shorter and/or the amount of added probe is reduced.
- *Extinction coefficient* – provides information about the amount of light of a specific wavelength that can be absorbed by a fluorescent molecule. The brightness of the fluorophore is defined as the product of absorption coefficient and quantum yield.

Since ancient times purple has been considered the color of royalty, great power, and highest majesty. Indeed, this color is a perfect match for the first synthetic dye, whose vibrant purple tones fascinated Queen Victoria and the Empress Eugenie of France. In 1856, 18-year-old William Henry Perkin was trying to synthesize the anti-malarial drug quinine and accidentally ended up with the development of mauveine [152]. The substance was very quickly patented and commercialized, as a much cheaper synthetic alternative to the commonly used natural dyes. However, the absolute breakthrough in fluorescence imaging of biological specimens was made by the three fathers of green fluorescent protein (GFP): Roger Y. Tsien, Osamu Shimomura, and Martin Chalfie, who were awarded the 2008 Nobel Prize in Chemistry "for the discovery and development of the green fluorescent protein, GFP". GFP was first purified in 1962 from the jellyfish *Aequorea Victoria* [153]. Nowadays, GFP is used as a tool to visualize gene expression patterns in living organisms such as bacteria, yeast, fish, and mammals. The synthesis of fluorophores is an ever-evolving area of research in which scientists are trying to create more stable, non-toxic, easy to incorporate probes that can be precisely localized to different regions of interest within the cell. In this chapter, I will discuss the most common types of fluorescent probes used in biological membrane research.

4.2.1 Phase-specific probes

The most straightforward approach to study membrane heterogeneities is the incorporation of lipid-based probes characterized by selective partitioning into L_d or L_o phase (see Figure 4.3 A). It should be noted that the vast majority of lipid-derived probes bind preferentially to more liquid regions, making labeling of the highly ordered and densely packed

L_o phase particularly difficult [154]. As discussed in the chapter 2.2, lipids are characterized by different combinations of fatty acid chains, which may be saturated, mono- or polyunsaturated. The degree of saturation and the length of the fatty acid chains determine the selective partitioning of lipids into the specific phase. However, the partitioning of lipid-derived probes is rarely determined by the lipid structure alone, but also depends on the type of fluorophore attached. Phospholipids can be fluorescently labeled in two locations of the lipid molecule: (i) at one of the acyl chains or (ii) at the head group. The head group labeled fluorescent probes based on the PE lipid with unsaturated fatty acid chains (e.g. Atto 633-DOPE) localize solely in L_d phase in model membranes. Saturated PE lipids (e.g. 1,2-dipalmitoyl-sn-glycero-3-phosphoethanolamine, DPPE) carrying fluorescent probes are characterized by less predictable partitioning. DPPE lipid bearing rhodamine-derived fluorophores such as e.g. Lissamine Rhodamine or Texas Red show preference towards L_d phase, despite the presence of L_o forming lipid in these lipid-dye complexes [155, 156]. In contrast, DPPE conjugated with small neutral dye nitrobenzoxadiazole (NBD) shows partitioning into L_d and L_o phases with a stronger preference towards a more fluid phase [156]. Remarkably, the degree of partitioning in the case of NBD-DPPE probe is strongly dependent on the used model system and its lipid composition. Although the above behavior of NBD-DPPE is valid for GUVs and SLBs, its partitioning in giant plasma membrane vesicles (GPMVs) is different; it entirely incorporates within the L_o phase [157]. Similar discrepancies in membrane partitioning are observed for head group-labeled SM-bearing analogs of Atto dye. Although SM is a main constituent of L_o phase, probes such SM-Atto532 or SM-Atto647N preferentially incorporate within the disordered phase. This arises from the relatively big size of the Atto fluorophore, which disturbs the partitioning of the probe in the densely packed L_o phase. As an alternative approach, the fluorophore can be attached to the lipid via a long hydrophilic linker (e.g. PEG2000 spacer), which has been shown to prevent probe exclusion from the L_o phase [158].

Modification of the lipids at their acyl chains puts additional requirements on the properties of the conjugated fluorophore. The need for small size and low polarity of the fluorophore precludes the use of the commonly used rhodamine or cyanine dyes. Lipids commonly used for acyl chain modification are derivatives of PC and SM labeled with 4,4-difluoro-4-bora-3a,4a-diaza-s-indacene (BODIPY) or NBD fluorophores. Similarly, fluorescent labeling of SM at the acyl chain with Atto dyes or their derivatives (such as Atto 647-GM1) leads to the selective partitioning of these probes in L_d phase and complete exclusion from L_o phase [159]. Modification of lipid at the fatty acid chain changes the size of the lipid-fluorophore complex and hampers its incorporation within the more densely packed L_o phase [154]. Overall, when selecting a lipid-based probe, several factors should be considered, such as the type of lipid, the size of the fluorophore, and the site of binding (head group or acyl chain), as they all contribute to the behavior and partitioning of the probe within the cell membrane.

Cholesterol is known to intercalate between lipids of both L_d and L_o phases with preferential incorporation within more ordered L_o phase. Taking this into account, it is expected that cholesterol-derived probes would partition in approximately the same ratio in both L_d and L_o regions of model cell membranes. Two cholesterol analogs NBD-cholesterol and TopFluor-cholesterol, both bearing fluorophore at the side chain show remarkably different partitioning in a lipid membrane. NBD-cholesterol due to the more

polar character of NBD dye shows preferential binding to L_d phase [155], while TopFluor-cholesterol tends to insert into L_o phase [159].

Lipophilic probes are not derived from lipids, but their structure and lipophilic or amphiphilic character resemble lipid molecules, allowing their incorporation into the membrane structure. This class of probes can be divided into two main groups: dye bearing long-chain hydrocarbons (LCH probes) and polycyclic aromatic hydrocarbons (PAH probes). LCH probes include cyanines (e.g. DiL, fast DiL, DiD, fast DiO) and rhodamines (e.g. Rhodamine-R18); both groups are characterized by high stability and brightness [154]. It should be noted that regardless of the degree of saturation in the hydrocarbon chain, LCH probes are generally excluded from the L_o phase, preferentially binding to more fluid membrane regions [160]. PAH dyes (terylene, naphthopyrene) are good alternatives for selective labeling of the L_o phase [160]. Relatively planar in structure, they intercalate between lipids from the L_o phase in a manner similar to cholesterol molecules.

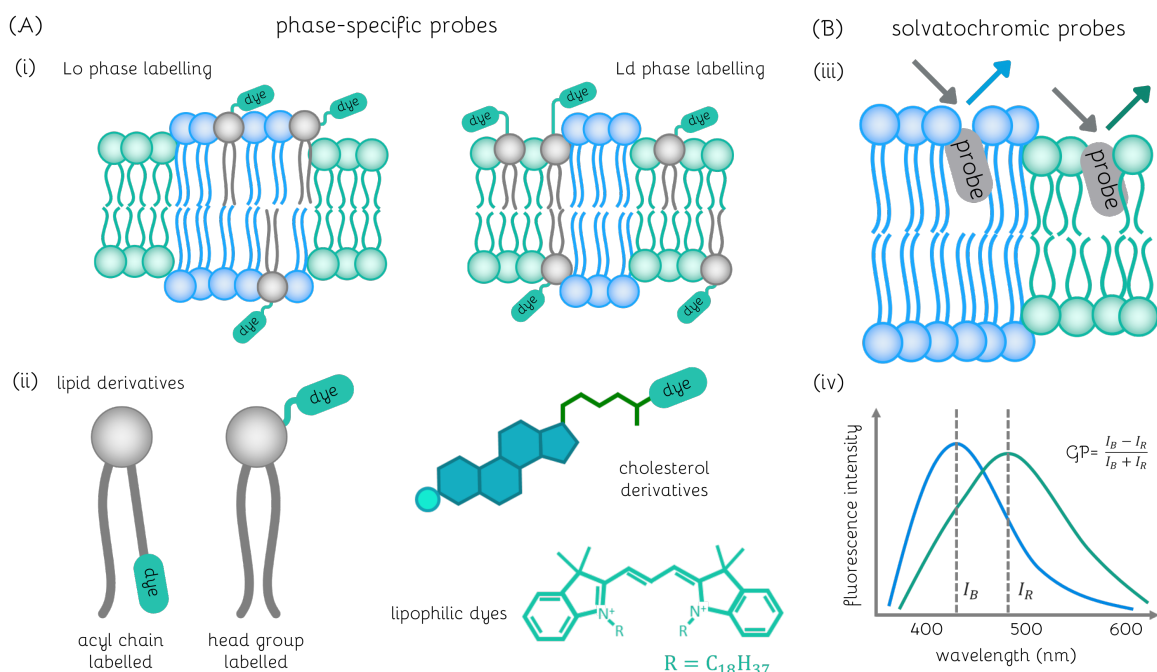


Figure 4.3: Two main classes of the membrane probes: (A) Phase specific probes: (i) schematic representation of the probes selectively incorporating within different membrane phases, (ii) representative classes of the phase specific membrane probes, (B) Solvatochromic probes: (iii) schematic representation of probe incorporation within membrane; probe binds to both membrane phases, (iv) emission spectrum for L_o (blue) and L_d (green) phases; GP value can be calculated from the emission maxima for both phases following the depicted formula.

4.2.2 Solvatochromic probes

Solvatochromic or environment-sensitive probes show affinity to L_o and L_d phases of the membrane and due to the changes in polarity of the surrounding environment, their emission spectrum shifts towards shorter (blue) or longer (red) wavelengths (see Figure

4.3 B). Thus, they provide information about a variety of membrane properties such as fluidity, viscosity, packing, and local hydration state. The high heterogeneity of the membrane is expressed in the form of different membrane phases: gel (L_β), ordered (L_o), and fluid (L_d , L_α). Gel and ordered phases are characterized by higher packing of constituent lipids, lower hydration, and increased viscosity compared to the fluid-disordered phases. The commonly used solvatochromic probes: Laurdan [161], Prodan [162], and di-ANEPPQ [163], show a significant red shift of the emission spectrum during the transition of the membrane from the gel/ordered to the fluid state. Despite the qualitative assessment of the membrane fluidity with these environment-sensitive probes, it is also possible to determine its degree of order using a quantitative parameter called generalized polarization (GP), which for Laurdan probe is defined as follows (4.2):

$$GP_{Laurdan} = \frac{I_{440} - I_{490}}{I_{440} + I_{490}} \quad (4.2)$$

where I_{440} and I_{490} are defined as the emission intensities at the wavelengths 440 nm (corresponding to the peak of characteristic for L_o phase) and 490 nm (intensity peak for L_d phase), respectively.

It should be noted that the wavelengths corresponding to the intensity peaks maxima can vary depending on the type of used solvatochromic probe, however, the general formula remains the same (4.3), where the peak at the shorter wavelength (I_B) corresponds to the more ordered phase, while the intensity maximum at longer wavelengths (I_R) is ascribed to the gel or ordered phase (Figure 4.3 A):

$$GP = \frac{I_B - I_R}{I_B + I_R} \quad (4.3)$$

The theoretical GP values vary from -1 to 1, where two extremes are ascribed to liquid disordered and gel phase, respectively. Experimentally values for the liquid phase range between 0.3 to -0.3, and for the gel phase, they oscillate at around 0.5-0.6 [164]. The differences in GP values can be calculated not only for model cell membranes but have been also successfully applied for determining membrane heterogeneities and local changes in membrane fluidity in bacteria [165], live cells [166], or zebrafish embryos [167].

The mechanism standing behind the phase dependent emission spectrum of Laurdan is the dipolar relaxation of molecular moieties surrounding Laurdan particle. The spectral shift occurs as a result of mutual interactions between the excited state dipole of the Laurdan probe and the dipoles of the surrounding solvent molecules. The molecular structure of Laurdan can be divided into two parts: the lauric acid acyl chain, which incorporates between lipids acyl chains, and the aromatic naphthalene ring, which is localized at the hydrophilic/hydrophobic interface of the lipid bilayer [168]. The dipole-carrying water molecules surrounding the naphthalene part of the Laurdan undergo relaxation. The rotational times of water dipoles are comparable to the fluorescence lifetime of Laurdan, which hence reports about the polarity of the surrounding environment [169]. The blue shift of the Laurdan's emission, inherently connected with lack of solvent relaxation points towards low water content in the local environment. These conditions are characteristic for L_o phase, where tightly packed, saturated lipids expel water from the headgroup region of the lipid membrane. In the more loosely packed L_d phase water molecules have more space to intercalate between lipid headgroups. The Laurdan's excited state dipole

moment is affected by the relaxation of this large population of water molecules [170]. The excited state energy of the probe is partially used to reorient the water dipoles, resulting in a shift of its emission towards longer wavelengths [171].

4.3 Atomic force microscopy

"There's plenty of room at the bottom³."

Richard Feynman

Atomic force microscopy (AFM) is a type of scanning probe microscopy, that provides information about the surface topography with subnanometer resolution. It was first presented in 1985 by Gerd Binnig and Heinrich Rohrer as an alternative technique to scanning tunneling microscope (STM) [172]. The atomic level resolution of STM opened up new possibilities for obtaining information about the shape, size, and organization of molecules [173]. However, Binnig and Rohrer quickly noticed that its use was limited only to the conductive samples and because of the vacuum conditions maintained during measurements, its applications were restricted to very specific types of specimens. AFM was a technique developed to overcome the shortcomings of its predecessor. It expanded the application of scanning probe microscopy into new areas of research such as the study of soft, non-conductive materials (e.g. polymers), thin films, coatings, and biological samples (e.g. proteins, tissues, cells).

The AFM is based on the use of a cantilever ended with a very sharp probe with a nanometer radius, which scans the surface of the specimen (see Figure 4.4 A) [174]. Cantilevers and probes come in different shapes, depending on the medium used for imaging and the type of sample. The most common cantilevers are triangular V-shaped or rectangular, while probes have a pyramidal or conical shape. When the tip is in proximity to the surface, the attractive (van der Waals, electrostatic, and chemical interactions [175]) and repulsive forces (Pauli repulsion and electron-electron Coulomb interactions [176]) between the tip and the measured sample lead to the deflection of the cantilever (see Figure 4.4. B). The cantilever deflection is then converted into an electrical signal, whose intensity is proportional to the deflection, and thus to the topography of the sample. The variety of scanning modes (contact, non-contact, tapping, quantitative imaging - QI) makes this technique a versatile tool for addressing a wide range of samples from very rigid metallic surfaces to extremely soft biological samples such as cells or membranes, in both air and liquid environments. In biomembrane research, AFM provides information about the overall bilayer thickness, height mismatch between different phases, and their potential changes with e.g. hydration level. Based on the overall bilayer thickness and the hydrophobic mismatch it is possible to calculate the line tension at the phase boundary, which is known to be one of the main factors leading to the phase separation in biological cell membranes.

³"There's Plenty of Room at the Bottom – An Invitation to Enter a New Field of Physics" was the title of a lecture given by physicist Richard Feynman at the American Physical Society meeting at Caltech in 1959. Prof. Feynman predicted that soon we will be able to not only observe molecules at the atomic level but also to induce their rearrangement and design specific molecular-level assemblies.

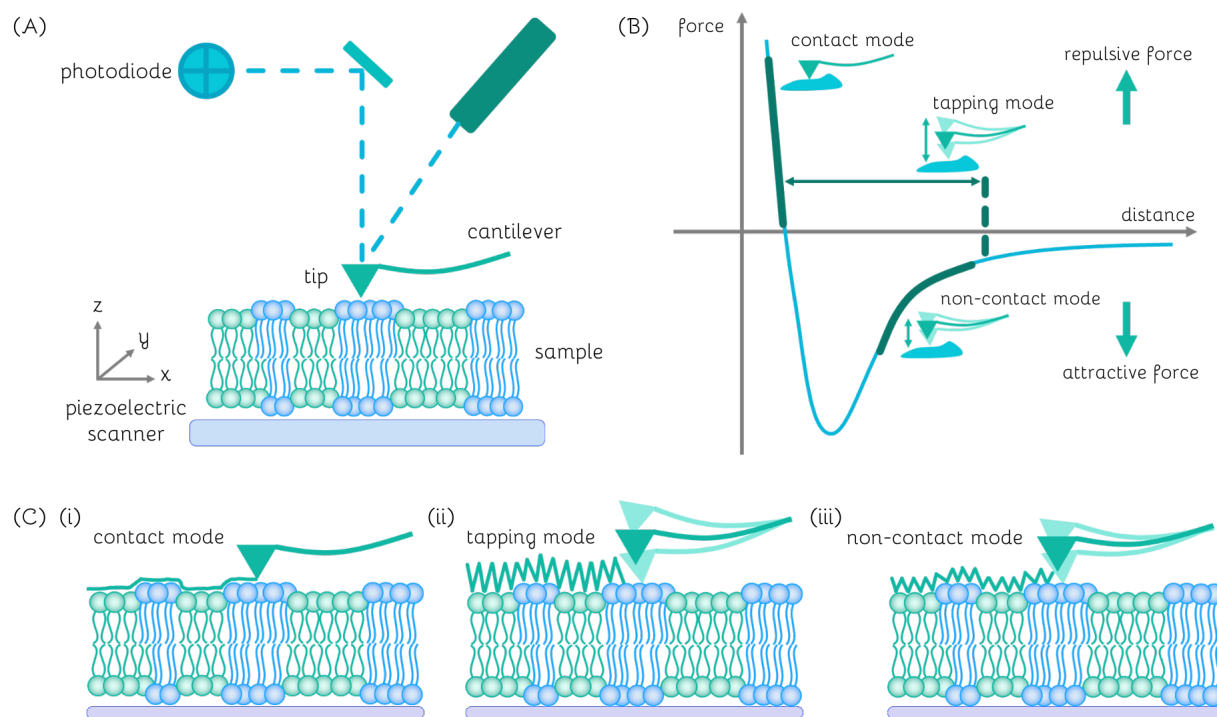


Figure 4.4: Schematic representation of: (A) Basic AFM setup, (B) Force regimes for different operating modes, (C) Most common AFM working modes: (i) contact mode, (ii) tapping mode, (iii) non-contact mode.

4.3.1 Imaging modes

In the *static* or *contact mode*, the probe remains in constant contact with the surface of the scanned sample as depicted in Figure 4.4 C(i). Two variants of this mode can be used; constant force and variable force. In the constant force mode, the deflection and consequently force of the cantilever are maintained by the feedback mechanism over the scanning trajectory. When encountering the protruding surface feature, the cantilever is deflected in the z -direction, and the differences in z -height are recorded as a function of x, y positions, to create a 3D map of the surface topography. Variable force imaging does not use the feedback mechanism, keeping the height of the cantilever always at a constant position. Although variable force imaging has its limitations and is best suited to scanning flat samples with subtle (low) surface features, it offers superior resolution compared to constant force mode. Contact mode can be applied for relatively hard and smooth samples. While contact mode is relatively easy to operate, and can be performed even by less experienced researchers, it has many disadvantages. Due to the constant contact with the sample, the tip can destroy and drag parts of soft, fragile surfaces such as biological specimens when too much force is applied. In this case, parts of the sample accumulate on the surface of the probe, leading to decreased imaging resolution and faster wear of the scanning tip. When the applied force is too high it can deform the sample, and as a consequence, the obtained height differences between particular surface features may become underestimated.

Biological samples such as cells, tissues, proteins, and membranes are very soft and fragile. Their imaging is usually done using an alternative scanning approach - *inter-*

mittent contact (tapping) mode [177]. In contrast to the contact mode, the tip touches the surface only intermittently during scanning, generally oscillating slightly above it at a frequency close to its resonance frequency (see Figure 4.4 C(ii)). As the tip scans the sample, it moves up and down, only intermittently making direct contact with the sample. When the cantilever encounters protruding features of the surface, its oscillatory amplitude changes. The feedback mechanism changes the z-height of the cantilever, in order to maintain the amplitude at the constant value. This tip-sample distance is recorded as a function of x,y position, which then can be used to reconstruct a 3D map of the surface topography. The main advantage of the tapping mode is its minimum-damage character, which makes it a versatile mode of operation for scanning a variety of soft, biological samples. Lateral forces and friction are significantly decreased, leading to better resolution and wear resistance of the tip.

Non-contact mode operates on a similar basis as tapping mode; the cantilever is also set into vibration but in this case, as shown in Figure 4.4 C(iii) the amplitude of resonance frequency oscillations is much smaller [178]. As the probe approaches the sample surface, van der Waals and electrostatic interactions occur between atoms in the probe and the sample, leading to a shift in the frequency of the cantilever oscillations. This phase shift is used to reposition the cantilever in the z-direction to keep it above the surface. In the non-contact mode, the tip does not come into direct contact with the scanned sample, which makes it a non-destructive method of imaging, widely used for the imaging of biological specimens.

4.3.2 AFM as a tool for line tension determination

The interplay of lipid-lipid and lipid-protein interactions leads to the specific lateral organization of lipid membranes both in vivo and in vitro [179]. All of these interactions are mediated by the water, which is the main driving force for the structural rearrangement of lipids, conformation and folding of transmembrane proteins, and formation of phase separation [180]. Different heights of membrane components lead to the formation of height mismatch between lipid and protein entities. Exposure of lipid tails or hydrophobic parts of the proteins to the aqueous environment is energetically unfavorable. As a consequence in order to minimize contact with water, lipids tend to phase separate, while proteins are forced to adopt certain conformations within the membrane structure.

Based on the fluorescence microscopy, it can be easily observed that membranes composed of ternary lipid mixtures containing PC, SM, and cholesterol tend to phase separate, where more saturated SM and cholesterol form domains within the sea of unsaturated PC. AFM and X-ray scattering studies consistently show that the L_o phase, characterized by the unsaturation of constituent lipids and their dense packing, typically exhibits a higher thickness than the L_d phase, which contains more loosely packed and unsaturated lipids. This “height mismatch” or “hydrophobic mismatch” leads to the formation of line tension at the boundary of two phases, which as a consequence promotes the formation of bigger and more round domains [34] as shown in Figure 4.5 A, B.

The transition between L_o and L_d phases is never a sharp step, which would lead to the exposure of hydrophobic tails to the aqueous environment (see Figure 4.5 C). As shown in Figure 4.5 D, in order to minimize the hydrophobic surface, lipids from the monolayer deform at the boundary. We can distinguish three lipid deformations:

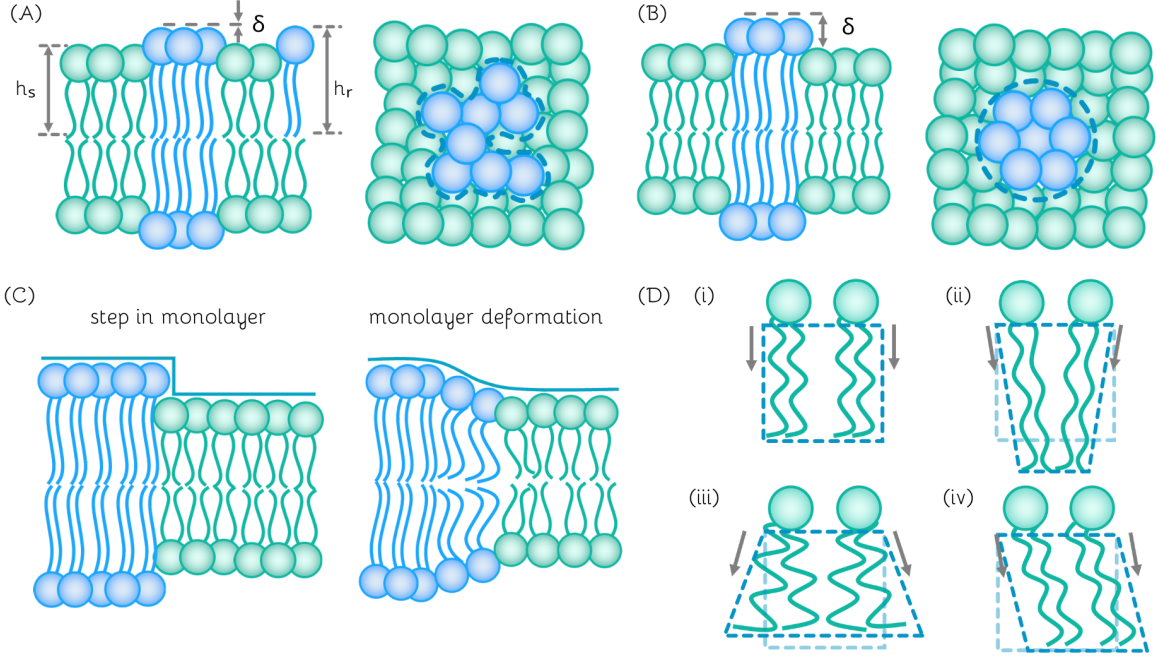


Figure 4.5: Schematic representation of: (A) Phase-separated lipid membrane, where height mismatch (δ) between phases is low, leading to low values of line tension (γ). Domains of L_o phase have an irregular shape, with low circularity. (B) Phase-separated lipid membrane, where height mismatch (δ) between phases is high, leading to high values of line tension (γ). In this case, domains of L_o phase are circular. (C) Raft boundary: step in monolayer leads to exposure of hydrophobic tails to the aqueous medium, while deformation at the boundary of phases decreases the exposed hydrophobic surface. (D) Possible deformations of monolayer: (i) undisturbed monolayer, (ii) monolayer with negative splay, (iii) monolayer with positive splay, (iv) tilted monolayer. The monolayer thickness is changed only by splay, whereas tilt does not affect this parameter. The volume per lipid stays constant regardless of the considered deformation.

splay (bending), tilt, and area compression, all of them can occur simultaneously or in different combinations. When lipids tilt, the area per lipid and monolayer thickness remain constant, to keep the overall volume the same, lipids acyl chains have to elongate. Contrary, splay influences the overall monolayer thickness. To maintain the volume, chains can behave in two ways; they either elongate during approaching each other (negative splay) or they shorten if they deviate from each other (positive splay). Negative splay leads to increased monolayer thickness, while the positive splay causes compression of the monolayer. In both cases, the area per lipid has to change, to keep the overall volume constant.

Cohen et al. developed theoretical model for calculation of line tension (4.4), which is correlated with the height mismatch between L_o and L_d phase [181].

$$\gamma = \frac{\sqrt{B_s K_s B_r K_r}}{\sqrt{B_r K_r} + \sqrt{B_s K_s}} \cdot \frac{\delta^2}{h_o^2} - \frac{1}{2} \cdot \frac{(J_s B_s - J_r B_r)^2}{\sqrt{B_r K_r} + \sqrt{B_s K_s}} \quad (4.4)$$

where γ is the line tension, δ is the phase height mismatch, h_o is the monolayer thickness, B is the elastic splay modulus, K is the tilt modulus and J is the spontaneous curvature

of the monolayer.

In case of "soft domains" B, K, and J take the following values: $B_r = B_s = 10kT$, $K_r = K_s = 40 \frac{mN}{m}$, and $J_r = J_s = 0$, where K_r , J_r , and B_r are parameters describing "rigid" domains, while K_s , J_s , and B_s apply to "soft" domains [34]. In the equation 4.4 the effective thickness of e.g. DMoPC bilayer measured at fully hydrated conditions is $3.86 \pm 0.02 \text{ nm}$ [182]. The values of height mismatch can be directly obtained from AFM measurements with a precision of 0.1 nm.

The monolayer thickness (4.5) is defined as an average thickness of L_d (h_s) and L_o phase (h_r) monolayers.

$$h_o = \frac{(h_r + h_s)}{2} \quad (4.5)$$

Modifying the disordered phase by using phosphatidylcholines of different acyl chain lengths leads to a bigger height difference between L_o and L_d lipid phases. Change of the number of carbon atoms in the acyl chain from 22 to 14, corresponding to the increase of height mismatch from 0.17 nm to 1.56 nm, led to the increase of line tension from 0.06 to 6 pN respectively and consequently, the formation of more round and bigger domains of L_o phase [34].

4.4 Fluorescence recovery after photobleaching

"Life is movement. Once you stop moving, you're dead."

Eugen Sandow⁴

Fluorescence recovery after photobleaching (FRAP) is a microscopy-based technique used to determine the mobility of fluorescently labeled molecules within living cells and model cell systems. FRAP is based on the photobleaching phenomenon in which the fluorescence intensity of the fluorophore or intrinsically fluorescent molecule decreases over time during its constant exposure to laser light. When exposed to high-intensity light, fluorescent molecules undergo irreversible photo-induced chemical damage, resulting in the cleavage of covalent bonds. These irreversible chemical alterations in the molecule ultimately result in permanent loss of its ability to fluoresce. When a population of molecules, each with a single lifetime τ is exposed to constant light absorption, its fluorescence intensity (I) will decrease over time in an exponential manner according to the following equation (4.6):

$$I(t) = I_0 e^{-\frac{t}{\tau}} \quad (4.6)$$

where I_0 is defined as the initial fluorescence intensity at the time t . The fluorescence lifetime τ is determined as the time required for the intensity to decrease to $1/e$, which equals to approximately 0.368 of its initial value.

Generally photobleaching is considered problematic in standard imaging, especially when the sample has to be monitored for a prolonged time and exposed to multiple illumination events, which cause gradual degradation of the fluorophore intensity and decreased signal-to-noise ratio. Contrary, FRAP relies on the permanent loss of fluorescence

⁴Eugen Sandow (April 2, 1867 – October 14, 1925) – a German bodybuilder and showman from Prussia.

in the molecules localized in the photobleached region of interest (ROI) [183].

A typical FRAP experiment can be divided into 3 main steps as shown in Figure 4.6 A [184]:

- Pre-bleaching – few images are obtained before bleaching, the acquisition is performed to record 3-10 frames to obtain the intensity of the analyzed fluorophore before the bleaching (Figure 4.6 A, panel i). The laser power at this stage is adjusted to minimize the photobleaching of the dye.
- Bleaching – a selected region of interest (ROI), which can be a circular spot or fringe pattern, is exposed to the high-intensity laser pulse to “switch off” localized there dye molecules (Figure 4.6 A, panel ii). The bleaching time should not exceed a tenth of time to half intensity recovery to prevent the diffusion of the molecules from the ROI vicinity, within the bleaching time.
- Recovery - the images are obtained after the bleaching (Figure 4.6 A, panel iii). The acquisition parameters are kept the same as for “pre-bleaching” phase to minimize the bleaching. The images are recorded until the intensity within ROI reaches plateau (Figure 4.6 A, panel iv), which typically requires 10-50 times longer time than the half time to full recovery.

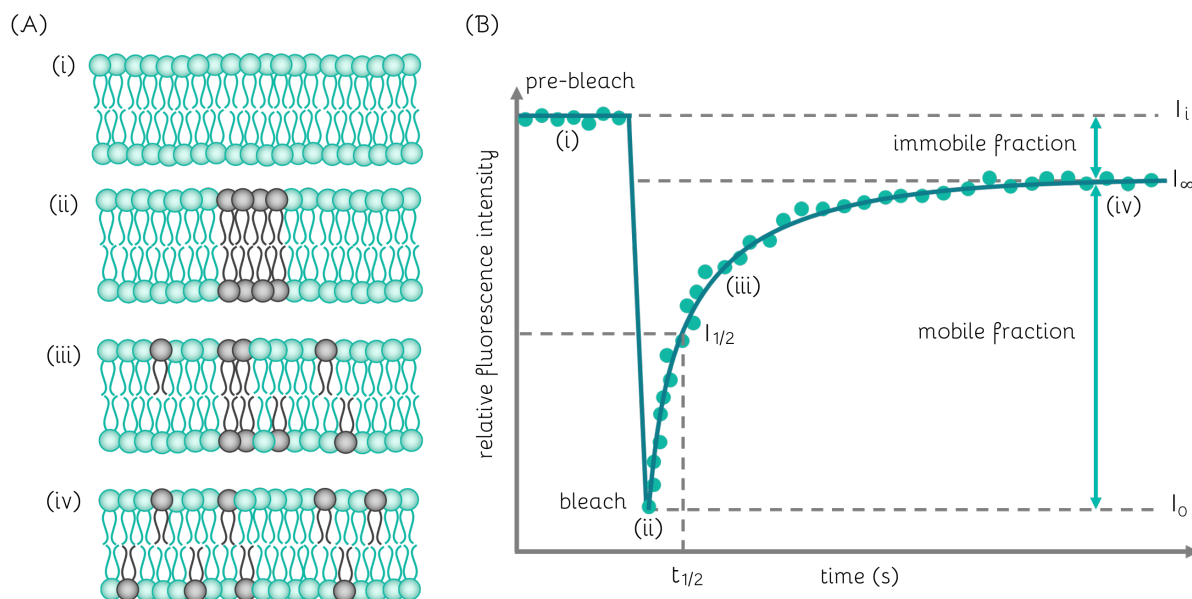


Figure 4.6: Schematic representation of the FRAP principle: (A) Distribution of bleached and unbleached fluorophores in SLB during FRAP experiment: (i) before photobleaching, (ii) immediately after photobleaching, (iii) few seconds after photobleaching (fluorescence recovery), (iv) after fluorescence recovery, (B) a typical FRAP trace, $t_{1/2}$ is defined as the half-time of recovery.

FRAP curve provides various parameters that overall build a comprehensive picture of the dynamics of diffusing molecules. The half-time of recovery ($t_{1/2}$) is defined as the time when the value of intensity after photobleaching reaches half of the final recovered

intensity (plateau region) [185]. This parameter can be extracted directly from the FRAP curve without applying any fitting or mathematical modeling. However, half-time of recovery is very sensitive to the user-defined experimental parameters such as the size of the bleached spot or intrinsic properties of the molecule (e.g. its dynamics). This makes ($t_{1/2}$) an empirical indicator of the recovery rate, which cannot be directly used to compare the movement of different diffusing molecules. The quantitative determination of the molecules' movement can be done by calculating the diffusion coefficient (D), which can be obtained by fitting the fluorescence recovery curve following, for instance, the modified Soumpasis formula ([186]):

$$f(t) = ae^{\frac{2\tau_D}{t}} \left[J_0 \left(\frac{2\tau_D}{t} \right) + J_1 \left(\frac{2\tau_D}{t} \right) \right] + b \quad (4.7)$$

where a is an amplitude of the fitted recovery curve, b is the fluorescence remaining after photobleaching, J_0 is a Bessel function of 0th order, J_1 is a Bessel function of 1st order.

The diffusion coefficient of a freely moving molecule is obtained from the following equation (4.8):

$$D = \frac{\omega^2}{4\tau_D} \quad (4.8)$$

where τ_D is the characteristic time constant extracted from the mathematical fitting of the FRAP curve and ω is a bleach area radius.

Another important parameter is the mobile fraction (MF), which informs about the percentage of molecules that are freely diffusing [185]. It is defined as the ratio of the characteristic intensities obtained before, during, and after photobleaching (4.9):

$$MF = \frac{I_\infty - I_0}{I_i - I_0} \quad (4.9)$$

where I_i is the initial intensity of the bleached spot recorded before the photobleaching, I_0 is the intensity within the bleached spot, immediately after photobleaching and I_∞ is the intensity of the bleached spot after an infinite time (maximal plateau value).

The fraction of molecules that cannot migrate freely between bleached and nonbleached regions is called the immobile fraction (IMF) and is defined as (4.10):

$$IMF = 1 - MF \quad (4.10)$$

It should be noted that FRAP can be very invasive type of technique, especially for living cells. It requires the introduction of fluorescently labeled molecules, which do not always reflect the behavior of native molecules within the cell. The strong laser pulse used for bleaching can cause local damage to the cell structure and perturb its proper functioning [187]. It should be noted that FRAP provides information about the diffusion of the population of molecules, assuming the homogeneity of the measured sample, and cannot distinguish the potential diffusion heterogeneity which is characteristic of biological samples such as cells or tissues. Moreover, the fitting of FRAP curves for slowly diffusing molecules is very challenging and their speed of movement can be recorded only if the diffusion coefficient is faster than $0.1 \mu m^2/s$. Despite these limitations, FRAP

inevitably is a very useful technique that provides information about the lateral movement of fluorescently labeled molecules within both model cell systems and living cells. It can be carried out on most confocal microscopes that allow the selection of ROI and its exposure to high laser power in order to induce local bleaching in this region. The measurement procedure and data analysis in FRAP are easier than in other commonly used techniques for diffusion determination (e.g. FCS or SPT) thus making it a very useful tool for the estimation of molecules' dynamics even for less experienced users.

4.5 Dynamic light scattering

"Colors come from a phenomenon called scattering. The wavelengths of light and the size of the particles determine the colors."

Francine Sandra Rivers⁵

Dynamic light scattering (DLS) also known as photon correlation spectroscopy is a technique commonly used to determine the size of particles such as vesicles, polymers, nanoparticles or proteins ranging from below 1 nm up to a few micrometers in diameter. In 1827 the Scottish botanist Robert Brown described the random motion of *Clarkia pulchella* pollens suspended in water, which nowadays is known as the Brownian motion [188]. This random movement of particles in solution forms the fundamental basis for DLS measurements. Particles following the Brownian motion are subject to constant collisions with solvent molecules, which results in energy transfer and further movement [189]. This intermolecular energy exchange remains relatively constant but exerts a more pronounced influence on smaller particles, causing them to move at higher speeds compared to larger ones. This relation between the speed of movement of the particles defined as the translational diffusion coefficient D , and their size is described by the Stokes-Einstein equation (4.11).

$$D = \frac{k_B T}{6\pi\eta R_H} \quad (4.11)$$

where D is defined as the translational diffusion coefficient, k_B is Boltzmann constant, T is temperature, η is viscosity, and R_H is a hydrodynamic radius.

In order to perform DLS measurement nanoparticles have to be dispersed in a liquid medium and placed in a transparent cuvette. The sample is then illuminated by a single-frequency laser beam, which upon reaching the particles, gets scattered in all directions. The scattered light is further detected by the fast photon detector over a specified time period in order to determine the movement of the suspended nanoparticles. Due to the random movement of the particles, the intensity of the scattered light fluctuates and the rate of this fluctuation is strongly dependent on the particles' size [190]. Larger particles are characterized by a slower movement which leads to lower fluctuations of the light intensity than observed for smaller particles (Figure 4.7 A). In contrast, particles of smaller size move faster, but the detected amplitudes of the scattered light intensities, expressed as the difference between the maximum and minimum light intensity, are much lower (Figure 4.7 B) [190]. The obtained trace, presenting intensity over a certain period of time, is further processed to create the correlation function describing for how long a

⁵Francine Sandra Rivers (born 1947) – an American novelist.

single particle stays in the same spot within the sample. For very short time intervals the particle is essentially in the same spot as the moment before, which results in the constant correlation function. When the particle starts moving and its position is different from the original localization, the correlation function decreases exponentially. The correlation function is again a straight line at the moment when the initial position of the particle and its localization after a certain time do not show any similarity. This second constant region of the correlation function is defined as a baseline. The time needed for the particle to change its initial position is represented in the decay of the correlation function. Smaller particles are characterized by very fast movement and rapid change of the localization, which is expressed as sharp decay. On the contrary, larger particles change their position at a slower pace, leading to slower decline of the correlation function.

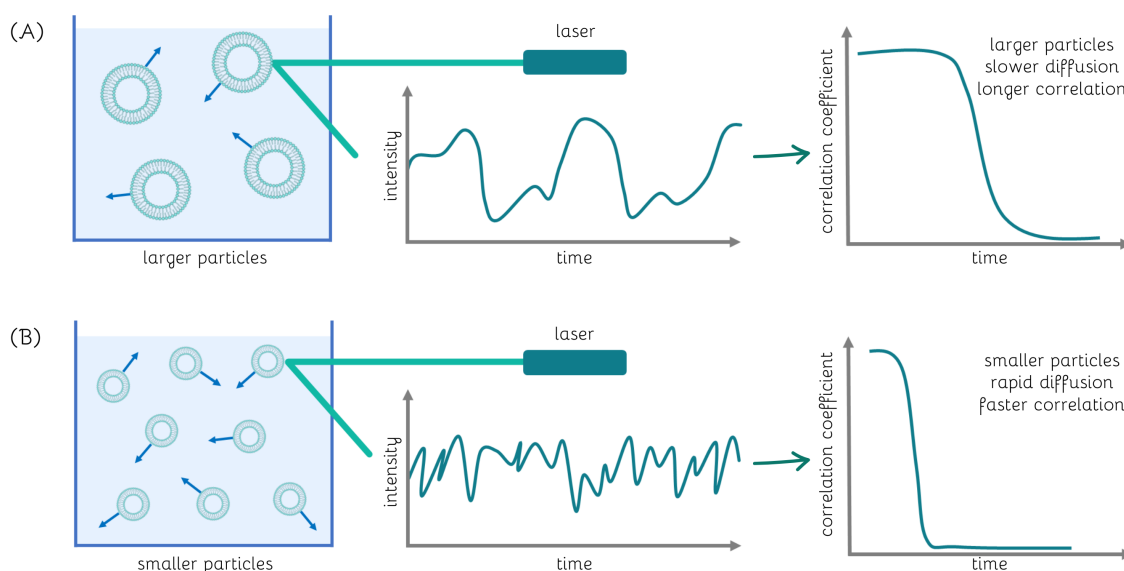


Figure 4.7: Schematic representation of the DLS principle: smaller particles are characterized by faster movement, which causes more rapid fluctuations of the light intensity than observed for larger particles. The correlation function, which is based on the intensity change is used to describe how long a single particle stays in the same spot within the sample. Smaller particles are characterized by sharp decay of the correlation function, while larger particles show delayed decline of the correlation function.

It should be noted that in order to obtain reliable and repeatable results of particle size using DLS several essential considerations should be taken into account:

- Particles should be suspended in a transparent fluid.
- The movement of the particles has to be based on Brownian motion.
- Particles should be stable and do not sediment over the course of measurements.
- The sample has to be homogenous in size, larger aggregates significantly influence the final results (light scattering depends on the 6th power of the particle size, $I \propto d^6$).

- The final intensity signal obtained from DLS depends not only on the particles' size but also on their concentration, thus proper optimization might be required.
- DLS measurements are very sensitive to the temperature variations and viscosity of the dispersing medium, both parameters influence the particles' movement speed.

DLS technique is based on indirect measurement of the particle size, which is obtained based on their movement. In general, each sample contains particles of a wide range of sizes and the width of this particle size distribution is described by the polydispersity index (PDI). Values of PDI below 5 % indicate that the sample is monodispersed in size, meaning that most of the particles have similar size [191]. However, in order to obtain information about the whole population of polydisperse samples in many cases it is required to analyze the particle size distribution chart which provides more meaningful data about the character of the measured particles. DLS can be used to determine the size of vesicles, and monitor alterations induced by variations in pH, temperature, or the introduction of other molecules [192]. It can detect the aggregation of vesicles or fusion events, both of which result in an increase of liposome size. To summarize, DLS technique has a lot of requirements regarding the sample's preparation and data validation, however, it is still a very powerful tool for fast measurements of particles' size in the nano- and even microscale.

4.6 Zeta potential measurements

"Protons give an atom its identity, electrons its personality."

Bill Bryson⁶

When a solid particle, liquid droplet, or porous body is dispersed in a liquid, a thin layer of ions is deposited on its surface as shown in Figure 4.8 A. The formed layer is known as Stern layer and contains ions of the opposite charge to the charge of the particle's surface. When moving further from the particle's surface, the more loosely connected ions of the opposite charge to the surface form the double layer. These counterions move together with the particle due to the Brownian motion or as a result of the sedimentation process. At the slipping plane, ions are no longer associated with the particle, and the voltage recorded at the edge of this plane is called the zeta potential. Finally, when the distance from the particle's surface is further increased, the surface potential decreases until the moment when its value reaches zero.

Zeta potential provides information about the stability of the analyzed particles suspended in aqueous solution. Particles with a large positive or negative net surface charge do not agglomerate due to the strong repulsion force occurring between them. The suspension is considered stable when zeta potential of the measured particles is higher than 30 mV or lower than -30 mV [193]. When the absolute value of zeta potential is $|\zeta| < 30 \text{ mV}$, the particles tend to form aggregates and sediment, which is a qualitative indicator of the unstable suspension.

Zeta potential can be calculated from the electrophoretic mobility, which is defined by Henry equation (4.12) [194]:

⁶Bill Bryson (born December 8, 1951) – an American–British journalist and author of scientific books.

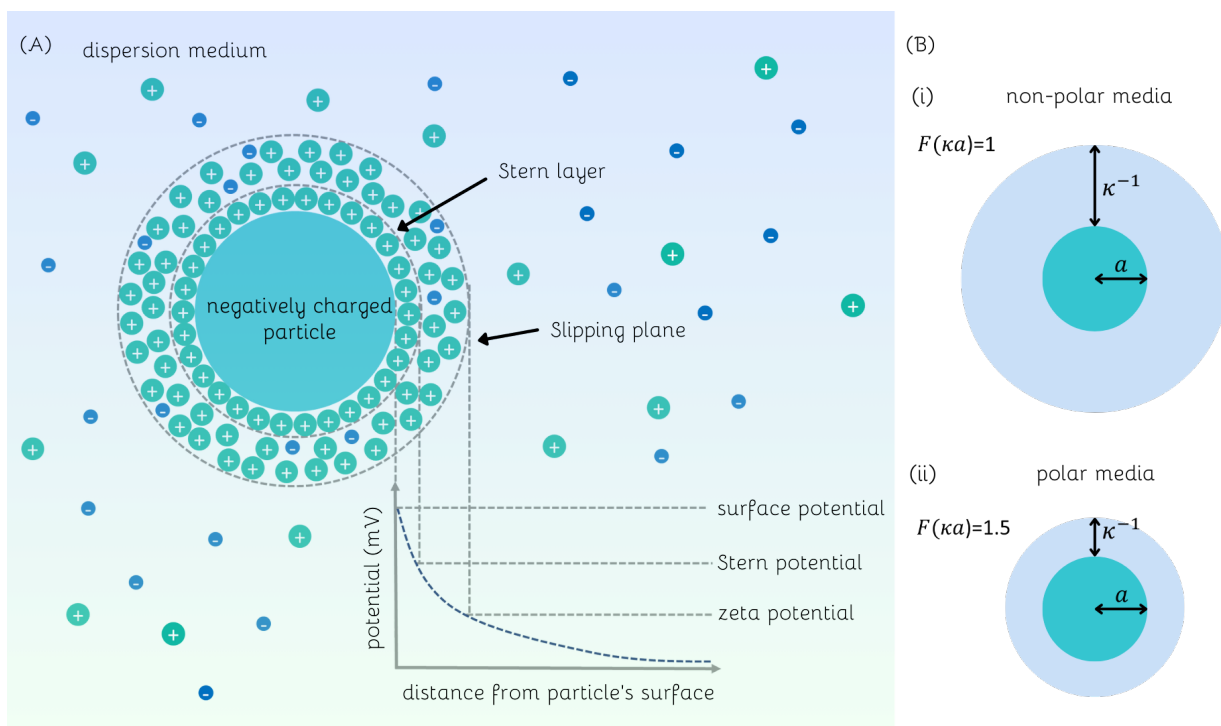


Figure 4.8: Schematic representation of: (A) the ionic concentration and potential difference as a function of distance from the particle's surface, (B) Huckel (i) and Smoluchowski's (ii) approximations used for simplification of Henry's function.

$$U_E = \frac{2\epsilon\zeta F(\kappa a)}{3\eta} \quad (4.12)$$

where U_E is the electrophoretic mobility, ζ is the zeta potential, ϵ is the solvent dielectric permittivity or solvent dielectric constant, η is the viscosity of the solvent, and $F(\kappa a)$ is the Henry's function.

The reciprocal of κ in Henry's function is called the Debye length, which is the distance calculated from the surface of the charged particle over which the charge of the particle is screened by the freely moving ions in the solution. The Debye length is often also defined as the thickness of the electrical double layer, that forms around the charged particle that is suspended in the aqueous solution. It is strongly dependent on the concentration of ions in the solution, meaning that the thickness of the double layer decreases with the increase of the solution's ionic strength. The second variable in Henry's function is the parameter "a", which is defined as the radius of the particle. When the radius of the particle is small compared to the Debye length and the used solution contains low salt concentration (low dielectric constant media such as non-polar solutions), the Henry's function is reduced to Hückel limit $F(\kappa a) = 1$ (see Figure 4.8 B, panel i) [195]. Alternatively, when the thickness of the electrical double layer (κ^{-1}) is relatively small when compared to the particle's radius (a), and the measurements are performed in high salt aqueous buffer, the Henry's function can be approximated to the Smoluchowski limit $F(\kappa a) = 1.5$ (see Figure 4.8 B, panel ii) [196].

The zeta potential is a key parameter used for determining the stability of colloids

and suspensions. It is widely used in the pharmaceutical, food, biomedical, and cosmetic industries where it is employed to assess the stability of drugs, and drug-loaded nanoparticles, monitor properties of food (aggregation or sedimentation processes), or as a tool for the development of stable cosmetic and emulsions. The measurements of zeta potential found their application also in membrane research as a valuable tool for characterizing LUVs, GUVs, or extracellular vesicles, where they can provide information about the vesicle's net charge and vesicle interactions with ions [197] or proteins [198, 199]. The zeta potential has been shown to correlate with the amount of negatively charged lipids (PG or PS) incorporated into the LUVs. For example, as the amount of negatively charged POPG increases, the zeta potential shifts to more negative values [200]. Thus, it can be used as an indirect indicator of the amount of incorporated negatively charged lipids within the bilayer.

Chapter 5

Lateral organization of biomimetic cell membranes in varying pH conditions

Cell membranes are characterized by the presence of local, spatial heterogeneities, which are associated with saturated lipids, cholesterol and very often enriched in proteins. These ordered lipid domains are the binding centers for specific biomolecules such as proteins, where they may undergo folding into specific spatial conformation. The high line tension boundaries between ordered and disordered phase function as preferred binding sites for HIV fusion peptides [21]. Moreover, membrane domains are responsible for various biological processes occurring at the cellular level such as ion-channel regulation, cell signaling, membrane trafficking and they actively participate in catalyzing and mediating the enzymatic reactions [3]. Finally, bacterial products such as toxins not only preferentially bind to raft-like domains but also migrate through these regions to the cell interior [22]. The undeniable significance of these raft-like regions in cellular activity stimulates the ongoing investigations on replicating and controlling local membrane heterogeneities in model membrane systems.

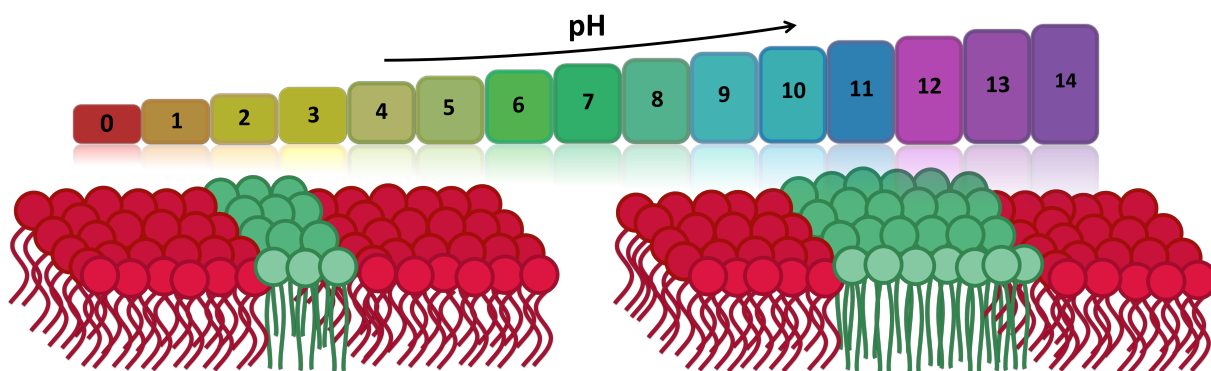


Figure 5.1: Graphical representation of the key findings presented in publication 1. Environmental pH influences the size of L_o phase domains, which opens up new possibilities for influencing the lateral organization of biomimetic cell membranes without changing the dynamics of constituent lipids.

In publication 1, I present how varying the environmental pH influences the formation, dynamics, and stability of phase-separated biomimetic cell membranes (Figure 5.1).

I investigated how domains of the L_o phase change in a broad range of pH 1.7-9.0 and observed an increase in the domain size with increasing pH of the buffer solution hydrating the lipid membrane. At the same time, the measurements of the diffusion coefficient for both ordered and disordered phases revealed that the diffusion remains the same in the whole range of the tested pH. I discovered a clear correlation between the increase of the domain size under increasing pH with the changes of the hydrophobic mismatch between the L_d and L_o phases. Furthermore, I showed that the architecture of the lipid membrane formed in the specific pH remains stable for up to 3 days upon replacement of the aqueous medium with the buffer of neutral pH. Thus the presented here novel approach of shaping the domains of L_o phase can be applied for further studies on interactions between proteins, incorporation of transmembrane channels for the measurements of selective permeability of the membrane, as well as, embedding of pH-sensitive molecules binding specifically to the L_o phase domains.



Lateral organization of biomimetic cell membranes in varying pH conditions



Emilia Krok^{*}, Agnieszka Batura, Madhurima Chattopadhyay, Hanna Orlikowska, Lukasz Piatkowski^{*}

Poznan University of Technology, Faculty of Materials Engineering and Technical Physics, Institute of Physics, Piotrowo 3, 60-965 Poznan, Poland

ARTICLE INFO

Article history:

Received 1 September 2021
Revised 11 October 2021
Accepted 19 October 2021
Available online 22 October 2021

Keywords:

Biomimetic cell membranes
Supported lipid bilayers
pH
Phospholipids
Lipid domains

ABSTRACT

Many studies have been devoted to investigation of phase separation and formation of lipid domains, which play crucial role in many biological processes. Here we present a complex study on the formation, dynamics, and stability of the phase-separated supported lipid membranes under varying pH conditions. The size and distribution of liquid-ordered (L_o) phase domains were investigated in a wide range (1.7–9.0) of buffer pH values and a strong correlation was found between the size of the L_o domains and pH of the buffer hydrating the lipid bilayer. Interestingly, the dynamics of lipids composing both L_o and L_d phase are insensitive to the pH of the buffer. Our findings demonstrate that by varying pH of the environment one can induce formation of domains with a specific size and shape without any external modification of the solid support or altering the membrane composition. Finally, we show that the architecture of the lipid membrane is stable even upon replacement of the aqueous medium with the buffer of neutral pH. Consequently, this method of patterning of L_o phase domains in biomimetic membranes is applicable to the studies involving binding of proteins or incorporation of other pH-sensitive molecules.

© 2021 The Author(s). Published by Elsevier B.V. This is an open access article under the CC BY license (<http://creativecommons.org/licenses/by/4.0/>).

1. Introduction

Biological membranes play a key role in the functioning of the cells. They are responsible for protecting the cell from changing external factors in the process called homeostasis. Moreover, they allow transportation of the ions and molecules such as glucose, amino acids, and lipids inside and outside the cell. The presented by Singer and Nicholson fluid mosaic model [1] is still the most accurate model describing the cell membrane. It proposes that cell membrane is composed of different types of lipids, forming more or less randomly organized fluid, in which there are embedded various components such as cholesterol, proteins, and carbohydrates. Sphingolipids and cholesterol form more organized micro- and nanoscopic domains, that are floating in the sea of phospholipids [2]. Sphingolipids with their long and saturated acyl chains allow the cholesterol to tightly intercalate with them, forming the liquid-ordered (L_o) phase [3]. On the other hand, unsaturated phospholipids are more loosely packed due to the structure of their acyl chains and are forming a liquid disordered (L_d) phase.

The lateral segregation in the membrane and compartmentalization by lipid domains are strongly related to many biological

processes occurring in the body such as protein sorting [4], ion-channel regulation [5,6], signaling [7,8], membrane trafficking [9,10], organization of cytoskeleton [11,12] and pathogen entry [13,14]. Moreover, cholesterol- and sphingomyelin-rich domains are connected with the binding of toxins and their penetration inside the cell, as well as they are suggested to create the microenvironment promoting the prion formation and aggregation of amyloids [15]. The importance of the lipid domains led to the studies on how to manipulate their size and shape and questions as to the relations between size, distribution and the density of the domains with other membrane parameters such as diffusion coefficient or rigidity. So far the membrane structure was altered by changing its composition [16–19], the composition of the aqueous environment [20], the addition of lineactants [21], nucleation and spinodal decomposition processes [22], or applying different temperature and cooling speed during lipid bilayer formation [23].

One of the factors that affect the biological cell membranes is the change of the pH inside the cell as well as in the surrounding environment. The variations in the concentration of H^+ and OH^- ions, that occur outside the cell are responsible for the functioning of the cell, regulating its mobility [24,25] and deformation [26,27]. The internal changes of pH in the cells take part in the signaling mechanism of many cellular processes such as regulation of the cell cycle [28], proliferation [29], differentiation [30], and cell apoptosis [31]. The patterning of pH occurring within the cell plays

^{*} Corresponding author.

E-mail addresses: emilia.krok@put.poznan.pl (E. Krok), lukasz.j.piatkowski@put.poznan.pl (L. Piatkowski).

<https://doi.org/10.1016/j.molliq.2021.117907>

0167-7322/© 2021 The Author(s). Published by Elsevier B.V.

This is an open access article under the CC BY license (<http://creativecommons.org/licenses/by/4.0/>).

CHAPTER 5. LATERAL ORGANIZATION OF BIOMIMETIC CELL MEMBRANES IN VARYING PH CONDITIONS

E. Krok, A. Batura, M. Chattopadhyay et al.

Journal of Molecular Liquids 345 (2022) 117907

a key role in the organization of the cytoskeleton [32] and regulates the migration of its components [33]. The abnormal increase in intracellular and decrease in extracellular pH are connected with the mutation of cancer cells and tumor progression [34]. Clearly, the understanding of the influence of pH on biological cell membranes has become of great interest to biophysicists, biologists, and biochemists.

The investigation of lipid membranes in native form is difficult due to the complexity of the living cells as well as all the chemical, biological and physical processes that can alter the studied properties. The changes in the structure and dynamics of lipid membranes upon exposure to different pH conditions were checked so far on the systems such as supported black lipid membranes [35], liposomes [36], or single component supported lipid bilayers (SLBs). However, due to the higher complexity of lipid membranes exhibiting phase separation than those comprised of only one type of lipids, the studies on the behavior of L_o lipid domains under varying pH conditions so far were not addressed in detail.

To understand the behavior of the cell membranes under varying pH conditions we used supported lipid bilayers (SLBs), which mimic well the natural cell membranes [37]. Here we show how phase-separated membranes behave under a wide range of environmental pH 1.7–9.0. We observed that the structure of lipid membranes is extremely sensitive to the changes in pH, with a clear increase of the L_o phase domains size with the increasing pH. At the same time, lipid membranes maintained their full mobility within the whole tested pH range. The formation of domains with specific size occurs on the solid support and results from the changes in the height difference between lipids composing L_o and L_d phase under different pH of the environment. These findings demonstrate that it is possible to prepare membranes with predefined size and shape of lipid domains without any external modification of their composition. The formation of lipid domains with a specific size makes them great platforms for studying the binding of proteins, signal transduction molecules, and incorporation of membrane channels for tracking transport across the membrane.

2. Materials and methods

2.1. Materials

1,2-Dimyristoleoyl-*sn*-glycero-3-phosphocholine (14:1 PC), egg yolk sphingomyelin (SM), and cholesterol were purchased from Avanti Polar Lipids, Alabaster AL, USA. Monosialoganglioside (GM1) from bovine brain and 1,2-Dioleoyl-*sn*-glycero-3-phosphoethanolamine labeled with Atto 633 (DOPE-Atto 633), sodium hydroxide (NaOH), and hydrogen chloride (HCl) were purchased from Merck KGaA, Darmstadt, Germany. N-2-Hydroxyethyl piperazine-N'-2-ethane sulphonic acid (HEPES PUFFERAN[®]) was obtained from Carl Roth GmbH & Co KG, Karlsruhe, Germany. Alexa Fluor 488 conjugated with cholera toxin B subunit (CTxB 488) was obtained from Molecular Probes, Life Technologies, Grand Island, NY, USA. Calcium chloride (CaCl_2) was purchased from CHEMPUR[®], Piekary Slaskie, Poland. Sodium chloride (NaCl) was obtained from P. P.H. STANLAB sp. j., Lublin, Poland. All the materials and reagents were used without further purification. Optical adhesive glue Norland 68 was purchased from Norland Products Inc., Cranbury, NJ, USA. The ultrapure water was obtained by using Milli-Q[®] Reference Water Purification System from Merck KGaA, Darmstadt, Germany.

2.2. Vesicles preparation

The SLBs were prepared by vesicles deposition on the solid support following the formerly established method [38]. In order to

form multilamellar vesicles (MLV), 14:1 PC, SM, and cholesterol in chloroform solution were mixed at the molar ratio 1:1:1 with addition of 0.1 mol% of GM1 and 0.1 mol% of DOPE-Atto 633 dye to form 10 mM solution of the lipids. The lipid mixture was dried under nitrogen gas leaving a thin film of lipids deposited on the bottom of the vial. To confirm the complete evaporation of the organic solvent, the dried lipid mixture was further desiccated in a vacuum-dry chamber for at least 2 h. The lipids were resuspended in the buffer solution (10 mM HEPES and 150 mM NaCl, pH adjusted to 7.4) and exposed to four cycles of heating on the hot plate at 60 °C and vortexing. Each step of heating and vortexing was performed for 1 min. Lipid suspension containing 10 μL of multilamellar vesicles (MLVs) was distributed into new sterilized glass vials. Aliquots were stored at $-20\text{ }^\circ\text{C}$ for further use and consumed within two weeks.

2.3. Vesicles characterization

Vesicles for determination of mean hydrodynamic diameter were prepared using the same composition and the same approach as for the formation of SLBs but with the final concentration of lipids 20 mM. After drying and desiccation, lipids were resuspended in 100 μL of the buffer solution (10 mM HEPES and 150 mM NaCl) with pH adjusted to the final values 2.2, 4.2, 7.2, and 9.0. Each sample was exposed to four cycles of heating on the hot plate at 60 °C and vortexing to produce multilamellar vesicles (MLVs). Subsequently, MLVs suspensions at different pH were exposed to 10 min of sonication to obtain small unilamellar vesicles (SUVs). Lipid suspensions were then diluted in the buffer of specific pH for the final lipids concentration of 0.727 mg/ml. The mean hydrodynamic diameter and polydispersity index (PDI) of the vesicles were determined from dynamic light scattering (DLS) measurements using Zetasizer Nano by Malvern Panalytical, Kassel, Germany. Prior to the measurement lipid suspensions were exposed to the ultrasound water bath for 5 min.

2.4. SLBs preparation

All buffers for SLBs preparation contained 10 mM HEPES and 150 mM NaCl. By using a suitable amount of 0.1 M HCl, pH of buffers was adjusted to the final values of 1.7, 2.2, 3.7, 4.2, 4.7, and 5.2. 0.5 M of NaOH was added to obtain buffers with pH 5.7, 6.2, 6.7, 7.2, 7.7, 8.2, 8.5, and 9.0. The adjustment was done by using pH meter ELMETRON[®] CP-461. Lipid vesicles were diluted 10 times by the addition of the HEPES buffer of the desired pH to obtain the final lipids concentration of 1 mM. Aliquots containing MLVs were bath-sonicated for 10 min at maximum power to generate SUVs. To prepare the solid support for lipids deposition, a thin layer of freshly cleaved mica was glued by UV-activated glue on the glass coverslip. A half-cut Eppendorf tube was placed on the top of the coverslip and sealed with silicone to create a water reservoir. 100 μL of SUVs solution was deposited on top of the mica at room temperature, followed by the addition of 2 μL of 0.1 M CaCl_2 solution and 8 μL of 0.01 mM CTxB 488 and allowed to settle down for 30 s before the consecutive addition of 400 μL of HEPES buffer with the desired pH. The sample was incubated for 30 min and washed by pipetting up and down with an overall of 20 ml of HEPES buffer with the corresponding pH to remove the excess, unburst vesicles. After the final wash, the Eppendorf tube was filled with the same buffer solution, closed with a glass coverslip, and sealed with medical silicone.

2.5. Confocal imaging and FRAP experiments

The confocal imaging and fluorescence recovery after photobleaching (FRAP) experiments were conducted using Zeiss LSM

710 microscope from Carl Zeiss, Jena, Germany with 40× 1.3NA oil immersion objective. Ar laser 488 nm was used for excitation of CTxB-Alexa Fluor 488. The excitation of Atto 633 was done using HeNe laser with the wavelength 633 nm. Emission was recorded at wavelength range 495–530 nm for green light channel (CTxB-Alexa Fluor 488) and 645–797 nm for red light channel (Atto 633 detection). The minimal laser powers were used to minimize photobleaching. For FRAP experiments a circular area with 10 μm diameter was bleached and the fluorescence recovery kinetics were recorded. Diffusion coefficients (D) of lipid molecules were obtained by fitting the fluorescence recovery curve following the modified Soumpasis formula (1) [39].

$$f(t) = a \cdot e^{-\frac{2\tau_D}{t}} \left(I_0\left(\frac{2\tau_D}{t}\right) + I_1\left(\frac{2\tau_D}{t}\right) \right) + b \quad (1)$$

where

$$\tau_D = \frac{w^2}{4D} \quad (2)$$

where a is an amplitude of the fitted recovery curve, b is the fluorescence remaining after photobleaching, w is a bleach area radius, and $I_0(t)$ and $I_1(t)$ are modified Bessel functions.

Fitting was performed for data normalized with respect to the reference intensity signal of the whole image (excluding the bleached area). The mobile fraction for the liquid disordered phase was calculated according to the formula (3).

$$R_{mobile} = \frac{a}{1-b} \quad (3)$$

where a and b parameters were obtained from fitting. The extracted diffusion coefficient (D) was finally averaged from FRAP traces acquired from 10 different areas within the sample of a specific pH. This approach of determining lipids diffusion coefficient was proven widely applicable for hydrated phase-separated membranes [40] as well as for membranes of varying hydration state [41]. In the experiments we choose to excite a spot that is sufficiently large (typically 10 μm) that for all tested pH values we probed diffusivity of lipids subjected to different microenvironments and hence exhibiting different diffusivity (for instance L_o lipids moving within the L_o domains (i), those moving from L_d into L_o phase and vice versa (ii), as well as, L_o lipids moving within the L_d phase (iii)). This way we measured average diffusion coefficient of lipids associated with each of the phases. This is particularly important for the presented experiments as we intended to compare dynamics of lipids solely as a function of changing pH conditions. Choosing smaller area could lead to probing different species of lipids resulting in (potentially additional) variation in diffusion coefficient of lipids between different pH values. To determine the average size of the lipid domains and total area occupied by domains, the original confocal images were converted to black and white binary versions by adjusting the threshold of contrast in the ImageJ software [42]. At least 10 different locations were chosen from 2 different samples of the same pH, for a total of 20 images 50×50 μm each. Circularity was calculated for samples prepared at pH 4.2, 5.7, 7.2, and 9.0 using ImageJ software based on the equation (4).

$$circularity = 4\pi \frac{area}{perimeter^2} \quad (4)$$

Images were converted to black and white binary versions and smoothed, by replacing each pixel with the average of its 3 × 3 neighborhood. At least 12 images, 50 × 50 μm in size from different spots within the same sample were analyzed, each contained 12–330 domains.

3. Results and discussion

3.1. Size of lipid domains as a function of pH

SLBs were prepared from a ternary lipid mixture of 14:1 PC/SM/cholesterol in the molar ratio 1:1:1. This commonly used membrane composition is characterized by phase separation (L_d and L_o), mainly due to the difference in the fatty acid chain length between 14:1 PC and SM [43]. L_d phase is built of shorter phosphatidylcholine and cholesterol, while L_o phase is composed of saturated sphingomyelin, interleaved tightly with cholesterol. The chosen ratio 1:1:1 of 14:1 PC, SM and cholesterol has been quite well characterized in the literature regarding both structure and dynamics [44–46], allowing us to verify consistency of our membranes at neutral conditions with those studied earlier.

For labelling of the L_d phase we used fluorescent lipid, which shows high affinity and specific partitioning to disordered phase. The fluorescent probe is an Atto 633 dye covalently attached to the hydrophilic headgroup of 1,2-dioleoyl-*sn*-glycero-3-phosphoethanolamine (DOPE). Labelling of the L_o phase was done using monosialoganglioside (GM1) – a receptor of the cholera toxin subunit B (CTxB), which partitions specifically in the L_o phase [47]. The imaging of CTxB is possible due to the conjugation of CTxB with Alexa Fluor 488 dye. In general ganglioside GM1 has been shown to partition into both phases but upon binding with CTxB it preferentially localizes in the L_o phase, allowing the visualization of sphingomyelin-rich domains [44].

The confocal images of phase-separated SLBs revealed that there is an extremely strong influence of the environmental pH on the structure of lipid membranes as presented in Fig. 1. As shown in Fig. 1A the domains of L_o phase could not be resolved in the membranes labeled with both dyes and prepared in pH below 3.7. These membranes were visible as a mixture of L_o and L_d phases. As presented in Fig. 1B and C membranes prepared at pH 4.2, and 4.7 had very small domains, while in the pH range 5.7–8.2 L_o phase formed more round, and larger domains. The representative images for pH 6.2 and 7.2 are shown in Fig. 1D and E. At pH 8.5 and 9.0 domains were merging into bigger entities with areas up to tens of μm². Membranes prepared in these conditions contained regions with inverse domains, where L_d phase formed round domains within the L_o phase as it is shown in Figs. 1F and S1. Membranes in the whole tested pH range 1.7 – 9.0 did not show any signs of peeling off from the substrate, formation of holes, or other intrinsic defects.

Membranes containing CTxB protein for labeling did not show significant phase separation at pH below 4. To eliminate the possible impact of denaturation of CTxB protein in pH values below 4 [48], some membranes were prepared without labeling the L_o phase with CTxB-AlexaFluor 488. As shown in Fig. S2 lipid bilayers prepared at pH 2.2 (A) and 3.7 (B) without the addition of CTxB protein contained small, distinguishable domains of L_o phase, which previously were not visible under the fluorescence microscope. CTxB is a 57 kDa pentamer protein [49], which in the folded state binds up to 5 GM1 molecules, that diffuse together. Upon denaturation in pH below 4, this big complex unfolds, exposing a larger surface area with the increased number of binding sites that can hamper many lipid molecules [50]. It is thus feasible that upon denaturation of CTxB the free movement of lipids composing L_o phase and their assembly into domains is hindered. It has to be emphasized that even in harsh acidic conditions lipid bilayer without the addition of CTxB was able to reorganize its structure, which was visible as merging of lipid domains over time as depicted in Fig. S2(C, D).

The increase of the pH in the range of 1.7–9.0 causes an increase in the average domain size. To quantify the observed variation of

CHAPTER 5. LATERAL ORGANIZATION OF BIOMIMETIC CELL MEMBRANES IN VARYING PH CONDITIONS

E. Krok, A. Batura, M. Chattopadhyay et al.

Journal of Molecular Liquids 345 (2022) 117907

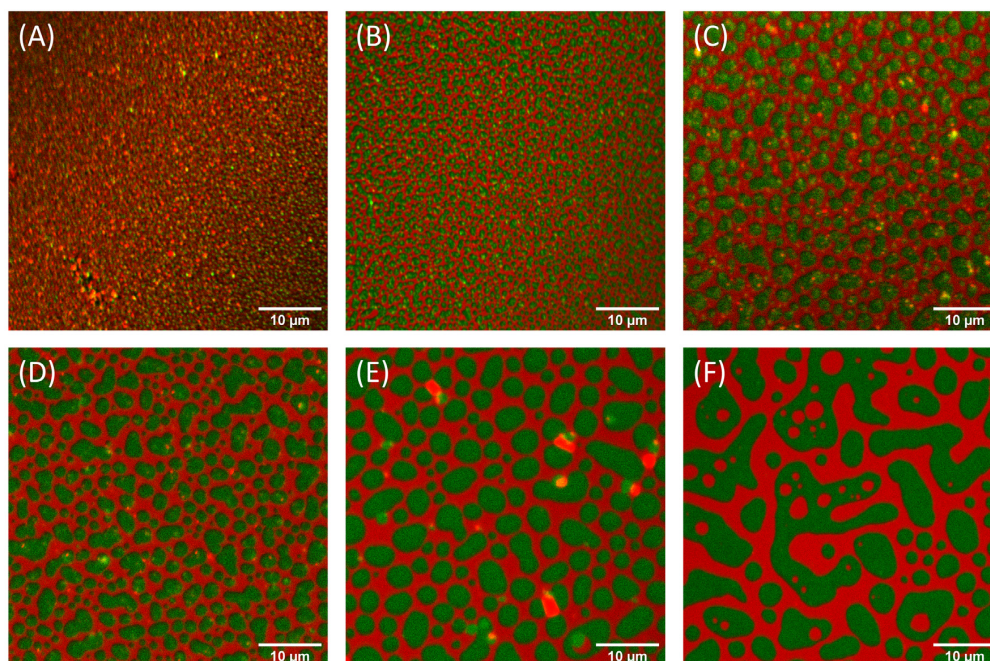


Fig. 1. Fluorescence images of supported lipid bilayers composed of 14:1 PC/SM/cholesterol and formed at pH: (A) 3.7, (B) 4.2, (C) 4.7, (D) 6.2, (E) 7.2, (F) 9.0. L_d phase was labelled with DOPE-Atto 633 (red), complex CTxB – AlexaFluor 488 marks L_0 phase domains (green). The increase of the size of L_0 phase domains is strongly related to the increase in the pH of the environment. (For interpretation of the references to colour in this figure legend, the reader is referred to the web version of this article.)

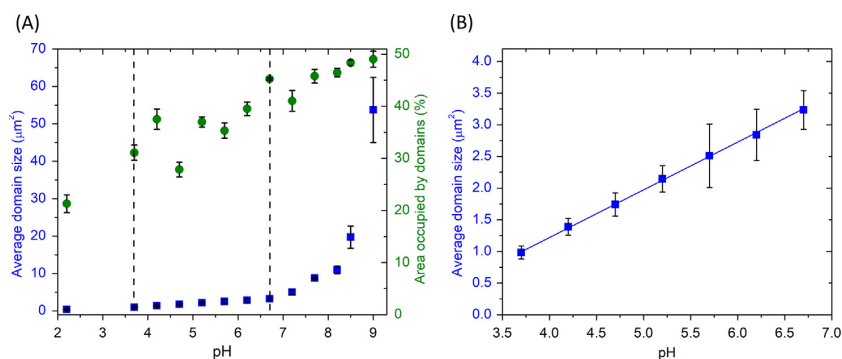


Fig. 2. (A) Average L_0 domain size (marked by blue squares) and area occupied by L_0 domains (green circles) as a function of pH, (B) linear dependence of the average domain size as a function of pH within the pH range 3.7 – 6.7, marked on panel (A) by two vertical, dashed lines. (For interpretation of the references to colour in this figure legend, the reader is referred to the web version of this article.)

domain sizes, lipid membranes were analyzed by using ImageJ. As presented in Fig. 2A the average L_0 phase domain size for lipid bilayers prepared in pH 2.2 was $0.37 \pm 0.13 \mu\text{m}^2$, whereas for near-neutral pH 7.2 it was $5.03 \pm 0.57 \mu\text{m}^2$. The further increase of the pH led to the rapid changes in the average size of the L_0 domains, which for the highest tested pH 9 was $53.71 \pm 8.70 \mu\text{m}^2$. Intriguingly, as shown in Fig. 2B the average domain size showed a linear dependence on the pH in the range of pH 3.7–6.7. In this range, the domain size increased on average by $0.38 \pm 0.03 \mu\text{m}^2$ with pH increase of 0.5. Due to the resolution limit of the confocal microscope, domains of L_0 phase for the sample prepared at pH 1.7 could not be resolved.

The area occupied by domains of L_0 phase was found to also increase with the increase of pH of the medium buffer. The small-

est area occupied by domains was observed for pH 2.2 with the value of 22%, which was more than two times smaller than for pH 9.0, where 49% of the total image area was occupied by domains of L_0 phase. It should be noted that the initial composition of membranes was the same for each tested pH condition. The decrease in the area occupied by L_0 phase could be caused by the occurrence of nanodomains embedded within L_d phase at lower pH, which could not be resolved by a confocal microscope. On the other hand, it has been shown that lowering of the pH causes a decrease in the area per lipid (A_L) [51,52]. At low pH, hydrocarbon chains are more closely organized due to the decreased headgroup repulsion. The headgroup rearrangement leads to the denser packing of the lipids, which in turn causes up to 33% decrease of the area per headgroup for lipid membranes in pH 5.5 compared

CHAPTER 5. LATERAL ORGANIZATION OF BIOMIMETIC CELL MEMBRANES IN VARYING PH CONDITIONS

E. Krok, A. Batura, M. Chattopadhyay et al.

Journal of Molecular Liquids 345 (2022) 117907

with pH 9.0. It is consistent with the presented here reduction of the area occupied by domains by approximately 28% (from 1225 μm^2 to 883 μm^2) for the same values of pH as evaluated in the molecular dynamics simulation [51].

It should be noted that both acidic and basic environment can catalyze the process of lipids hydrolysis. Phosphatidylcholine can be hydrolyzed at four locations, influencing carboxy esters at *sn*-1 and *sn*-2 positions and phosphate ester bonds [53]. Lipid suspensions containing phosphatidylcholine have been proven to be stable for 140 h at pH 4, 7 and 10 and slowly hydrolyzed at pH 1 with a half-time of 50 h [54]. In our experiments, bilayers were monitored for no longer than 24 h. Within this time scale, only a small amount of phosphatidylcholine undergoes hydrolysis, and it can be concluded that this reaction does not influence the formation of lipid domains under both acidic and basic pH. Moreover, the hydrolysis rate reported in literature for the pH range tested in this research (1.7–9.0), would result in the formation of a negligible amount of hydrolyzed lipids, that potentially could cause a change in the architecture of the membrane.

Shaping of the lipid membranes by the formation of L_0 phase domains with controlled size opens up a wide range of possibilities for potential studying of protein binding and incorporation of membrane channels that are placed specifically within the domains. However, the use of different types of proteins requires neutral or near-neutral pH of the buffer solution. To confirm the applicability of our technique for future experiments involving proteins, membrane stability was tested after the replacement of the acidic/basic buffer with a buffer of pH 7.4. The lipid membranes were prepared in pH 4.2 and 9.0 to form domains of specific size and then the liquid medium was replaced (multiple, thorough washing) with the buffer of neutral pH 7.4. After 1 h of incubation in the buffer of pH 7.4, lipid membrane domains did not change, maintaining their size and shape (see Fig. S3). The stability of the membranes was tested for 72 h. Despite the normal merging of the domains that is a natural process occurring over time, we did not observe any abnormal rearrangement of the L_0 phase. It can be concluded that presented here technique of shaping of the lipid membrane allows the formation of lipid domains with a specific size in the buffer of corresponding pH, and further transfer into the medium of neutral pH for subsequent studies involving proteins and other pH sensitive molecules.

3.2. Lipids mobility under different pH conditions

To determine whether the increase of the domains size is related to the changes in mobility of the lipids at different pH values, FRAP technique was applied [55,56]. FRAP traces presenting the recovery trajectories with time after bleaching for SLBs prepared at pH 4.2, 5.7, 7.2, and 9.0 are shown in Fig. 3A. The observed recovery of the fluorescence indicated the formation of stable and continuous lipid bilayers regardless of pH conditions. In the presence of defects such as membrane perforations, curling up or detachment from the support, both fluorescence recovery as well as mobile fraction would be hampered [57]. Diffusion coefficients were determined separately for L_d and L_0 phase as depicted in Fig. 3B, because of the significant differences in the mobility of the unsaturated lipids forming disordered phase and the more packed saturated lipids that belong to the ordered domains. The obtained values for the diffusion coefficient are in the range of 1.03–1.29 $\mu\text{m}^2/\text{s}$ (Fig. 3B) and are in full agreement with the work by Kataoka-Hamai, who reported that the diffusion coefficient for zwitterionic DOPC in a single component SLBs did not show significant differences (from 1.1 to 1.8 $\mu\text{m}^2/\text{s}$), when measured for pH values of 3, 4, 7.2, and 8.3 [58]. The diffusion coefficient for the sphingomyelin-rich L_0 phase was 4.5–10 fold slower than for L_d phase, and varied between 0.10 $\mu\text{m}^2/\text{s}$ for pH 4.2 and 4.7, to

0.18–0.24 $\mu\text{m}^2/\text{s}$ for pH range 5.2–9.0. These results are consistent with the findings reported by Bacia et al. [47] for neutral pH condition, where depending on cholesterol concentration the diffusion coefficient between L_0 and L_d phase can be 6–50-fold lower. We note here that the L_0 phase is probed through CTxB molecules, which can bind to multiple GM1 molecules (from 1 to 5 units) [59]. Consequently, the diffusion coefficient measured through CTxB complex corresponds to an average diffusivity of individual lipids and also of larger lipid complexes (1–5 molecules). Hence the diffusion of L_0 phase lipids is very slow and the mobile fraction is approximately around 30–40% with very little variation across the entire tested pH range. The diffusion coefficient of L_0 phase lipids for SLBs prepared at pH lower than 4 could not be determined due to the plausible denaturation of the CTxB protein, which is a compound linking AlexaFluor dye with the GM1. In this case, FRAP traces could not be fitted due to the lack of fluorescence recovery, indicating that L_0 phase lipids were effectively immobile. It should also be noted that lipids diffusion was not affected by the buffer replacement from pH 4.2 to 7.4 and from pH 9.0 to 7.4 (Fig. S4). Lipid membranes prepared in the buffer with specific pH can be transferred to the buffer of neutral pH without hampering the mobility of lipids.

Although changes in the pH of the environment did not affect the diffusion of the lipids in the whole range of tested pH, they influenced the mobile fraction of L_d phase. The mobile fraction for the L_d phase was increasing with the pH, showing values in the range ~70–90% with a significantly lower value of 49% for pH 3.7. The isoelectric point for a mixture of PC composed of different chain length lipids (16:0, 18:0, 18:1, 18:2, and 20:4) was found to be at pH 4.12 [60], and for SM around pH 4.01 [36]. It thus look that the reduced mobile fraction at the pH of ~3.7 is related with the isoelectric point of our membrane. Zimmermann et al. suggested that SLB composed of DOPC undergoes a charge-induced transition from a liquid-crystalline bilayer into a more ordered/gel phase bilayer at the isoelectric point [61]. At the same time they observed a gradual reduction of the diffusion coefficient below the isoelectric point. In the work by Petelska et al. they observed (supported by theoretical models) an abrupt, over a 2-fold increase of an interfacial tension for SLBs composed of PC, PS, PE and SM at their isoelectric points [36,60,62]. The observed in our data sudden reduction in the mobile fraction at the isoelectric point is in line with the mentioned, possible changes of the structural properties (phase transition and interfacial tension) in such conditions. Above the isoelectric point, the force balance between van der Waals interactions and electrostatic repulsion is maintained, which allows lipids to move freely within the bilayer, which was reflected here by the higher values of mobile fraction than for more acidic pH values [63]. However, the exact mechanism behind the observed lowering of mobile fraction at the isoelectric point remains unclear.

3.3. Rearrangement of lipid domains under different pH conditions

Based on the FRAP experiments it is clear that the formation of lipid domains with different size at different pH values is not related to the potential changes in lipids mobility. In order to determine whether variation in domain size occurs at the stage of vesicle formation, the DLS measurements were applied. The pH of the buffer in which vesicles were formed was 2.2, 4.2, 7.2, and 9.0. As shown in Fig. S5 there was no difference in the mean hydrodynamic diameter of the vesicles. Mean hydrodynamic diameter was 94 ± 3 nm, 91 ± 3 nm, 104 ± 3 nm, and 98 ± 5 nm for pH 2.2, 4.2, 7.2, and 9.0 respectively, which is a typical size for SUVs prepared by sonication method, reported in the literature [64,65]. The polydispersity index was 0.3 ± 0.04 , 0.36 ± 0.09 , 0.4 ± 0.03 , and 0.34 ± 0.06 for pH 2.2, 4.2, 7.2, and 9.0 respectively, indicating

CHAPTER 5. LATERAL ORGANIZATION OF BIOMIMETIC CELL MEMBRANES IN VARYING PH CONDITIONS

E. Krok, A. Batura, M. Chattopadhyay et al.

Journal of Molecular Liquids 345 (2022) 117907

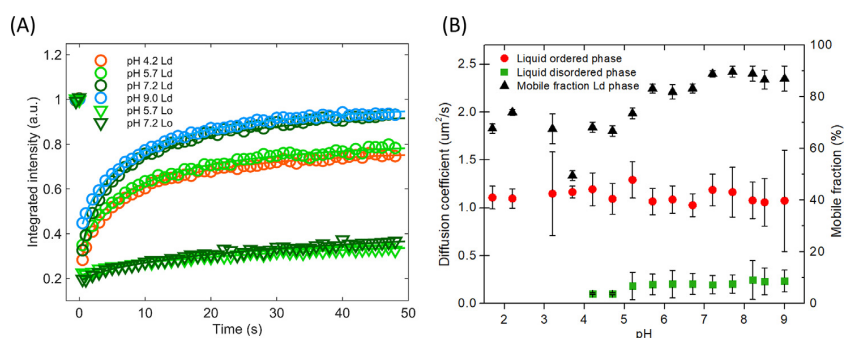


Fig. 3. (A) FRAP curves for L_d phase of SLBs prepared at pH 4.2, 5.7, 7.7 and 9.0 and for L_o phase prepared at pH 5.7 and 7.2, (B) Diffusion coefficient for L_d (red circles) and L_o (green squares) phases of SLBs and mobile fraction for L_d phase (black triangles) as a function of pH of the buffer. (For interpretation of the references to colour in this figure legend, the reader is referred to the web version of this article.)

that the obtained samples were relatively homogenous [66]. Evidently, the presence of different size of domains was not the result of the formation of bigger vesicles but must occur as a consequence of rearrangement of the lipids upon deposition onto the solid support.

To induce sample homogeneity, create the same sample thermal history in the experiment, and enable observation of the growth of the domains, samples were prepared at increased temperature, which allowed complete mixing of L_o and L_d phase lipids. Samples prepared at pH 4.2, 7.2, and 9.0 were heated during the sonication, deposition, and incubation to 65 °C, which is higher than the 14:1 PC and SM miscibility temperature [43]. The samples were imaged immediately after removing from the hot plate and domains growth was observed over time. Right after removal from the hot plate, membrane constituents were homogeneously distributed, without the presence of any visible phase separation, regardless of the tested pH. The nucleation process was visible once the samples started to cool down, but the growth of domains was different for each pH as shown in Figs. 4A and S6. The beginning of the domains nucleation for the SLB prepared at pH 4.2 was visible 5 min after removal from the hot plate. However, at this time point domains were too small for quantification due to the resolution limit of the confocal microscope. After 30 min lipid domains had an average size of $0.76 \pm 0.12 \mu\text{m}^2$. Within 1 h, they doubled their size to the average value of $1.35 \pm 0.13 \mu\text{m}^2$. The domains size was checked also 3 h after removal from the hot plate

and was estimated to be $1.29 \pm 0.16 \mu\text{m}^2$, indicating that the equilibration of the sample with ambient temperature and domains growth occurs within the first hour after removal from the hot plate. The same time intervals were used for checking lipid membranes prepared at pH 7.2 and 9.0. For all the samples the growth of the L_d phase occurred within the first 1 h, when domains reached the size characteristic for the tested pH and remained stable for another 2 h. The rapid merging of the domains was observed for the sample prepared at pH 9.0 as presented in [supplementary Movie M1](#). The time-dependent evolution of the domains size for the three tested pH conditions follows the trend presented by Giocondi et al. [67] where the growth of domains prepared at neutral pH 7.4 was rapid within the first 45 min after temperature quench from 60 °C to 23 °C. It has to be emphasized that the final size of the obtained domains was different for each tested pH, even though all samples had the same starting point of a complete mixture of both phase constituents. Regardless of the tested pH, domains of L_o phase equilibrated within 1 h, obtaining exactly the same average size as when the samples were not exposed to the heating (see Fig. 2A) and did not show further significant growth for the next 2 h.

The average domain size is strongly related to the tendency of a lipid mixture to phase separate, which is regulated by three factors opposing each other. Entropy and electrostatic repulsion lead to lipid mixing and formation of small domains [68]. On the other hand, the size of domains is increased by the line tension occurring

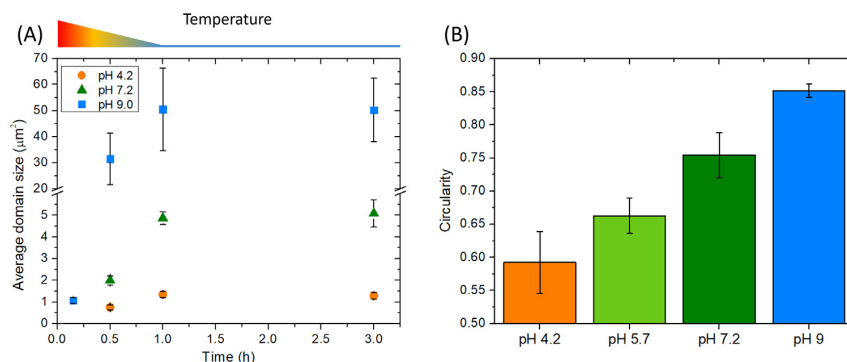


Fig. 4. (A) L_d phase domains growth as a function of time for the lipid bilayers prepared at pH 4.2, 7.2 and 9.0. Each point presenting the average domain size corresponds to the minimum of 10 images collected from 10 different areas of the lipid membrane, each analyzed image presented a minimum of 12 domains for pH 9 to approximately 330 domains for pH 4.2. (B) Circularity of the L_d domains at pH 4.2, 5.7, 7.2 and 9.0 calculated based on at least 10 different areas containing 12–330 domains each. Domains at higher pH tend to be more circular to minimize the energy at the phase boundary.

at the boundary of two phases, which tries to reduce the perimeter of the domain that is exposed to the water interface [69]. AFM studies have proven that for the ternary lipid mixture of DOPC, SM and cholesterol, L_o phase is thicker than the surrounding L_d phase [70]. This height difference leads to the phenomenon called hydrophobic mismatch, which occurs at the boundary of the two phases. The mismatch in the height is energetically unfavorable and leads to the formation of high line tension at the boundary of L_o and L_d phases. Thus, under the presence of higher line tension, the lipid membrane rearranges itself to minimize the length of the boundary at the interface of two phases, which in consequence leads to the formation of bigger domains.

According to Deplazes et al. [71] the zwitterionic lipids change their height upon pH variation. Bilayer composed of POPC, which is a zwitterionic lipid forming L_d phase, increased its thickness from 3.6 at neutral pH to 4.2 nm upon exposure to $[H_3O^+]$ ions (addition of 0.4 M of hydronium ions). The addition of $[H_3O^+]$ ions leads to the formation of acidic environment reducing the membrane fluidity and making lipid tails more straight and rigid. At low pH lipid hydrocarbon chains have higher orientational order, and a decreased headgroup repulsion [51]. Consequently, the tails of PC lipids can pack more densely, forming a more ordered state. Under acidic conditions, the height difference between protruding lipids of L_o phase and thinner L_d phase is reduced, leading to the lower hydrophobic mismatch and thus reducing the need to form bigger domains, decreasing the interfacial boundary between the two phases and enhancing their miscibility. Indeed, as presented in Fig. 4B membranes prepared in the higher pH are characterized by higher line tension, which is associated with the formation of more circular lipid domains. It is evident that the observed in this study differences in the size of domains in buffers containing different concentration of H^+ and OH^- ions are directly related to the changes in the height mismatch between L_o and L_d phases, that lead to an increase of the line tension at the phase boundary.

4. Conclusions

It has been shown that pH of the environment has a strong influence on the formation and size of the domains of L_o phase in supported lipid bilayers. The increase of pH of the environment leads to the formation of bigger L_o phase domains, exceeding the factor of 50 for pH values from 1.7 to 9.0. The increase in average L_o phase domain size is associated with an increase in the line tension and formation of rounder domains at higher pH values. Our findings are consistent with the MD simulations, which showed that unsaturated lipids take up straighter conformation under acidic pH (thickening of the L_d phase bilayer) [71]. In return this leads to the reduction of height difference between disordered and ordered phase and formation of smaller domains. On the other hand, the hydrophobic mismatch is more prominent under basic pH, which leads to the formation of bigger domains and higher line tension. We show here that the process of domains reorganization is not a result of the formation of larger vesicles but occurs at the stage of membrane establishment on the solid support. Adjustment of the environmental pH enables the control of the formation and size of domains without the introduction of mechanical boundaries that would modulate the size of lipid domains [72], use of lineactants [73], or modification of the membrane composition [74]. Given the high importance of lipid domains in many biological processes, the possibility to create these entities with a specific and repeatable size gives a wide range of new experimental opportunities. Lipid domains with fully controlled size can serve as platforms for the binding of different types of proteins such as caveolins [75], signal transduction molecules [76], and incorporation of membrane channels [77]. The diffusion of the lipid mem-

brane proteins is normally limited by the size of the domains. Each domain can usually carry around 10 to 30 proteins [15]. The formation of bigger lipid domains gives the possibility to create binding sites for a higher amount of proteins and to observe the mutual interactions between them and other chemical complexes. It should be noted that lipid membranes prepared in different pH conditions do not lose their mobility. The measurements of the diffusion for both phases showed that although there is a significant difference in the phase separation architecture of the membranes prepared at different pH conditions, the diffusion coefficient of the lipids is not affected by pH of the environment. Finally, lipid membranes formed in specific pH do not rearrange their structure upon replacement of the basic or acidic buffer to the buffer of neutral pH. Thus presented here technique of domains shaping, enables the further studying of the lipid membranes interacting with molecules that require neutral environmental conditions.

CRediT authorship contribution statement

Emilia Krok: Conceptualization, Methodology, Validation, Writing – original draft, Visualization. **Agnieszka Batura:** Conceptualization, Investigation, Writing – original draft. **Madhurima Chattopadhyay:** Methodology, Software, Writing – review & editing. **Hanna Orlikowska:** Methodology, Writing – review & editing. **Lukasz Piatkowski:** Formal analysis, Writing – review & editing, Supervision.

Declaration of Competing Interest

The authors declare that they have no known competing financial interests or personal relationships that could have appeared to influence the work reported in this paper.

Acknowledgments

The authors acknowledge the financial support from the EMBO Installation Grant (IG 4147) and from the Ministry of Science and Higher Education of Poland in the year 2021 (Project No. 0512/SBAD/2120). L.P. acknowledges the financial support from the First TEAM Grant (POIR.04.04.00-00-5D32/18-00), provided by the Foundation for Polish Science and Opus Grant (UMO-2020/37/B/ST4/01785) from the National Science Centre, Poland. This work was financed from the budget funds allocated for science in the years 2019–2023 as a research project under the “Diamond Grant” program (Decision No. 0042/DIA/2019/48). The authors thank prof. Filip Ciesielczyk for his assistance in DLS measurements.

Appendix A. Supplementary material

Supplementary data to this article can be found online at <https://doi.org/10.1016/j.molliq.2021.117907>.

References

- [1] S.J. Singer, G.L. Nicolson, The fluid mosaic model of the structure of cell membranes, *Science* 175 (4023) (1972) 720–731, <https://doi.org/10.1126/science.175.4023.720>.
- [2] K. Simons, E. Ikonen, Functional rafts in cell membranes, *Nature* 387 (6633) (1997) 569–572, <https://doi.org/10.1038/42408>.
- [3] J. Hjort Ipsen, G. Karlström, O.G. Mouritsen, H. Wennerström, M.J. Zuckermann, Phase equilibria in the phosphatidylcholine-cholesterol system, *BBA – Biomembr.* 905 (1) (1987) 162–172, [https://doi.org/10.1016/0005-2736\(87\)90020-4](https://doi.org/10.1016/0005-2736(87)90020-4).
- [4] K. Simons, J.L. Sampaio, Membrane organization and lipid rafts, *Cold Spring Harb. Perspect. Biol.* 3 (10) (2011) a004697, <https://doi.org/10.1101/cshperspect.a004697>.
- [5] C. Dart, Lipid microdomains and the regulation of ion channel function, *J. Physiol.* 588 (2010) 3169–3178, <https://doi.org/10.1113/jphysiol.2010.191585>.

CHAPTER 5. LATERAL ORGANIZATION OF BIOMIMETIC CELL MEMBRANES IN VARYING PH CONDITIONS

E. Krok, A. Batura, M. Chattopadhyay et al.

Journal of Molecular Liquids 345 (2022) 117907

- [6] T.S. Tillman, M. Cascio, Effects of membrane lipids on ion channel structure and function, *Cell Biochem. Biophys.* 38 (2003) 161–190, <https://doi.org/10.1385/CBB:38:2:161>.
- [7] K. Simons, D. Toomre, Lipid rafts and signal transduction, *Nat. Rev. Mol. Cell Biol.* 1 (1) (2000) 31–39, <https://doi.org/10.1038/35036052>.
- [8] J.F. Hancock, Lipid rafts: Contentious only from simplistic standpoints, *Nat. Rev. Mol. Cell Biol.* 7 (6) (2006) 456–462, <https://doi.org/10.1038/nrm1925>.
- [9] D.A. Brown, E. London, Functions of lipid rafts in biological membranes, *Annu. Rev. Cell Dev. Biol.* 14 (1) (1998) 111–136, <https://doi.org/10.1146/annurev.cellbio.14.1.111>.
- [10] E. Ikonen, Roles of lipid rafts in membrane transport, *Curr. Opin. Cell Biol.* 13 (4) (2001) 470–477, [https://doi.org/10.1016/S0955-0674\(00\)00238-6](https://doi.org/10.1016/S0955-0674(00)00238-6).
- [11] G.R. Chichili, W. Rodgers, Cytoskeleton-membrane interactions in membrane raft structure, *Cell. Mol. Life Sci.* 66 (14) (2009) 2319–2328, <https://doi.org/10.1007/s00118-009-0022-6>.
- [12] B.F. Lillemeier, J.R. Pfeiffer, Z. Surviladze, B.S. Wilson, M.M. Davis, Plasma membrane-associated proteins are clustered into islands attached to the cytoskeleton, *Proc. Natl. Acad. Sci. U. S. A.* 103 (50) (2006) 18992–18997, <https://doi.org/10.1073/pnas.0609009103>.
- [13] C.M. Rosenberger, J.H. Brumell, B.B. Finlay, Microbial pathogenesis: Lipid rafts as pathogen portals, *Curr. Biol.* 10 (22) (2000) R823–R825, [https://doi.org/10.1016/S0969-9822\(00\)00788-0](https://doi.org/10.1016/S0969-9822(00)00788-0).
- [14] D.W. Zaas, M. Duncan, J.o. Rae Wright, S.N. Abraham, The role of lipid rafts in the pathogenesis of bacterial infections, *Biochim. Biophys. Acta - Mol. Cell Res.* 1746 (3) (2005) 305–313, <https://doi.org/10.1016/j.bbamcr.2005.10.003>.
- [15] K. Simons, E. Ikonen, How Cells Handle Cholesterol, *Science* 290 (5497) (2000) 1721–1726, <https://doi.org/10.1126/science.290.5497.1721>.
- [16] J.M. Holopainen, H.L. Brockman, R.E. Brown, P.K.J. Kinnunen, Interfacial interactions of ceramide with dimyristoylphosphatidylcholine: Impact of the N-acyl chain, *Biophys. J.* 80 (2) (2001) 765–775, [https://doi.org/10.1016/S0006-3495\(01\)76056-0](https://doi.org/10.1016/S0006-3495(01)76056-0).
- [17] R. Tero, K. Fukumoto, T. Motegi, M. Yoshida, M. Niwano, A. Hirano-Iwata, Formation of Cell Membrane Component Domains in Artificial Lipid Bilayer, *Sci. Rep.* 7 (2017) 1–10, <https://doi.org/10.1038/s41598-017-18242-9>.
- [18] F. Vega Mercado, B. Maggio, N. Wilke, Modulation of the domain topography of biphasic monolayers of stearic acid and dimyristoyl phosphatidylcholine, *Chem. Phys. Lipids* 165 (2) (2012) 232–237, <https://doi.org/10.1016/j.chemphyslip.2012.01.003>.
- [19] J. Zhao, J. Wu, F.A. Heberle, T.T. Mills, P. Klawitter, G. Huang, G. Costanza, G.W. Feigenson, Phase studies of model biomembranes: Complex behavior of DSPC/DOPC/Cholesterol, *Biochim. Biophys. Acta - Biomembr.* 1768 (11) (2007) 2764–2776, <https://doi.org/10.1016/j.bbamem.2007.07.008>.
- [20] F.V. Mercado, B. Maggio, N. Wilke, Phase diagram of mixed monolayers of stearic acid and dimyristoylphosphatidylcholine. Effect of the acid ionization, *Chem. Phys. Lipids* 164 (5) (2011) 386–392, <https://doi.org/10.1016/j.chemphyslip.2011.05.004>.
- [21] A.A. Bischof, A. Mangiarotti, N. Wilke, Searching for line active molecules on biphasic lipid monolayers, *Soft Matter* 11 (11) (2015) 2147–2156, <https://doi.org/10.1039/C5SM00022J>.
- [22] A. Arnold, I. Cloutier, A.M. Ritchey, M. Auger, Temperature and pressure dependent growth and morphology of DMPC/DSPC domains studied by Brewster angle microscopy, *Chem. Phys. Lipids* 133 (2) (2005) 165–179, <https://doi.org/10.1016/j.chemphyslip.2004.09.020>.
- [23] U. Bhojoo, M. Chen, S. Zou, Temperature induced lipid membrane restructuring and changes in nanomechanics, *Biochim. Biophys. Acta - Biomembr.* 1860 (3) (2018) 700–709, <https://doi.org/10.1016/j.bbamem.2017.12.008>.
- [24] R.K. Paradise, M.J. Whitfield, D.A. Lauffenburger, K.J. Van Vliet, Directional cell migration in an extracellular pH gradient: A model study with an engineered cell line and primary microvascular endothelial cells, *Exp. Cell Res.* 319 (4) (2013) 487–497, <https://doi.org/10.1016/j.yexcr.2012.11.006>.
- [25] E. Takahashi, D. Yamaguchi, Y. Yamaoka, A relatively small gradient of extracellular pH directs migration of MDA-MB-231 cells in vitro, *Int. J. Mol. Sci.* 21 (2020) 2565–2580, <https://doi.org/10.3390/ijms21072565>.
- [26] N. Khalifat, N. Puff, S. Bonneau, J.-B. Fournier, M.L. Angelova, Membrane deformation under local pH gradient: Mimicking mitochondrial cristae dynamics, *Biophys. J.* 95 (10) (2008) 4924–4933, <https://doi.org/10.1529/biophysj.108.136077>.
- [27] C.C. Yao, Z. gang Zha, Effects of incubation pH on the membrane deformation of a single living human red blood cell, *Curr. Appl. Phys.* 7 (2007) 11–14, <https://doi.org/10.1016/j.cap.2006.11.005>.
- [28] C.R. Kruse, M. Singh, S. Targosinski, I. Sinha, J.A. Sørensen, E. Eriksson, K. Nuutila, The effect of pH on cell viability, cell migration, cell proliferation, wound closure, and wound reepithelialization: In vitro and in vivo study, *Wound Repair Regen.* 25 (2) (2017) 260–269, <https://doi.org/10.1111/wrr.12526>.
- [29] M. Flinck, S.H. Kramer, S.F. Pedersen, Roles of pH in control of cell proliferation, *Acta Physiol.* 223 (3) (2018) e13068, <https://doi.org/10.1111/apha.13068>.
- [30] A. Boussouf, S. Gaillard, Intracellular pH changes during oligodendrocyte differentiation in primary culture, *J. Neurosci. Res.* 59 (2000) 731–739, [https://doi.org/10.1002/\(SICI\)1097-4547\(20000315\)59:6<731::AID-JNR5>3.0.CO;2-G](https://doi.org/10.1002/(SICI)1097-4547(20000315)59:6<731::AID-JNR5>3.0.CO;2-G).
- [31] D. Lagadic-Gossman, L. Huc, V. Lecreur, Alterations of intracellular pH homeostasis in apoptosis: Origins and roles, *Cell Death Differ.* 11 (9) (2004) 953–961, <https://doi.org/10.1038/sj.cdd.4401466>.
- [32] S.P. Denker, D.C. Huang, J. Orłowski, H. Furthmayr, D.L. Barber, Direct binding of the Na-H exchanger NHE1 to ERM proteins regulates the cortical cytoskeleton and cell shape independently of H⁺ translocation, *Mol. Cell.* 6 (6) (2000) 1425–1436, [https://doi.org/10.1016/S1097-2765\(00\)00139-8](https://doi.org/10.1016/S1097-2765(00)00139-8).
- [33] M. Motizuki, S. Yokota, K. Tsurugi, Effect of low pH on organization of the actin cytoskeleton in *Saccharomyces cerevisiae*, *Biochim. Biophys. Acta - Gen. Subj.* 1780 (2) (2008) 179–184, <https://doi.org/10.1016/j.bbagen.2007.10.003>.
- [34] K.A. White, B.K. Grillo-Hill, D.L. Barber, Cancer cell behaviors mediated by dysregulated pH dynamics at a glance, *J. Cell Sci.* 130 (2017) 663–669, <https://doi.org/10.1242/jcs.195297>.
- [35] R. Zimmermann, D. Küttner, L. Renner, M. Kaufmann, J. Zitzmann, M. Müller, C. Werner, Charging and structure of zwitterionic supported bilayer lipid membranes studied by streaming current measurements, fluorescence microscopy, and attenuated total reflection Fourier transform infrared spectroscopy, *Biointerphases* 4 (1) (2009) 1–6, <https://doi.org/10.1116/1.3082042>.
- [36] A.D. Petelska, Z.A. Figaszewski, pH effect of the sphingomyelin membrane interfacial tension, *J. Membr. Biol.* 230 (1) (2009) 11–19, <https://doi.org/10.1007/s00232-009-9181-5>.
- [37] J. Andersson, I. Köper, Biomimetic Membranes, *Compr. Nanosci. Nanotechnol.* 1–5 (2019) 49–64, <https://doi.org/10.1016/B978-0-12-803581-8.10447-3>.
- [38] S. Chiantia, N. Kahya, P. Schwille, Dehydration damage of domain-exhibiting supported bilayers: An AFM study on the protective effects of disaccharides and other stabilizing substances, *Langmuir* 21 (2005) 6317–6323, <https://doi.org/10.1021/la050115m>.
- [39] D.M. Soumpasis, Theoretical analysis of fluorescence photobleaching recovery experiments, *Biophys. J.* 41 (1) (1983) 95–97, [https://doi.org/10.1016/S0006-3495\(83\)84410-5](https://doi.org/10.1016/S0006-3495(83)84410-5).
- [40] K. Sumitomo, A. Oshima, Liquid-Ordered/Liquid-Crystalline Phase Separation at a Lipid Bilayer Suspended over Microwells, *Langmuir* 33 (46) (2017) 13277–13283, <https://doi.org/10.1021/acs.langmuir.7b02156>.
- [41] M. Chattopadhyay, E. Krok, H. Orlikowska, P. Schwille, H.G. Franquelim, L. Piatkowska, Hydration Layer of Only a Few Molecules Controls Lipid Mobility in Biomimetic Membranes, *J. Am. Chem. Soc.* 143 (36) (2021) 14551–14562, <https://doi.org/10.1021/jacs.1c04314>.
- [42] C.A. Schneider, W.S. Rasband, K.W. Eliceiri, NIH Image to ImageJ: 25 years of image analysis, *Nat. Methods* 9 (7) (2012) 671–675, <https://doi.org/10.1038/nmeth.2089>.
- [43] A.J. García-Sáez, S. Chiantia, P. Schwille, Effect of line tension on the lateral organization of lipid membranes, *J. Biol. Chem.* 282 (46) (2007) 33537–33544, <https://doi.org/10.1074/jbc.M706162200>.
- [44] N. Kahya, D. Scherfeld, K. Bacia, B. Poolman, P. Schwille, Probing lipid mobility of raft-exhibiting model membranes by fluorescence correlation spectroscopy, *J. Biol. Chem.* 278 (30) (2003) 28109–28115, <https://doi.org/10.1074/jbc.M302969200>.
- [45] K. Bacia, D. Scherfeld, N. Kahya, P. Schwille, Fluorescence correlation spectroscopy relates rafts in model and native membranes, *Biophys. J.* 87 (2) (2004) 1034–1043, <https://doi.org/10.1529/biophysj.104.040519>.
- [46] M. Chattopadhyay, H. Orlikowska, E. Krok, L. Piatkowska, Sensing hydration of biomimetic cell membranes, *Biosensors* 11 (7) (2021) 241, <https://doi.org/10.3390/bios11070241>.
- [47] K. Bacia, P. Schwille, T. Kurzchalia, Sterol structure determines the separation of phases and the curvature of the liquid-ordered phase in model membranes, *Proc. Natl. Acad. Sci. U. S. A.* 102 (2005) 3272–3277, <https://doi.org/10.1073/pnas.0408215102>.
- [48] M.J.S. De Wolf, G.A.F. Van Dessel, A.R. Lagrou, H.J.J. Hilderson, W.S.H. Dierck, pH-Induced Transitions in Cholera Toxin Conformation: A Fluorescence Study, *Biochemistry* 26 (13) (1987) 3799–3806, <https://doi.org/10.1021/bi00387a010>.
- [49] M. Komiazyk, M. Palczewska, I. Sitkiewicz, S. Pikula, P. Groves, Neutralization of cholera toxin by Rosaceae family plant extracts, *BMC Complement. Altern. Med.* 19 (2019) 1–14, <https://doi.org/10.1186/s12906-019-2540-6>.
- [50] X.S. Sun, Soy Protein Adhesives, in: *Bio-Based Polym. Compos.*, Academic Press, 2005, pp. 327–368, <https://doi.org/10.1016/B978-012763952-9/50011-3>.
- [51] K. Lähdesmäki, O.H.S. Ollila, A. Koivuniemi, P.T. Kovanen, M.T. Hyvönen, Membrane simulations mimicking acidic pH reveal increased thickness and negative curvature in a bilayer consisting of lysophosphatidylcholines and free fatty acids, *Biochim. Biophys. Acta* 1798 (5) (2010) 938–946, <https://doi.org/10.1016/j.bbamem.2010.01.020>.
- [52] H.A.F. Santos, D. Vila-Viçosa, V.H. Teixeira, A.M. Baptista, M. Machuqueiro, Constant-pH MD Simulations of DMPA/DMPK Lipid Bilayers, *J. Chem. Theory Comput.* 11 (12) (2015) 5973–5979, <https://doi.org/10.1021/acs.jctc.5b00956>.
- [53] C.R. Kensil, E.A. Dennis, Alkaline Hydrolysis of Phospholipids in Model Membranes and the Dependence on Their State of Aggregation, *Biochemistry* 20 (21) (1981) 6079–6085, <https://doi.org/10.1021/bi00524a025>.
- [54] R.J.Y. Ho, M. Schmetz, D.W. Deamer, Nonenzymatic hydrolysis of phosphatidylcholine prepared as liposomes and mixed micelles, *Lipids* 22 (3) (1987) 156–158, <https://doi.org/10.1007/BF02537295>.
- [55] M. Sarkar, J.G. Koland, Fluorescence recovery after photobleaching analysis of the diffusional mobility of plasma membrane proteins: HER3 mobility in breast cancer cell membranes, in: *Methods Mol. Biol.*, 2016, pp. 97–105, https://doi.org/10.1007/978-1-4939-3170-5_9.
- [56] N.W. Goehring, D. Chowdhury, A.A. Hyman, S.W. Grill, FRAP analysis of membrane-associated proteins: Lateral diffusion and membrane-cytoplasmic exchange, *Biophys. J.* 99 (8) (2010) 2443–2452, <https://doi.org/10.1016/j.bpj.2010.08.033>.

CHAPTER 5. LATERAL ORGANIZATION OF BIOMIMETIC CELL MEMBRANES IN VARYING PH CONDITIONS

E. Krok, A. Batura, M. Chattopadhyay et al.

Journal of Molecular Liquids 345 (2022) 117907

- [57] E.A.J. Reits, J.J. Neefjes, From fixed to FRAP: Measuring protein mobility and activity in living cells, *Nat. Cell Biol.* 3 (6) (2001) E145–E147, <https://doi.org/10.1038/35078615>.
- [58] C. Kataoka-Hamai, M. Higuchi, Packing Density Changes of Supported Lipid Bilayers Observed by Fluorescence Microscopy and Quartz Crystal Microbalance-Dissipation, *J. Phys. Chem. B* 118 (37) (2014) 10934–10944, <https://doi.org/10.1021/jp503905r>.
- [59] A.M. Kabbani, K. Raghunathan, W.I. Lencer, A.K. Kenworthy, C.V. Kelly, Structured clustering of the glycosphingolipid GM1 is required for membrane curvature induced by cholera toxin, *Proc. Natl. Acad. Sci. U. S. A.* 117 (26) (2020) 14978–14986, <https://doi.org/10.1073/pnas.2001119117>.
- [60] A.D. Petelska, Z.A. Figaszewski, Effect of pH on the interfacial tension of lipid bilayer membrane, *Biophys. J.* 78 (2) (2000) 812–817, [https://doi.org/10.1016/S0006-3495\(00\)76638-0](https://doi.org/10.1016/S0006-3495(00)76638-0).
- [61] R. Zimmermann, D. Küttner, L. Renner, M. Kaufmann, C. Werner, Fluidity Modulation of Phospholipid Bilayers by Electrolyte Ions: Insights from Fluorescence Microscopy and Microslit Electrokinetic Experiments, *J. Phys. Chem. A* 116 (25) (2012) 6519–6525, <https://doi.org/10.1021/jp212364q>.
- [62] A.D. Petelska, Z.A. Figaszewski, Effect of pH on the interfacial tension of bilayer lipid membrane formed from phosphatidylcholine or phosphatidylserine, *Biochim. Biophys. Acta - Biomembr.* 1561 (2) (2002) 135–146, [https://doi.org/10.1016/S0005-2736\(01\)00463-1](https://doi.org/10.1016/S0005-2736(01)00463-1).
- [63] P.S. Cremer, S.G. Boxer, Formation and Spreading of Lipid Bilayers on Planar Glass Supports, *J. Phys. Chem. B* 103 (13) (1999) 2554–2559, <https://doi.org/10.1021/jp983996x>.
- [64] C.-M. Lin, C.-S. Li, Y.-J. Sheng, D.T. Wu, H.-K. Tsao, Size-dependent properties of small unilamellar vesicles formed by model lipids, *Langmuir* 28 (1) (2012) 689–700, <https://doi.org/10.1021/la203755v>.
- [65] C.F. de Freitas, I.R. Calori, A.L. Tessaro, W. Caetano, N. Hioka, Rapid formation of Small Unilamellar Vesicles (SUV) through low-frequency sonication: An innovative approach, *Colloids Surf. B Biointerfaces* 181 (2019) 837–844.
- [66] M. Danaei, M. Dehghankhold, S. Ataei, F. Hasanzadeh Davarani, R. Javanmard, A. Dokhani, S. Khorasani, M.R. Mozafari, Impact of particle size and polydispersity index on the clinical applications of lipidic nanocarrier systems, *Pharmaceutics* 10 (2018) 1–17, <https://doi.org/10.3390/pharmaceutics10020057>.
- [67] M.-C. Giocondi, V. Vié, E. Lesniewska, P.-E. Milhiet, M. Zinke-Allmang, C. Le Grimellec, Phase Topology and Growth of Single Domains in Lipid Bilayers, *Langmuir* 17 (5) (2001) 1653–1659, <https://doi.org/10.1021/la0012135>.
- [68] P.I. Kuzmin, S.A. Akimov, Y.A. Chizmadzhev, J. Zimmerberg, F.S. Cohen, Line tension and interaction energies of membrane rafts calculated from lipid splay and tilt, *Biophys. J.* 88 (2) (2005) 1120–1133, <https://doi.org/10.1529/biophysj.104.048223>.
- [69] A. Mangiarotti, N. Wilke, Electrostatic interactions at the microscale modulate dynamics and distribution of lipids in bilayers, *Soft Matter* 13 (3) (2017) 686–694, <https://doi.org/10.1039/C6SM01957A>.
- [70] D.E. Saslow, J. Lawrence, X. Ren, D.A. Brown, R.M. Henderson, J.M. Edwardson, Placental alkaline phosphatase is efficiently targeted to rafts in supported lipid bilayers, *J. Biol. Chem.* 277 (30) (2002) 26966–26970, <https://doi.org/10.1074/jbc.M204669200>.
- [71] E. Deplazes, D. Poger, B. Cornell, C.G. Cranfield, The effect of hydronium ions on the structure of phospholipid membranes, *Phys. Chem. Chem. Phys.* 20 (1) (2018) 357–366, <https://doi.org/10.1039/C7CP06776C>.
- [72] A.R. Sapuri-Butti, Q. Li, J.T. Groves, A.N. Parikh, Nonequilibrium patterns of cholesterol-rich chemical heterogeneities within single fluid supported phospholipid bilayer membranes, *Langmuir* 22 (12) (2006) 5374–5384, <https://doi.org/10.1021/la052248d10.1021/la052248d.s001>.
- [73] R. Brewster, S.A. Safran, Line active hybrid lipids determine domain size in phase separation of saturated and unsaturated lipids, *Biophys. J.* 98 (6) (2010) L21–L23, <https://doi.org/10.1016/j.bpj.2009.11.027>.
- [74] S.L. Goh, J.J. Amazon, G.W. Feigenson, Toward a better raft model: Modulated phases in the four-component bilayer, DSPC/DOPC/POPC/CHOL, *Biophys. J.* 104 (4) (2013) 853–862, <https://doi.org/10.1016/j.bpj.2013.01.003>.
- [75] T. Harder, K. Simons, Caveolae, DIGS, and the dynamics of sphingolipid-cholesterol microdomains, *Curr. Opin. Cell Biol.* 9 (4) (1997) 534–542, [https://doi.org/10.1016/S0955-0674\(97\)80030-0](https://doi.org/10.1016/S0955-0674(97)80030-0).
- [76] M.J. Langton, L.M. Scriven, N.H. Williams, C.A. Hunter, Triggered Release from Lipid Bilayer Vesicles by an Artificial Transmembrane Signal Transduction System, *J. Am. Chem. Soc.* 139 (44) (2017) 15768–15773, <https://doi.org/10.1021/jacs.7b07747>.
- [77] J.R. Martens, K. O'Connell, M. Tamkun, Targeting of ion channels to membrane microdomains: Localization of K⁺ V channels to lipid rafts, *Trends Pharmacol. Sci.* 25 (1) (2004) 16–21, <https://doi.org/10.1016/j.tips.2003.11.007>.

Supplementary Information for

Lateral organization of biomimetic cell membranes in varying pH conditions

Emilia Krok^a, Agnieszka Batura^a, Madhurima Chattopadhyay^a, Hanna Orlikowska^a, Lukasz Piatkowski^a

^a Poznan University of Technology, Faculty of Materials Engineering and Technical Physics, Institute of Physics, Piotrowo 3, 60-965 Poznan, Poland

Table of contents:

Supplementary figures S1 – S6.

Figure S1

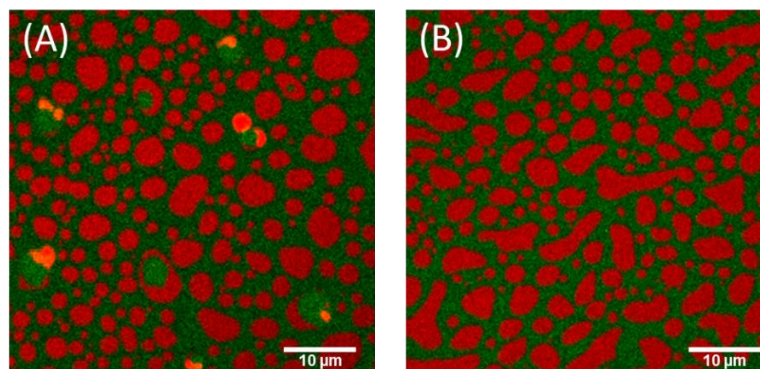


Figure S1 Exemplary fluorescence images of lipid membrane with inverse domains prepared at pH: (A) 8.5 and (B) 9.0.

Figure S2

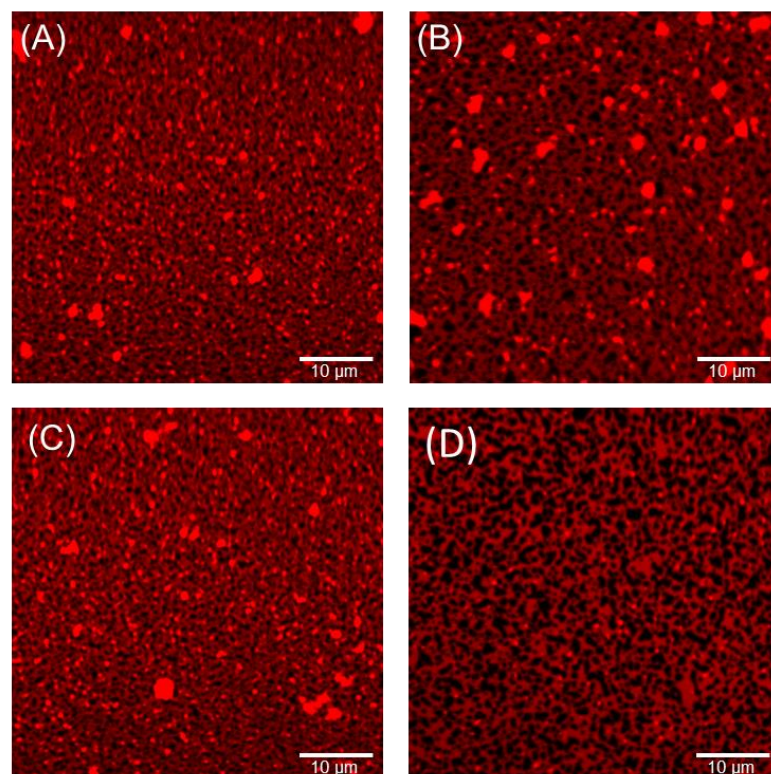


Figure S2 Fluorescence images of supported lipid bilayers with L_{α} phase labeled with Atto 633 dye and no labeling of L_o phase, formed at pH: (A) 2.2, (B) 3.7. Reorganization of the L_o domains in SLBs prepared at pH 2.2 imaged (C) right after preparation, (D) 24h after preparation.

Figure S3

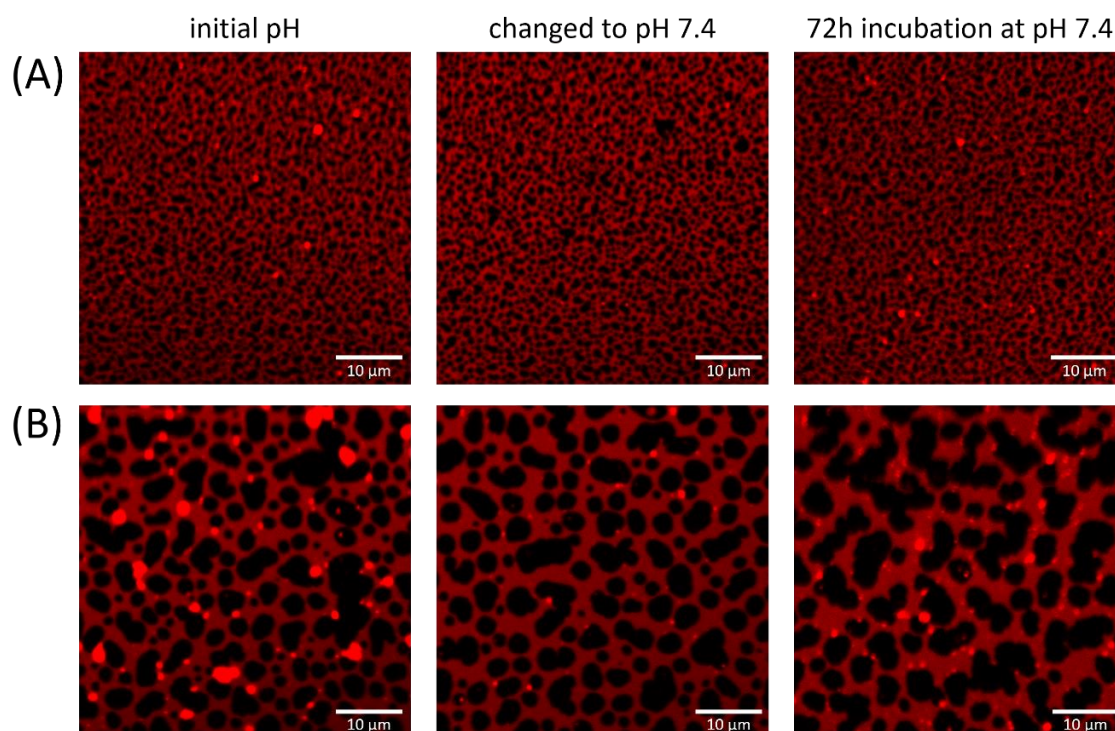


Figure S3 Preparation of SLBs at pH (A) 4.2 and (B) 9.0 with subsequent replacement of the buffer with pH 7.4 and further incubation at pH 7.4 for 72h. The use of a buffer with specific pH allows the formation of domains with controlled size. Changing the buffer to pH 7.4 did not influence the architecture of the membranes. Once formed domains with the specific size remain stable for at least 72h in neutral conditions.

Figure S4

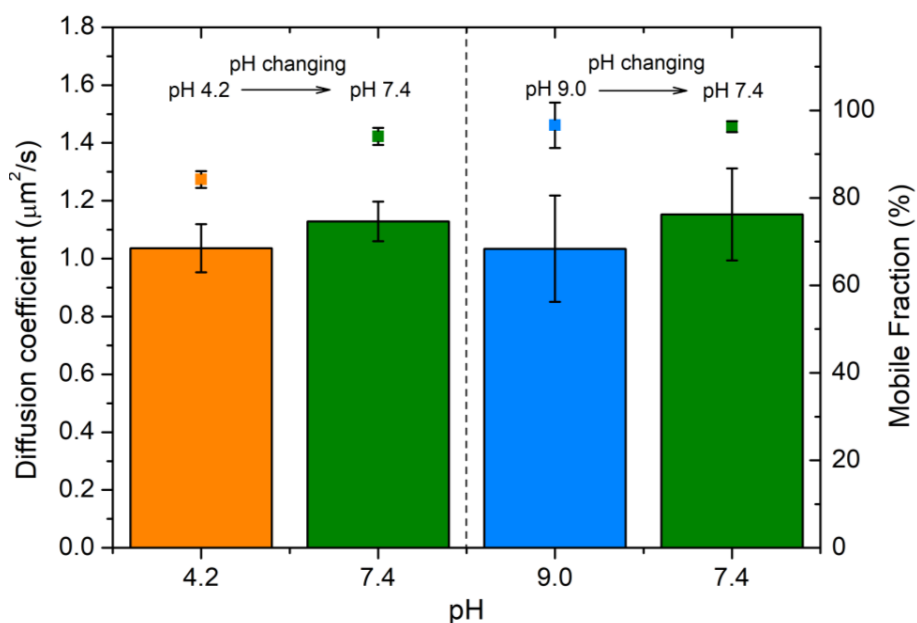


Figure S4 Diffusion coefficient (bar plot) and mobile fraction (scatter plot) before and after changing of the buffer from pH 4.2 to pH 7.4 and from pH 9.0 to pH 7.4. The diffusion coefficient of the lipids doesn't change upon replacement with the buffer of neutral conditions (pH 7.4).

Figure S5

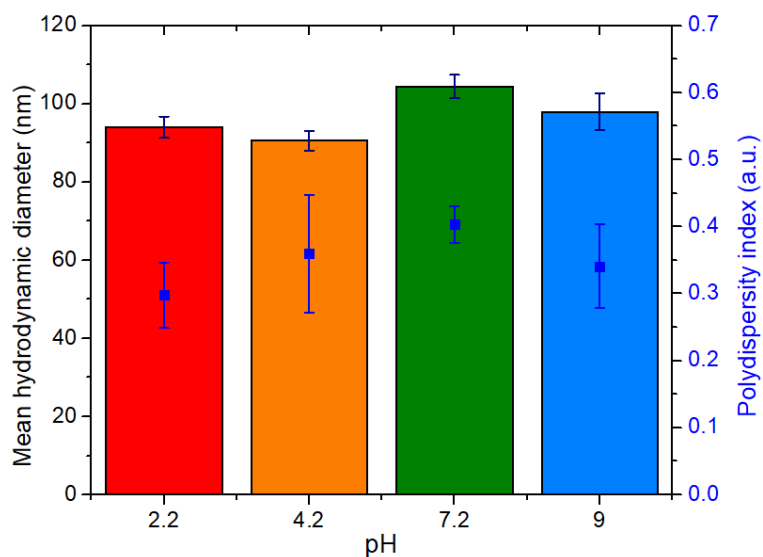


Figure S5 Mean hydrodynamic diameter and polydispersity index of vesicles prepared at pH 2.2, 4.2, 7.2 and 9.0, determined by DLS measurements. The hydrodynamic diameter was similar (~100 nm) for all tested pH values, and was characteristic for SUVs prepared by the sonication method.

Figure S6

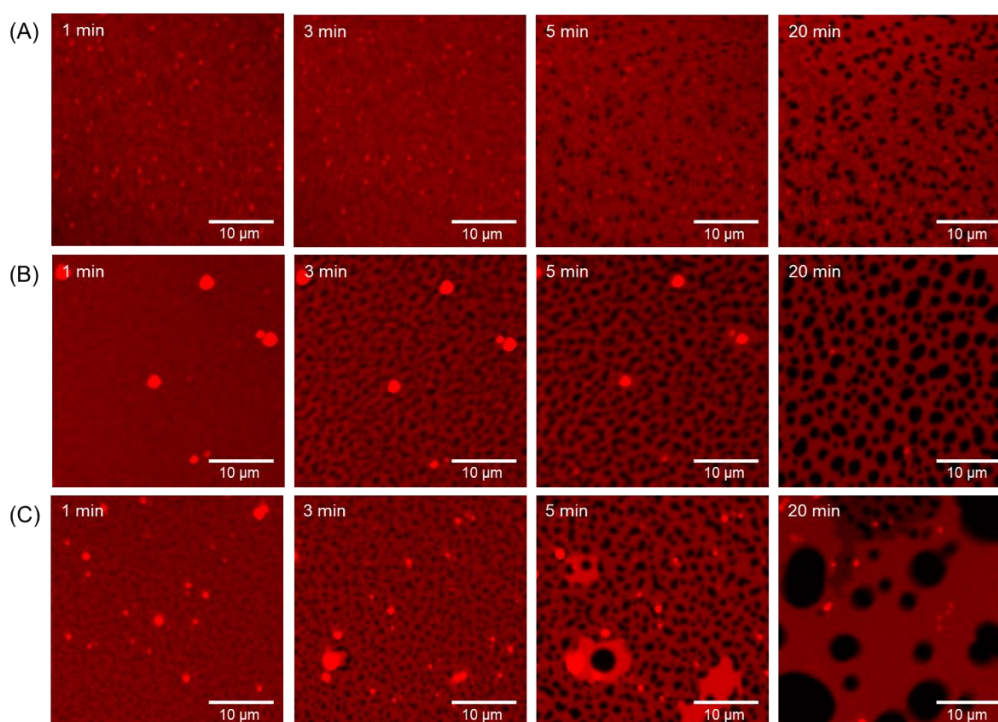


Figure S6 Fluorescence images of the domains formation process at pH: (A) 4.2, (B) 7.2, (C) 9.0. Lipid membranes were prepared on the hot plate at 60 °C and the process of nucleation and domains growth was observed over time. Domains nucleation for the SLB prepared at pH 4.2 was visible after 5 min. but the quantification was possible after 20 min. when the size of the domains was bigger than the resolution limit of the confocal microscope. Domains of L_0 phase for pH 7.2 and 9.0 were visible 3 min after removal from the hot plate. For all tested pH the growth significantly slowed down 1h after the removal from the hot plate, when domains reached the characteristic size for each pH.

Chapter 6

Nanoscale structural response of biomimetic cell membranes to controlled dehydration

The genesis of phase separation and the dimensions of the resulting ordered phase domains are influenced by a dynamic interplay of molecular interactions between membrane constituents, among them we can distinguish lipid-lipid [3], and lipid-protein interactions [33]. Moreover, membrane segregation into phases is affected by external-environmental factors such as temperature, pH, or hydration [46]. In the following publication, I focused on the last factor, which is the presence of water - molecules indispensable for sustaining life in all organisms. Water exerts a distinct influence on the membrane, especially in the presence of the so-called hydrophobic mismatch, a phenomenon that arises when the thickness of different membrane constituents does not match, resulting in the exposure of hydrophobic moieties to water [181]. This hydrophobic interaction is energetically unfavorable and is considered to be one of the primary mechanisms driving the phase separation in membranes of living cells and in biomimetic models [51]. Indeed, the bigger the hydrophobic mismatch between L_o and L_d phases, the stronger is the line tension at their boundary, which consequently leads to the increased degree of membrane phase separation, expressed as the formation of larger L_o phase domains [34]. While water undeniably plays a pivotal role in organizing cell membranes and forming regions comprised of molecules with similar heights, its impact on parameters such as hydrophobic mismatch and line tension remains not fully understood.

In this publication, I undertook the challenge of unraveling the nanoscale structural response of the phase-separated SLBs to a wide range of hydration conditions (Figure 6.1). Using the developed in our research group method I was able to not only track the structural reorganization of membranes under varying hydration conditions but also in a state of complete desiccation, importantly without the introduction of any membrane stabilizing agents or mechanical modifications of the solid support. Fluorescence microscopy imaging revealed significant changes in the shape of the L_o domains, which with lowering the hydration were characterized by a more jagged perimeter and decreased circularity. The analysis of the intensity of L_d -labeling fluorescent probe DOPE-Atto 633 within L_o phase regions, pointed out towards increased migration of lipids forming L_d phase inside membrane domains. To overcome the diffraction limit of the fluorescence microscope and

investigate the nanoscale structural reorganization of the membrane, I performed AFM measurements. The decreasing of the membrane hydration state led to an enhanced mixing of lipids forming the L_d phase with those composing the L_o phase. Analysis of AFM height profiles allowed the calculation of the height mismatch between phases, which was 2-fold lower for completely desiccated membrane than for fully hydrated. This was associated with a 3-fold decrease in the line tension. Importantly, this process was entirely reversible, and upon subsequent rehydration, the height mismatch returned to its initial value.

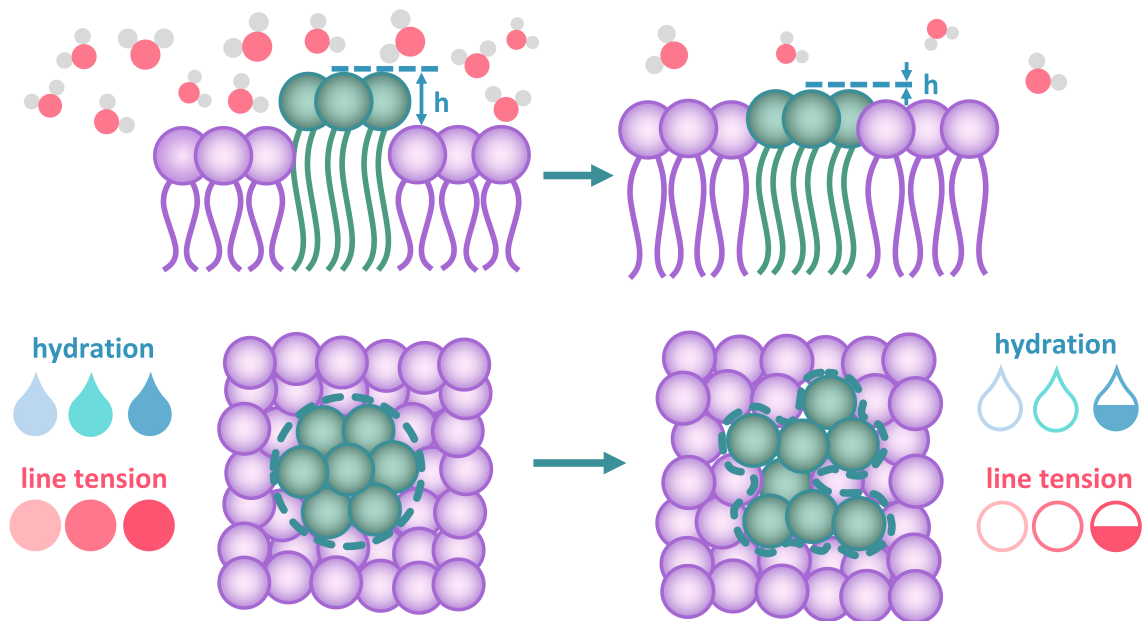
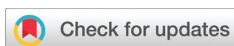


Figure 6.1: Graphical representation of the key findings presented in publication 2.

It should be noted that this research is novel in two areas: science and engineering. First of all, it broadens our understanding of processes that require transient, local dehydration of the cell membranes, such as endo- and exocytosis, viral entry, fertilization, and various cell fusion events. Secondly, it highlights a new methodology of AFM measurements under varying hydration conditions, which can successfully be applied to study other model cell systems.

Cite this: *Nanoscale*, 2024, **16**, 72

Nanoscale structural response of biomimetic cell membranes to controlled dehydration†

 Emilia Krok, ^{*a} Henri G. Franquelim, ^{b,c} Madhurima Chattopadhyay, ^a Hanna Orlikowska-Rzeznik, ^a Petra Schuille ^b and Lukasz Piatkowski ^{*a}

Although cell membranes exist in excess of water under physiological conditions, there are a number of biochemical processes, such as adsorption of biomacromolecules or membrane fusion events, that require partial or even complete transient dehydration of lipid membranes. Even though the dehydration process is crucial for understanding all fusion events, still little is known about the structural adaptation of lipid membranes when their interfacial hydration layer is perturbed. Here, we present the study of the nanoscale structural reorganization of phase-separated, supported lipid bilayers (SLBs) under a wide range of hydration conditions. Model lipid membranes were characterised using a combination of fluorescence microscopy and atomic force microscopy and, crucially, without applying any chemical or physical modifications that have previously been considered essential for maintaining the membrane integrity upon dehydration. We revealed that decreasing the hydration state of the membrane leads to an enhanced mixing of lipids characteristic of the liquid-disordered (L_d) phase with those forming the liquid-ordered (L_o) phase. This is associated with a 2-fold decrease in the hydrophobic mismatch between the L_d and L_o lipid phases and a 3-fold decrease in the line tension for the fully desiccated membrane. Importantly, the observed changes in the hydrophobic mismatch, line tension, and lipid miscibility are fully reversible upon subsequent rehydration of the membrane. These findings provide a deeper insight into the fundamental processes, such as cell–cell fusion, that require partial dehydration at the interface of two membranes.

Received 26th June 2023,
Accepted 15th November 2023
DOI: 10.1039/d3nr03078d
rsc.li/nanoscale

1 Introduction

Biological cell membranes are permeable barriers responsible for maintaining homeostasis and protecting the cell from the surrounding environment.¹ They act as gateways, mediating the selective transport of ions and biomacromolecules such as glucose or amino acids.² They also play a key role in cell compartmentalisation, allowing mutually exclusive biochemical processes to occur simultaneously within the cell.³ The study of cellular membranes in their native form is very challenging due to the high structural complexity of these systems and the plethora of chemical, biological and physical processes that occur within the cell. For this reason, model biological cell

membranes are often used, such as giant unilamellar vesicles (GUVs) or supported lipid bilayers (SLBs), which have analogous physical and structural properties to native cell membranes, but at the same time can be modified and simplified to focus on specific biophysical properties.^{4–9}

The lateral organisation of lipid membranes is driven by the interplay of lipid–lipid and lipid–protein interactions.¹⁰ However, this biological system is not complete without water, the presence of which is considered to be an indispensable factor that modulates the structural organisation of membranes, phase separation, as well as the spatial arrangement of transmembrane proteins, both in model membrane systems and living cells.^{11–13} Water acts on the membrane in particular in the presence of the so-called hydrophobic mismatch, which occurs when the thickness of different membrane constituents is different, leading to an exposure of the hydrophobic moieties to water.¹⁴ This hydrophobic interaction is energetically unfavourable and is therefore one of the main mechanisms driving the phase separation.¹⁵ García-Sáez *et al.* modified the thickness of the disordered phase using phosphatidylcholines with different acyl chain lengths and showed that the bigger the difference between the hydrophobic parts of the membrane, the stronger the phase separation, and the higher the

^a Poznan University of Technology, Faculty of Materials Engineering and Technical Physics, Institute of Physics, Piotrowo 3, 60-965 Poznan, Poland.

E-mail: emilia.krok@put.poznan.pl, lukasz.j.piatkowski@put.poznan.pl

^b Department of Cellular and Molecular Biophysics, Max Planck Institute of Biochemistry, Am Klopferspitz 18, 82152 Martinsried, Germany

^c Leipzig University, Research and Transfer Center for Bioactive Matter, Deutscher Platz 5, 04103 Leipzig, Germany

† Electronic supplementary information (ESI) available. See DOI: <https://doi.org/10.1039/d3nr03078d>



line tension at the boundary between the two phases.¹⁶ Line tension is also responsible for the self-healing properties of the cell membranes by facilitating the closure of transient pores within the structure of the lipid bilayer.¹⁷ Line tension for single component membranes can be determined by inducing the formation of transient pores in the membrane structure and observing the rate of pore closure. Srividya *et al.* showed that the line tension in single phase membranes increases with the acyl chain length of the constituting lipids.¹⁸

Although lipid membranes under natural conditions indeed exist in excess of water, there are biological processes that require at least partial interfacial dehydration of lipid bilayers. Processes such as endo- and exocytosis,¹⁹ neurotransmission,²⁰ viral entry,²¹ fertilization,²² or cell fusion during embryogenesis²³ and morphogenesis²⁴ involve the fusion of two lipid membranes. All of these membrane fusion events rely on interactions between lipids, proteins, and water hydrating the two interfacing membranes.²⁵ When the two bilayers come in close contact and the distance between them is reduced to about 2–3 nm, a strong hydration repulsion, also known as the “hydration force”, occurs between their hydrophilic surfaces.^{26–28} At this stage the thin water layer separating the membranes must be expelled for hemi-fusion to occur.

Thus, to fully understand the intricate interactions between membrane constituents and the membrane hydration layer, as well as the biophysical consequences of these interactions, it is crucial to gain insight into the structural properties of cellular membranes when their hydration state is altered. Indeed, Chiantia *et al.* reported on the structure of SLBs composed of DOPC/SM/cholesterol under conditions of complete dehydration using atomic force microscopy (AFM).²⁹ They showed that in the absence of stabilising agents such as trehalose, the membranes lose their integrity upon abrupt dehydration and subsequent rehydration and severe structural damage is observed in the form of holes, aggregates and delimitation of membranes.³⁰ Similar results were reported by Iriarte-Alonso *et al.* for single-component DOPC membranes, where abrupt dehydration resulted in the formation of multiple defects and holes, and consequently loss of membrane continuity.³¹ Many attempts have been made to preserve the structure of desiccated lipid membranes and prevent them from rapid vesiculation. These include the use of saccharides, which are known to increase the spacing between lipids in the dry state and thus prevent them from collapsing,^{30,32} the modification of lipid head groups to improve the interactions between the lipids and the solid support^{33–35} or the introduction of physical confinement, which prevents the interfacial peeling force from causing destructive membrane delamination.³⁶ All of these approaches, although successful in membrane preservation, involve alteration of the native properties of lipid membranes due to the introduced chemical or physical modifications of either the membrane or the solid support. Recently, we presented a novel method for membrane preservation under dehydration conditions based on the controlled steady

decrease of environmental humidity, which provides new possibilities to study the behavior and properties of membranes without altering their chemical composition or physical features.^{37,38}

In this study, we have used a combination of fluorescence and atomic force microscopy to investigate the nanoscale structural response of phase-separated SLBs to a wide range of hydration conditions. Our results demonstrate that the structure of lipid membranes can be preserved even under conditions of complete desiccation without the use of stabilising agents, if the dehydration process is carried out in a gradual and controlled manner. The dehydration method used here allowed the overall structural organisation of the membrane to be maintained without the appearance of defects or holes. At the same time, the removal of bulk water led to a prominent nanoscale structural reorganisation within the membrane. We observed that the dehydration process causes a significant decrease in the hydrophobic mismatch between the L_d and L_o phases, and consequently lowers the line tension at their interface. Importantly, this process is fully reversible and upon subsequent rehydration, the height mismatch increases to its initial state. We show that the removal of bulk water leads to an extensive mixing of the liquid-disordered (L_d) and liquid-ordered (L_o) phase lipids and changes in the borderline of the L_o phase domains. Finally, the present study employs a pioneering methodology of AFM measurements under controlled humidity, which can be applied to study other model cell systems under varying hydration conditions.

2 Materials and methods

2.1 Materials

1,2-Dimyristoleoyl-*sn*-glycero-3-phosphocholine (14:1 PC or DMOPC), egg yolk sphingomyelin (SM), and cholesterol were purchased from Avanti Polar Lipids, Alabaster AL., USA. Monosialoganglioside (GM1) from bovine brain, 1,2-dioleoyl-*sn*-glycero-3-phosphoethanolamine labeled with Atto 633 (DOPE-Atto 633), sodium hydroxide (NaOH), calcium chloride (CaCl_2), and sodium chloride (NaCl) were purchased from Merck KGaA, Darmstadt, Germany. Alexa Fluor 488 conjugated with a cholera toxin B subunit (CTxB-Alexa 488) was obtained from Molecular Probes, Life Technologies, Grand Island, NY, USA. *N*-2-Hydroxyethyl piperazine-*N'*-2-ethane sulphonic acid (HEPES PUFFERAN) was obtained from Carl Roth GmbH & Co KG, Karlsruhe, Germany. All the materials and reagents were used without further purification. Optical adhesive glue Norland 68 was purchased from Norland Products Inc., Cranbury, NJ, USA. Ultrapure water was obtained using a Milli-Q reference water purification system from Merck KGaA, Darmstadt, Germany.

2.2 Vesicles' preparation

Multilamellar vesicles (MLVs) were formed by dissolving DMOPC, SM, and cholesterol in chloroform in a 1:1:1 molar ratio with the addition of 0.1 mol% of DOPE-Atto 633 dye,



resulting in a 10 mM solution of the lipids. For the representative fluorescence imaging purposes 0.1 mol% of GM1 was added for further labelling with CTxB-Alexa 488. The lipid mixture was dried under nitrogen gas for 20 minutes, leaving a thin film of lipids deposited on the bottom of the vial. The dried lipid mixture was further desiccated in a vacuum dry chamber for at least 2 h to ensure the complete removal of the organic solvent. The lipids were resuspended in a buffer solution (10 mM HEPES and 150 mM NaCl, pH adjusted to 7.4 with NaOH) and subjected to four cycles of heating on a hot plate at 60 °C and vortexing. Each heating and vortexing step was performed for 1 min. 10 µL aliquots of the lipid suspension containing MLVs were distributed into new sterilised glass vials and stored at -20 °C until further use.

2.3 SLB preparation

SLBs were formed using a previously reported method.³⁹ Briefly, lipid vesicles were diluted 10 times to a final lipid concentration of 1 mM by addition of HEPES buffer. Aliquots containing MLVs were sonicated in a Bransonic 1800 ultrasonic bath for 10 min to generate small unilamellar vesicles (SUVs). To prepare a solid support for lipid deposition, a thin layer of freshly cleaved mica was glued using UV-activated glue onto a round glass coverslip. A half-cut 2 ml Eppendorf tube was placed on top of the coverslip and sealed with silicone to provide a temporary water reservoir necessary for SLB formation, incubation and washing. 100 µL of SUV solution was deposited on top of the mica. 2 µL of 0.1 M CaCl₂ was added to promote vesicle bursting, followed by the addition of 600 µL of buffer (10 mM HEPES and 150 mM NaCl). 9 µL of 0.01 mM CTxB-Alexa 488 was added only to the SLBs containing GM1 to label the L_o phase domains. The two-color labelling (DOPE-Atto 633 for the L_d phase and GM1 CTxB-Alexa 488 complex for the L_o phase) was used only for the preparation of the representative images to ensure the reader that the membranes were free of holes and defects in both the L_d and L_o phases at each hydration level. All other data (fluorescence and AFM) were acquired on SLBs labelled with the L_d phase probe only to exclude the potential impact of GM1 on the membrane response to dehydration. The sample was incubated for 40 min and then washed to remove the excess vesicles with a total of 20 ml of Milli-Q water. Unless otherwise stated, Milli-Q water was used instead of HEPES buffer for washing to avoid the possible formation of salt crystals on top of the membrane during dehydration. After the final washing step, the Eppendorf tube was gently removed and the sample was transferred to the AFM holder, which was then filled with Milli-Q water to allow proper hydration. For measurements under different hydration conditions, the bulk water was gently removed with a pipette and the sample was mounted in the coverslip holder. Nitrogen gas at >90% RH was immediately flushed through the two ports of the AFM holder.

2.4 Hydration control

Control over the membrane hydration state was done using a home-made control unit as previously described.³⁷ The relative

humidity (RH) of nitrogen gas was adjusted and maintained by mixing wet (saturated with water vapour, 95% RH) and dry (~5% RH) N₂ gas. The final relative humidity and temperature of the N₂ gas were continuously monitored using an electronic thermohygrometer in a range of 0–95% RH and an accuracy of 1%. Samples were exposed to a RH of 90% (62 × 10¹⁹ water molecules per min), 70% (48 × 10¹⁹ water molecules per min), 50% (34 × 10¹⁹ water molecules per min), and 30% (20 × 10¹⁹ water molecules per min), and completely dry conditions (~5% RH) during dehydration and rehydration cycles. It should be noted that although the relative humidity of the environment in which the SLB is placed is not a direct property of the lipid membrane, we present our results in terms of RH throughout the manuscript because this is the parameter that we directly controlled in the experiments. However, the environmental RH can be directly translated into a hydration state of the lipid membrane, expressed in terms of the number of water molecules per lipid molecule, as shown in previous works.^{37,40,41} Briefly, the conversion is based on the experimental data of Hristova *et al.* (X-ray diffraction) and of Piatkowski *et al.* (infrared spectroscopy), which showed that stacked DOPC lipid bilayers equilibrated at 95% RH contain approximately 11–12 water molecules per lipid in their first hydration shell.^{40,41} Lower RH values of 75, 50, and 25% correspond to approximately 6.3, 3.6, and 2.4 water molecules per lipid, respectively. SLBs were incubated at each hydration state for approximately 30 min prior to imaging to ensure proper equilibration of the membrane.

2.5 AFM imaging

AFM measurements were performed using a NanoWizard III system from JPK Instruments, Berlin, Germany, mounted on a Zeiss LSM 510 Meta fluorescence microscope. Measurements were performed using a Biolever Mini cantilever (BL-AC40TS-C2) from Olympus, Tokyo, Japan. Images were acquired in contact mode using a silicon tetrahedral tip with a radius of 10 nm and a spring constant of 0.09 N m⁻¹. The scan rate was set to 1–2 Hz. The force was kept as low as possible. Both topography and deflection (error) signals were measured simultaneously for the trace and retrace directions. The images were post-processed by applying line fitting, which corrects for the offset within the image, using JPK processing software from JPK Instruments, Berlin, Germany. Final image analysis was performed using ImageJ⁴² and Gwyddion software.⁴³ Height mismatch between phases was determined by analyzing height distribution histograms.

2.6 Line tension calculation

Line tension was calculated based on the theoretical model developed by Cohen *et al.*, in which the line tension is directly related to the height mismatch between the L_o and L_d phases:¹⁴

$$\gamma = \frac{\sqrt{B_s K_s B_r K_r}}{\sqrt{B_r K_r} + \sqrt{B_s K_s}} \cdot \frac{\delta^2}{h_0^2} - \frac{1}{2} \cdot \frac{(J_s B_s - J_r B_r)^2}{\sqrt{B_r K_r} + \sqrt{B_s K_s}} \quad (1)$$



where γ is the line tension, δ is the phase height mismatch, h_o is the monolayer thickness, B is the elastic splay modulus, K is the tilt modulus and J is the spontaneous curvature of the monolayer. The monolayer thickness is defined as an average thickness of L_d (h_s) and L_o phase (h_r) monolayers:

$$h_o = \frac{(h_r + h_s)}{2} \quad (2)$$

Following the model assumptions presented by García-Sáez *et al.*, we considered the values of $B_r = B_s = 10$ kT, $K_r = K_s = 40$ mN m⁻¹, and $J_r = J_s = 0$, which describe the scenario of “soft” domains.¹⁶ We determined that the thickness of the DMoPC bilayer (L_d phase) measured at 90% RH was 3.87 ± 0.21 nm, while the thickness of the L_o phase was calculated by adding the value of the height mismatch between the two phases to the height of the L_d phase.

2.7 Confocal imaging

Confocal imaging for sample localisation prior to AFM measurements was performed on a Zeiss LSM 510 Meta Carl Zeiss, Jena, Germany, using a 20x, 0.75NA objective. Confocal images were obtained by using the excitation light from a He-Ne laser at 633 nm for Atto 633 and an Ar laser was used for excitation of Alexa Fluor 488. Emission was collected in the wavelength range of 645–797 nm for the red light channel (Atto 633 detection) and 495–530 nm for the green light channel (Alexa Fluor 488). High quality images were obtained by using a Zeiss 710 microscope with a 40x 1.3 NA oil immersion objective. Minimal laser power was used in all imaging experiments to minimise photobleaching. To quantify the shape of the lipid domains based on the confocal images obtained at different hydration states, the circularity parameter was calculated as follows:

$$\text{circularity} = 4\pi \frac{\text{area}}{\text{perimeter}^2} \quad (3)$$

Image processing and calculation of domain circularity were done using ImageJ/Fiji software.⁴⁴

3 Results and discussion

3.1 Analysis of fluorescence in dehydrated lipid membranes

Nanoscale characterisation of the supported lipid bilayers (SLBs) in different hydration states has been carried out for membranes reconstituted from a ternary lipid mixture of DMoPC/SM/cholesterol in a molar ratio of 1 : 1 : 1. This membrane composition leads to the formation of L_o domains enriched in sphingomyelin and cholesterol embedded in the L_d phase composed of more loosely packed PC lipids. The structure of the membranes with this lipid composition has been well characterised in the literature in terms of domain size and shape¹⁶ and membrane dynamics⁴⁵ under conditions of full hydration, where the membrane is embedded in an aqueous environment. In contrast, here we focused on elucidating the structural properties of lipid bilayers in a wide range of hydration states: from full hydration (bulk hydration)

to dry membranes containing only a few water molecules per lipid. The degree of membrane hydration was tuned and controlled using the previously described humidity control setup schematically shown in Fig. 1a, in which water-enriched nitrogen is supplied directly to the membrane (see Materials and methods).³⁷ The coupling of a confocal microscope with an AFM system allowed the simultaneous observation of microscale and nanoscale changes in the lateral organisation of the membrane as a function of its hydration state. Analysis of the fluorescence images showed that the overall membrane structure was unaffected by dehydration. Despite the small number of vesicles and aggregates that were deposited on top of the bilayer during dehydration, the membrane remained intact with readily distinguishable phase separation.

However, as the hydration of the membrane is reduced, small changes in the shape of the L_o domains become apparent in the form of a more jagged perimeter of the L_o phase domains, as shown in Fig. 1b. To provide quantitative information about these differences in the domain shape, we calculated the circularity parameter by analysing all clearly resolvable domains from at least four images of two different samples. The domain circularity decreased with decreasing humidity, as shown in Fig. 2a. Under fully hydrated conditions the domain circularity was 0.82 ± 0.02 , while at 5% RH it decreased to 0.51 ± 0.01 . To verify that the changes in domain circularity were caused solely by the hydration state of the membrane, we performed additional experiments, where after 0.5 h of incubation time at 70% RH, the membrane was monitored for a further 0.5 h under exactly the same humidity conditions to record any potential changes in the shape and circularity of the L_o phase domains. As shown in Fig. S1a and b,† there were no visible changes in the shape or distribution of the domains. Quantitative analysis confirmed this result (Fig. S1c†) – the calculated circularity parameters were the same: 0.61 ± 0.07 and 0.63 ± 0.07 , measured immediately after sample equilibration to 70% RH and after 30 min of further incubation under the same humidity conditions, respectively. It should be noted that the subsequent restoration of high membrane hydration led to the reappearance of domain circularity. The domain circularity values corresponding to the specific hydration levels were the same for the dehydration and rehydration trajectories within the range of 5–70% RH. However, at 90% RH during the rehydration cycle, the domain circularity decreased to a value of 0.53 ± 0.03 (see the purple triangle in Fig. 2a). As shown in Fig. S2a and b,† we observed that at this value of environmental humidity, the domains largely merged and formed elongated structures composed of a few integrated domains, leading to a significant decrease in the circularity parameter. In agreement with our previous reports, under high humidity conditions the lipids regain their initial mobility, which favours the merging of the lipid domains.³⁷ In addition to the global analysis (of the entire images) of the circularity of the L_o phase at 90% RH, we also analysed 25 domains that did not undergo merging (see Fig. S2c†) and observed that their circularity regained the initial value upon rehydration.



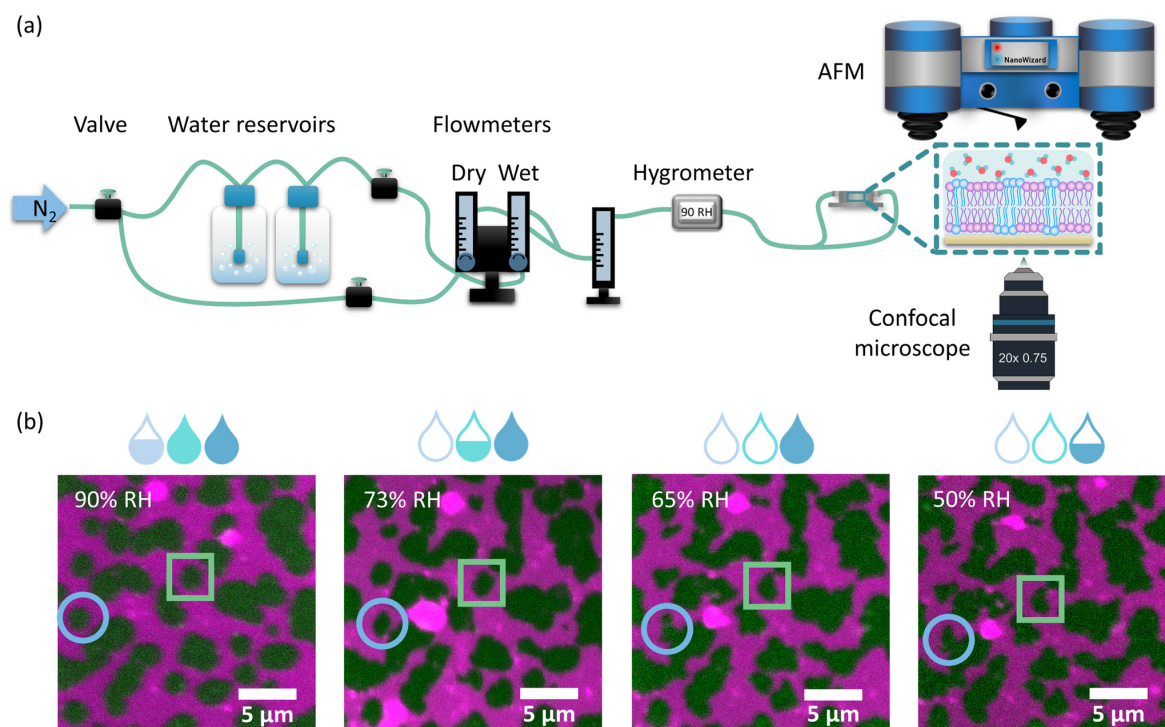


Fig. 1 (a) Schematic representation of the home-built humidity control setup, which allows simultaneous AFM and confocal measurements of biomimetic cell membranes under varying hydration conditions. The setup consists of a source of nitrogen gas (N₂), two reservoirs of water, 3 flow meters, providing information on the dry, wet and final flow reaching the sample, 3 manual valves for precise control of the flow rate, and an electronic thermohygrometer. (b) Fluorescence images of the representative SLB showing phase separation into L_d (labelled with DOPE-Atto 633, shown in magenta) and L_o (labelled with CTxB-Alexa 488, shown in green) domains under different hydration conditions of: 90% RH, 73% RH, 65% RH, and 50% RH. Domains of the L_o phase become less circular with decreasing hydration level (see, e.g. domains indicated by blue circles and green squares). Experiments were carried out in 10 mM HEPES and 150 mM NaCl buffer.

The observed changes in the shape of the L_o domains suggest an increased miscibility of the lipids composing both phases. If indeed true, this could also be manifested in the fluorescence signal, as one would expect higher L_d label fluorescence intensity within the L_o phase, due to lipid admixing. To monitor whether the compositional changes occurred within the domains of the L_o phase, we measured the average fluorescence intensity of the L_d phase labelling dye DOPE-Atto 633 within the domains (I_D) and divided this by the average intensity of this dye at 1 μm from the domain boundary (I_N). By taking the ratio (I_D/I_N) of the fluorescence intensities measured within the L_o domain and immediately adjacent within the L_d phase, we ensure that any potential mechanisms affecting the detected fluorescence signal of the dye in both phases, such as for instance a change in the quantum efficiency of the dye or focusing of the objective (hence the fluorescence collection efficiency), are divided out. Interestingly, we observed more than a 3-fold increase in the I_D/I_N ratio for the membranes equilibrated at 90, 70, 50, 30, and 0% RH compared to the membrane containing bulk water as shown in Fig. 2b. Upon dehydration, there was a clear

increase in the fluorescence intensity of DOPE-Atto 633 within the L_o domains. The observed increase in fluorescence may in principal be due either to the increased migration of lipids from the L_d phase to the L_o phase or to changes in the photo-physical properties of the label fluorophore. To investigate this, we performed additional control experiments and determined the changes in the fluorescence intensity as a function of membrane hydration for a single component, non-phase separated SLB composed of 14 : 1 PC doped with 0.1 mol% of DOPE-Atto 633 (please see ESI note 1 and Fig. S3† for control experiments and further discussion). We found that dehydration increased the detected fluorescence signal by a factor of approximately 1.6 (Fig. S3a†). Given the very high fluorescence quantum yield (QE) of Atto 633 (64% in water), it is not physically possible that the observed increase is solely due to the increase in the QE of the dye, as this would indicate that the QE increases to a value >100%. It should be noted here that the optical properties of the studied system also change as a function of hydration. In particular, the fluorescence collection efficiency is affected by the refractive index of the medium in which the emitting dipoles are placed.⁴⁶ In bulk water, fluo-



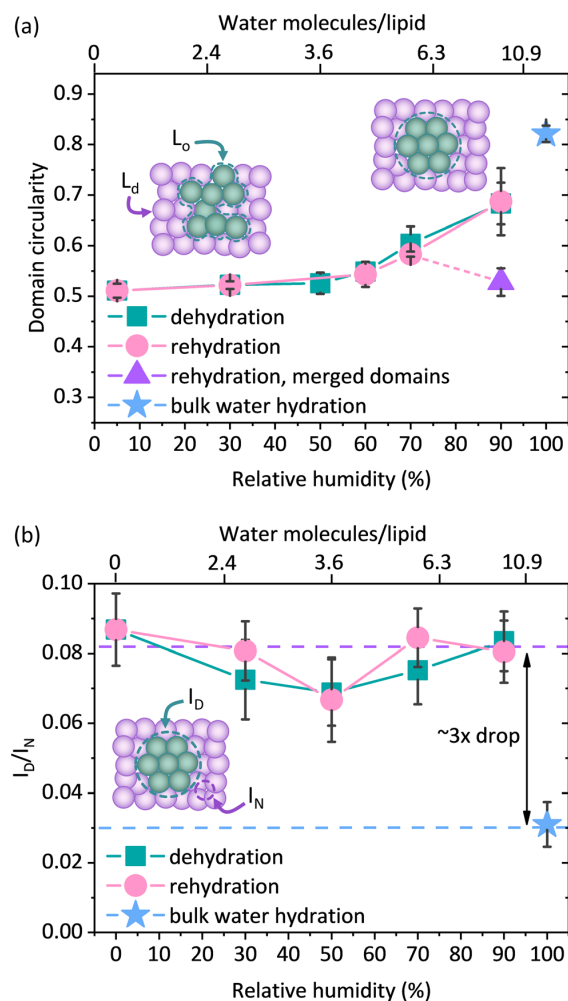


Fig. 2 (a) Circularity of the L_o phase domains calculated from the confocal images for the fully hydrated sample during the cycle of dehydration (90, 70, 60, 50, 30, and 5% RH) and subsequent rehydration (5, 30, 60, 70 and 90% RH). The violet triangle corresponds to the domain circularity calculated for 25 unmerged domains from three different areas. (b) Fluorescence intensity within the domain (I_D) divided by the intensity in the region adjacent to the domain (I_N) as a function of membrane hydration. Experiments were performed in buffer containing 10 mM HEPES and 150 mM NaCl. Four different areas (size $50 \times 50 \mu\text{m}$) of 2 individual SLBs were analysed. Each area contained approximately 200 domains. The bottom x-axis shows the values of relative humidity, which can be correlated with the number of water molecules per lipid (see the upper x-axis).

rescence is emitted more symmetrically with respect to the substrate plane, whereas under dehydrated conditions, fluorescence is emitted predominantly towards the substrate. Thus, the observed increase in the fluorescence intensity of DOPE-Atto 633 in the single component membrane most likely includes a contribution from the optical effects. Regardless of the exact contributions of the effects discussed above (which

are very difficult, if not impossible, to disentangle), we clearly observed (Fig. S3b†) that the fluorescence signal of Atto 633 increases much less in the L_d phase ($\sim \times 1.5$) than in the L_o phase ($\sim \times 4.7$). In fact, if the redistribution of DOPE-Atto 633 were the only (or main) mechanism, then one should observe an increase in the fluorescence intensity in the L_o domain and a decrease (by the same absolute amount) in the fluorescence intensity in the adjacent L_d phase area. Indeed, if we correct the observed increase in fluorescence intensity in the L_o/L_d phases by a factor of 1.6, determined from the single-component membrane, we found (Fig. S3c†) that the fluorescence intensity in the L_o phase increases by approximately 600 counts, whereas in the L_d phase we observed a decrease in fluorescence intensity by approximately 600 counts. The observed changes, *i.e.* the decrease in fluorescence in the L_d phase and the increase in fluorescence in the L_o phase, correlate very well. All the evidence suggests that the observed 3-fold increase in fluorescence intensity is due to the diffusion of the Atto dye-carrying lipids from the disordered to the ordered phase.

Altogether, the analysis of domain circularity and fluorescence intensity within the L_o domains consistently points toward the enhanced lateral reorganisation of the membrane constituents under dehydration conditions. The size of the ordered phase domains in this study was approximately $1\text{--}5 \mu\text{m}^2$, so the details of the structural reorganisation are hidden below the resolution limit of the fluorescence microscope and could not be resolved based on the fluorescence signal.

3.2 Nanoscale structural changes under dehydration conditions

The macroscopic structural analysis of the SLBs under different hydration conditions suggests a structural rearrangement of the lipids at the nanoscale. To identify the exact origin of the observed changes within the lipid domains, we used AFM imaging. A home-built hydration setup was connected directly to the AFM JPK coverslip holder *via* perfusion inlets, allowing for continuous gas flow within the chamber, as shown in Fig. 1a. In the presence of excess water, we observed a well-defined phase separation as shown in Fig. 3a (bulk water). The unlabelled areas measured by confocal microscopy corresponded to the more protruding regions detected by AFM and are identified as L_o phase lipid domains.⁴⁷ Lipid domains under fully hydrated conditions had a round shape with smooth edges. Upon removal of bulk water and a subsequent gradual decrease in membrane hydration, the boundaries between the L_o and L_d phases became jagged, as shown in Fig. S4† (90–5% RH). At the same time, we observed the formation of small areas of lower height, which we attributed to the L_d phase nanodomains formed within the L_o phase domains, reminiscent of admixing phenomena recently observed for similar mixtures of photoswitchable lipids.^{48,49} Measurements immediately after the removal of bulk water required constant adjustment of the applied force and performing of many scans to remove aggregates deposited on top



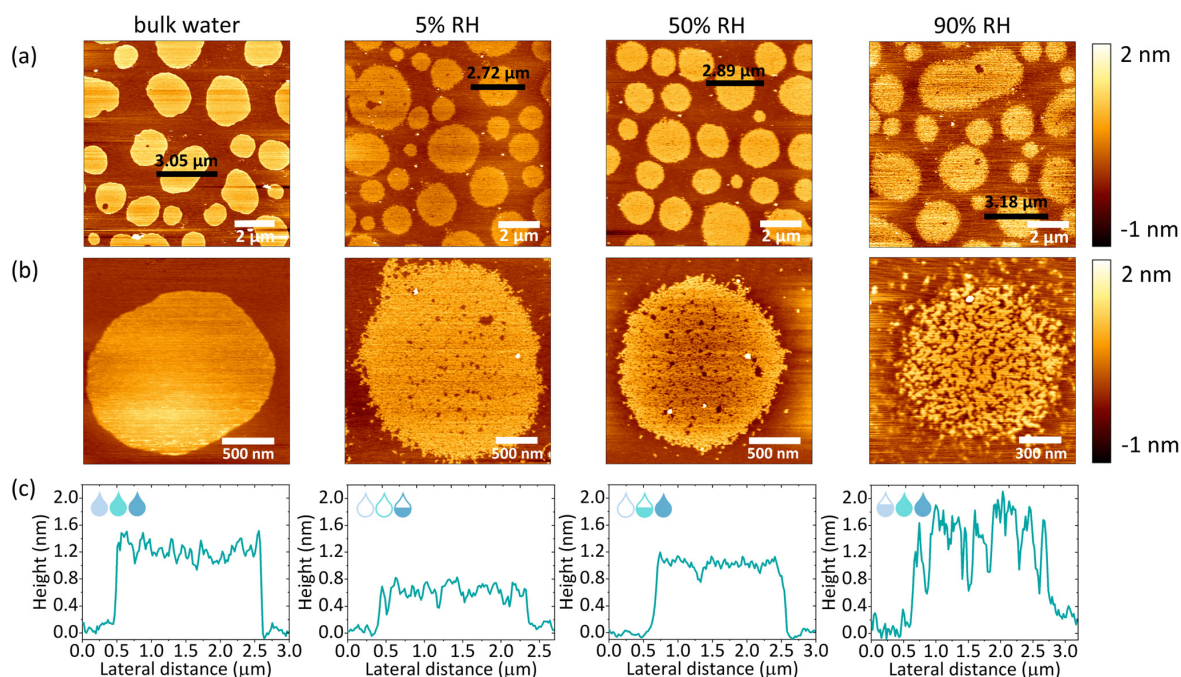


Fig. 3 (a) Representative images of the fully hydrated SLB and SLBs after removal of bulk water and equilibrated at 5, 50 and 90% RH. (b) High-resolution images of single domains at different hydration levels (bulk water hydration, 5, 50 and 90% RH). (c) Height profiles corresponding to the black horizontal lines shown in (a).

of the membrane. In addition, at high humidity, the membrane is very sticky and adheres to the AFM tip during scanning, which can drag membrane fragments as shown in Fig. S5.† Consequently, measurements at high humidity levels required constant changing of the measured spot, thus during the dehydration cycle (Fig. S4†) we did not follow the structural reorganization of the membrane in the exact same area but rather focused on the global characterisation of the sample.

It should be emphasised that a gradual decrease in hydration did not lead to such a pronounced reorganisation of the domain shape (domain boundary) throughout the dehydration and rehydration cycles, as it was observed in the case of confocal imaging. From our previous studies, it is clear that as hydration decreases, the diffusion of lipids, as well as their mobile fraction, decreases abruptly when the number of water molecules hydrating the membrane falls below a certain value.^{37,50} At 50% RH and below, the mobility of lipids is almost completely ceased, due to the breaking of the first hydration shell surrounding a single lipid head group moiety. In addition, other recent studies of ours have shown that the dynamics of lipids under dehydration conditions is strongly influenced by the ionic composition of the buffer hydrating the membrane.⁵¹ Although lipids remain mobile in the presence of Na⁺ ions at humidity above 50% RH, their mobility is significantly reduced in MilliQ water upon dehydration to 85% RH. In the course of the measurements presented here, we decided to perform AFM scanning in the absence of salt-

enriched buffer, which could lead to salt crystallisation on the membranes. Therefore, membranes prepared in HEPES buffer, were thoroughly washed with MilliQ water to remove any residual salt. The absence of Na⁺ ions in the residual water leads to lower (<0.2 μm² s⁻¹) lipid mobility under reduced hydration conditions, explaining the lack of macroscopic circularity changes within the membranes at low humidity. However, it should be noted that although lipid mobility is affected under dehydration conditions, there was a noticeable structural reorganisation in the partially dehydrated membrane compared to the membrane under fully hydrated conditions.

After dehydration, a gradual rehydration of the membrane was performed to confirm the complete preservation of the structure throughout the entire cycle of lowering and raising the humidity. As shown in Fig. 3a and S6a,† throughout the entire rehydration process the integrity of the lipid membranes remained intact. Iriarte-Alonso *et al.* reported that pure DOPC membranes lose their structural arrangement and membrane continuity upon abrupt and complete dehydration and rehydration, resulting in an abundance of various defects and holes exposing the bare support.³¹ This gives even more importance to the dehydration method presented in our research, which allows the membrane and lipids to adapt to the slowly changing hydration state of the membrane. The high resolution images of individual domains revealed increased mixing of the L_o and L_d phases as shown in Fig. 3b and S6b.† As



shown in Fig. 3c, the AFM height profiles across the domains showed that the height mismatch between the L_d and L_o phases was different under different hydration conditions. Thus, we concluded that the more pronounced phase mixing at higher hydration values was due to two phenomena: (i) the gradual recovery of lipid mobility, leading to a more dynamic membrane reorganisation and (ii) the increase in hydrophobic mismatch between phases, promoting phase separation. Consequently, the lipids of the L_d phase separate from the L_o phase and merge to minimise the perimeter exposed to water (see Fig. S7†).

Based on the AFM images, we determined the total bilayer thickness for the membrane without bulk water (90% RH) by selecting areas with membrane defects as shown in Fig. 4a. The formation of holes was induced by applying an abrupt dehydration procedure, which is based on the rapid aspiration of water with a pipette. Moreover, in order to find ruptured parts of the membrane, we selected areas near the edges of the solid substrate, which are more susceptible to the air–water interfacial peeling force acting during dehydration. We extracted cross-sectional profiles over the areas containing three types of features: holes, and L_o and L_d phases, and found that the height difference between the L_d phase and the surface of the bare substrate was 3.87 ± 0.21 nm, which we attributed to the thickness of the DMOPC bilayer. It should be noted that this

value is in agreement with the bilayer thickness of 3.86 nm reported by Lee *et al.* for a fully hydrated membrane also composed of DMOPC lipids.⁵² From the height profiles, it was possible to distinguish the domains of the L_o phase protruding approximately 1.3 nm from the L_d phase. Furthermore, the height profiles along the domains confirmed that the intermediate height regions represent the L_d phase trapped within the L_o domains, as the height difference obtained corresponds to the L_o/L_d height mismatch (see Fig. 4b).

3.3 Hydrophobic mismatch and line tension under dehydration conditions

The preparation of lipid membranes from the ternary lipid mixture used in this study results in the formation of lipid domains composed of the L_o phase embedded in the L_d lipid matrix. AFM^{53,54} and X-ray scattering^{55,56} studies clearly show that the L_o phase, due to the presence of saturated and more densely packed lipids, is thicker than the L_d phase which contains unsaturated lipids. This results in the so-called “height mismatch” or “hydrophobic mismatch” between the two phases. Although this height difference is well defined for SLBs composed of phospholipids with different fatty acid chain lengths in bulk water, it has not been measured under reduced hydration conditions due to the problems in maintaining the structural integrity of the membrane during desic-

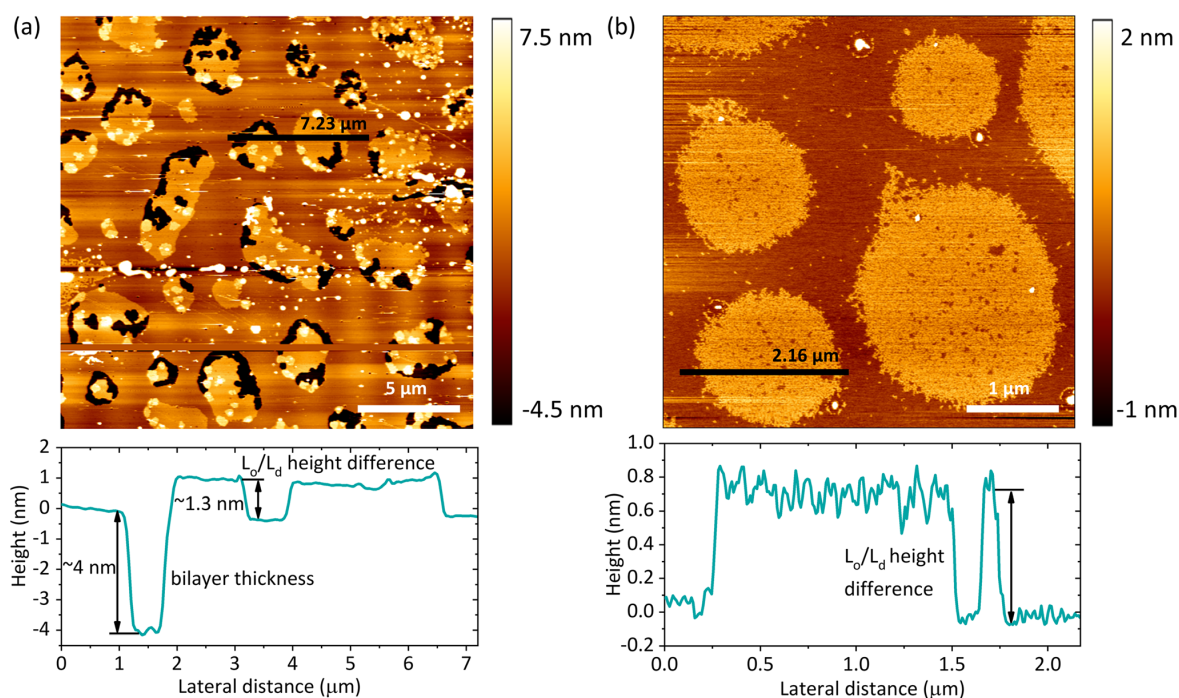


Fig. 4 (a) SLB after abrupt removal of bulk water and subsequent equilibration at 90% RH. The bilayer thickness at 90% RH was approximately 4 nm with a height difference between the L_o and L_d phases of approximately 1.3 nm. (b) SLB after careful removal of bulk water and subsequent equilibration at 5% RH. The intermediate height regions within the L_o phase domains correspond to the L_d phase. The height difference between the phases under these hydration conditions was about 0.8 nm.



cation.¹⁶ From the height distribution histograms (see Fig. S8†), we determined the height mismatch between phases in a wide range of membrane hydration states, as shown in Fig. 5a. We observed that the height mismatch decreased from 1.36 ± 0.19 nm at 90% RH to 0.8 ± 0.04 nm at 5% RH during dehydration. These changes were almost completely reversible upon rehydration. Importantly, measurements in bulk water

and under all hydration conditions were made with the same cantilever and in one mode (contact mode) to ensure that the values obtained were comparable. The sudden increase in the height mismatch observed when going from bulk hydration (100% RH) to 90% RH is an experimental artifact due to abrupt changes in the balance between attractive and repulsive forces to which the AFM tip is subjected immediately after the removal of bulk water (see ESI note 2†).

The height mismatch between the L_o and L_d phases changes gradually (Fig. 5a). One would therefore expect that with dehydration there should be a steady increase in the number of L_d phase lipids diffusing into the L_o zone. However, in the fluorescence data (Fig. 2b) we observed more of a step-wise behaviour, where after an initial increase in the fluorescence intensity of the L_d phase probe in the L_o domain, we observed a fairly constant intensity at all other humidities. At first glance, it may seem somewhat surprising that the trends in the fluorescence data and the height contrast data are different. However, it is important to note that the changes in the height mismatch are in no way related to the mobility of the lipids. The observed changes in lipid partitioning are associated with the decreased hydrophobic mismatch, but unlike the height mismatch data, they are also strongly dependent on the lipid mobility. Since lipid mobility decreases strongly with decreasing membrane hydration,^{37,50,51} it is not too surprising that we do not see a steady increase in the partitioning of the L_d phase lipids into the L_o phase. At lower membrane hydration states, we observed a competition between the lower hydrophobic mismatch, which favours lipid admixing, and the lower diffusivity, which hinders mixing.

The lateral organisation of the membrane, the distribution of the domains, and their size and shape are all driven, among other things, by the height mismatch between the L_d and L_o phases, which is a key factor leading to the occurrence of line tension at the boundary between two phases. Exposure of the hydrophobic tails of the lipids to the aqueous environment is energetically unfavorable. Therefore, the lipids of the L_o phase tend to organise themselves into domains in order to reduce the exposure to the aqueous medium. The theoretical model developed by Cohen *et al.* showed that the line tension increases quadratically with the phase height mismatch.¹⁴ Experimental work based on this model has shown that by varying the length of the PC acyl chain from 22 to 14 carbons, the height difference between the phases increases from 0.17 ± 0.9 nm to 1.56 ± 0.13 nm, leading to a 100-fold increase in the values of the line tension, from 0.06 to 6 pN, respectively.¹⁶ Line tensions of a similar order of magnitude have also been obtained using other approaches such as the measurement of the domain nucleation rate⁵⁷ or the analysis of the vesicle geometry based on the Jülicher and Lipowsky theory.⁵⁸ Surprisingly, the line tension in membranes has never been calculated or measured as a function of its main determinant, which is the presence of water. From the extracted profiles for samples at 90% RH, it could be concluded that the total lipid bilayer thickness does not appear to change upon removal of bulk

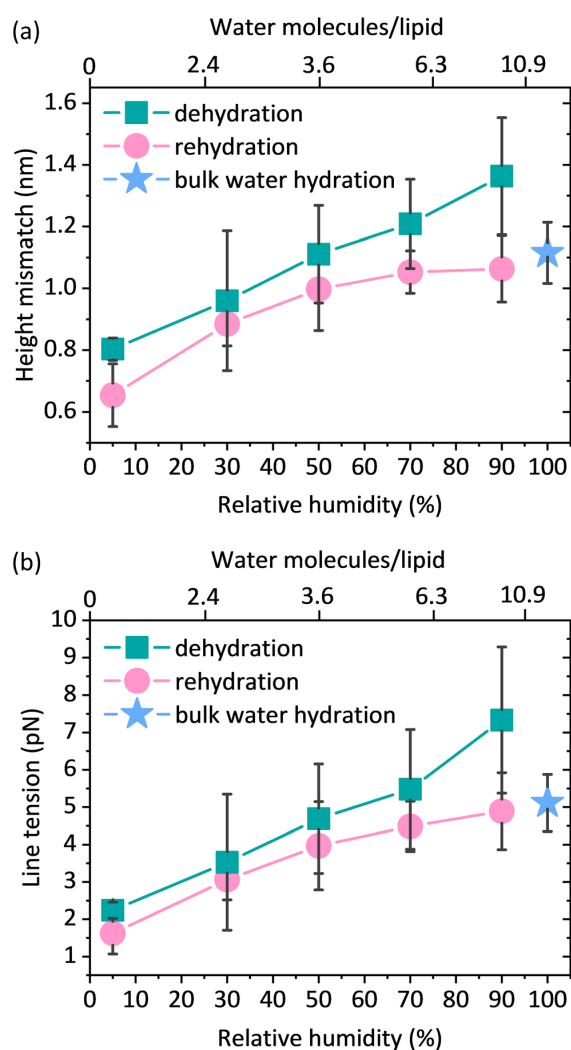


Fig. 5 (a) Height mismatch between the L_o and L_d phases during dehydration and rehydration analysed from the height histograms of 3–8 different images containing multiple domains of the L_o phase. (b) Line tension during dehydration and rehydration calculated from the model assuming the presence of soft domains, no spontaneous curvature, and no change in the height of the L_o phase during the hydration change cycle. Height mismatch and line tension were determined from 3–8 images (depending on the hydration level) of 3 individual SLBs; each image contained multiple L_o domains. The bottom x-axis shows the values of relative humidity, which can be correlated with the number of water molecules per lipid (see the upper x-axis).



water, as the bilayer thickness measured at 90% RH of 3.87 nm is consistent with the value of 3.86 nm reported in the literature for a fully hydrated DMOPC bilayer.⁵² The determination of the effective thickness of the L_o and L_d phases was not possible for each hydration level, because the lipid membranes did not show any defects in the form of holes and membrane disruptions that would provide the reference plane for height measurements. While it is relatively easy to induce holes in the membrane, as it requires the abrupt removal of bulk water, once membrane defects are formed and the hydration is further gradually reduced, they behave in an unpredictable manner; they rapidly expand in all directions, and the edges of the membrane curl up. This progressive degradation of the membrane makes it difficult to follow the absolute thickness of the bilayer as the hydration changes. However, NMR and X-ray diffraction experiments on the membranes under lower hydration conditions showed that the lipids forming the L_d phase are more susceptible to height changes during dehydration. The lipids of the L_d phase undergo a straightening of the acyl chains, leading to a decrease in the lateral area per lipid molecule and consequently an increase in their hydrophobic thickness.^{59,60} Moreover, recent simulation results on the behavior of lipid membranes under reduced hydration clearly show that, in the absence of water, the lipids of the L_d phase undergo a liquid-gel transition and exhibit properties of an ordered membrane, which is stiffer with the acyl chains of the lipids more densely packed.⁶⁰ With this in mind, we infer that the change in height mismatch and the consequent change in the line tension are caused by the straightening of the fatty acid chains of the lipids composing the L_d phase, rather than a change in the thickness of the L_o phase. We calculated the line tension using the equation proposed by Cohen *et al.*¹⁴ (see the Materials and methods section), assuming that the difference in height was caused by the increase in the thickness of the L_d phase. We observed that there was a linear dependence of the line tension on the degree of hydration (Fig. 5b).

While all the evidence discussed above suggests that it is the L_d phase that changes its height when the membrane hydration is altered, we also considered two other scenarios, in which a decrease in the hydrophobic mismatch is caused by a decrease in the thickness of the L_o phase or by both phases having the opposite effect, *i.e.* the thickness of the L_d phase increases with a simultaneous decrease in the thickness of the L_o phase (see Fig. S9a†). Regardless of the assumptions, for all three scenarios we observed the same trend in the changes of the line tension at varying hydration levels, *i.e.* an almost 3-fold decrease of the line tension for the lowest humidity of 5% RH when compared to 90% RH (see Fig. S9b and S9c†).

4 Conclusions

In this paper, we have presented a methodology for AFM measurements under varying hydration conditions, in which biomimetic membranes are directly subjected to the slow

gradual changes of their hydration state. The phase-separated lipid membranes, characterised by the presence of the L_d and L_o phases, were exposed to a wide range of environmental humidities and fluorescence images as well as membrane topography information were acquired simultaneously. We observed that the overall lateral organisation of the lipid membranes, *i.e.* the presence of phase separation and the continuity of the structure, did not change upon removal of bulk water and subsequent gradual dehydration of the membrane. However, the absence of bulk water leads to an increased miscibility of the lipids constituting the L_d phase within the domains of the L_o phase, as compared to fully hydrated conditions. We investigated the response of biomembranes to the dehydration conditions in terms of the line tension, which has only been measured as a function of lipid chain length and never through the direct effect of water content. We observed a 3-fold difference in the line tension between the two extreme hydration states. The significant drop in line tension at the L_d and L_o phase interface explains the tendency of lipids from different phases to mix more freely at reduced membrane hydration.

Local dehydration of two merging cell membranes is an indispensable prerequisite for all fusion events that occur during biological processes such as viral entry, endo- and exocytosis, neurotransmission or fertilisation. Fusion can be modulated in two ways: using different types of fusogenic proteins, such as SNAREs, or by structural, local adaptation of the membrane lipid composition.⁶¹ It has been shown that cholesterol accumulates in the regions of high curvature during stalk formation in fusion events.⁶² This is attributed to the ability of cholesterol to increase the membrane fluidity and induce the formation of negative curvature. Sphingomyelin is known to promote the formation of a denser and less fluid L_o phase, effectively inhibiting the membrane fusion.⁶³ The opposite effect is induced by unsaturated lipids, which form the L_d phase, stimulating membrane curvature and promoting the formation of fusion intermediates.⁶⁴ Although the fusion of two membranes preferentially occurs in the regions of high fluidity, viral protein elements such as HIV fusion peptides have been shown to bind to high line tension L_o - L_d interface regions, where they promote the membrane fusion of the HIV viral envelope with the host cell membrane.⁶⁵ The revised stalk-pore model, extended to heterogeneous membranes (exhibiting L_o - L_d phase coexistence), proposes that the reduction of line tension at the lipid phase boundary during stalk formation generates additional energy for the fusion, facilitating viral entry through phase boundary regions.⁶⁶ As we have shown here, the reduction in line tension under dehydration conditions is associated with an extensive lipid migration between the L_d and L_o phases. It is therefore possible that the observed changes in local membrane fluidity and flexibility, as well as the reduced line tension, are yet another factor required for the fusion to occur.

While partial dehydration of the membranes has been presented as an inherent requirement for the mechanism of membrane fusion, the term 'dehydration' is far from well



defined, as it is not clear to what extent membranes actually become dehydrated. One way of describing membrane dehydration would be to define a state where the amount of hydrating water decreases to a level where the dynamic or structural properties of the membrane begin to be affected. Based on the experiments reported here as well as our recent works,^{37,50,51} both the dynamics and the structure of the membrane are gradually affected when the first hydration shell of the lipids is perturbed. In the case of the zwitterionic phosphocholine lipids, this happens when the hydration drops below about 12 molecules per lipid. Thus, the thickness of the water layer is at most 1–2 monolayers of water on top of the membrane. This suggests that biomimetic membranes don't really 'feel' any changes in hydration properties beyond their first hydration shell. Certainly, it would be fascinating to monitor membrane's properties while controlling the thickness of the hydrating water layer from a few nanometers all the way down to a few water molecules per lipid, in the regime that is directly relevant to the mechanism of membrane fusion, but the question of how to control the thickness of the hydrating layer beyond the first hydration shell remains open.

In conclusion, our results provide new insights into the behavior of biological membranes under water shortage conditions in terms of their lateral organisation and adaptation to membrane dehydration. The results presented here bring a new perspective to the processes that require local membrane dehydration, such as cell fusion, fertilisation or binding of macromolecules. Finally, the methodology proposed in this research for AFM measurements in varying hydration states provides new possibilities for studying other biological systems and their interactions with water.

Author contributions

Emilia Krok: conceptualization, validation, investigation, writing – original draft, visualization, and funding acquisition. Henri G. Franquelim: conceptualization, validation, investigation, resources, and writing – review and editing. Madhurima Chattopadhyay: conceptualization, validation, and writing – review and editing. Hanna Orlikowska-Rzeznik: validation and writing – review and editing. Petra Schwill: writing – review and editing, resources, and supervision. Lukasz Piatkowski: conceptualization, validation, supervision, writing – original draft, and funding acquisition.

Conflicts of interest

There are no conflicts to declare.

Acknowledgements

The authors acknowledge the financial support from the EMBO Installation Grant 2019 (IG 4147). LP acknowledges the financial support from the First TEAM Grant No.

POIR.04.04.00-00-5D32/18-00 provided by the Foundation for Polish Science (FNP). EK acknowledges the financial support from the Ministry of Education and Science of Poland in the year 2022 (Project No. 0512/SBAD/6212). HOR acknowledges the financial support from the National Science Centre (Poland) through OPUS grant, project no. 2020/37/B/ST4/01785.

References

- 1 J. Lombard, Once upon a Time the Cell Membranes: 175 Years of Cell Boundary Research, *Biol. Direct*, 2014, **9**, 32.
- 2 N. J. Yang and M. J. Hinner, Getting across the Cell Membrane: An Overview for Small Molecules, Peptides, and Proteins, *Methods Mol. Biol.*, 2015, **1266**, 29–53.
- 3 L. Schoonen and J. C. M. Van Hest, Compartmentalization, Approaches in Soft Matter Science: From Nanoreactor Development to Organelle Mimics, *Adv. Mater.*, 2016, **28**, 1109–1128.
- 4 J. A. Jackman and N. J. Cho, Supported Lipid Bilayer Formation: Beyond Vesicle Fusion, *Langmuir*, 2020, **36**, 1387–1400.
- 5 L. Picas, F. Rico and S. Scheuring, Direct Measurement of the Mechanical Properties of Lipid Phases in Supported Bilayers, *Biophys. J.*, 2012, **102**, L01–L03.
- 6 A. E. Vallejo and C. A. Gervasi, Impedance Analysis of Ion Transport through Gramicidin Channels in Supported Lipid Bilayers, *Bioelectrochemistry*, 2002, **57**, 1–7.
- 7 E. London, Insights into Lipid Raft Structure and Formation from Experiments in Model Membranes, *Curr. Opin. Struct. Biol.*, 2002, **12**, 480–486.
- 8 J. M. Crane and L. K. Tamm, Fluorescence Microscopy to Study Domains in Supported Lipid Bilayers, *Methods Mol. Biol.*, 2007, **400**, 481–488.
- 9 E. Krok, M. Stephan, R. Dimova and L. Piatkowski, Tunable Biomimetic Bacterial Membranes from Binary and Ternary Lipid Mixtures and Their Application in Antimicrobial Testing, *Biochim. Biophys. Acta, Biomembr.*, 2023, **1865**(7), 184194.
- 10 L. J. Pike, Rafts Defined: A Report on the Keystone Symposium on Lipid Rafts and Cell Function, *J. Lipid Res.*, 2006, **47**, 1597–1598.
- 11 J. D. Nickels and J. Katsaras, Water and Lipid Bilayers, *Subcell. Biochem.*, 2015, **71**, 45–67.
- 12 F. Martelli, C. Calero and G. Franzese, Redefining the Concept of Hydration Water near Soft Interfaces, *Biointerphases*, 2021, **16**, 020801.
- 13 P. Jungwirth, Biological Water or Rather Water in Biology?, *J. Phys. Chem. Lett.*, 2015, **6**, 2449–2451.
- 14 P. I. Kuzmin, S. A. Akimov, Y. A. Chizmadzhev, J. Zimmerberg and F. S. Cohen, Line Tension and Interaction Energies of Membrane Rafts Calculated from Lipid Splay and Tilt, *Biophys. J.*, 2005, **88**, 1120–1133.
- 15 E. E. Meyer, K. J. Rosenberg and J. Israelachvili, Recent Progress in Understanding Hydrophobic Interactions, *Proc. Natl. Acad. Sci. U. S. A.*, 2006, **103**, 15739–15746.



- 16 A. J. García-Sáez, S. Chiantia and P. Schwille, Effect of Line Tension on the Lateral Organization of Lipid Membranes, *J. Biol. Chem.*, 2007, **282**, 33537–33544.
- 17 Y. Zhen, M. Radulovic, M. Vietri and H. Stenmark, Sealing Holes in Cellular Membranes, *EMBO J.*, 2021, **40**, e106922.
- 18 N. Srividya and S. Muralidharan, Determination of the Line Tension of Giant Vesicles from Pore-Closing Dynamics, *J. Phys. Chem. B*, 2008, **112**, 7147–7152.
- 19 M. B. Jackson and E. R. Chapman, The Fusion Pores of Ca²⁺-Triggered Exocytosis, *Nat. Struct. Mol. Biol.*, 2008, **15**, 684–689.
- 20 J. Rizo and C. Rosenmund, Synaptic Vesicle Fusion, *Nat. Struct. Mol. Biol.*, 2008, **15**, 665–674.
- 21 S. C. Harrison, Viral Membrane Fusion, *Nat. Struct. Mol. Biol.*, 2008, **15**, 690–698.
- 22 P. Primakoff and D. G. Myles, Cell-Cell Membrane Fusion during Mammalian Fertilization, *FEBS Lett.*, 2007, **581**, 2174–2180.
- 23 R. D. Byrne, S. Veeriah, C. J. Applebee and B. Larijani, Conservation of Proteo-Lipid Nuclear Membrane Fusion Machinery during Early Embryogenesis, *Nucleus*, 2014, **5**, 441–448.
- 24 G. Shemer and B. Podbilewicz, Fusomorphogenesis: Cell Fusion in Organ Formation, *Dev. Dyn.*, 2000, **218**(1), 30–51.
- 25 S. Aeffner, T. Reusch, B. Weinhausen and T. Salditt, Energetics of Stalk Intermediates in Membrane Fusion Are Controlled by Lipid Composition, *Proc. Natl. Acad. Sci. U. S. A.*, 2012, **109**, E1609–E1618.
- 26 S. L. Leikin, M. M. Kozlov, L. V. Chernomordik, V. S. Markin and Y. A. Chizmadzhev, Membrane Fusion: Overcoming of the Hydration Barrier and Local Restructuring, *J. Theor. Biol.*, 1987, **129**, 411–425.
- 27 S. Aeffner, T. Reusch, B. Weinhausen and T. Salditt, Membrane Fusion Intermediates and the Effect of Cholesterol: An in-House X-Ray Scattering Study, *Eur. Phys. J. E: Soft Matter Biol. Phys.*, 2009, **30**, 205–214.
- 28 A. Joardar, P. G. Prasad and H. Chakraborty, Mechanism of Membrane Fusion: Interplay of Lipid and Peptide, *J. Membr. Biol.*, 2022, **255**, 211–224.
- 29 S. Chiantia, N. Kahya and P. Schwille, Dehydration Damage of Domain-Exhibiting Supported Bilayers: An AFM Study on the Protective Effects of Disaccharides and Other Stabilizing Substances, *Langmuir*, 2005, **21**, 6317–6323.
- 30 M. Del, F. Amalfa, A. M. Nuñez, S. Díaz, A. C. Biondi De Lopez and E. A. Disalvo, Effect of Trehalose and Sucrose on the Hydration and Dipole Potential of Lipid Bilayers, *Biophys. J.*, 2000, **78**, 2452–2458.
- 31 M. A. Iriarte-Alonso, A. M. Bittner and S. Chiantia, Influenza A Virus Hemagglutinin Prevents Extensive Membrane Damage upon Dehydration, *BBA Adv.*, 2022, **2**, 100048.
- 32 S. Ohtake, C. Schebor and J. J. de Pablo, Effects of Trehalose on the Phase Behavior of DPPC-Cholesterol Unilamellar Vesicles, *Biochim. Biophys. Acta, Biomembr.*, 2006, **1758**, 65–73.
- 33 Y. Deng, Y. Wang, B. Holtz, J. Li, N. Traaseth, G. Veglia, B. J. Stottrup, R. Elde, D. Pei, A. Guo and X. Y. Zhu, Fluidic and Air-Stable Supported Lipid Bilayer and Cell-Mimicking Microarrays, *J. Am. Chem. Soc.*, 2008, **130**, 6267–6271.
- 34 B. P. Oberts and G. J. Blanchard, Formation of Air-Stable Supported Lipid Monolayers and Bilayers, *Langmuir*, 2009, **25**, 2962–2970.
- 35 R. M. Fabre and D. R. Talham, Stable Supported Lipid Bilayers on Zirconium Phosphonate Surfaces, *Langmuir*, 2009, **25**, 12644–12652.
- 36 C. T. Han and L. Chao, Creating Air-Stable Supported Lipid Bilayers by Physical Confinement Induced by Phospholipase A2, *ACS Appl. Mater. Interfaces*, 2014, 6378–6383.
- 37 M. Chattopadhyay, E. Krok, H. Orlikowska, P. Schwille, H. G. Franquelim and L. Piatkowski, Hydration Layer of Only a Few Molecules Controls Lipid Mobility in Biomimetic Membranes, *J. Am. Chem. Soc.*, 2021, **143**, 14551–14562.
- 38 H. Orlikowska-Rzeznik, E. Krok, M. Chattopadhyay, A. Lester and L. Piatkowski, Laurdan Discerns Lipid Membrane Hydration and Cholesterol Content, *J. Phys. Chem. B*, 2023, **127**, 3382–3391.
- 39 E. Krok, A. Batura, M. Chattopadhyay, H. Orlikowska and L. Piatkowski, Lateral Organization of Biomimetic Cell Membranes in Varying PH Conditions, *J. Mol. Liq.*, 2022, **345**, 117907.
- 40 L. Piatkowski, J. De Heij and H. J. Bakker, Probing the Distribution of Water Molecules Hydrating Lipid Membranes with Ultrafast Förster Vibrational Energy Transfer, *J. Phys. Chem. B*, 2013, **117**, 1367–1377.
- 41 K. Hristova and S. H. White, Determination of the Hydrocarbon Core Structure of Fluid Dioleoylphosphocholine (DOPC) Bilayers by x-Ray Diffraction Using Specific Bromination of the Double-Bonds: Effect of Hydration, *Biophys. J.*, 1998, **74**, 2419–2433.
- 42 C. A. Schneider, W. S. Rasband and K. W. Eliceiri, NIH Image to ImageJ: 25 Years of Image Analysis, *Nat. Methods*, 2012, **9**, 671–675.
- 43 D. Nečas and P. Klapetek, Gwyddion: An Open-Source Software for SPM Data Analysis, *Cent. Eur. J. Phys.*, 2012, **10**, 181–188.
- 44 J. Schindelin, I. Arganda-Carreras, E. Frise, V. Kaynig, M. Longair, T. Pietzsch, S. Preibisch, C. Rueden, S. Saalfeld, B. Schmid, J. Y. Tinevez, D. J. White, V. Hartenstein, K. Eliceiri, P. Tomancak and A. Cardona, Fiji: An Open-Source Platform for Biological-Image Analysis, *Nat. Methods*, 2012, **9**, 676–682.
- 45 J. Ries, S. Chiantia and P. Schwille, Accurate Determination of Membrane Dynamics with Line-Scan FCS, *Biophys. J.*, 2009, **96**, 1999–2008.
- 46 D. Axelrod, Evanescent Excitation and Emission, in *Fluorescence Microscopy: Super-Resolution and other Novel Techniques*, Academic Press, 2014, pp. 1–14.
- 47 E. Sezgin, P. Schwille and T. Dresden, Molecular Membrane Biology Model Membrane Platforms to Study Protein-Membrane Interactions Model Membrane



- Platforms to Study Protein-Membrane Interactions, *Mol. Membr. Biol.*, 2012, **29**, 144–154.
- 48 N. Hartrampf, S. M. Leitao, N. Winter, H. Toombs-Ruane, J. A. Frank, P. Schwille, D. Trauner and H. G. Franquelim, Structural Diversity of Photoswitchable Sphingolipids for Optodynamic Control of Lipid Microdomains, *Biophys. J.*, 2023, **122**(11), 2325–2341.
- 49 J. A. Frank, H. G. Franquelim, P. Schwille and D. Trauner, Optical Control of Lipid Rafts with Photoswitchable Ceramides, *J. Am. Chem. Soc.*, 2016, **138**, 12981–12986.
- 50 M. Chattopadhyay, H. Orlikowska, E. Krok and L. Piatkowski, Sensing Hydration of Biomimetic Cell Membranes, *Biosensors*, 2021, **11**(7), 241.
- 51 M. Chattopadhyay, E. Krok, H. Orlikowska-Rzeczniak and L. Piatkowski, Cooperativity between Sodium Ions and Water Molecules Facilitates Lipid Mobility in Model Cell Membranes, *Chem. Sci.*, 2023, **14**, 4002–4011.
- 52 T. H. Lee, M. A. Sani, S. Overall, F. Separovic and M. I. Aguilar, Effect of Phosphatidylcholine Bilayer Thickness and Molecular Order on the Binding of the Antimicrobial Peptide Maculatin 1.1, *Biochim. Biophys. Acta, Biomembr.*, 2018, **1860**, 300–309.
- 53 S. Chiantia, N. Kahya, J. Ries and P. Schwille, Effects of Ceramide on Liquid-Ordered Domains Investigated by Simultaneous AFM and FCS, *Biophys. J.*, 2006, **90**, 4500–4508.
- 54 S. Chiantia, J. Ries, N. Kahya and P. Schwille, Combined AFM and Two-Focus SFCS Study of Raft-Exhibiting Model Membranes, *ChemPhysChem*, 2006, **7**, 2409–2418.
- 55 T. J. McIntosh, X-Ray, Diffraction to Determine the Thickness of Raft and Nonraft Bilayers, *Methods Mol. Biol.*, 2007, **398**, 221–230.
- 56 M. Gandhavadi, D. Allende, A. Vidal, S. A. Simon and T. J. McIntosh, Structure, Composition, and Peptide Binding Properties of Detergent Soluble Bilayers and Detergent Resistant Rafts, *Biophys. J.*, 2002, **82**, 1469–1482.
- 57 C. D. Blanchette, W. C. Lin, C. A. Orme, T. V. Ratto and M. L. Longo, Using Nucleation Rates to Determine the Interfacial Line Tension of Symmetric and Asymmetric Lipid Bilayer Domains, *Langmuir*, 2007, **23**, 5875–5877.
- 58 T. Baumgart, S. T. Hess and W. W. Webb, Imaging Coexisting Fluid Domains in Biomembrane Models Coupling Curvature and Line Tension, *Nature*, 2003, **425**, 821–824.
- 59 B. W. Koenig, H. H. Strey and K. Gawrisch, Membrane Lateral Compressibility Determined by NMR and X-Ray Diffraction: Effect of Acyl Chain Polyunsaturation, *Biophys. J.*, 1997, **73**, 1954–1966.
- 60 Y. G. Smirnova, S. Aeffner, H. J. Risselada, T. Salditt, S. J. Marrink, M. Müller and V. Knecht, Interbilayer Repulsion Forces between Tension-Free Lipid Bilayers from Simulation, *Soft Matter*, 2013, **9**, 10705–10718.
- 61 A. Sardar, N. Dewangan, B. Panda, D. Bhowmick and P. K. Tarafdar, Lipid and Lipidation in Membrane Fusion, *J. Membr. Biol.*, 2022, **255**, 691–703.
- 62 W. Wang, L. Yang and H. W. Huang, Evidence of Cholesterol Accumulated in High Curvature Regions: Implication to the Curvature Elastic Energy for Lipid Mixtures, *Biophys. J.*, 2007, **92**, 2819–2830.
- 63 E. Haque, T. J. McIntosh and B. R. Lentz, Influence of Lipid Composition on Physical Properties and PEG-Mediated Fusion of Curved and Uncurved Model Membrane Vesicles: “Nature’s Own” Fusogenic Lipid Bilayer, *Biochemistry*, 2001, **40**, 4340–4348.
- 64 M. Pinot, S. Vanni, S. Pagnotta, S. Lacas-Gervais, L. A. Payet, T. Ferreira, R. Gautier, B. Goud, B. Antonny and H. Barelli, Polyunsaturated Phospholipids Facilitate Membrane Deformation and Fission by Endocytic Proteins, *Science*, 2014, **345**, 693–697.
- 65 S. T. Yang, V. Kiessling, J. A. Simmons, J. M. White and L. K. Tamm, HIV Gp41-Mediated Membrane Fusion Occurs at Edges of Cholesterol-Rich Lipid Domains, *Nat. Chem. Biol.*, 2015, **11**, 424–431.
- 66 S. T. Yang, V. Kiessling and L. K. Tamm, Line Tension at Lipid Phase Boundaries as Driving Force for HIV Fusion Peptide-Mediated Fusion, *Nat. Commun.*, 2016, **7**, 11401.



Supplementary Information for

Nanoscale structural response of biomimetic cell membranes to controlled dehydration.

Emilia Krok^{a*}, Henri G. Franquelim^{b,c}, Madhurima Chattopadhyay^a, Hanna Orlikowska-Rzeznik^a, Petra Schwille^b, Lukasz Piatkowski^{a*}

^a Poznan University of Technology, Faculty of Materials Engineering and Technical Physics, Institute of Physics, Piotrowo 3, 60-965 Poznan, Poland

^b Department of Cellular and Molecular Biophysics, Max Planck Institute of Biochemistry, Am Klopferspitz 18, 82152 Martinsried, Germany

^c Leipzig University, Research and Transfer Center for Bioactive Matter, Deutscher Platz 5, 04103 Leipzig, Germany

*corresponding authors

Table of contents:

Supplementary notes 1-2

Supplementary figures S1-S8

Supplementary note 1

To verify whether there are any changes in the detected fluorescence intensity of the Atto 633 dye due to other effects independent of the spatial rearrangement of the probe (partitioning), we acquired additional, control data and quantified the changes in the fluorescence intensity as a function of membrane hydration for a single-component, non-phase-separated SLB composed of 14:1 PC doped with DOPE-Atto 633 (0.1 mol%). Figure S3a shows that the detected fluorescence signal increases by a factor of approximately 1.6 with dehydration. Given the very high fluorescence quantum yield (QE) of Atto 633 (64% in water), it is not physically possible that the observed increase is solely due to the increase in QE of the dye, as this would indicate that the QE increases to a value >100%. We could not identify any theoretical or experimental work that would provide explicit information on the possible changes in QE of Atto 663 when dissolved in water and embedded in an SLB. However, recent experimental results have shown that the QE of Atto 647N and Atto 655 increases by 25% and 48% respectively when embedded in an SLB compared to when dissolved in water¹. Similarly, extensive studies by Frantzeskos have shown that the QE of the basic Atto 633 chromophore - CP 149 - does not change by more than 30% when dissolved in solvents of different polarity².

The optical properties of the studied system also change as a function of hydration. For example, the efficiency of fluorescence collection is influenced (among other things) by the refractive index of the medium in which the emitting dipoles are located³. In bulk water, the fluorescence is emitted more symmetrically with respect to the substrate plane, whereas in dehydrated conditions (higher refractive index mismatch between the membrane (~1.47^{4,5}) and air), the fluorescence is mostly emitted towards the substrate. Thus, the observed increase in fluorescence intensity most likely includes a contribution from the optical effects.

Irrespective of the exact contributions of the effects discussed above, we clearly observed (Fig. S3b) that the fluorescence signal of Atto 633 increases much less in the L_d phase (~x1.5) than in the L_o phase (~x4.7). Indeed, if redistribution of DOPE-Atto 633 were the only mechanism, one should observe an increase in fluorescence intensity in the L_o domain and a decrease (by the same absolute amount) of the fluorescence intensity in the adjacent L_d phase region. If we correct the observed increase in fluorescence intensity in the L_o/L_d phases by a factor of 1.6, determined from the single-component membrane, we find (Fig. S3c) that indeed the fluorescence intensity in the L_o phase increases (~600 counts), while in the L_d phase we observe a decrease in fluorescence intensity (~600 counts). Of course, any quantitative conclusions should be made with great caution, as not all the effects involved here are easily identifiable and quantifiable, but the acquired fluorescence data give a very solid indication of the increased mixing of lipids associated with the two phases.

Supplementary note 2

In the interphase height mismatch data shown in Figure 5a, we observed a sudden increase in the L_d - L_o height mismatch for the membrane in humid air (90% RH) compared to the membrane in water (100% RH). We consider this to be an artifact due to abrupt changes in the balance of attractive and repulsive forces to which the AFM tip is subjected immediately after the removal of bulk water. As mentioned in the main text, it was experimentally very difficult to obtain AFM images immediately after removal of bulk water. These samples were extremely sticky and the AFM tip dragged considerably, requiring multiple scans to first remove the membrane aggregates. This additional stickiness was mainly observed in AFM images taken during the dehydration trajectory (immediately after bulk water removal), as opposed to the rehydration trace (from dry to humid air). This is probably due to the presence of strong capillary and adhesive forces between the tip and sample during the dehydration phase, likely caused by the residual water molecules adsorbed on the silicon tip and the formation of a nanoscopic water meniscus^{6,7}. These stronger tip-sample adhesion forces can lead to membrane deformation/compression⁸, especially of the softer L_d regions, and consequently to an “overestimation” of the recorded L_d - L_o height difference values.

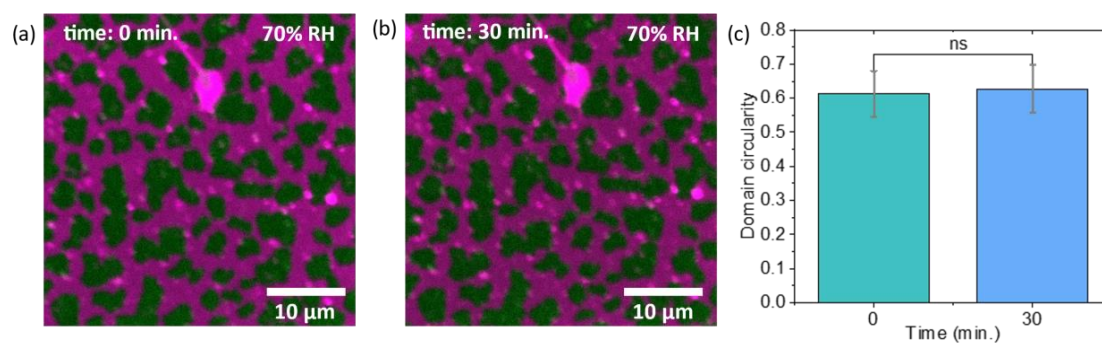


Fig. S1 Domains circularity measured as a function of time.

Fluorescence images of a representative SLB showing phase separation into L_d (labelled with DOPE-Atto 633, shown in magenta) and L_o (labelled with CTxB-Alexa 488, shown in green): (a) measured after equilibration with 70% RH and (b) after 30 min. incubation at 70% RH. (c) Domain circularity determined from the domains shown in (a) and (b).

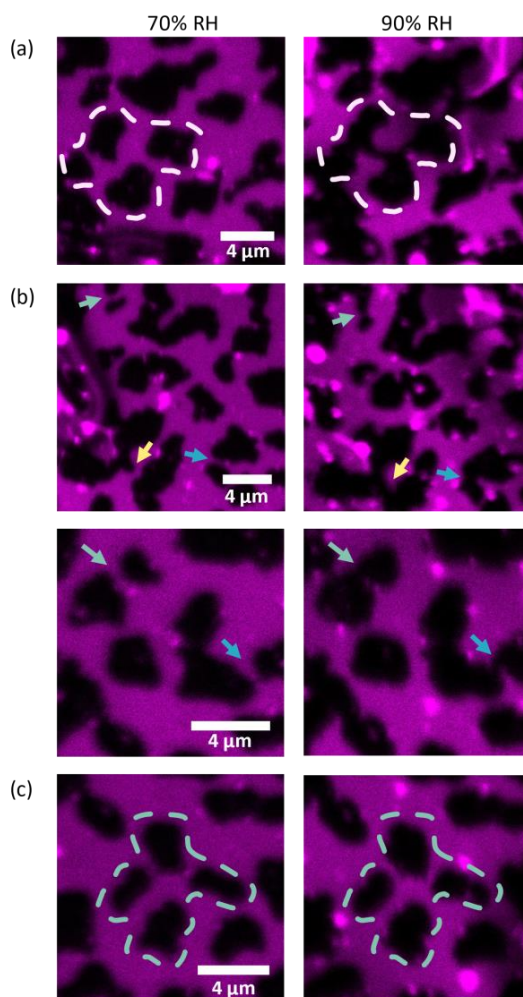


Fig. S2 Changes of the domains shape during rehydration

(a) Merging of domains as relative humidity is increased from 70 to 90% RH. The blue dashed lines mark the outlines of four merging domains. (b) Merging of domains during humidity increase, arrows indicate the merging points of the domains at 70 (left) and 90% RH (right). (c) Domains that did not merge during the increase of the environment relative humidity. Confocal imaging was performed in 10 mM HEPES and 150 mM NaCl buffer.

CHAPTER 6. NANOSCALE STRUCTURAL RESPONSE OF BIOMIMETIC CELL MEMBRANES TO CONTROLLED DEHYDRATION

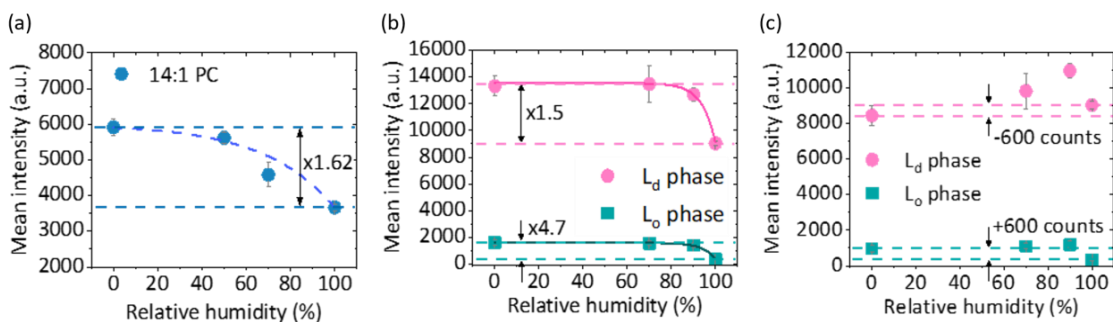


Fig. S3 Fluorescence signal from DOPE-Atto 633 probe as a function of membrane hydration

(a) Changes in the fluorescence intensity of the L_d phase probe - DOPE-Atto 633 during the dehydration cycle of a single component SLB composed of 14:1 PC. (b) Changes in the fluorescence intensity of the DOPE-Atto 633 probe measured separately in the L_d and L_o phases during dehydration of a phase-separated SLB. (c) Corrected changes in the fluorescence intensity of the DOPE-Atto 633 probe during dehydration. The correction factor of 1.62 was calculated from the changes in fluorescence intensity observed for a single component membrane.

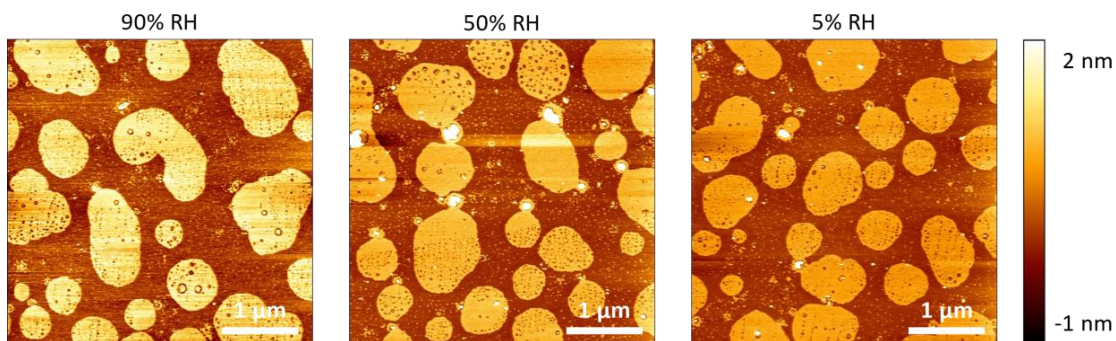


Fig. S4 AFM topography images of SLBs during dehydration

Representative images of SLBs during the dehydration cycle. The membrane was equilibrated at 90, 50 and 5% RH.

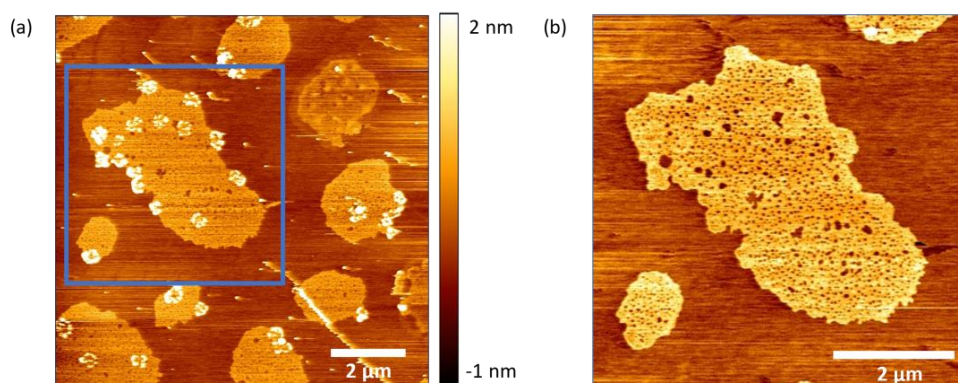


Fig. S5 AFM topography images of SLBs right after removal of bulk water

(a) Representative image of the lipid bilayer immediately after removal of bulk water and equilibration to 90% RH. The blue square indicates the area shown in high resolution images of the lipid bilayer at 90% RH (b). The lipid membrane was sticky at high humidity, small aggregates on the surface were dragged by the tip, causing distortions in the measurements. (b) After further equilibration and sweeping with the AFM tip over the surface, the aggregates on top of the membrane were removed and the topography could be measured more reliably.

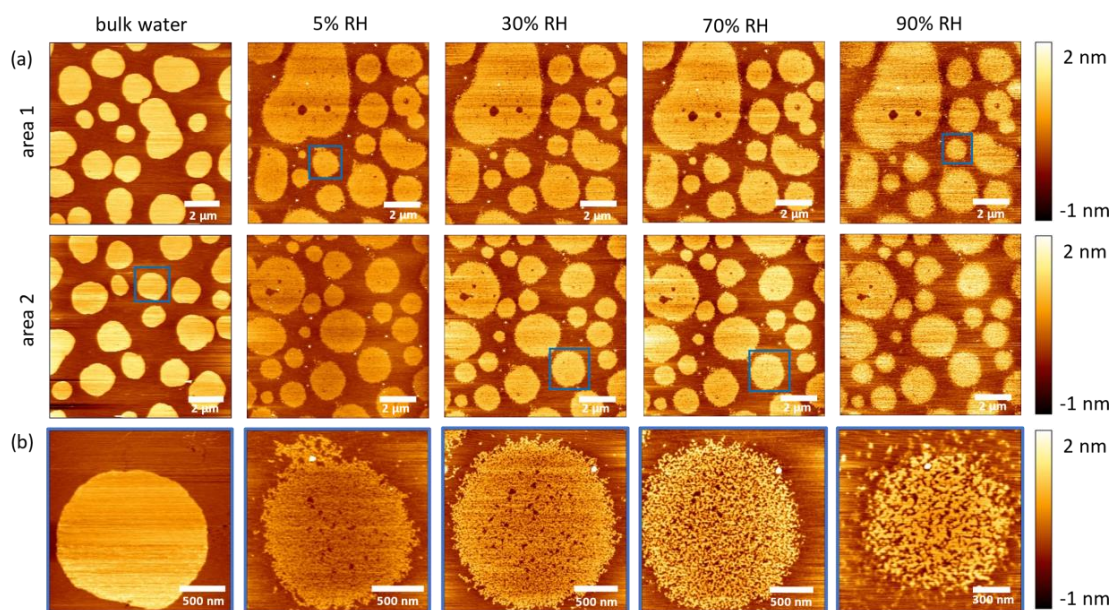


Fig. S6 AFM topography images of SLBs at different hydration levels.

(a) Representative images of fully hydrated SLB, and SLB after removal of bulk water and equilibration at 5, 30, 70 and 90% RH. The top and middle rows correspond to two different regions of the SLB. (b) High resolution images of individual areas (indicated by blue squares in panel (a)) at different hydration levels.

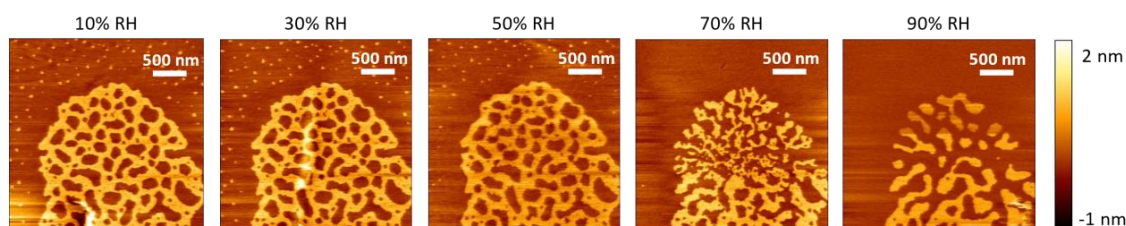


Fig. S7 High resolution AFM topography images of single L_o phase domain at different hydration levels. High resolution single domain images during membrane rehydration revealed the evolution of the L_d nanodomains trapped within the L_o phase. At 70% RH, it is evident that the L_d phase nanodomains merge to minimize the phase boundary.

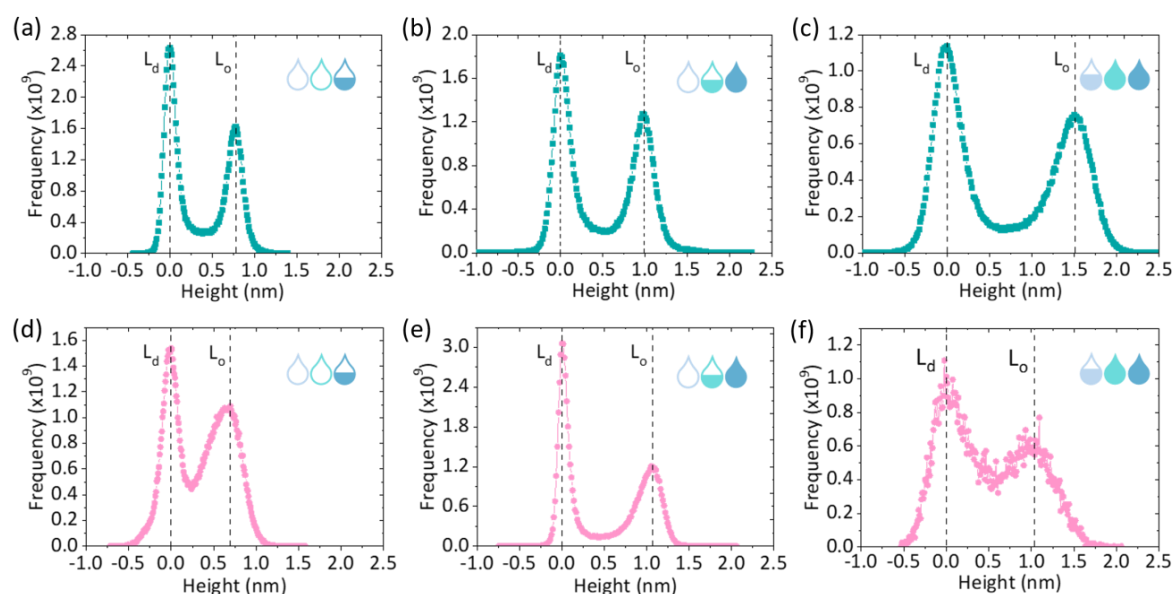


Fig. S8 Quantification of the height difference between the L_d and L_o phase from the AFM images. Height distribution histograms for the membrane subjected to dehydration (top row, green) at (a) 5% RH, (b) 50% RH, and (c) 90% RH, and rehydration (bottom row, pink) at (d) 5% RH, (e) 50% RH, and (f) 90% RH. The profiles have been offset corrected so that the L_d peak is centered at 0 nm.

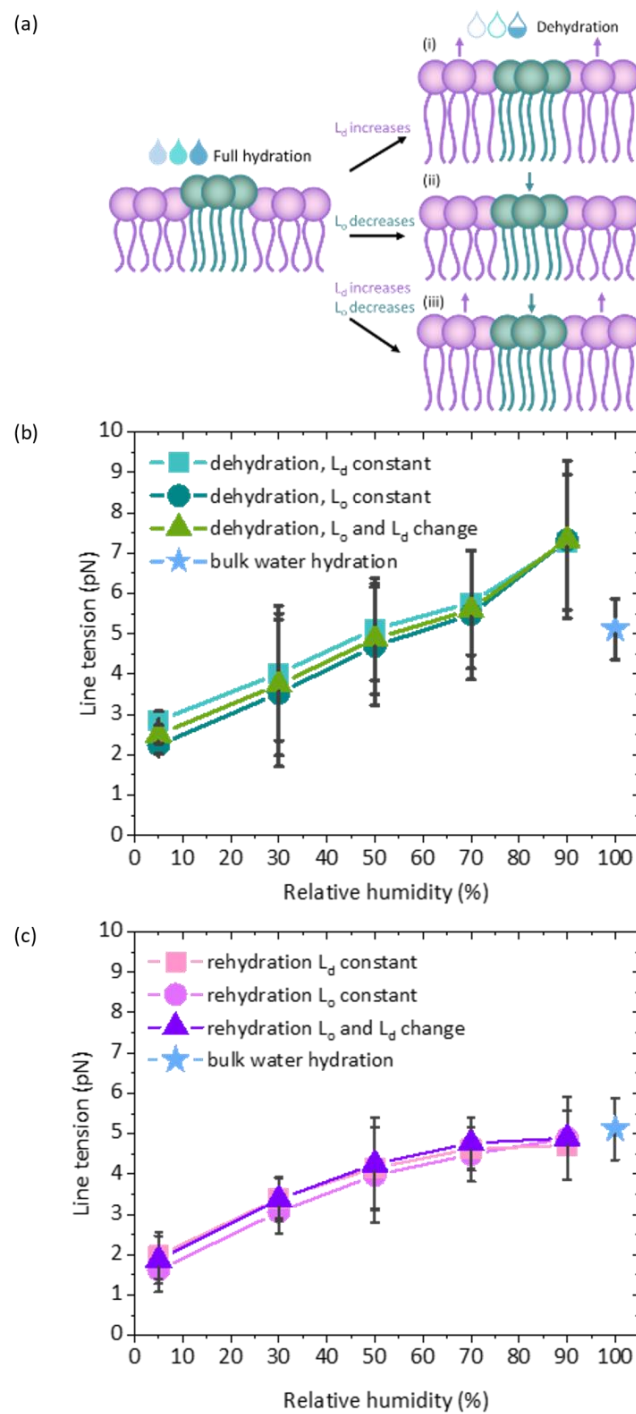


Fig. S9 Line tension at different hydration levels during dehydration and rehydration of the lipid bilayer.

(a) Three scenarios for the line tension calculation: (i) the L_d phase thickness increases, while the L_o phase does not change, (ii) the L_o phase thickness decreases, while the L_d phase thickness does not change, (iii) the L_d phase increases and the L_o phase decreases. (b) Line tension during dehydration calculated from the model assuming a soft domain and no spontaneous curvature for the three different scenarios shown in (a). (c) Line tension during rehydration calculated for the three different scenarios presented in (a).

References:

- 1 F. Schneider, D. Ruhlandt, I. Gregor, J. Rg Enderlein and A. I. Chizhik, Quantum Yield Measurements of Fluorophores in Lipid Bilayers Using a Plasmonic Nanocavity, *J. Phys. Chem. Lett.*, 2017, **8**, 1472–1475.
- 2 Jörg Frantzeskos, *Neue langwellige Fluoreszenzfarbstoffe zur Markierung von Biomolekülen*, Shaker Publishing House, 2001.
- 3 D. Axelrod, in *Fluorescence Microscopy: Super-Resolution and other Novel Techniques*, Academic Press, 2014, pp. 1–14.
- 4 D. F. Kienle, J. V. De Souza, E. B. Watkins and T. L. Kuhl, Thickness and refractive index of DPPC and DPPE monolayers by multiple-beam interferometry, *Anal. Bioanal. Chem.*, 2014, **406**, 4725–4733.
- 5 A. Gadomski, N. Kruszewska and J. M. Rubi, Derivation of the refractive index of lipid monolayers at an air-water interface, *Opt. Mater.*, 2019, **93**, 1–5.
- 6 X. Xiao and L. Qian, Investigation of humidity-dependent capillary force, *Langmuir*, 2000, **16**, 8153–8158.
- 7 D. I. Kim, J. Grobelny, N. Pradeep and R. F. Cook, Origin of adhesion in humid air, *Langmuir*, 2008, **24**, 1873–1877.
- 8 A. San Paulo and R. García, High-Resolution Imaging of Antibodies by Tapping-Mode Atomic Force Microscopy: Attractive and Repulsive Tip-Sample Interaction Regimes, *Biophys. J.*, 2000, **78**, 1599–1605.

Chapter 7

Tunable biomimetic bacterial membranes from binary and ternary lipid mixtures and their application in antimicrobial testing

The intricate composition of bacterial cell membranes determines their ability to survive direct exposure to extreme environmental conditions and is responsible for the development of resistance toward membrane-targeting antibiotics. The inherent complexity of prokaryotic membranes, complicated isolation process, as well as high biosafety risk associated with handling of bacterial cells, led to the development of different model membranes. The commonly used biomimetic models do not mimic well the characteristics of mammalian cell membranes, and due to the differences in lipid profile as well as in structural and organizational features, they fail to portray the characteristics of bacterial membranes. Moreover, the experimental results obtained for gram-negative bacterial models, which gained interest due to the availability of the ready-made lipid extracts (e.g. *E.coli* polar extract), are often extrapolated to explain processes occurring in other gram-negative bacteria and even in gram-positive bacteria despite the significant differences in membrane structure and composition. Indisputably the available models are far from mimicking the complexity of natural prokaryotic cell membranes, while the scarce, available ones reflect only very specific strains.

In publication 3, I demonstrate the reconstruction of biomimetic cell membranes with increasing levels of complexity developed from binary and ternary lipid mixtures (Figure 7.1). First, I characterized the most commonly used models containing phosphatidylcholine PC and PE or PC and PG and pointed out the differences in structural organization compared to the models comprising only the typical bacterial lipids PE and PG. This comparison allowed me to demonstrate how inaccurate the commonly used model bacterial membranes can be. In the next step, I focused on the preparation of membranes from complex lipid mixtures containing PE, PG, and cardiolipin and showed that even small changes in the lipid profile can have a tremendous impact on the basic properties of the formed GUVs such as membrane curvature, size, leaflets asymmetry (associated with the enhanced formation of nanotubes inside vesicles lumen) or presence of phase separation. Importantly, by varying the relative amount of membrane constituents I sampled a broad

CHAPTER 7. TUNABLE BIOMIMETIC BACTERIAL MEMBRANES FROM BINARY AND TERNARY LIPID MIXTURES AND THEIR APPLICATION IN ANTIMICROBIAL TESTING

area within the compositional map characteristic of different bacterial strains, demonstrating that the proposed here bottom-up approach of reconstituting cellular membranes by mixing the desired ratio of lipids gives the possibility to reproduce, and most importantly tune, the structural and organizational characteristics for both gram-negative and gram-positive bacterial cell membranes. Finally, to validate the bio-application of the reconstructed model gram-positive bacterial membranes I exposed them to the commonly used lipopeptide antibiotic daptomycin. I quantified the daptomycin binding efficiency as a function of the amount of negatively charged lipid species in the membrane.

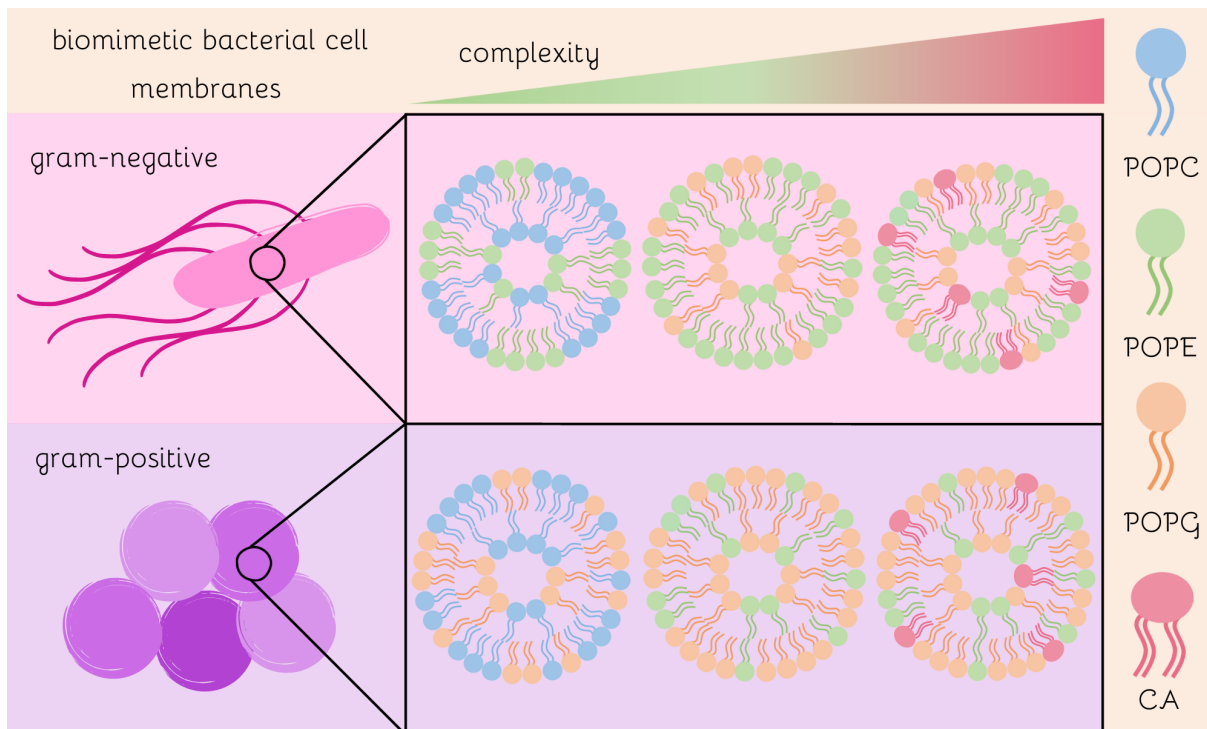


Figure 7.1: Graphical representation of the bottom-up approach used in publication 3 for reconstruction of cell membranes characteristic for gram-negative and gram-positive bacteria.

CHAPTER 7. TUNABLE BIOMIMETIC BACTERIAL MEMBRANES FROM BINARY AND TERNARY LIPID MIXTURES AND THEIR APPLICATION IN ANTIMICROBIAL TESTING

BBA - Biomembranes 1865 (2023) 184194



Contents lists available at [ScienceDirect](https://www.sciencedirect.com)

BBA - Biomembranes

journal homepage: www.elsevier.com/locate/bbamem



Tunable biomimetic bacterial membranes from binary and ternary lipid mixtures and their application in antimicrobial testing

Emilia Krok^{a,b,*}, Mareike Stephan^b, Rumiana Dimova^{b,**}, Lukasz Piatkowski^a

^a Poznan University of Technology, Faculty of Materials Engineering and Technical Physics, Institute of Physics, Piotrowo 3, 60-965 Poznan, Poland

^b Max Planck Institute of Colloids and Interfaces, Science Park Golm, 14476 Potsdam, Germany

ARTICLE INFO

Keywords:

Bacterial membranes
Model cell membranes
Giant unilamellar vesicles
Phase separation
Antimicrobial peptides
Fluorescence microscopy

ABSTRACT

The reconstruction of accurate yet simplified mimetic models of cell membranes is a very challenging goal of synthetic biology. To date, most of the research focuses on the development of eukaryotic cell membranes, while reconstitution of their prokaryotic counterparts has not been fully addressed, and the proposed models do not reflect well the complexity of bacterial cell envelopes. Here, we describe the reconstitution of biomimetic bacterial membranes with an increasing level of complexity, developed from binary and ternary lipid mixtures. Giant unilamellar vesicles composed of phosphatidylcholine (PC) and phosphatidylethanolamine (PE); PC and phosphatidylglycerol (PG); PE and PG; PE, PG and cardiolipin (CA) at varying molar ratios were successfully prepared by the electroformation method. Each of the proposed mimetic models focuses on reproducing specific membrane features such as membrane charge, curvature, leaflets asymmetry, or the presence of phase separation. GUVs were characterized in terms of size distribution, surface charge, and lateral organization. Finally, the developed models were tested against the lipopeptide antibiotic daptomycin. The obtained results showed a clear dependency of daptomycin binding efficiency on the amount of negatively charged lipid species present in the membrane. We anticipate that the models proposed here can be applied not only in antimicrobial testing but also serve as platforms for studying fundamental biological processes in bacteria as well as their interaction with physiologically relevant biomolecules.

1. Introduction

Bacterial lipid membranes differ significantly from their mammalian analogs in terms of composition and structural organization. Mammalian cytoplasmic membranes are composed of different phospholipids such as phosphatidylcholine (PC), phosphatidylserine (PS), phosphatidylethanolamine (PE), sphingomyelin (SM) and cholesterol [1], while bacterial membranes contain mostly PE, phosphatidylglycerol (PG), and cardiolipin (CA). However, the differences between mammalian and bacterial cell membranes go beyond just the lipid composition, as they are distinct also in terms of structural organization. The gram-negative bacterial cell envelope is composed of two membranes separated by the periplasm, which is a gel like substance containing a thin layer of peptidoglycans [2]. The outer membrane (OM) is composed of phospholipids, lipoproteins, OM proteins and glycolipids, of which the most common are lipopolysaccharides. The inner membrane consists of

phospholipids such as PE, PG and CA [3]. Contrary to gram-negative bacteria, the cell envelope of gram-positive bacteria is simpler and does not contain the OM. To withstand the potentially unfavorable environmental conditions their cell membranes are surrounded by a much thicker layer of peptidoglycans, compared to those present in gram-negative bacteria. Moreover, the composition of the inner membrane (IM) differs significantly, it contains mostly PG, lyso-PG, and a much higher amount of CA than in gram-negative bacteria [4].

The widely used biomimetic models reflect well the characteristics of mammalian cell membranes. On the contrary, the models of prokaryotic membranes are usually very simple, composed of one type of lipids. Alternatively, in many cases, some characteristic lipids are replaced by their mammalian substitutes (such as phosphatidylcholine), which are easier to incorporate within the model membranes [5,6]. Such oversimplification can lead to misinterpretation of the obtained results and formulation of false conclusions. On the other hand, studies on bacterial

* Correspondence to: E. Krok, Poznan University of Technology, Faculty of Materials Engineering and Technical Physics, Institute of Physics, Piotrowo 3, 60-965 Poznan, Poland

** Corresponding author.

E-mail addresses: emilia.krok@put.poznan.pl (E. Krok), rumiana.dimova@mpik.mpg.de (R. Dimova).

<https://doi.org/10.1016/j.bbamem.2023.184194>

Received 13 February 2023; Received in revised form 5 June 2023; Accepted 8 June 2023

Available online 14 June 2023

0005-2736/© 2023 Published by Elsevier B.V.

CHAPTER 7. TUNABLE BIOMIMETIC BACTERIAL MEMBRANES FROM BINARY AND TERNARY LIPID MIXTURES AND THEIR APPLICATION IN ANTIMICROBIAL TESTING

E. Krok et al.

BBA - Biomembranes 1865 (2023) 184194

cell membranes reconstituted from lipids extracted directly from bacterial cells are difficult to perform. Although bacterial cell membranes derive from simpler organisms than eukaryotic cells do, they are still characterized by a high level of complexity due to the presence of numerous lipids, proteins, and carbohydrates, which makes it difficult to identify the specific membrane constituents responsible for the observed processes [7]. The sophisticated structure of natural bacterial membranes together with the possible biosafety risks inevitably associated with the handling of bacterial cells has led to the development of biomimetic membrane models with different levels of complexity [8].

A variety of model membranes, such as supported lipid bilayers [3,9–11], tethered bilayer lipid membranes [12–14], and liposomes [15–17] have been used to mimic prokaryotic cell membranes. Giant unilamellar vesicles (GUVs) have received great interest as cell membrane mimetics due to their tractable geometry such as spherical shape and size, which is comparable to the dimensions of natural cells [18–20]. The elimination of solid support (inherent to planar model systems) abolishes the impact of the substrate on one of the leaflets, and allows for the use of symmetric or asymmetric solutions across the membrane, consequently giving the possibility to study processes such as division [21,22], deformation [23], invagination [24], diffusion [25] or transport and release of biomolecules as the basic models of *exo-* and *endo-*cytosis [26]. Although GUVs have been widely employed in studying eukaryotic cell membranes [27–29], the research on prokaryotic GUVs is still limited and the scarce literature reports focus mostly on the gram-negative inner bacterial cell membranes [30–33], and do not address the structurally different membranes of the gram-positive bacteria.

The simplistic, yet accurate models of cell membranes, whether developed from synthetic lipids or natural polar lipid extracts, are necessary for studying the impact of ions [34,35], molecules [36], hydration [37], or antimicrobial agents [38–40] on the prokaryotic membranes. The use of models with well-defined compositions significantly eliminates the effect of other compounds present in native membranes that could influence the obtained results. Usually, the determination of exact factors responsible for specific cellular responses is far from trivial when studying live cells *in vitro*. Indisputably, there is a strong need for accurate, stable, and fully tunable models of prokaryotic membranes that could mimic differences in cell envelopes not only between gram-positive and gram-negative bacteria but also between specific strains, which deviate significantly in terms of lipid composition and as a consequence structural and mechanical properties such as membrane charge, leaflet asymmetry, and presence or absence of phase separation, just to mention a few.

The present study sought to develop biomimetic membranes resembling those present in gram-positive and gram-negative bacteria with an increasing level of complexity. We applied the commonly used electroformation method to form GUVs composed of different molar ratios of PC and PG; PC and PE; PE and PG, ending with the most accurate models containing PE, PG, and CA. All models were prepared from binary or ternary lipid mixtures, allowing for tuning of the final lipid composition to mimic membranes characteristic for specific bacterial strains. We show that depending on the used lipids and their final ratio, the obtained models differ significantly in terms of size, membrane curvature, charge and lateral organization. We demonstrate that the interchangeable use of lipids with similar chemical structures or restricting the model membrane composition to only one or two lipid species can drastically change the overall properties of bacterial membranes and lead to false conclusions. Finally, as a proof of concept, we tested the obtained models containing PG and CA against the lipopeptide antibiotic daptomycin and presented the clear dependency of its binding efficiency on the amount of negatively charged lipids present in the membrane.

2. Materials and methods

2.1. Materials

1-palmitoyl-2-oleoyl-sn-glycero-3-phosphocholine (POPC) and 1-palmitoyl-2-oleoyl-sn-glycero-3-phospho-(1'-rac-glycerol) (sodium salt) (POPG), 1-palmitoyl-2-oleoyl-sn-glycero-3-phosphoethanolamine (POPE), 1,2-dioleoyl-sn-glycero-3-phosphoethanolamine (DOPE), 1',3'-bis[1,2-dioleoyl-sn-glycero-3-phospho]-glycerol (sodium salt) (18:1 CA), and 1,2-dipalmitoyl-sn-glycero-3-phosphoethanolamine-N-(7-nitro-2-1,3-benzoxadiazol-4-yl) (ammonium salt) (16:0 NBD-DPPE), 1,1',2,2'-tetraoleoyl cardiolipin[4-(dipyrrometheneboron difluoride) butanoyl] (ammonium salt) TopFluor® Cardiolipin (TF-CA) and daptomycin were obtained from Avanti Polar Lipids, Alabaster, AL, USA. 1,2-Dioleoyl-sn-glycero-3-phosphoethanolamine labeled with Atto 633 (DOPE-Atto 633), sucrose (BioUltra, HPLC grade), glucose (D-(+)-Glucose, BioUltra, HPLC grade), β -casein (from bovine milk), and chloroform (LiChrosolv®) were purchased from Merck KGaA, Darmstadt, Germany. The ultrapure water was obtained by using Milli-Q® Reference Water Purification System from Merck KGaA, Darmstadt, Germany. All the materials were used without further purification.

2.2. Electroformation of GUVs

GUVs were prepared by the electroformation method following the previously reported protocols [41]. Chloroform stock solutions of POPC-POPE, POPC-POPG, POPE-POPG, or POPE-POPG-CA were mixed at desired molar ratio to the final lipid concentration of 4 mM in each mixture. For imaging purposes, 0.1 mol% of DOPE-Atto 633, 0.5 mol% of NBD-DPPE or 0.5 mol% of Top Fluor-CA were added. 10 μ L of as prepared stock solutions were spread on two conductive indium tin oxide (ITO)-coated glasses (50 mm \times 50 mm, resistance 20 Ω /sq., Präzisions Glas & Optik, Iserlohn, Germany), equipped with a pair of adhesive copper strips (3 M, Cergy-Pontoise, France) and placed in a desiccator for 2 h to remove residual traces of chloroform. To assemble the chamber, a 2 mm thick Teflon spacer was placed between the ITO-glasses, and the formed chamber was filled with 2 mL sucrose solution with an osmolarity of 100 ± 1 mOsmol/kg for vesicles made of the binary mixtures or sucrose solution with an osmolarity 300 ± 1 mOsmol/kg for GUVs composed from ternary lipid mixtures (POPE, POPG and CA). The osmolarity was measured with a freezing point osmometer Osmomat 3000 (Gonotec, Berlin, Germany). The electroformation was done by applying AC electric field at 10 Hz with a peak-to-peak voltage of 1.6 V for 1 h. In the case of vesicles made from ternary lipid mixtures, the electroformation was performed at 65 °C, which is above the phase transition temperature of cardiolipin (60 °C). The vesicles were harvested from the chamber using a 1 mL pipette and transferred to Eppendorf tube for further imaging on the same day.

2.3. Vesicle imaging

Observation chambers were constructed from two coverslips and a spacer (CoverWell™ incubation chamber, Grace Bio-Labs, Oregon, USA). To prevent vesicles from bursting upon contact with glass, the coverslips were coated with β -casein (2 mg/mL), and left for 15 min to dry. 10 μ L of GUVs solution was deposited onto the coverslip together with 10 μ L glucose solution with the same osmolarity as the inside sucrose solution (100 mOsmol/kg or 300 mOsmol/kg for GUVs composed of binary or ternary lipid mixtures respectively). The sucrose-glucose solution density difference induced GUVs sedimentation onto the glass coverslip. In each experiment GUVs were allowed to settle for around 30 min prior to imaging.

The fluorescence imaging was done using Leica SP5 or Leica SP8 confocal microscopes (Leica Microsystems, Mannheim, Germany). Argon laser with wavelength 488 nm was used for NBD-DPPE and TF-CA excitation. The emitted light was collected in the wavelength range of

CHAPTER 7. TUNABLE BIOMIMETIC BACTERIAL MEMBRANES FROM BINARY AND TERNARY LIPID MIXTURES AND THEIR APPLICATION IN ANTIMICROBIAL TESTING

E. Krok et al.

BBA - Biomembranes 1865 (2023) 184194

500–550 nm. The excitation of Atto 633 was done using HeNe laser with wavelength 633 nm, and the emission was collected in the range of 650–750 nm. Images were obtained using 40 \times , NA 1.3 oil immersion objective (Leica SP8) or 40 \times , NA 0.75 dry objective (Leica SP5) in bidirectional scan mode at 400 Hz. Minimal laser powers were used to minimize the photobleaching. To determine the size distribution of GUVs at least 150 GUVs from 3 different preparations of the same lipid composition were analyzed using Fiji (ImageJ) software [42]. We performed 3–5 scans in the z-direction over large imaging areas to include vesicles of different sizes and ensure that always the equatorial cuts are analyzed. Vesicles with diameters smaller than 1 μ m were not considered in the analysis.

2.4. Preparation of LUVs for zeta potential measurements

Chloroform stock solutions of POPC-POPG, POPE-POPG, and POPE-POPG-CA were mixed at the desired molar ratio to the final lipid concentration of 10 mM in each mixture. Lipid films were dried under a nitrogen stream and left under a vacuum pump for overnight incubation, to ensure the removal of residual organic solvent. The films were rehydrated with 2 mL of the sucrose buffer with an osmolarity of 100 mOsmol/kg and exposed to four cycles of heating on a hot plate (65 $^{\circ}$ C) and vortexing. Each step of heating and vortexing was performed for 1 min. The lipid suspension containing multilamellar vesicles was extruded 21 times through a polycarbonate membrane with a 100 nm pore diameter using a mini-extruder from Avanti Polar Lipids.

2.5. Zeta potential measurements

Zeta potential measurements were performed on GUVs and on large unilamellar vesicles (LUVs) using ZetaSizer Nano ZS (Malvern, UK). The measurements of zeta potential on GUVs are challenging due to low stability and sedimentation of the vesicles during repeated measurements. According to Carvalho et al. [43], the zeta potential measured on GUVs correlates well with the values obtained for LUVs, thus we tested both model systems to quantify the surface charge. Approximately 600 μ L of GUVs or LUVs suspension in the symmetric sucrose solution was placed directly in DTS1070 folded capillary cell with integrated gold electrodes (Malvern). All measurements were performed at 21 $^{\circ}$ C. The electrostatic potential at the shear plane was calculated using the Helmholtz-Smoluchowski Eq. (1)

$$\xi = \frac{\mu\eta}{\epsilon\epsilon_0} \quad (1)$$

where μ is the electrokinetic mobility of the vesicle, η is the viscosity of the aqueous solution (sucrose in this case), ϵ is the dielectric constant of the aqueous medium, and ϵ_0 is the permittivity of free space.

2.6. Binding of daptomycin to GUVs and imaging

GUVs composed of binary lipid mixtures containing POPE:POPG in molar ratios 7:3, 1:1 and 3:7, and from ternary lipid mixtures POPE:POPG:CA in molar ratios 7:2:1 and 3:6:1 were prepared in 300 mM sucrose solution using the electroformation method. The samples were mixed by placing 10 μ L of glucose containing 20 mM CaCl₂ with the final osmolarity of 300 mOsmol/kg followed by the addition of 10 μ L of GUVs suspension. GUVs were allowed to settle for 10 min prior to the addition of 1 μ L of 22 μ M daptomycin (in water). Daptomycin is intrinsically fluorescent due to its kynurenine residue which can be excited using 405 nm laser diode, giving the possibility for imaging without an additional fluorescent probe bound to this antibiotic. The emitted light was collected in the wavelength range of 415–470 nm. The images for intensity analysis were acquired at fixed laser power and gain, 30 min after the addition of daptomycin to ensure the same incubation time for all samples. The intensity analysis of GUVs was performed using the

ImageJ plugin Radial Profile Angle. The fluorescence intensity was plotted as a function of normalized radial coordinate after subtracting the background intensity using peak finder in OriginLab software.

3. Results and discussion

3.1. POPC/POPE GUVs as basic models of the inner cell membrane of gram-negative bacteria

Phosphatidylethanolamine (PE) is one of the major lipid components of all prokaryotic cell membranes and the most abundant constituent of the inner membrane of gram-negative bacteria [44]. The inner cell membrane of *E. coli* is composed of 70 % of PE, 25 % of PG, and around 5 % of CA. The chemical structure and zwitterionic character of PE make it very similar to phosphatidylcholine (PC), which differs only in the methylation of the amine group. Consequently, PC, which due to its cylindrical shape favors flat bilayer structures, has been widely used as a substitute for PE in most studies. However, some of the intrinsic properties of PE lipid, for instance the ability to be a hydrogen bond donor [45], or PE membrane properties such as increased curvature [46], which in native membranes leads to stabilization of transmembrane proteins [47], make it a unique membrane constituent.

In order to recreate the most basic model of the inner cell membrane of gram-negative bacteria and to assess whether PC and PE can truly be used interchangeably at any ratio, we explored four different mixtures of lipids, containing POPC:POPE in molar ratios 9:1, 7:3, 1:1 and 3:7. We have chosen lipids with one saturated 16:0 and one unsaturated 18:1 fatty acid chain, which are the most abundant types of acyl chains present in cell membranes of both gram-negative and gram-positive bacteria [48,49]. Moreover, the eukaryotic and prokaryotic cell membranes *in vivo* contain high content of lipids with mixed acyl chains (such as POPE or POPC), while lipids with both monounsaturated acyl chains (such as e.g. DOPE or DOPC) are sparsely present in the biological systems [50]. As presented in Fig. 1A, GUVs with 10 % of POPE did not show any signs of phase separation. When the amount of POPE increased to 30 % we observed membrane domains with different (lower) fluorescence intensities of the labeling dye NBD-DPPE. At 21 $^{\circ}$ C, which is the temperature maintained during all measurements reported here, POPC which has a phase transition temperature of -2 $^{\circ}$ C, is in a disordered liquid crystalline phase (L_d), while POPE with its phase transition temperature of 25 $^{\circ}$ C remains in ordered gel phase (S_b) [51]. The difference in lipid packing is the main driving force leading to the observed phase separation. Given the melting temperatures of the two lipids and the increasing area fractions of the domains with increasing POPE mole fraction, we conclude that the dark domains are POPE-rich. The irregular shape of the domains (see Fig. S1) and the fact that their morphology does not change over time corroborate the conclusion that they are solid-like. They could drift along the vesicle surface confirming that the surrounding phase is fluid. NBD-DPPE appeared to be distributed in the fluid POPC-rich regions rather than POPE phase, consistent with previous observations for preferential partitioning to liquid disordered phases [52]. To further confirm the partitioning of NBD-DPPE dye to POPC-rich domains we introduced the dye Atto-DOPE as an additional fluorescent marker. We observed that regions of higher NBD-DPPE intensity colocalize perfectly with Atto-DOPE labeled areas (see Fig. S2). Thus we conclude that NBD-DPPE prefers the higher fluidity regions over areas composed of lipids with the same headgroup. It should be noted that PE derivatives with saturated chains are characterized by a rather unpredictable partitioning within membranes, and many of them (such as Rh-DPPE) prefer incorporation within fluid-like regions over ordered phases [53].

Images of the equatorial cross-section of GUVs showed that regions of POPE bend inward (towards the vesicle interior) while the saddle-shaped rims of the domain boundaries are occupied by the more flexible fluid POPC-rich phase (consistent with the previous observations [54]). The polar headgroup of POPE has a smaller diameter than its

CHAPTER 7. TUNABLE BIOMIMETIC BACTERIAL MEMBRANES FROM BINARY AND TERNARY LIPID MIXTURES AND THEIR APPLICATION IN ANTIMICROBIAL TESTING

E. Krok et al.

BBA - Biomembranes 1865 (2023) 184194

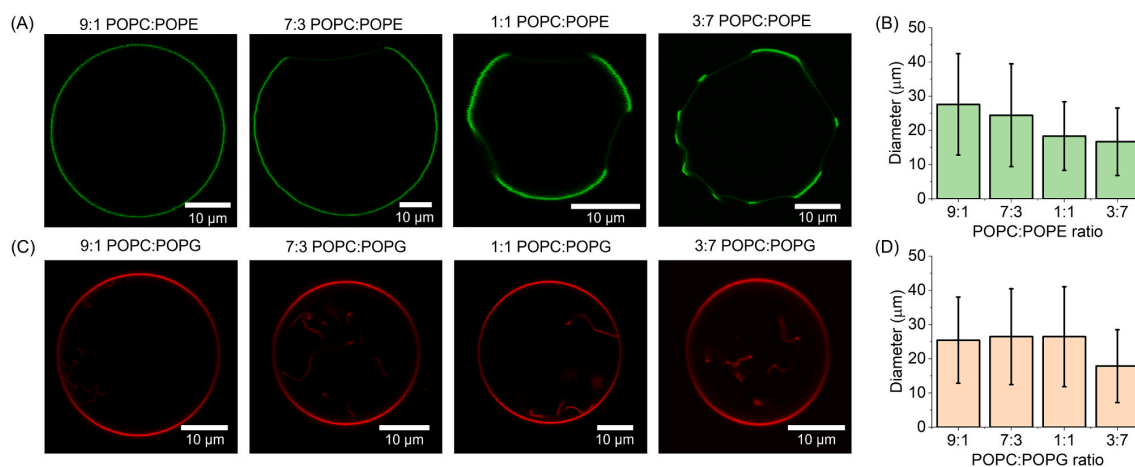


Fig. 1. Phase separation and sizes of GUVs prepared from binary lipid mixtures containing POPC and lipids typical for bacterial cell membranes: (A) Confocal cross section images of GUVs mimicking gram-negative bacterial cell membranes composed of POPC and POPE in molar ratios 9:1, 7:3, 1:1 and 3:7, labeled with 0.5 mol% of fluorescent probe NBD-DPPE. The low-intensity regions were ascribed to the POPE-rich phase. (B) Average diameter of GUVs containing POPC:POPE at different molar ratios, error bars correspond to the standard deviation. Number of analyzed vesicles was $N_{9:1} = 352$, $N_{7:3} = 292$, $N_{1:1} = 268$, $N_{3:7} = 517$. (C) Confocal cross section images of GUVs mimicking gram-positive bacterial cell membranes prepared from binary lipid mixture of POPC and POPG in molar ratios 9:1, 7:3, 1:1 and 3:7, labeled with 0.1 mol% of fluorescent probe DOPE-Atto 633. (D) Average diameter of GUVs containing POPC:POPG at different molar ratios, error bars correspond to the standard deviation. Number of analyzed vesicles was $N_{9:1} = 255$, $N_{7:3} = 308$, $N_{1:1} = 215$, $N_{3:7} = 151$. See Figs. S3 and S4 for size distribution histograms. Image acquisition was done at 21 °C.

hydrocarbon chain (truncated cone shape geometry), leading to its affinity to assemble and stabilize hexagonal phases. POPE molecules are characterized by high negative curvature of approximately -0.33 nm^{-1} [55], while POPC which can be considered as having a cylindrical shape, favors lamellar phases as its curvature is 0.022 nm^{-1} [55,56]. These molecular curvatures are not to be confused with the curvature of the membrane, which in our system is relatively low and of the order of 0.1 nm^{-1} . High membrane curvature is typically generated by asymmetry of the bilayer leaflet composition [57–60] or the solution across the membrane [35,61], whereby the latter was also shown to modulate the phase state of charged membranes [62–64].

We noticed that the relative content of POPC and POPE had a strong influence on the size of the formed GUVs. Size distribution is one of the most important parameters determining the potential application of GUVs. When used as drug delivery agents, GUVs should be bigger than the volume of the desired cargo [65], while those used as simple models of eukaryotic or prokaryotic cells, should have dimensions compatible with the size of natural cells, which for the most bacterial strains varies between 1 and 2 μm. To determine the size distribution of GUVs with different POPC and POPE ratio at least 250 GUVs were analyzed from 3 different sample preparations. As shown in Figs. 1B and S3 we observed clear dependence between the POPE content and GUVs size, where the latter decreased with the increasing amount of POPE. It should be noted that the area per lipid, which is a parameter describing the packing of lipids within the membrane differs significantly for POPE (56.6 \AA^2) [66] and POPC (68.1 \AA^2) [67]. The smaller size of GUVs containing higher amounts of POPE can be explained two-fold: on the one hand, the higher population of more densely packed lipids might lead to the decreased size of the formed GUVs; and on the other hand, the differences in molecular curvatures force vesicles to adopt more energetically favorable shape.

The observed changes in lateral organization, curvature and size clearly show that PC and PE should not be used interchangeably to model bacterial membranes as membranes composed of one or the other lipid (or with varying relative ratio) exhibit very different properties.

3.2. POPC/POPG GUVs as basic models of gram-positive bacterial cell membranes

The cell membranes of gram-positive bacteria such as *S. aureus* (responsible for 34 % of post-implantation infections) or *B. subtilis* (pivotal strain used in fermentation processes) contain up to 70 % of negatively charged PG lipids. To mimic the gram-positive bacterial cell membrane it is therefore crucial to incorporate large fractions of negatively charged lipids. Thus, the most basic model of these membranes, proposed here consists of POPC:POPG lipids at molar ratio 9:1, 7:3, 1:1, and 3:7. We observed that membranes containing >30 % of POPG exhibited inward-pointing protrusions in the form of tubes and buds (see Fig. 1C). This is consistent with earlier reports [68] showing the presence of nanotubes in GUVs containing PC and PG lipids prepared by the electroformation method. The tubes are stabilized by negative spontaneous curvature resulting from the transbilayer lipid membrane asymmetry between the inner and outer leaflet. The latter is caused by the presence of the electrode electrostatic charge that is inseparable factor driving GUVs formation in this technique. As shown in [68], this asymmetry can easily be eliminated by using gel-assisted swelling [69], an alternative method, which allows formation of GUVs at high salt concentrations that screen the negatively charged POPG. It should be noted that the asymmetrical assembly of different types of lipids is highly desirable, as this type of arrangement emerges as the preferential structural organization in all prokaryotic [33,70,71], and eukaryotic cell membranes [72–74]. Membrane asymmetry affects basic membrane properties [57,59,68,75,76] such as surface charge, permeability, curvature, shape, stability, mechanics and membrane potential, and it is essential for a wide range of biologically relevant processes, among them signal transduction [73], apoptosis [77], cell-cell fusion [78] and immune response of the cell [79]. Consequently, the formation of GUVs with different lipid compositions in the inner and outer leaflets can be considered as a more accurate and biologically significant model of naturally occurring cell membranes.

It should be noted that we did not observe phase separation for any of the tested POPC:POPG lipids compositions. The transition temperature of POPC and POPG is -2 °C , which means that at room temperature ($\sim 21 \text{ °C}$) both lipids are in liquid disordered phase [51]. Moreover,

CHAPTER 7. TUNABLE BIOMIMETIC BACTERIAL MEMBRANES FROM BINARY AND TERNARY LIPID MIXTURES AND THEIR APPLICATION IN ANTIMICROBIAL TESTING

E. Krok et al.

BBA - Biomembranes 1865 (2023) 184194

POPC and POPG are characterized by the same chain length and almost zero spontaneous curvature, which are other important factors that could influence the lateral organization.

Furthermore, contrary to GUVs composed of POPC and POPE, there was no compositional dependence on the size of POPG-doped GUVs. As shown in Figs. 1D and S4, only vesicles that contained 70 % of POPG had a significantly smaller diameter. It should be noted that these samples exhibited also a very high content of tubes. These inward-pointing protrusions are good mimics of mesosomes – convoluted membranous structures present in prokaryotic cells upon their exposure to perturbing events such as mechanical contraction or cell injury [80]. This specific type of invagination of the plasma membrane has not been well studied; however, the presence of mesosomes has been proven as inseparable during the replication and separation of chromosomes, cell division, and extracellular transport [81]. Moreover, mesosomes are considered to be prokaryotic equivalents of eukaryotic mitochondria - a connection that still has not been well understood [82]. The model of gram-positive cell membranes proposed here lays the groundwork for the follow-up research on both asymmetric membranes as well as on the behavior of mesosomes and their role in various cellular mechanisms.

3.3. POPE/POPG binary lipid mixtures as model bacterial cell membranes

It is estimated that only 10 % of all gram-positive and gram-negative bacteria possess PC as a membrane lipid and only up to 15 % of them have the ability to synthesize this lipid [83]. Although the structure of PC is very similar to PE, which explains its use in model bacterial cell membranes, it cannot be considered as a typical lipid constituting bacterial cell membranes. We analyzed lipid profiles of the most common bacterial strains from gram-positive and gram-negative groups. Most of them are composed of high fractions of PE and PG and differ only in their relative ratio as presented in Fig. 2A (dark violet and pink dots correspond to the most common strains of gram-positive and gram-negative bacteria, respectively) and in Supplementary Table 1. Thus, in the

next step towards the development of bacterial cell membranes we chose to use PE and PG lipids without the addition of PC. As shown in Fig. 2B–D, despite the high content of negatively charged POPG, we were able to form defect-free GUVs, which in general did not contain tubes or vesicles trapped inside. Contrary to vesicles containing POPC and POPE, there was no phase separation observed for any of the tested compositions (7:3, 1:1 and 3:7) containing POPE and POPG. The absence of micrometer size domains does not exclude their potential presence on the nanometer scale, i.e., below the resolution limit of the fluorescence microscope. However, AFM measurements reported in [84] revealed that phase separation in the binary lipid mixture of POPE:POPG strongly depends on the presence of Ca^{2+} ions. In the absence of this divalent cation, supported lipid bilayers composed of POPE and POPG do not exhibit phase separation, which is consistent with our findings for POPE/POPG GUVs obtained in sucrose/glucose buffer. Moreover, we did not observe variation in membrane local curvature in GUVs containing POPE and POPG, contrary to the models that were composed of POPE and POPC. This clearly shows that the replacement of POPE or POPG with POPC, which is commonly applied in the preparation of bacterial models, can drastically change the overall membrane properties. The analysis of size presented in Figs. 2E and S5, revealed that these GUVs did not show any variation in size regardless of the used POPE:POPG ratio. However, it should be noted that vesicles containing only POPG and POPG had a maximum diameter not exceeding 45 μm (see Fig. S5), which makes them much smaller than GUVs containing POPC as the major component.

3.4. Gram-positive and gram-negative cell membranes reconstructed from ternary lipid mixtures

Gram-positive bacterial cell membranes are characterized by a high content of negatively charged lipids such as POPG and CA and in most cases only a small amount of POPE [85]. A model of gram-positive bacterial cell membrane was prepared from ternary lipid mixture of POPE:POPG:CA in a molar ratio 3:6:1. To prepare GUVs mimicking the

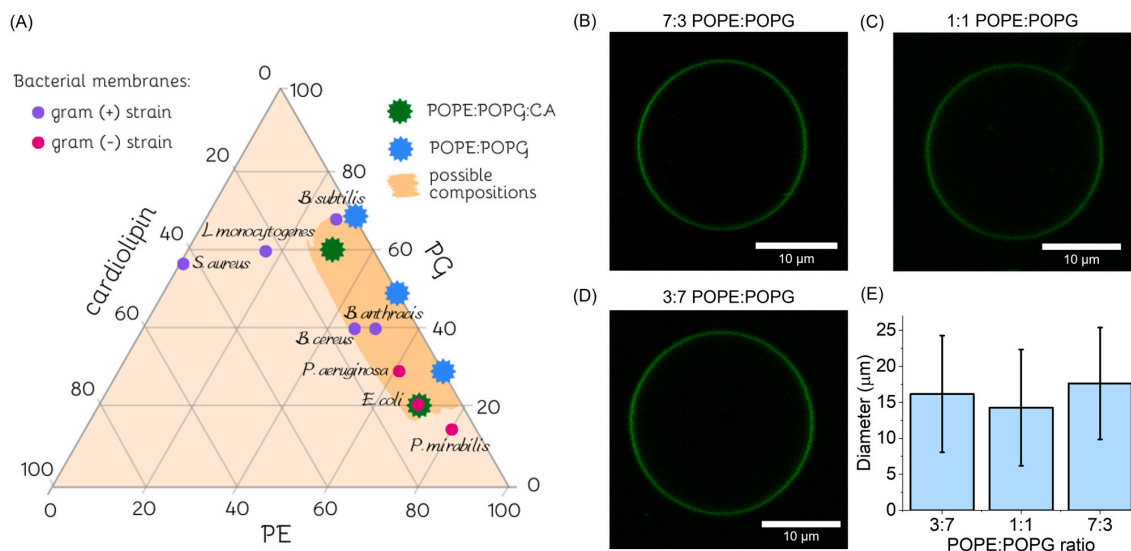


Fig. 2. (A) Ternary diagram of lipid membrane compositions for the most common gram-positive (dark violet dots) and gram-negative (magenta dots) bacterial strains; green and blue stars correspond to the lipid compositions tested in this study; rectangular, orange area indicates the compositions for GUV preparation that could readily be achieved by mixing the desired ratio of POPE:POPG:CA (see section on membrane models obtained from ternary lipid mixtures); see Supplementary Table S1 for details on membrane compositions. (B) Fluorescence image of GUVs containing POPE and POPG in molar ratio 7:3, (C) POPE:POPG 1:1, and (D) POPE:POPG 3:7, GUVs were labeled with 0.5 mol% NBD-PPPE. (E) Average diameter of GUVs prepared from binary lipid mixture of POPE and POPG. Number of analyzed vesicles was $N_{3:7} = 185$, $N_{1:1} = 174$, $N_{7:3} = 128$. See Fig. S5 for size distribution histograms. Image acquisition was done at 21 °C. (For interpretation of the references to colour in this figure legend, the reader is referred to the web version of this article.)

CHAPTER 7. TUNABLE BIOMIMETIC BACTERIAL MEMBRANES FROM BINARY AND TERNARY LIPID MIXTURES AND THEIR APPLICATION IN ANTIMICROBIAL TESTING

E. Krok et al.

BBA - Biomembranes 1865 (2023) 184194

inner cell membrane of gram-negative bacteria we have chosen the ternary lipid mixture of POPE:POPG:CA in a molar ratio 7:2:1, which resembles well the composition of commonly used *E. coli* polar extract. The incorporation of CA in models of gram-positive and gram-negative bacterial cell membranes is crucial, as this unique lipid is abundantly present in prokaryotic membranes (see Fig. 2A) and plays a pivotal role in creating binding sites for membrane-specific proteins [86].

Both mixtures of POPE:POPG:CA in molar ratio 3:6:1 and 7:2:1 corresponding to gram-positive and gram-negative bacterial cell membranes respectively, resulted in the successful formation of GUVs. We are not aware of studies where the electroformation method has been applied for preparing bacterial GUVs with such a high content of negatively charged lipids, which is characteristic for membranes of gram-positive bacteria. The available literature proposes only the use of PVA gel-assisted swelling as successful formation technique [38].

As shown in Fig. 3A, the labeling of the membranes with NBD-DPPE revealed the formation of patches with brighter fluorescence intensity in 7:2:1 POPE:POPG:CA GUVs. Addition of a second probe - Atto-633 DOPE, which is known to incorporate within L_d phase, showed that NBD-DPPE resides preferentially in the fluid phase. To clarify further the origin and character of the clearly visible phase separation and the role of CA in this lateral arrangement we performed an additional experiment where NBD-DPPE was replaced by another fluorescent probe Top Fluor-CA (see Fig. S6). Because regions containing Atto-633 DOPE and Top Fluor-CA showed perfect colocalization, we assigned them to more fluid and CA-rich areas, which is in agreement with results reported by Khoury et al. [87], where GUVs composed of PE:PG:CA in molar ratio 60:21:11 contained flower-like CA domains. Moreover, as shown in Fig. S7A we have prepared GUVs with the lipid composition DOPE:POPG:CA at molar ratio 7:2:1, which differ in the replacement of POPE with more unsaturated (fluid) lipid DOPE. Although, the relative lipid composition was the same as for GUVs composed of POPE:POPG:CA, we obtained homogeneous GUVs with no signs of phase-separation in the form of cardiolipin-rich domains. As presented in Fig. S7B we have also prepared GUVs with varying ratio of POPE and POPG, keeping the

amount of CA constant and observed that formation of domains occurs solely for one specific lipid composition 7:2:1 characterized by a large fraction of POPE. Surprisingly, as shown in Figs. 3B and S6, and despite containing the same CA amount, GUVs that possessed a higher fraction of POPG (reflecting gram-positive bacterial membranes) were characterized by homogeneous distribution. They lacked the presence of CA-rich microdomains, which were clearly visible in GUVs composed predominantly of POPE with only 20 % of POPG and 10 % of CA (Fig. 3A).

Undoubtedly, the presence of CA leads to the structural changes within the membrane, as no phase separation was observed for GUVs containing only POPE and POPG. The formation of lipid domains or so-called "lipid rafts" in bacterial cell membranes is still debatable, however, recent publications clearly state that specific strains of gram-positive and gram-negative bacteria can exhibit phase separation within their cell envelopes [87–89]. The CA-specific fluorescent dye 10-N-nonyl-acridine orange revealed lateral heterogeneities in *E. coli* membranes, where CA-rich domains localized preferentially in septal regions and on the poles of the bacterial cell envelope [90]. Moreover, the formation of phosphatidylethanolamine (PE)-rich domains in *B. subtilis* cells was detected by using the cyclic peptide probe Ro09-0198, which binds specifically to PE lipids [91]. The proposed models reflect the CA segregation observed *in vitro*, thus they can successfully be applied to study changes in the lateral organization and structural heterogeneities in bacterial membranes; to investigate the lipid-protein interactions, since domains are the preferential binding sites for some membrane proteins [92]; as well as used in antimicrobial testing of phase-specific drugs.

The sizes of GUVs composed of ternary lipid mixtures were smaller (on average between 5 and 10 μm in diameter) than those of GUVs made of membranes containing PC (Fig. 3C, D). Mohanan et al. [79] obtained vesicles with an average size of 45 and 43 μm for gram-negative and gram-positive bacterial membranes respectively, using PVA gel-assisted swelling in HEPES buffer, suggesting that the size of bacterial GUVs depends on the formation technique and type of the swelling solution. The small size of GUVs can limit their application in studying the

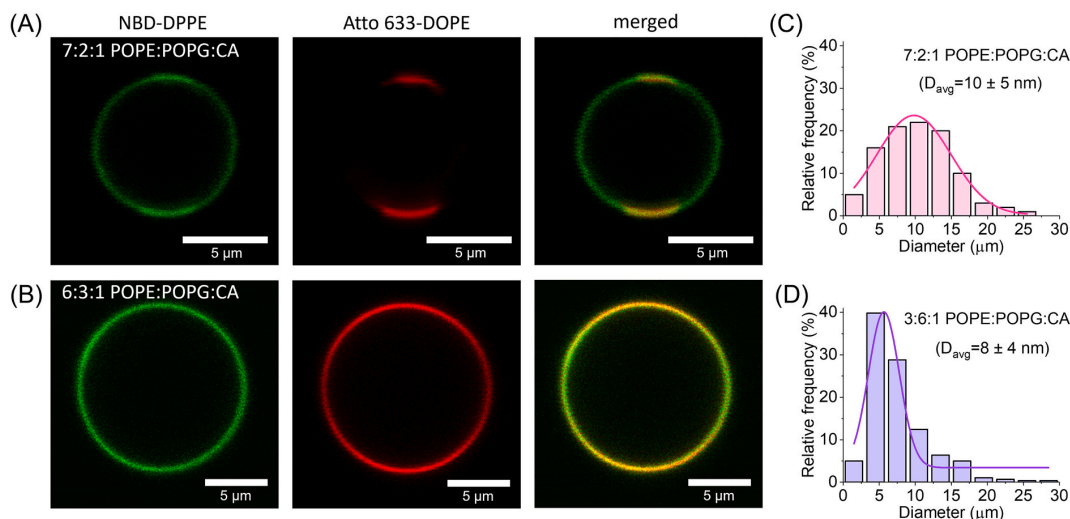


Fig. 3. Appearance and size distribution of GUVs mimicking bacterial cell membranes reconstituted from ternary lipid mixture of POPE, POPG and CA: (A) Confocal cross section images of GUVs with lipid composition characteristic for the inner cell membrane of gram-negative bacteria, containing POPE:POPG:CA in molar ratio 7:2:1, labeled with 0.5 mol% of NBD-DPPE and 0.1 mol% of DOPE-Atto 633. Atto-labeled regions correspond to the more fluid domains rich in CA and POPG. (B) Fluorescence images of GUVs with lipid composition characteristic for the inner cell membrane of gram-positive bacteria, containing POPE:POPG:CA in molar ratio 3:6:1, labeled with 0.5 mol% of NBD-DPPE and 0.1 mol% of DOPE-Atto 633. (C) Histogram of size distribution of GUVs mimicking cell membranes of gram-negative, D_{avg} refers to the average diameter of GUVs, number of analyzed vesicles $N = 165$ from 3 different samples preparations. (D) Histogram of size distribution of GUVs mimicking cell membranes gram-positive bacteria, D_{avg} refers to the average diameter of GUVs, number of analyzed vesicles $N = 281$ from 3 different samples preparations. Image acquisition was done at 21 °C.

CHAPTER 7. TUNABLE BIOMIMETIC BACTERIAL MEMBRANES FROM BINARY AND TERNARY LIPID MIXTURES AND THEIR APPLICATION IN ANTIMICROBIAL TESTING

E. Krok et al.

BBA - Biomembranes 1865 (2023) 184194

diffusion of lipids and incorporated molecules. Methods such as fluorescence recovery after photobleaching, which is based on the bleaching of a small spot, and observation of its recovery, will not be applicable in determining diffusion coefficient as the standard size of the spot (typically a few micrometers in diameter) is usually comparable with the average size of the GUVs obtained here (~5–10 μm); an approach based on half-vesicle bleaching might still be applicable [58]. Nevertheless, the average size of the bacterial cell lies between 1 and 2 μm , with only a few exceptions such as e.g. *T. majus*, which can reach up to 20 μm [93]. Therefore, the formation of biomimetic membranes with dimensions similar to bacterial cells seems more reasonable than the use of models with sizes adapted to mimic eukaryotic cells.

We noticed that the production yield differed for both membrane models. To study the stability as well as to obtain an idea about the formation yield, GUVs from both groups were harvested and placed in an observation chamber followed by 24 h incubation. As shown in Fig. S8 the population number was much higher for GUVs containing POPE:POPG:CA at molar ratio 3:6:1 (mimicking gram-positive bacterial cell membranes) than for 7:2:1 POPE:POPG:CA GUVs (corresponding to cell membranes of gram-negative bacteria). Presumably, the high amount of negatively charged lipid species in gram-positive membranes leads to more efficient production when using electroformation method; as demonstrated earlier, vesicle growth may be improved if the phospholipid mixtures contain charged lipids [94]. The number of GUVs composed of POPE:POPG:CA at molar ratio 3:6:1 was so high that they completely covered the whole observation area and scanning in the z-direction confirmed the presence of multiple layers of GUVs. Thus, for prolonged experiments performed on this model, it is recommended to further dilute the GUVs solution, to obtain more dispersed and easier to image samples.

As presented in Fig. S8, 3:6:1 POPE:POPG:CA GUVs (containing high content of negatively charged lipids characteristic for gram-positive bacteria) had a strong tendency to form multivesicular structures. This suggests that the electroformation of gram-positive GUVs can be used as an alternative protocol for the formation of multivesicular structures or so-called “vesosomes” [95]. These structures are mother vesicles encapsulating non-concentrically arranged vesicles trapped inside their lumen. Vesosomes can be treated as very basic models of primitive cells, where internal vesicles mimic well cellular compartmentalization. Moreover, vesosomes are widely applied as drug delivery systems, where molecules trapped inside inner vesicles are protected by the mother vesicle from contact with body fluids [96]. Finally, they are commonly used as confined reaction compartments for enzymatic reactions [97].

The reconstitution of model gram-positive and gram-negative bacterial cell membranes was performed in this research by mixing the appropriate ratio of lipids instead of using commercially available extracts. *E. coli* total and polar extract are the most common lipid mixtures used for the preparation of bacterial cell membranes. Both extracts are obtained from *E. coli* B (strain nomenclature: ATCC 11303) grown in Kornberg Minimal media at 37 °C and taken at 3/4 log growth phase. *E. coli* polar extract has been successfully used for studying the impact of antimicrobial peptides such as ciprofloxacin [98], norfloxacin [38], gramicidin S [99], ovispirin-1, and magainin 2 [100] on the reconstructed model bacterial cell membranes. Moreover, GUVs developed from *E. coli* extract were reported as simplistic, yet accurate models for studying interactions of bacterial membranes with magainin 2 [101], lactoferricin B [102,103], melittin [104] and AMPR-11 [105]. Bacterial extract can be considered as a more biologically relevant lipid mixture due to the presence of higher level of lipid tails diversity. In general, extracts are not limited to PG and PE lipids with specific fatty acid chains, but contain lipids with a wider variety of chain lengths, and different degree of saturation, including also branched fatty acids commonly present in bacterial membranes. The physical properties of the lipid membranes such as fluidity, bending modulus, membrane permeability and phase separation are directly related to the types of

hydrocarbon chains and their relative amount within the lipid bilayer. However, it should be emphasized that contrary to the extracted lipid mixtures, the proposed bottom-up approach gives the possibility for modifying the GUVs composition in a controlled fashion and for preparing membranes with specific lipid profile characteristic not only for *E. coli* inner cell membrane but also for other gram-negative bacteria. By varying the ratio of PE, PG and CA we are also able to recreate membranes of gram-positive bacteria mimic, for which there are no extracts available. Finally, it should be noted that the exact lipid composition in the bacterial extracts can vary even between different cultures of the same strain and firmly depends on the growth parameters, which in consequence can influence the reproducibility of the obtained experimental results [106]. These differences in GUVs final lipid profile are significantly reduced when preparing model membranes by mixing the desired ratio of lipids.

3.5. Zeta potential measurements

In general and within the same sample, vesicles made of the ternary mixture can vary in composition [107], presumably, because during handling, GUVs can bud, pinching off a domain of certain composition. GUVs composed of POPC and POPE showed phase separation and formation of POPE-rich domains, which increased in size with the increasing POPE content. Thus, it is very likely that these model membranes contained both types of lipids. To corroborate the presence of negatively charged POPG in GUVs that were not characterized by phase separation we measured the zeta potential. We are aware that zeta potential measurements are subject to errors and cannot be directly used to quantitatively compare amounts of negatively charged lipids in GUVs of different composition. Nevertheless, zeta potential measurements were applied here to confirm that GUVs indeed contained negatively charged lipids, which was a key prerequisite for the subsequent experiments with the antimicrobial peptide daptomycin (see Fig. S9).

From the size histograms, it was clear that our GUVs were very polydisperse in size. Sample heterogeneity is disadvantageous in zeta potential measurements as it leads to a quasi-average value from the whole population [68]. Moreover, GUVs containing high content of negatively charged lipids are not stable in the electric field, which is inherently applied during the measurement. However, it has been shown that zeta potential values for GUVs correlate well with those measured for LUVs of the same lipid composition [43]. Consequently, the prepared MLVs were extruded through a 100 nm pore size filter in order to decrease and homogenize their size.

Both PG and CA are negatively charged lipids, with the latter carrying two negative charges. As presented in Fig. 4, zeta potential was negative for all samples, which confirmed the presence of negatively charged lipids in all tested systems containing POPG and/or CA. Moreover, increasing POPG content for LUVs formed from binary lipid mixtures led to more negative zeta potential. This effect is also evident for the samples composed of ternary lipid mixtures, where LUVs composed of POPE:POPG:CA at molar ratio 7:2:1 (mimicking gram-negative bacterial membranes) and POPE:POPG:CA at molar ratio 3:6:1 (proposed model for gram-positive bacterial membranes) had zeta potential values of -54 ± 5 mV and -67 ± 5 mV, respectively. As discussed previously, membranes of gram-positive bacteria were composed of a much higher content of negatively charged POPG and CA, which is the reason for this significantly lower value of zeta potential when compared with LUVs mimicking gram-negative bacterial membranes.

As shown in Figs. 4 and S9, the zeta potential values did not scale proportionally with the increase of the fraction of negatively charged lipids for both LUVs and GUVs, which could lead to the conclusion that the amount of POPG incorporated in the membrane was lower than the initial composition of stock solutions. However, as shown in [108,109] the changes of zeta potential with increasing amount of negatively charged lipids are minor when performed in pure sucrose buffer or in sucrose containing low (1–5 mM) concentrations of NaCl. The

CHAPTER 7. TUNABLE BIOMIMETIC BACTERIAL MEMBRANES FROM BINARY AND TERNARY LIPID MIXTURES AND THEIR APPLICATION IN ANTIMICROBIAL TESTING

E. Krok et al.

BBA - Biomembranes 1865 (2023) 184194

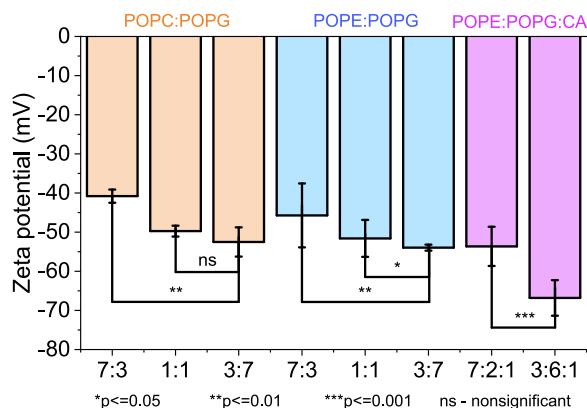


Fig. 4. Zeta potential measurements of LUVs in sucrose solution. LUVs prepared by extrusion of MLVs made of POPC:POPG mixtures at molar ratio: 7:3, 1:1, 3:7; POPE:POPG 7:3, 1:1, 3:7; POPE:POPG:cardiolipin in molar ratio: 7:2:1 and 3:6:1 corresponding to gram-negative and gram-positive bacterial cell membranes, respectively. The error bars represent the standard deviation of the calculated values. Student's *t*-tests were performed to determine the *p*-values and to verify whether the differences in the measured zeta potential values are statistically significant. We consider $p > 0.05$ to indicate not statistically significant difference (ns).

dependence of the zeta potential on the membrane surface charge becomes prominent when the amount of NaCl is increased to 100 mM. The screening effect in the presence of high salt concentration leads to the partial neutralization of the vesicles charge. Overall, the zeta potential measurements can be a reasonable indicator of the incorporation of negatively charged lipids into the membrane, however they cannot be used for directly correlating the zeta potential values with the fraction of negatively charged lipids in the membrane, as this correlation strongly depends on the ionic strength of the buffer.

3.6. Application of proposed model prokaryotic membranes in antimicrobial testing

To validate the applicability of the proposed model bacterial membranes to study membrane response to antimicrobial drugs, we exposed GUVs to the commonly used antibiotic daptomycin. *In vitro*, daptomycin has a strong activity against gram-positive bacteria at very low concentrations, ranging from nM to μ M. The exact mechanism of action is not known, however many studies propose that most likely daptomycin alters the membrane curvature, and induces holes which lead to potassium ion leakage, consequently causing the loss of membrane potential [110,111]. Daptomycin is an acidic, 13-amino acid cyclic lipopeptide, which preferentially binds to anionic lipids such as PG [112], which are abundantly found in membranes of gram-positive bacteria [113]. The activity of daptomycin as well as other antimicrobial peptides strongly depends on the ionic composition of the local environment. The electrostatic interactions between the antimicrobial agents and lipid membrane influence not only the process of binding but also the final response of the bacterial membrane expressed by the formation of pores [114], local changes of the bilayer curvature [115] or increase of lipid dynamics [116], to name a few. Additionally, antimicrobial peptides have found utility beyond physiological environments (e.g. with applications in non-physiological settings such as food preservation and crop protection). Here, among diverse physiologically relevant ions, we focus on Ca^{2+} cations, which possess unique properties, making them crucial for effective binding of daptomycin to the bacterial cell membrane as well as for facilitating daptomycin antimicrobial activity [117–119]. The role of Ca^{2+} ions in the mechanism of daptomycin binding is threefold: (i) neutralization of daptomycin charge, (ii) bonding the lipids and

daptomycin and (iii) induction of two daptomycin conformational changes: the first one exposes the hydrophobic surface of daptomycin, enabling interaction with negatively charged lipids, while the second conformational change allows deeper insertion of daptomycin into the lipid membrane [120]. We examined the binding of daptomycin to GUVs containing negatively charged lipids, composed of binary lipid mixtures of POPE and POPG in molar ratio 7:3, 1:1 and 3:7 and ternary lipid mixtures resembling gram-positive (POPE:POPG:CA in molar ratio 3:6:1) and gram-negative bacterial cell membranes (POPE:POPG:CA in molar ratio 7:2:1). For the outside medium, we used a solution containing 240 mM glucose supplemented with 20 mM CaCl_2 with a final osmolarity of 300 mOsmol/kg. The lipid membrane was visualized with NBD-DPPE and Atto-633 DOPE dyes, which were incorporated during GUVs preparation, while daptomycin was imaged through its intrinsic fluorescence signal.

The binding of daptomycin to the membrane was confirmed in all tested model GUVs, however, the efficiency of this process was clearly dependent on the amount of negatively charged lipids present in the membrane (see Fig. 5A). To quantify the dependence of daptomycin binding on the GUV composition, samples containing negatively charged lipids were supplemented with 1 μ L of 22 μ M daptomycin to the final daptomycin concentration 1.05 μ M in the GUVs suspension. GUVs were imaged 30 min after the addition of daptomycin, using fixed imaging conditions such as detection settings and laser power. We also selected vesicles that of similar size. The membrane fluorescence was determined for spherical GUVs by measuring the fluorescence intensity profile as a function of the distance from the center of the vesicle (Fig. 5B) following an approach reported in [121]. The average integrated fluorescence intensities as assessed from the peak areas were 5 ± 3 , 90 ± 40 , and 290 ± 60 for GUVs composed of POPE:POPG in molar ratio 7:3, 1:1 and 3:7, respectively, showing a significant increase with the increasing POPG content as presented in Fig. 5C. It is expected that daptomycin intensity would be similar for GUVs containing POPC instead of POPE, as both of these lipids do not bind daptomycin due to their zwitterionic character (see Fig. S10). However, as shown by Kreuzberger et al. [122], when exposed to daptomycin, GUVs composed of POPC:POPG tend to form domains rich in anionic lipids. In contrast, we did not observe local aggregation of POPG lipids in any of the tested samples. We conclude that although the net charge of membranes composed of POPE:POPG and POPC:POPG is the same for the specific ratio of both lipids, the response to daptomycin in terms of structural organization is different. GUVs with the composition characteristic for the gram-positive bacterial cell membranes (POPE:POPG:CA 3:6:1 molar ratio) exhibited fluorescence intensity 320 ± 50 which is similar to the value of 290 ± 60 measured for GUVs composed from binary lipid mixture POPE:POPG in molar ratio 3:7, although the amount of POPG in these vesicles was lower than for 3:7 POPE:POPG GUVs. This indicates that daptomycin does not bind only to PG lipids, but also to CA, which carries two negative charges. The intensity of GUVs mimicking the inner cell membrane of gram-negative bacteria (POPE:POPG:CA 7:2:1 molar ratio) had a value of 70 ± 30 , which is slightly below the results obtained for 1:1 POPE:POPG. Indeed, the amount of negatively charged lipids in gram-negative GUVs (20 % of POPG, each lipid carrying one negative charge and 10 % CA with two negative charges) is similar to 1:1 POPE:POPG composition. Finally, GUVs incubated for >1 h in glucose- CaCl_2 buffer containing daptomycin started to collapse and burst on the glass coverslip, which is shown in Fig. S11.

To confirm that the bursting of GUVs was indeed caused by the antimicrobial peptide, we incubated reference GUVs for 1 h in the same experimental conditions, using identical buffer composition (glucose with 20 mM CaCl_2 with the final osmolarity 300 mOsmol/kg) but in the absence of daptomycin. In this case, the bursting of GUVs was negligible, showing that the GUVs were stable for much longer than the timescale of the experiment and discarding the possibility that the composition of the outside solution (presence of CaCl_2) contributed to the extensive

CHAPTER 7. TUNABLE BIOMIMETIC BACTERIAL MEMBRANES FROM BINARY AND TERNARY LIPID MIXTURES AND THEIR APPLICATION IN ANTIMICROBIAL TESTING

E. Krok et al.

BBA - Biomembranes 1865 (2023) 184194

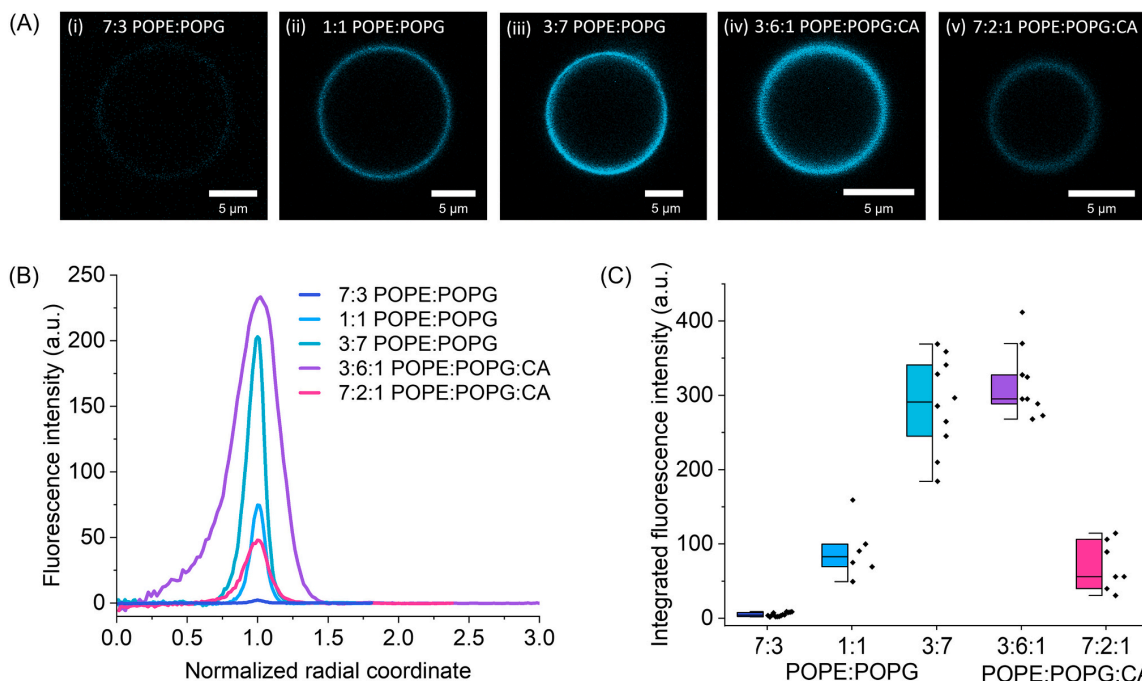


Fig. 5. Binding daptomycin strongly depends on the amount of negatively charged lipids: (A) Confocal cross sections of GUVs showing brightness differences for membranes composed of POPE:POPG in molar ratios (i) 7:3, (ii) 1:1, (iii) 3:7 and POPE:POPG:CA in molar ratio (iv) 3:6:1 mimicking gram-positive, and (v) 7:2:1 mimicking gram-negative bacterial cell membrane. The vesicles were imaged at 21 °C, 30 min after addition of daptomycin. (B) Fluorescence intensity as a function of radial coordinate (normalized by the vesicle radius) measured for the GUVs shown in (A). (C) Integrated fluorescence intensity for GUVs composed of POPE:POPG in molar ratios: 7:3, 1:1 and 3:7 (blue), and GUVs composed from ternary lipid mixtures POPE:POPG:CA 3:6:1 mimicking gram-positive and POPE:POPG:CA 7:2:1 mimicking gram-negative bacterial cell membranes. (For interpretation of the references to colour in this figure legend, the reader is referred to the web version of this article.)

rupturing of GUVs. Clearly, the enhanced bursting of GUVs is associated with the presence of daptomycin, in agreement with the findings in a recent report [122]. It should be noted that the exact mechanism of daptomycin-induced membrane rupture is still debated among researchers. As shown in [123] the exposure of GUVs containing PG lipids to daptomycin resulted in the extensive leak-in of the Ca^{2+} ions and

increase of the inside osmolarity. To equilibrate the increasing osmotic pressure, water molecules tend to flow to the vesicle interior [124]. This water influx causes extensive swelling of the vesicle, which progresses until the moment when the membrane reaches the critical line tension and collapses. The increased ions permeability of membranes upon exposure to daptomycin was also ascribed to other mechanisms such as

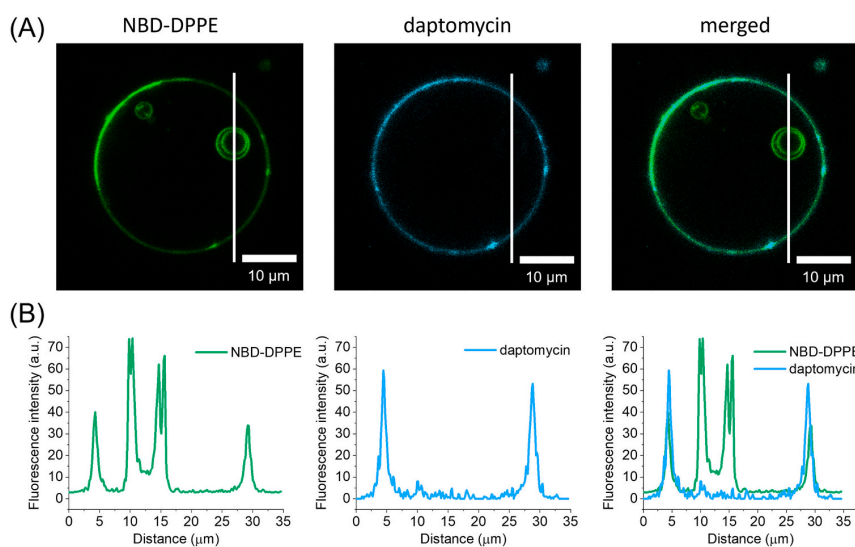


Fig. 6. Binding of daptomycin to GUVs mimicking cell membrane of gram-positive bacteria: (A) A single, defect-free vesicle incubated in 22 mM daptomycin and 20 mM $CaCl_2$, green channel corresponds to NBD-DPPE fluorescence, cyan represents daptomycin. Daptomycin is not membrane permeable and thus, inner vesicles that are not directly exposed to the daptomycin solution do not exhibit fluorescence in the daptomycin emission spectrum. The white lines indicate the position of the fluorescence intensity profiles shown below. (B) Fluorescence intensity profiles along the lines in (A) for NBD-PE and daptomycin channels. Image acquisition was done at 21 °C. (For interpretation of the references to colour in this figure legend, the reader is referred to the web version of this article.)

CHAPTER 7. TUNABLE BIOMIMETIC BACTERIAL MEMBRANES FROM BINARY AND TERNARY LIPID MIXTURES AND THEIR APPLICATION IN ANTIMICROBIAL TESTING

E. Krok et al.

BBA - Biomembranes 1865 (2023) 184194

lipid extracting effect [125] or to the increase of the hydrophobic mismatch at the boundary between the more rigid domains composed of daptomycin-PG aggregates and the surrounding more fluid phase [126]. One should note that the most plausible cause of the GUVs rupture is not a single effect but rather a synergic combination of the above mentioned mechanisms that lead to the increased membrane permeability.

We analyzed daptomycin binding to the GUVs complexes consisting of a mother vesicle and vesicles trapped inside the lumen (Fig. 6A). We observed that daptomycin bound evenly to the outside (mother) vesicle however, the vesicles in the lumen did not show fluorescence in the daptomycin channel, and presumably remained completely unaffected by its activity. According to recent molecular dynamics simulations, upon contact with Ca^{2+} ions daptomycin forms tetramers, which can reversibly flip between the outer and inner leaflets of the membrane [127]. We cannot unambiguously conclude whether daptomycin embeds only in the outer leaflet or integrates also in the inner monolayer of the membrane. We performed a quantitative analysis of intensity along the line crossing the mother GUV and trapped in its lumen liposomes as presented in Fig. 6B. The intensity in the daptomycin channel for GUVs trapped inside the mother vesicle was almost equal to the background intensity, leading to the conclusion that daptomycin does not internalize into the lumen.

4. Conclusions

The composition of bacterial cell membranes differs significantly from their mammalian analogs. Mammalian cytoplasmic membranes are composed mainly of phospholipids such as PC, phosphatidylserine (PS) as well as sphingomyelin (SM), and cholesterol, whereas bacterial membranes contain mostly PE, PG, and CA, while usually lacking cholesterol. Some strains such as *Helicobacter* [128], *Chlamydia* [129] or *Mycoplasma* [130] are able to obtain cholesterol from their host but they cannot synthesize it intrinsically. The control of membrane fluidity in bacteria is accomplished by constant adjustment in the ratio of saturated and unsaturated lipids or it is maintained by hopanoids, sterol-surrogates that are considered to be bacterial equivalent of the eukaryotic cholesterol [131]. The divergent lipid composition of bacterial cell membranes distinguishes them from their mammalian counterparts, which is expressed by the different structural organization, packing density, surface charge, and membrane curvature. Consequently, the commonly used models mimicking eukaryotic cell membranes cannot be applied for studying prokaryotic membranes. Furthermore, the lipid composition of bacterial cell membranes differs not only for gram-negative and gram-positive bacteria but can vary significantly even between individual strains.

We successfully prepared models of gram-negative and gram-positive cell membranes with increasing level of complexity, starting with binary mixtures of POPC with POPE or POPG and extending our studies to ternary systems containing lipids present solely in prokaryotic cell membranes. We proposed a bottom-up approach where instead of using the commercially available lipid extracts, membranes were reconstituted from lipid mixtures. The presented methodology allows one to tune the lipid composition towards cell membranes characteristic for particular bacterial strains.

The used electroformation method led to the successful formation of GUVs with diverse properties. The simplest GUVs containing POPC and POPE exhibited phase separation and their size was strongly dependent on the amount of POPE incorporated within the membrane. On the other hand, model membranes composed of POPC and POPG were characterized by leaflets asymmetry, which was expressed by formation of inward protruding tubes and buds.

For the membranes formed from ternary lipid mixtures we observed an intriguing interplay between POPE, POPG and CA, which had a strong influence on the lateral organization of the membranes. GUVs composed solely of POPE and POPG did not present phase separation, whereas liposomes of the same POPE:POPG content but with the

addition of CA showed clear phase separation. While the exact composition of the two phases is unclear, it is evidently caused by the preferential interactions of CA with POPE or POPG (presumably through their head groups, as the hydrophobic tails are the same for the two lipids).

Depending on the purpose of the conducted research, the presented membrane models can be tuned appropriately to study a variety of processes occurring in prokaryotic cell membranes such as changes in the membrane structure, permeability, and alterations in mechanical properties or dynamics under different environmental conditions.

Finally, we tested the proposed models against antimicrobial lipopeptide daptomycin. We observed not only strong interaction of this drug with the bacterial GUVs but also showed that the binding efficiency strongly depends on the amount of negatively charged lipids incorporated in the membrane. Moreover, based on the fluorescence intensity analysis of the mother vesicle and those trapped within, we conclude that daptomycin does not internalize in the GUV lumen. We anticipate that the models proposed here can successfully be applied in testing of antimicrobial agents and serve as non-toxic and safer in handling platforms for studying the fundamental biological processes and mechanisms laying behind bacterial antibiotic resistance.

CRediT authorship contribution statement

Emilia Krok: Conceptualization, Validation, Investigation, Writing – original draft, Visualization, Funding acquisition. **Mareike Stephan:** Methodology, Validation, Writing – review & editing. **Rumiana Dimova:** Conceptualization, Resources, Writing – review & editing, Supervision. **Lukasz Piatkowski:** Conceptualization, Writing – review & editing, Funding acquisition, Supervision.

Declaration of competing interest

The authors declare that they have no known competing financial interests or personal relationships that could have appeared to influence the work reported in this paper.

Acknowledgments

This work has been supported by the Polish National Agency for Academic Exchange (NAWA) under the STER programme, Towards Internationalization of Poznan University of Technology Doctoral School (2022–2024), grant number 4009/NAWA/0005-2/M-I/01. L.P. and E.K. acknowledge the financial support from the EMBO Installation Grant (IG 4147). E.K. acknowledges the financial support from the Ministry of Education and Science of Poland in the year 2023 (Project No. 0512/SBAD/6214). M.S. acknowledges funding from the International Max Planck Research School on Multiscale BioSystems.

Appendix A. Supplementary data

Supplementary data to this article can be found online at <https://doi.org/10.1016/j.bbamem.2023.184194>.

References

- [1] T. Harayama, H. Riezman, Understanding the diversity of membrane lipid composition, *Nat. Rev. Mol. Cell Biol.* 19 (2018) 281–296.
- [2] T.J. Silhavy, D. Kahne, S. Walker, The bacterial cell envelope, *Cold Spring Harb. Perspect. Biol.* 2 (2010).
- [3] Y. Kakimoto, R. Tero, Supported lipid bilayers of *Escherichia coli* extracted lipids and their calcium dependence, *Front. Mater.* 5 (2018).
- [4] H. Masaaki, O. Akinobu, K. Reiko, A. Masufumi, K. Yasuhiro, Lipid composition of *Staphylococcus aureus* and its derived L-forms, *Microbiol. Immunol.* 23 (1979) 435–442.
- [5] R. Leber, M. Pachler, I. Kabelka, I. Svoboda, D. Enkoller, R. Vácha, K. Lohner, G. Pabst, Synergism of antimicrobial frog peptides couples to membrane intrinsic curvature strain, *Biophys. J.* 114 (2018) 1945–1954.

CHAPTER 7. TUNABLE BIOMIMETIC BACTERIAL MEMBRANES FROM BINARY AND TERNARY LIPID MIXTURES AND THEIR APPLICATION IN ANTIMICROBIAL TESTING

E. Krok et al.

BBA - Biomembranes 1865 (2023) 184194

- [6] L. Niu, T. Wohland, W. Knoll, I. Köper, Interaction of a synthetic antimicrobial peptide with a model bilayer platform mimicking bacterial membranes, *Biointerphases*. 12 (2017) 04E404.
- [7] H. Strahl, J. Errington, Bacterial membranes: structure, domains, and function, *Annu. Rev. Microbiol.* 71 (2017) 519–538.
- [8] A.B. Carey, A. Ashenden, I. Köper, Model architectures for bacterial membranes, *Biophys. Rev.* 14 (2022) 111–143.
- [9] L. Picas, M.T. Montero, A. Morros, M.E. Cabañas, B. Seantier, P.E. Milhiet, J. Hernández-Borrell, Calcium-induced formation of subdomains in phosphatidylethanolamine- phosphatidylglycerol bilayers: a combined DSC, ³¹P NMR, and AFM study, *J. Phys. Chem. B* 113 (2009) 4648–4655.
- [10] Y. Kakimoto, R. Tero, Formation of supported lipid bilayers of *Escherichia coli* extracted lipids and their surface morphologies, *Jpn. J. Appl. Phys.* 58 (2019).
- [11] D. Konarzewska, J. Juhaniwicz, A. Güzeloglu, S. Şek, Characterization of planar biomimetic lipid films composed of phosphatidylethanolamines and phosphatidylglycerols from *Escherichia coli*, *Biochim. Biophys. Acta Biomembr.* 2017 (1859) 475–483.
- [12] S.A. Weiss, R.J. Bushby, S.D. Evans, L.J.C. Jeuken, A study of cytochrome bo3 in a tethered bilayer lipid membrane, *Biochim. Biophys. Acta Bioenerg.* 1797 (2010) 1917–1923.
- [13] Y. Nakatani, Y. Shimaki, D. Dutta, S.P. Muench, K. Ireton, G.M. Cook, L.J. C. Jeuken, Unprecedented properties of phenothiazines unraveled by a NDH-2 bioelectrochemical assay platform, *J. Am. Chem. Soc.* 142 (2020) 1311–1320.
- [14] L.J.C. Jeuken, S.D. Connell, M. Nurnabi, J. O'Reilly, P.J.F. Henderson, S.D. Evans, R.J. Bushby, Direct electrochemical interaction between a modified gold electrode and a bacterial membrane extract, *Langmuir*. 21 (2005) 1481–1488.
- [15] A. Som, G.N. Tew, Influence of lipid composition on membrane activity of antimicrobial phenylene ethynylene oligomers, *J. Phys. Chem. B* 112 (2008) 3495–3502.
- [16] O. Domenech, G. Francius, P.M. Tulkens, F. Van Bambeke, Y. Dufrene, M. P. Mingeot-Leclercq, Interactions of oritavancin, a new lipoglycopeptide derived from vancomycin, with phospholipid bilayers: effect on membrane permeability and nanoscale lipid membrane organization, *Biochim. Biophys. Acta Biomembr.* 1788 (2009) 1832–1840.
- [17] A. Marín-Menéndez, C. Montis, T. Díaz-Calvo, D. Carta, K. Hatzixanthis, C. J. Morris, M. McArthur, D. Berti, Antimicrobial Nanoplexes meet model bacterial membranes: the key role of Cardiolipin, *Sci. Rep.* 7 (2017).
- [18] R. Dimova, Giant vesicles and their use in assays for assessing membrane phase state, curvature, mechanics, and electrical properties, *Annu. Rev. Biophys.* 48 (2019) 93–119.
- [19] R. Dimova, S. Aranda, N. Bezlyepkina, V. Nikolov, K.A. Riske, R. Lipowsky, A practical guide to giant vesicles. Probing the membrane nanoregime via optical microscopy, *J. Phys. Condens. Matter*. 18 (2006).
- [20] S.F. Fenz, K. Sengupta, Giant vesicles as cell models, *Integr. Biol. (Camb.)* 4 (2012) 982–995.
- [21] A. Martos, M. Jiménez, G. Rivas, P. Schwillle, Towards a bottom-up reconstitution of bacterial cell division, *Trends Cell Biol.* 22 (2012) 634–643.
- [22] J. Steinkühler, R.L. Knorr, Z. Zhao, T. Bhatia, S.M. Bartelt, S. Wegner, R. Dimova, R. Lipowsky, Controlled division of cell-sized vesicles by low densities of membrane-bound proteins, *Nat. Commun.* 11 (2020) 1–11.
- [23] F. Fanalista, A. Birnie, R. Maan, F. Burla, K. Charles, G. Pawlik, S. Deshpande, G. H. Koenderink, M. Dogterom, C. Dekker, Shape and size control of artificial cells for bottom-up biology, *ACS Nano* 13 (2019) 5439–5450.
- [24] G.E. Rydell, L. Svensson, G. Larson, L. Johannes, W. Römer, Human GII.4 norovirus VLP induces membrane invaginations on giant unilamellar vesicles containing secretor gene dependent α1,2-fucosylated glycosphingolipids, *Biochim. Biophys. Acta Biomembr.* 1828 (2013) 1840–1845.
- [25] M. Przybylo, J. Sýkora, J. Humpolciová, A. Benda, A. Zan, M. Hof, Lipid diffusion in giant unilamellar vesicles is more than 2 times faster than in supported phospholipid bilayers under identical conditions, *Langmuir*. 22 (2006) 9096–9099.
- [26] S. Li, P.C. Hu, N. Malmstadt, Imaging molecular transport across lipid bilayers, *Biophys. J.* 101 (2011) 700–708.
- [27] L.R. Montes, A. Alonso, F.M. Goñi, L.A. Bagatolli, Giant unilamellar vesicles electroformed from native membranes and organic lipid mixtures under physiological conditions, *Biophys. J.* 93 (2007) 3548–3554.
- [28] N. Kahya, D. Scherfeld, K. Bacia, B. Poolman, P. Schwillle, Probing lipid mobility of raft-exhibiting model membranes by fluorescence correlation spectroscopy, *J. Biol. Chem.* 278 (2003) 28109–28115.
- [29] A.J. García-Sáez, S. Chiantia, P. Schwillle, Effect of line tension on the lateral organization of lipid membranes, *J. Biol. Chem.* 282 (2007) 33537–33544.
- [30] H. Behuria, N. Pal, R. Munda, S. Sahu, Preparation of giant unilamellar vesicles (GUVs) from bacterial polar lipid extract: developing a prokaryotic model membrane system, in: H. Thatoi, S.K. Nayak (Eds.), *Biotechnology for Sustainable Utilization of Bioresources*, Astral International Pvt. Ltd, 2020, pp. 309–320.
- [31] M. Jiménez, A. Martos, M. Vicente, G. Rivas, Reconstitution and organization of *Escherichia coli* proto-ring elements (FtsZ and FtsA) inside giant unilamellar vesicles obtained from bacterial inner membranes, *J. Biol. Chem.* 286 (2011) 11236–11241.
- [32] J. Kubiak, J. Brewer, S. Hansen, L.A. Bagatolli, Lipid lateral organization on giant unilamellar vesicles containing lipopolysaccharides, *Biophys. J.* 100 (2011) 978–986.
- [33] L. Paulowski, A. Donoghue, C. Nehls, S. Groth, M. Koistinen, S.O. Hagge, A. Böhlmg, M. Winterhalter, T. Gutschmann, The beauty of asymmetric membranes: reconstitution of the outer membrane of gram-negative bacteria, *Front. Cell Dev. Biol.* 8 (2020).
- [34] E. Krok, A. Batura, M. Chattopadhyay, H. Orlikowska, L. Piatkowski, Lateral organization of biomimetic cell membranes in varying pH conditions, *J. Mol. Liq.* 345 (2022).
- [35] M. Karimi, J. Steinkühler, D. Roy, R. Dasgupta, R. Lipowsky, R. Dimova, Asymmetric ionic conditions generate large membrane curvatures, *Nano Lett.* 18 (2018) 7816–7821.
- [36] N. Kahya, Protein-protein and protein-lipid interactions in domain-assembly: lessons from giant unilamellar vesicles, *Biochim. Biophys. Acta Biomembr.* 1798 (2010) 1392–1398.
- [37] M. Chattopadhyay, E. Krok, H. Orlikowska, P. Schwillle, H.G. Franquelim, L. Piatkowski, Hydration layer of only a few molecules controls lipid mobility in biomimetic membranes, *J. Am. Chem. Soc.* 143 (2021) 14551–14562.
- [38] G. Mohanan, K.S. Nair, K.M. Nampoothiri, H. Bajaj, Engineering bio-mimicking functional vesicles with multiple compartments for quantifying molecular transport, *Chem. Sci.* 11 (2020) 4669–4679.
- [39] Y. Tamba, M. Yamazaki, Single giant unilamellar vesicle method reveals effect of antimicrobial peptide magainin 2 on membrane permeability, *Biochemistry*. 44 (2005) 15823–15833.
- [40] T.M. Domingues, K.A. Riske, A. Miranda, Revealing the lytic mechanism of the antimicrobial peptide gomesin by observing giant unilamellar vesicles, *Langmuir*. 26 (2010) 11077–11084.
- [41] M.I. Angelova, D.S. Dimitrov, Liposome electroformation, *Faraday Discuss. Chem. Soc.* 81 (1986) 303–311.
- [42] J. Schindelin, I. Arganda-Carreras, E. Frise, V. Kaynig, M. Longair, T. Pietzsch, S. Preibisch, C. Rueden, S. Saalfeld, B. Schmid, J.Y. Tinevez, D.J. White, V. Hartenstein, K. Eliceiri, P. Tomancak, A. Cardona, Fiji: an open-source platform for biological-image analysis, *Nat. Methods* 9 (2012) 676–682.
- [43] K. Carvalho, L. Ramos, C. Roy, C. Picart, Giant unilamellar vesicles containing phosphatidylinositol(4,5) bisphosphate: characterization and functionality, *Biophys. J.* 95 (2008) 4348–4360.
- [44] G. Cho, E. Lee, J. Kim, Structural insights into phosphatidylethanolamine formation in bacterial membrane biogenesis, *Sci. Rep.* 11 (2021).
- [45] Z.T. Graber, J. Thomas, E. Johnson, A. Gericke, E.E. Kooijman, Effect of H-bond donor lipids on phosphatidylinositol-3,4,5-trisphosphate ionization and clustering, *Biophys. J.* 114 (2018) 126–136.
- [46] H.T. McMahon, E. Boucrot, Membrane curvature at a glance, *J. Cell Sci.* 128 (2015) 1065–1070.
- [47] S. Aimon, A. Callan-Jones, A. Berthaud, M. Pinot, G.E.S. Toombes, P. Bassereau, Membrane shape modulates transmembrane protein distribution, *Dev. Cell* 28 (2014) 212–218.
- [48] J. Pramanik, J.D. Keasling, Stoichiometric model of *Escherichia coli* metabolism: incorporation of growth-rate dependent biomass composition and mechanistic energy requirements, *Biotechnol. Bioeng.* 56 (1997) 398–421.
- [49] M.C. Trombe, M.A. Lanéele, G. Lanéele, Lipid composition of aminopterin-resistant and sensitive strains of *Streptococcus pneumoniae*. Effect of aminopterin inhibition, *Biochim. Biophys. Acta - Mol. Cell Biol. Lipids.* 574 (1979) 290–300.
- [50] H.I. Petrache, Lipid Bilayer Structure, *Comprehensive Biophysics*, Elsevier Inc., 2012, pp. 3–15.
- [51] R. Dimova, C. Marques, *The Giant Vesicle Book*, CRC Press, 2020.
- [52] T. Baumgart, G. Hunt, E.R. Farkas, W.W. Webb, G.W. Feigensohn, Fluorescence probe partitioning between Lo/Ld phases in lipid membranes, *Biochim. Biophys. Acta Biomembr.* 1768 (2007) 2182–2194.
- [53] A.S. Klymchenko, R. Kreder, Fluorescent probes for lipid rafts: from model membranes to living cells, *Chem. Biol.* 21 (2014) 97–113.
- [54] T. Baumgart, S.T. Hess, W.W. Webb, Imaging coexisting fluid domains in biomembrane models coupling curvature and line tension, *Nature*. 425 (2003) 821–824.
- [55] M.K. Dymond, R.J. Gillams, D.J. Parker, J. Burrell, A. Labrador, T. Nylander, G. S. Attard, Lipid spontaneous curvatures estimated from temperature-dependent changes in inverse hexagonal phase lattice parameters: effects of metal cations, *Langmuir*. 32 (2016) 10083–10092.
- [56] C. Kluge, M. Pöhl, R.A. Böckmann, Spontaneous local membrane curvature induced by transmembrane proteins, *Biophys. J.* 121 (2022) 671–683.
- [57] R. Dasgupta, M.S. Miettinen, N. Fricke, R. Lipowsky, R. Dimova, The glycolipid GM1 reshapes asymmetric biomembranes and giant vesicles by curvature generation, *Proc. Natl. Acad. Sci. U. S. A.* 115 (2018) 5756–5761.
- [58] M. Stephan, V. Dunsing, S. Pramanik, S. Chiantia, S. Barbirz, T. Robinson, R. Dimova, Biomimetic asymmetric bacterial membranes incorporating lipopolysaccharides, *Biophys. J.* 122 (2023) 2147–2161.
- [59] M. Aleksanyan, R.B. Lira, J. Steinkühler, R. Dimova, GM1 asymmetry in the membrane stabilizes pores, *Biophys. J.* 121 (2022) 3295–3302.
- [60] P. Bassereau, R. Jin, T. Baumgart, M. Deserno, R. Dimova, V.A. Frolov, P. V. Bashkurov, H. Grubmüller, R. Jahn, H.J. Risselada, L. Johannes, M.M. Kozlov, R. Lipowsky, T.J. Pucadyil, W.F. Zeno, J.C. Stachowiak, D. Stamou, A. Breuer, L. Lauritsen, C. Simon, C. Sykes, G.A. Voth, T.R. Weikl, The 2018 biomembrane curvature and remodeling roadmap, *J. Phys. D. Appl. Phys.* 51 (2018) 343001.
- [61] T. Bhatia, S. Christ, J. Steinkühler, R. Dimova, R. Lipowsky, Simple sugars shape giant vesicles into multispheres with many membrane necks, *Soft Matter* 16 (2020) 1246–1258.
- [62] B. Kubsch, T. Robinson, R. Lipowsky, R. Dimova, Solution asymmetry and salt expand fluid-fluid coexistence regions of charged membranes, *Biophys. J.* 110 (2016) 2581–2584.
- [63] B. Kubsch, T. Robinson, J. Steinkühler, R. Dimova, Phase behavior of charged vesicles under symmetric and asymmetric solution conditions monitored with fluorescence microscopy, *J. Vis. Exp.* 2017 (2017).

CHAPTER 7. TUNABLE BIOMIMETIC BACTERIAL MEMBRANES FROM BINARY AND TERNARY LIPID MIXTURES AND THEIR APPLICATION IN ANTIMICROBIAL TESTING

E. Krok et al.

BBA - Biomembranes 1865 (2023) 184194

- [64] C.C. Vequi-Suplicy, K.A. Riske, R.L. Knorr, R. Dimova, Vesicles with charged domains, *Biochim. Biophys. Acta Biomembr.* 1798 (2010) 1338–1347.
- [65] O. Stauer, S. Antona, D. Zhang, J. Csatári, M. Schröter, J.W. Janiesch, S. Fabritz, I. Berger, I. Platzman, J.P. Spatz, Microfluidic production and characterization of biofunctionalized giant unilamellar vesicles for targeted intracellular cargo delivery, *Biomaterials*. 264 (2021), 120203.
- [66] U.D. Chowdhury, A. Paul, B.L. Bhargava, The effect of lipid composition on the dynamics of tau fibrils, *Proteins*. 90 (2022) 2103–2115.
- [67] D. Drabik, G. Chodaczek, S. Kraszewski, M. Langner, Mechanical properties determination of DMPC, DPPC, DSPC, and HSPC solid-ordered bilayers, *Langmuir*. 36 (2020) 3826–3835.
- [68] J. Steinkühler, P. de Tillieux, R.L. Knorr, R. Lipowsky, R. Dimova, Charged giant unilamellar vesicles prepared by electroformation exhibit nanotubes and transbilayer lipid asymmetry, *Sci. Rep.* 8 (2018).
- [69] A. Weinberger, F.C. Tsai, G.H. Koenderink, T.F. Schmidt, R. Itri, W. Meier, T. Schmatko, A. Schröder, C. Marques, Gel-assisted formation of giant unilamellar vesicles, *Biophys. J.* 105 (2013) 154–164.
- [70] J. Abellón-Ruiz, S.S. Kaptan, A. Baslé, B. Claudi, D. Bumann, U. Kleinekathöfer, B. van den Berg, Structural basis for maintenance of bacterial outer membrane lipid asymmetry, *Nat. Microbiol.* 2 (2017) 1616–1623.
- [71] J.E. Rothman, E.P. Kennedy, Asymmetrical distribution of phospholipids in the membrane of *Bacillus megaterium*, *J. Mol. Biol.* 110 (1977) 603–618.
- [72] A. Yamaji-Hasegawa, M. Tsujimoto, Asymmetric distribution of phospholipids in biomembranes, *Biol. Pharm. Bull.* 29 (2006) 1547–1553.
- [73] A.J. Verkleij, J.A. Post, Membrane phospholipid asymmetry and signal transduction, *J. Membr. Biol.* 178 (2000) 1–10.
- [74] P.F. Devaux, Static and dynamic lipid asymmetry in cell membranes, *Biochemistry*. 30 (1991).
- [75] D. Marquardt, B. Geier, G. Pabst, Asymmetric lipid membranes: towards more realistic model systems, *Membranes (Basel)*. 5 (2015) 180–196.
- [76] J. Steinkühler, P. Fonda, Z. Zhao, F.S.C. Leomil, R. Lipowsky, R. Dimova, Superelasticity of plasma- and synthetic membranes resulting from coupling of membrane asymmetry, curvature, and lipid sorting, *Adv. Sci.* 8 (2021) 2102109.
- [77] K. Balasubramanian, A.J. Schroit, Aminophospholipid asymmetry: a matter of life and death, *Annu. Rev. Physiol.* 65 (2003) 701–734.
- [78] P.M. Kasson, V.S. Pande, Control of membrane fusion mechanism by lipid composition: predictions from ensemble molecular dynamics, *PLoS Comput. Biol.* 3 (2007) 2228–2238.
- [79] M. Doktorova, J.L. Symons, I. Levental, Structural and functional consequences of reversible lipid asymmetry in living membranes, *Nat. Chem. Biol.* 16 (2020) 1321–1330.
- [80] S. Raj, B. Omar, T. Hamidah, A. Suhana, N. Asih, Mesosomes are a definite event in antibiotic-treated *Staphylococcus aureus* ATCC 25923, *Trop. Biomed.* 24 (2007) 105–109.
- [81] X. Li, L.P. Yang, W.X. Zhu, X.Y. Pang, H.Q. Feng, Mesosomes, unique membranous structures in bacteria, *Adv. Mater. Res.* 894 (2014) 316–320.
- [82] J.W. Greenawalt, T.L. Whiteside, Mesosomes: membranous bacterial organelles, *Bacteriol. Rev.* 39 (1975) 405–463.
- [83] C. Sohlenkamp, I.M. Lopez-Lara, O. Geiger, Biosynthesis of phosphatidylcholine in bacteria, *Prog. Lipid Res.* 42 (2003) 115–162.
- [84] L. Picas, C. Suárez-Germá, M.T. Montero, Ó. Doménech, J. Hernández-Borrell, Miscibility behavior and nanostructure of monolayers of the main phospholipids of *Escherichia coli* inner membrane, *Langmuir*. 28 (2012) 701–706.
- [85] S. Clejan, T.A. Krulwich, K.R. Mondrus, D. Seto-Young, Membrane lipid composition of obligately and facultatively alkaliphilic strains of *Bacillus* spp., *J. Bacteriol.* 168 (1986) 334–340.
- [86] J. Planas-Iglesias, H. Dwarakanath, D. Mohammadyani, N. Yanamala, V.E. Kagan, J. Klein-Seetharaman, Cardiolipin interactions with proteins, *Biophys. J.* 109 (2015) 1282–1294.
- [87] M. el Khoury, J. Swain, G. Sautrey, L. Zimmermann, P. van der Smissen, J. L. Décout, M.P. Mingeot-Leclercq, Targeting bacterial cardiolipin enriched microdomains: an antimicrobial strategy used by amphiphilic aminoglycoside antibiotics, *Sci. Rep.* 7 (2017).
- [88] K. Matsumoto, J. Kusaka, A. Nishibori, H. Hara, Lipid domains in bacterial membranes, *Mol. Microbiol.* 61 (2006) 1110–1117.
- [89] M. Gohrbandt, A. Lipski, J.W. Grimshaw, J.A. Buttress, Z. Baig, B. Herkenhoff, S. Walter, R. Kurre, G. Deckers-Hebestreit, H. Strahl, Low membrane fluidity triggers lipid phase separation and protein segregation in living bacteria, *EMBO J.* 41 (2022), e109800.
- [90] E. Mileyskoykaya, W. Dowhan, Visualization of phospholipid domains in *Escherichia coli* by using the cardiolipin-specific fluorescent dye 10-N-nonyl acridine orange, *J. Bacteriol.* 182 (2000) 1172–1175.
- [91] A. Nishibori, J. Kusaka, H. Hara, M. Umeda, K. Matsumoto, Phosphatidylethanolamine domains and localization of phospholipid synthases in *Bacillus subtilis* membranes, *J. Bacteriol.* 187 (2005) 2163–2174.
- [92] I. Barak, K. Muchová, The role of lipid domains in bacterial cell processes, *Int. J. Mol. Sc.* 14 (2013) 4050–4065.
- [93] A.P. Petroff, A.L. Pasulka, N. Soplop, X.-L. Wu, A. Libchaber, Biophysical basis for convergent evolution of two well-forming microbes, *R. Soc. Open Sci.* 2 (2015).
- [94] K.I. Akashi, H. Miyata, H. Itoh, K. Kinoshita, Preparation of giant liposomes in physiological conditions and their characterization under an optical microscope, *Biophys. J.* 71 (1996) 3242.
- [95] C.B. Giuliano, N. Cvjetan, J. Ayache, P. Walde, Multivesicular vesicles: preparation and applications, *ChemSystemsChem.* 3 (2021).
- [96] E.T. Kisac, B. Coldren, C.A. Evans, C. Boyer, J.A. Zasadzinski, The vesosome—a multicompartiment drug delivery vehicle, *Curr. Med. Chem.* 11 (2004) 1241–1253.
- [97] P. Walde, S. Ichikawa, Enzymes inside lipid vesicles: preparation, reactivity and applications, *Biomol. Eng.* 18 (2001) 143–177.
- [98] S. Merino, Ó. Doménech, I. Díez, F. Sanz, M. Viñas, M.T. Montero, J. Hernández-Borrell, Effects of ciprofloxacin on *Escherichia coli* lipid bilayers: an atomic force microscopy study, *Langmuir*. 19 (2003) 6922–6927.
- [99] F. Staudegger, J. Prenner, M. Kriechbaum, G. Degovics, N.A.H. Lewis, R. N. Mcelhane, K. Löhner, X-ray studies on the interaction of the antimicrobial peptide gramicidin S with microbial lipid extracts: evidence for cubic phase formation, *Biochim. Biophys. Acta* 1468 (2000) 213–230.
- [100] L. Soblosky, A. Ramamoorthy, Z. Chen, Membrane interaction of antimicrobial peptides using *E. coli* lipid extract as model bacterial cell membranes and SFG spectroscopy, *Chem. Phys. Lipids* 187 (2015) 20–33.
- [101] M.M. Billah, M.M. Or Rashid, M. Ahmed, M. Yamazaki, Antimicrobial peptide magainin 2-induced rupture of single giant unilamellar vesicles comprising *E. coli* polar lipids, *Biochim. Biophys. Acta Biomembr.* 1865 (2023), 184112.
- [102] F. Hossain, H. Dohra, M. Yamazaki, Effect of membrane potential on entry of Lactoferricin B-derived 6-residue antimicrobial peptide into single *Escherichia coli* cells and lipid vesicles, *J. Bacteriol.* 203 (2021), e00021.
- [103] F. Hossain, M. Mizanur Rahman Moghal, M. Zahidul Islam, M. Moniruzzaman, X. Masahito Yamazaki, Membrane potential is vital for rapid permeabilization of plasma membranes and lipid bilayers by the antimicrobial peptide lactoferricin B, *J. Biol. Chem.* 294 (2019) 10449–10462.
- [104] S. Nandi, K.S. Nair, H. Bajaj, Bacterial outer-membrane-mimicking giant unilamellar vesicle model for detecting antimicrobial permeability, *Langmuir*. 39 (2023) 5891–5900.
- [105] H.R. Lee, D.G. You, H.K. Kim, J.W. Sohn, M.J. Kim, J.K. Park, G.Y. Lee, Y. Do Yoo, Romo1-derived antimicrobial peptide is a new antimicrobial agent against multidrug-resistant bacteria in a murine model of sepsis, *MBio*. 11 (2020).
- [106] N. Hassan, A.M. Anesio, M. Rafiq, J. Holtvoeth, I. Bull, A. Haleem, A.A. Shah, F. Hasan, Temperature driven membrane lipid adaptation in glacial psychrophilic bacteria, *Front. Microbiol.* 11 (2020).
- [107] N. Bezlyepkina, R.S. Graciá, P. Shchelokovskyy, R. Lipowsky, R. Dimova, Phase diagram and tie-line determination for the ternary mixture DOPC/eSM/cholesterol, *Biophys. J.* 104 (2013) 1456–1464.
- [108] H.A. Faizi, S.L. Frey, J. Steinkühler, R. Dimova, P.M. Vlahovska, Bending rigidity of charged lipid bilayer membranes, *Soft Matter* 15 (2019) 6006.
- [109] N. Marusic, L. Otrin, J. Rauchhaus, Z. Zhao, F.L. Kyriilis, F. Hamdi, P.L. Kastiris, R. Dimova, I. Ivanov, K. Sundmacher, Increased efficiency of charge-mediated fusion in polymer/lipid hybrid membranes, *Proc. Natl. Acad. Sci. U. S. A.* 119 (2022), e2122468119.
- [110] W.R. Miller, A.S. Bayer, C.A. Arias, Mechanism of action and resistance to daptomycin in *Staphylococcus aureus* and enterococci, *Cold Spring Harb. Perspect. Med.* 6 (2016).
- [111] H.W. Huang, DAPTOMYCIN, its membrane-active mechanism vs. that of other antimicrobial peptides, *Biochim. Biophys. Acta Biomembr.* 1862 (2020).
- [112] J. Larsen, N.S. Hatzakis, D. Stamou, Observation of inhomogeneity in the lipid composition of individual nanoscale liposomes, *J. Am. Chem. Soc.* 133 (2011) 10685–10687.
- [113] A. Pokorny, P.F. Almeida, The antibiotic peptide daptomycin functions by reorganizing the membrane, *J. Membr. Biol.* 254 (2021) 97–108.
- [114] A.D. Cirac, G. Moiset, J.T. Mika, A. Koçer, P. Salvador, B. Poolman, S.J. Marrink, D. Sengupta, The molecular basis for antimicrobial activity of pore-forming cyclic peptides, *Biophys. J.* 100 (2011) 2422.
- [115] N.W. Schmidt, G.C.L. Wong, Antimicrobial peptides and induced membrane curvature: geometry, coordination chemistry, and molecular engineering, *Curr. Opin. Solid State Mater. Sci.* 17 (2013) 151.
- [116] J.E. Nielsen, V.A. Bjørnstad, V. Pipich, H. Jessen, R. Lund, Beyond structural models for the mode of action: how natural antimicrobial peptides affect lipid transport, *J. Colloid Interface Sci.* 582 (2021) 793–802.
- [117] S.W. Ho, D. Jung, J.R. Calhoun, J.D. Lear, M. Okon, W.R.P. Scott, R.E. W. Hancock, S.K. Straus, Effect of divalent cations on the structure of the antibiotic daptomycin, *Eur. Biophys. J.* 37 (2008) 421–433.
- [118] A.L. Barry, P.C. Fuchs, S.D. Brown, In vitro activities of daptomycin against 2,789 clinical isolates from 11 north american medical centers, *Antimicrob. Agents Chemother.* 45 (2001) 1919–1922.
- [119] A. Pokorny, T.O. Khatib, H. Stevenson, A quantitative model of daptomycin binding to lipid bilayers, *J. Phys. Chem. B* 122 (2018) 9137–9146.
- [120] L. Robbel, M.A. Marahiel, Daptomycin, a bacterial lipopeptide synthesized by a nonribosomal machinery, *J. Biol. Chem.* 285 (2010) 27501–27508.
- [121] S. Pramanik, J. Steinkühler, R. Dimova, J. Spatz, R. Lipowsky, Binding of His-tagged fluorophores to lipid bilayers of giant vesicles, *Soft Matter* 18 (2022) 6372–6383.
- [122] M.A. Kreutzberger, A. Pokorny, P.F. Almeida, Daptomycin-phosphatidylglycerol domains in lipid membranes, *Langmuir*. 33 (2017) 13669–13679.
- [123] M.T. Lee, P.Y. Yang, N.E. Charron, M.H. Hsieh, Y.Y. Chang, H.W. Huang, Comparison of the effects of daptomycin on bacterial and model membranes, *Biochemistry*. 57 (2018) 5629–5639.
- [124] X. Cheng, P.M. Pinsky, The balance of fluid and osmotic pressures across active biological membranes with application to the corneal endothelium, *PLoS One* 10 (2015), e0145422.
- [125] Y.-F. Chen, T.-L. Sun, Y. Sun, H.W. Huang, Interaction of daptomycin with lipid bilayers: a lipid extracting effect, *Biochem.* 53 (2014) 5384–5392.

CHAPTER 7. TUNABLE BIOMIMETIC BACTERIAL MEMBRANES FROM BINARY AND TERNARY LIPID MIXTURES AND THEIR APPLICATION IN ANTIMICROBIAL TESTING

E. Krok et al.

BBA - Biomembranes 1865 (2023) 184194

- [126] A. Müller, M. Wenzel, H. Strahl, F. Grein, T.N.V. Saaki, B. Kohl, T. Siersma, J. E. Bandow, H.G. Sahl, T. Schneider, L.W. Hamoen, Daptomycin inhibits cell envelope synthesis by interfering with fluid membrane microdomains, *Proc. Natl. Acad. Sci. U. S. A.* 113 (2016) E7077–E7086.
- [127] A.H. Nguyen, K.S. Hood, E. Mileykovskaya, W.R. Miller, T.T. Tran, Bacterial cell membranes and their role in daptomycin resistance: a review, *Front. Mol. Biosci.* 9 (2022) 1–10.
- [128] M. Haque, Y. Hirai, K. Yokota, K. Oguma, Steryl glycosides: a characteristic feature of the *Helicobacter* spp.? *J. Bacter.* 177 (1995) 5334–5337.
- [129] R.A. Carabeo, D.J. Mead, T. Hackstadt, Golgi-dependent transport of cholesterol to the *Chlamydia trachomatis* inclusion, *Proc. Natl. Acad. Sci. U. S. A.* 100 (2003) 6771–6776.
- [130] P.F. Smith, Biosynthesis of cholesteryl glucoside by *Mycoplasma gallinarum*, *J. Bacteriol.* 108 (1971) 986–991.
- [131] J.P. Sáenz, D. Grosser, A.S. Bradley, T.J. Lagny, O. Lavrynenko, M. Broda, K. Simons, Hopanoids as functional analogues of cholesterol in bacterial membranes, *Proc. Natl. Acad. Sci. U. S. A.* 112 (2015) 11971–11976.

Supplementary figures

Tunable biomimetic bacterial membranes from binary and ternary lipid mixtures and their application in antimicrobial testing

Emilia Krok ^{a,b}, Mareike Stephan^a, Rumiana Dimova^a, Lukasz Piatkowski^b

* Address for correspondence: emilia.krok@put.poznan.pl, rumiana.dimova@mpikg.mpg.de

^a Max Planck Institute of Colloids and Interfaces, Science Park Golm, 14467 Potsdam, Germany

^b Poznan University of Technology, Faculty of Materials Engineering and Technical Physics, Institute of Physics, Piotrowo 3, 60-965 Poznan, Poland

Figure S1

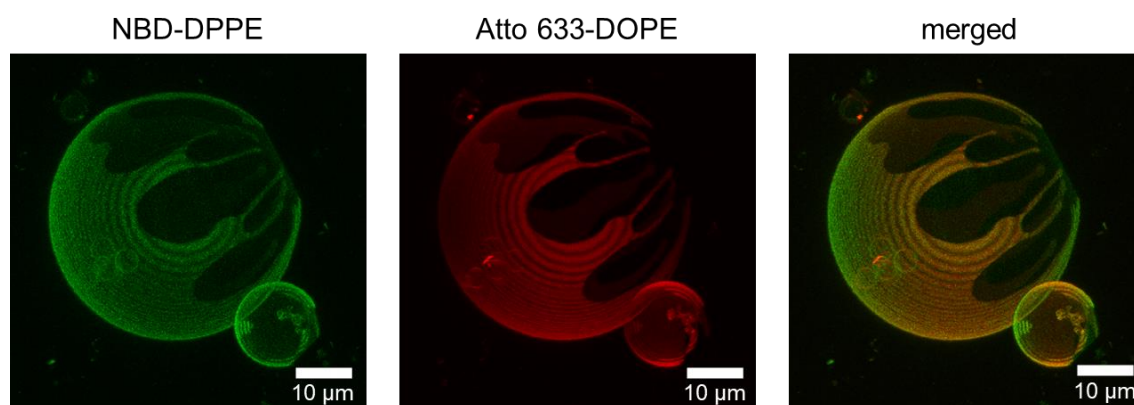


Figure S1 GUVs mimicking gram-negative cell membranes reconstituted from binary lipid mixture of POPC and POPE in molar ratio 7:3, labelled with 0.5 mol% of the fluorescent probe NBD-DPPE (green) and 0.1 mol% of Atto 633-DOPE (red). The irregular shape of the domains and the fact that their morphology does not change over time point out to their solid-like character. Image acquisition was done at 21°C.

Figure S2

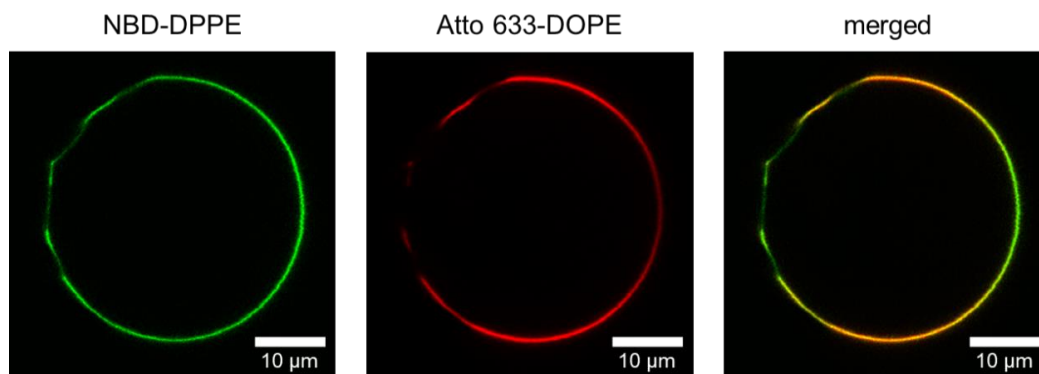


Figure S2 GUVs mimicking gram-negative cell membranes reconstituted from binary lipid mixture of POPC and POPE in molar ratio 7:3, labelled with 0.5 mol% of the fluorescent probe NBD-DPPE (green) and 0.1 mol% of Atto 633-DOPE (red). Atto 633-DOPE is known to bind to more fluid regions due to the unsaturated tails of DOPE and is an unambiguous indicator of the presence of L_d phase. The low-intensity areas in NBD-DPPE channel were ascribed to the POPE-rich regions. At the same time the regions of higher intensity colocalized perfectly with Atto-DOPE labeled areas. In the merged image, the variation in the coloring (orange/green) is due to polarization effects of the red dye (producing lower intensity in the horizontal direction with respect to the vertical direction). Images were recorded at 21°C.

Figure S3

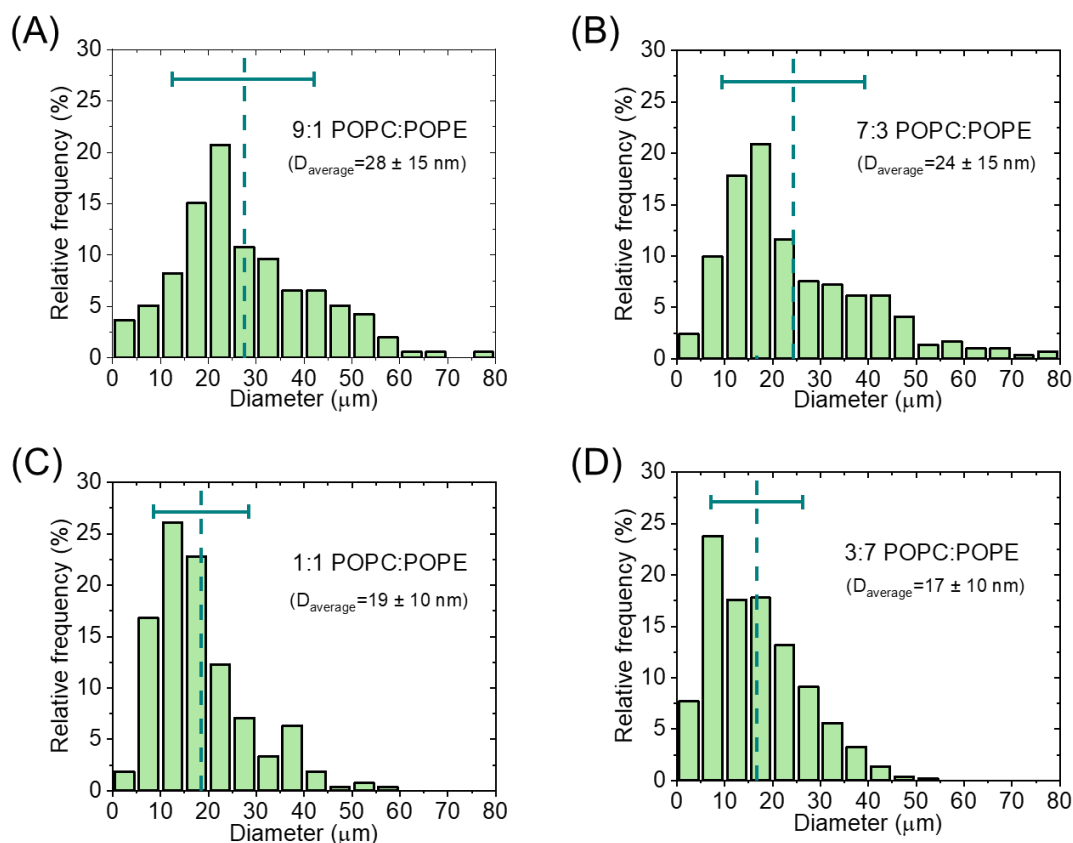


Figure S3 Histograms of size distributions of GUVs mimicking gram-negative bacterial cell membranes reconstituted from binary lipid mixtures of POPC and POPE at molar ratios: (A) 9:1, (B) 7:3, (C) 1:1 and (D) 3:7. The average size of GUVs decreases with increasing content of POPE. Dashed lines correspond to the average GUVs diameter, horizontal bars represent the standard deviations.

Figure S4

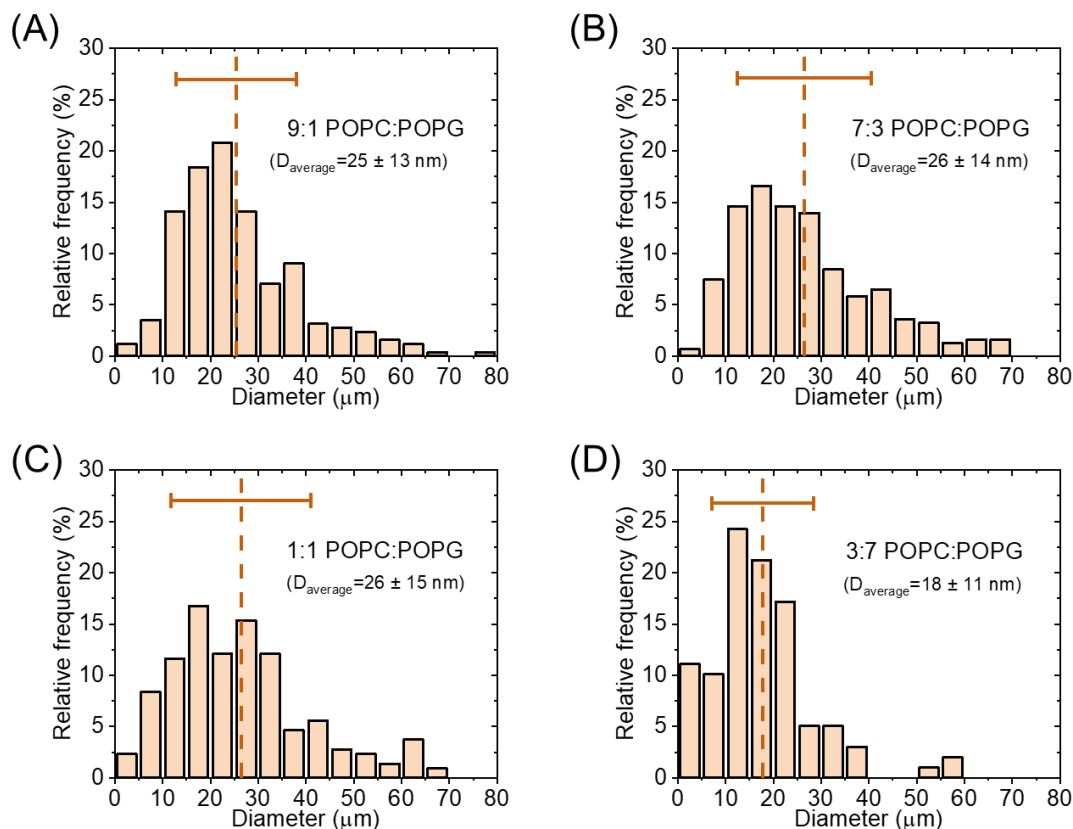


Figure S4 Histograms of size distributions of GUVs mimicking gram-negative bacterial cell membranes reconstituted from binary lipid mixtures of POPC and POPG at molar ratios: (A) 9:1, (B) 7:3, (C) 1:1 and (D) 3:7. The increasing amount of POPG did not influence the average GUVs size. Dashed lines correspond to the average GUV diameter, horizontal bars represent the standard deviations.

Table S1 Major lipid components in the membranes of the most common gram-negative (pink) and gram-positive bacteria (violet) together with the lipid compositions tested in this research. Values are expressed as a percentage of the overall membrane lipid content.

Bacterial strain	PE	PG	CA	References
<i>P. mirabilis</i>	80	15	5	[1]
<i>P. aeruginosa</i>	60	21	11	[2]
<i>E. coli</i>	67	23	10	[3]
proposed model of gram-negative bacterial cell membrane	70	20	10	this research
<i>S. aureus</i>	0	54	43	[4]
<i>L. monocytogenes</i>	9	52	22	[5]
<i>B. cereus</i>	43	40	17	[6]
<i>B. subtilis</i>	12	70	4	[7]
proposed model of gram-positive bacterial cell membrane	30	60	10	this research
3:7 POPE:POPG	30	70	-	this research
1:1 POPE:POPG	50	50	-	this research
7:3 POPE:POPG	70	30	-	this research

Figure S5

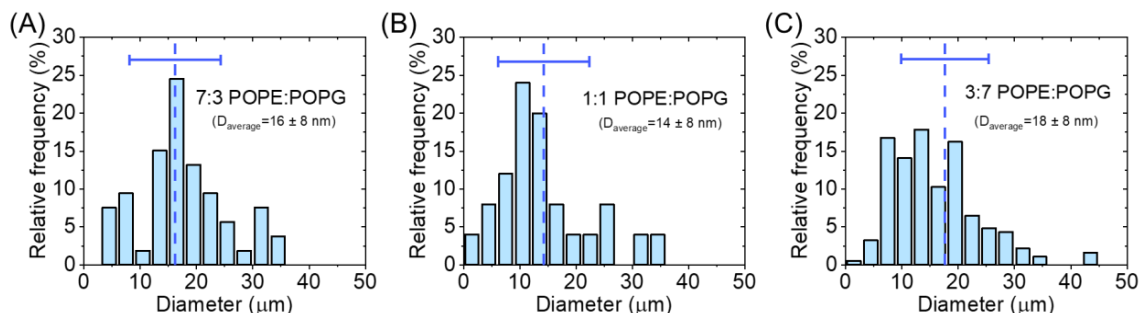


Figure S5 Histograms of size distributions in GUVs mimicking gram-negative bacterial cell membranes reconstituted from binary lipid mixtures of POPE and POPG at molar ratios: (A) 7:3, (B) 1:1, and (C) 3:7. The relative concentration of POPE and POPG does not influence the average size of the GUVs, however, GUVs with these lipid compositions are smaller than GUVs containing POPC (see Figure S2 and S3). Dashed lines correspond to the average GUV diameter; horizontal bars represent the standard deviations.

Figure S6

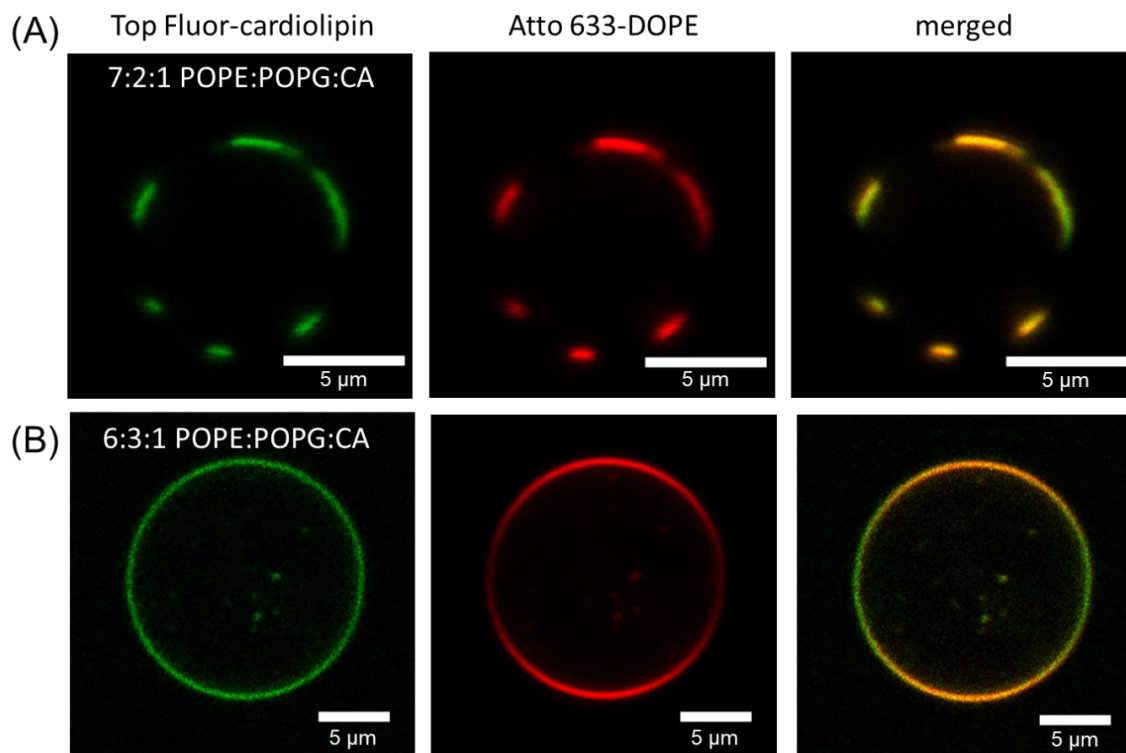


Figure S6 GUVs mimicking bacterial cell membranes reconstituted from ternary lipid mixture of POPE, POPG and cardiolipin: (A) Confocal equatorial cross sections of a GUV with lipid composition characteristic for the inner cell membrane of gram-negative bacteria, containing POPE:POPG:cardiolipin in molar ratio 7:2:1, labelled with 0.5 mol% of Top Fluor-cardiolipin and 0.1 mol% of DOPE-Atto 633. Atto-labeled regions overlap with Top Fluor-cardiolipin areas and correspond to the more fluid domains composed of cardiolipin and POPG, (B) Confocal equatorial cross sections of a GUV with lipid composition characteristic for the inner cell membrane of gram-positive bacteria, containing POPE:POPG:cardiolipin in molar ratio 3:6:1, labelled with 0.5 mol% of Top Fluor-cardiolipin and 0.1 mol% of DOPE-Atto 633. Phase separation was not visible in GUVs mimicking gram-positive bacterial membranes. Image acquisition was done at 21°C.

Figure S7

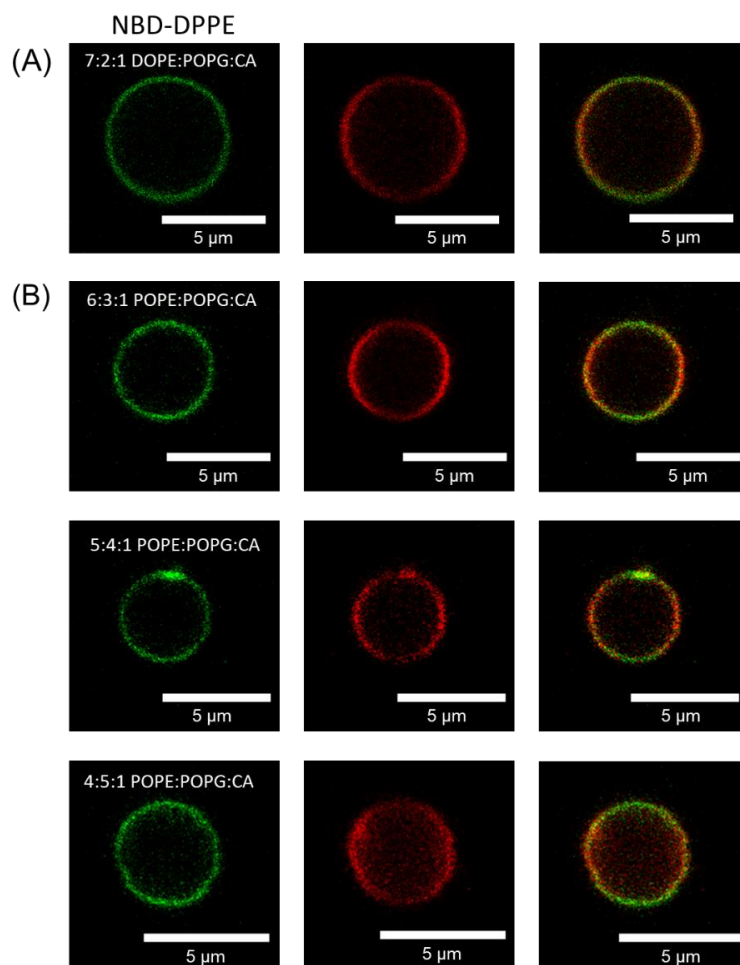


Figure S7 GUVs reconstituted from ternary lipid mixture of (A) DOPE:POPG:CA in molar ratio 7:2:1. (B) POPE:POPG:CA in molar ratio: 6:3:1; 5:4:1, 4:5:1. Contrary to the model composed of POPE, POPG and cardiolipin (7:2:1 molar ratio), there was no phase separation in any of the tested compositions. Temperature during acquisition was 21°C.

Figure S8

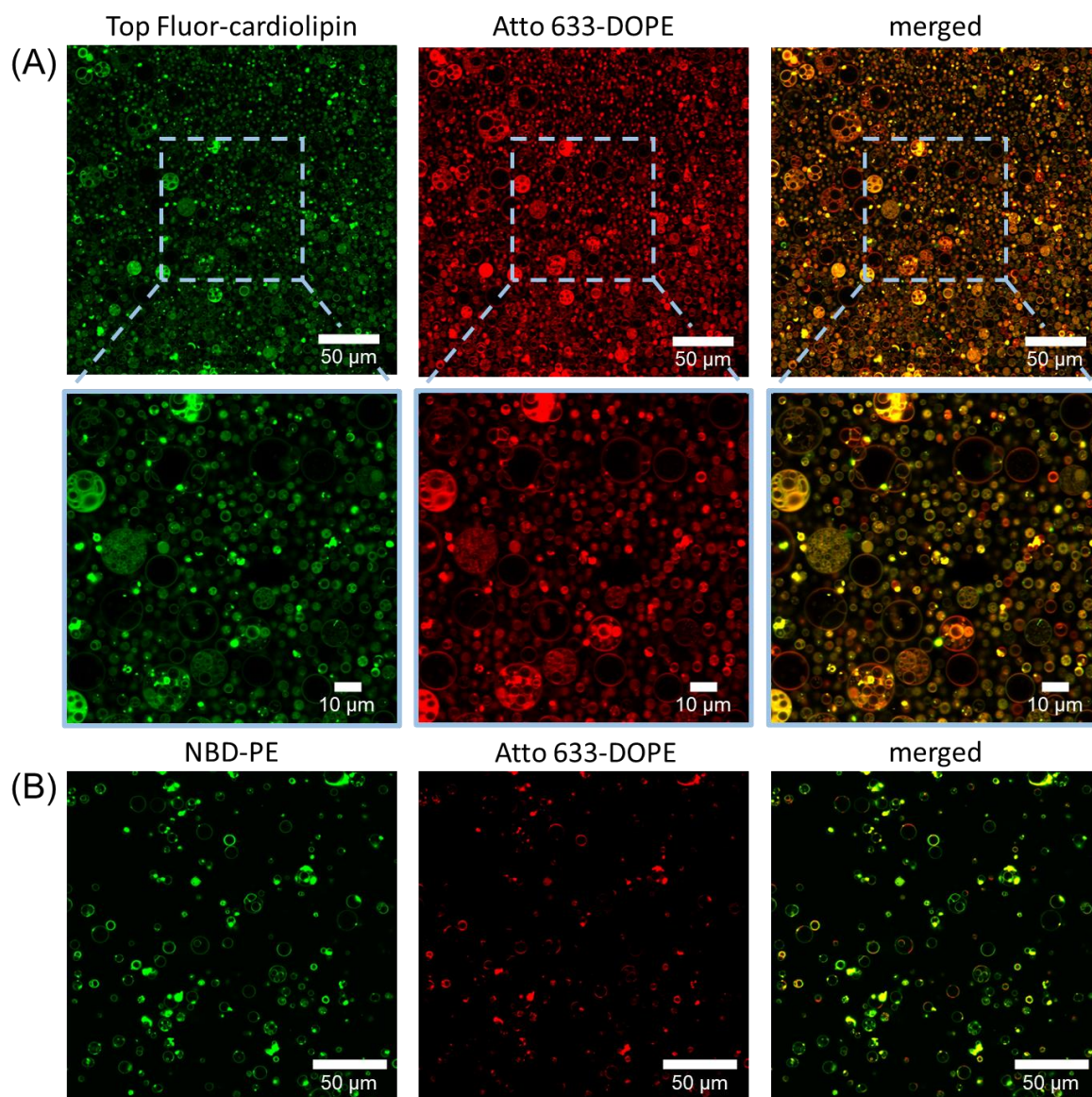


Figure S8 Formation yield for GUVs composed of: (A) POPE:POPG:cardiolipin in molar ratio 3:6:1, which is a lipid composition characteristic for gram-positive bacterial cell membranes, and (B) POPE:POPG:cardiolipin in molar ratio 7:2:1 mimicking gram-negative bacterial cell membranes. The production yield for gram-positive GUVs was much higher than for gram-negative GUVs. Moreover, GUVs containing high amount of negatively charged lipids (A) were more likely to form vesosomes – multivesicular structures where the mother vesicle contains multiple vesicles trapped inside. Image acquisition was done at 21°C.

Figure S9

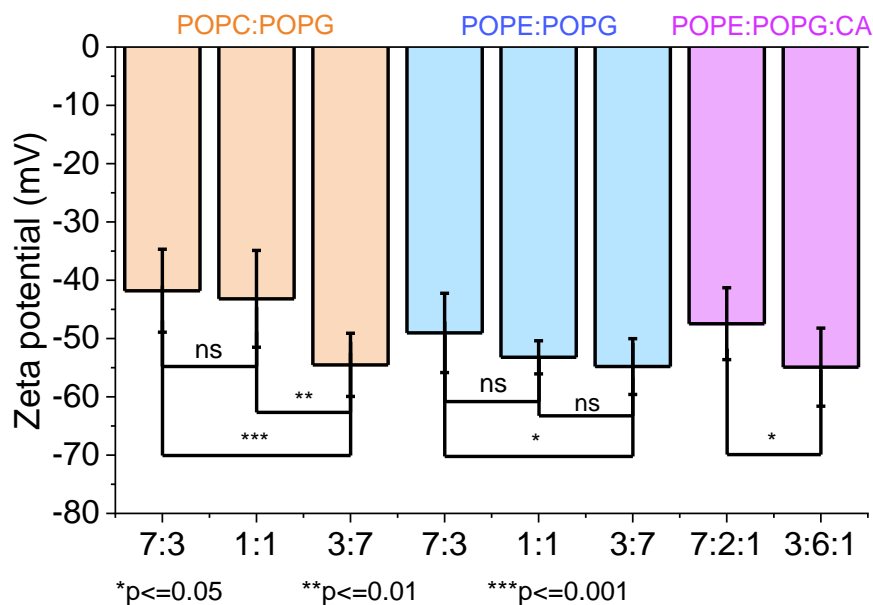


Figure S9 Zeta potential measurements of GUVs in sucrose solution. GUVs prepared by electroformation method, made of POPC:POPG mixtures at molar ratio: 7:3, 1:1, 3:7; POPE:POPG 7:3, 1:1, 3:7; POPE:POPG:cardiolipin in molar ratio: 7:2:1 and 3:6:1 corresponding to gram-negative and gram-positive bacterial cell membranes, respectively. The error bars represent the standard deviation of the calculated values. Student's t-tests were performed to determine the p-values and to verify whether the differences in the measured zeta potential values for membranes with different composition are statistically significant. We consider $p > 0.05$ to indicate not statistically significant difference (ns).

Figure S10

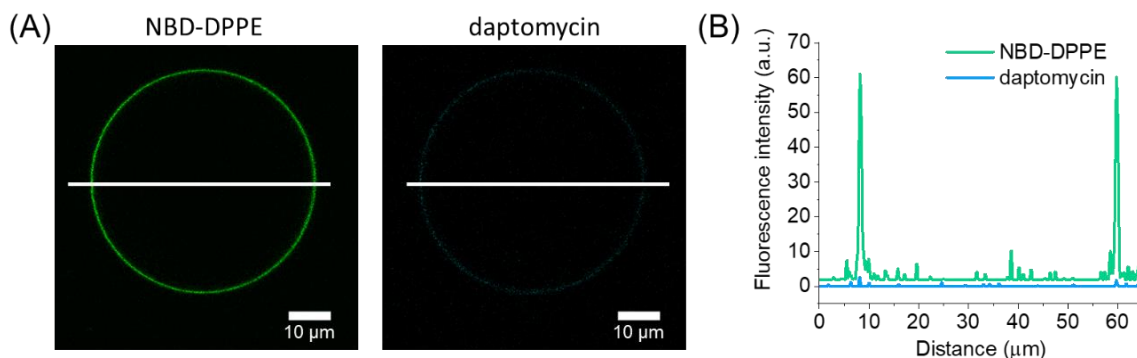


Figure S10 Binding of daptomycin to GUVs composed solely of zwitterionic POPC lipid: (A) A single defect-free GUV composed of POPC incubated in 22 mM daptomycin and 20 mM CaCl_2 , green channel corresponds to NBD-DPPE fluorescence, cyan represents daptomycin. (B) Fluorescence intensity profiles along the lines in (A) for NBD-DPPE and daptomycin channels.

Figure S11

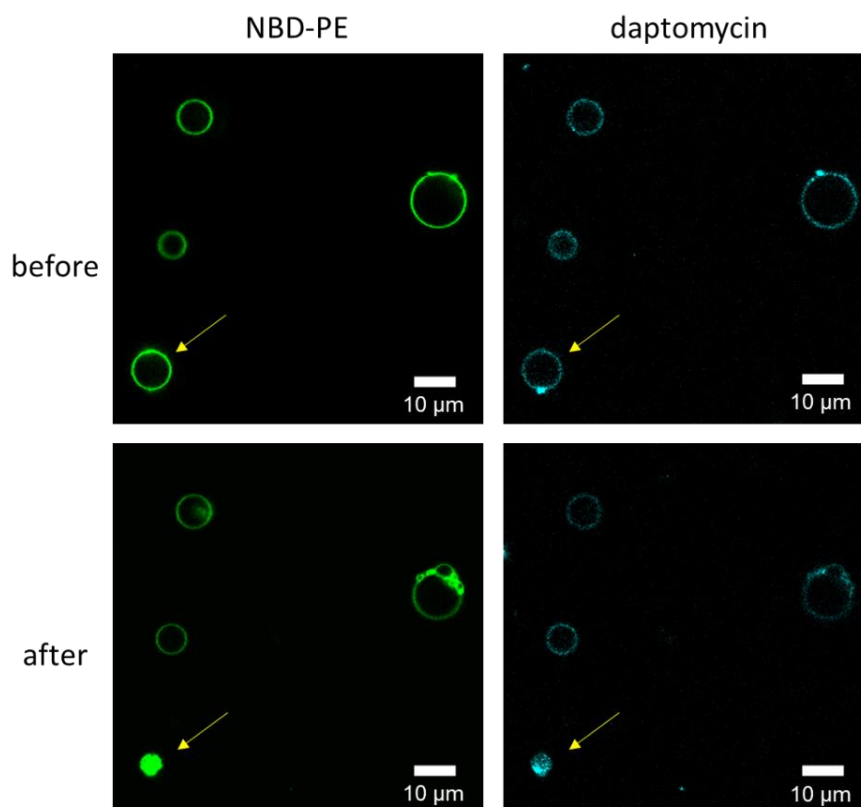


Figure S11 GUVs right after exposure to daptomycin (before) and 1 h upon its addition (after). Prolonged incubation in daptomycin-rich solution (22 mM daptomycin, 20 mM CaCl_2) leads to vesicles bursting (see yellow arrow).

CHAPTER 7. TUNABLE BIOMIMETIC BACTERIAL MEMBRANES FROM BINARY AND TERNARY LIPID MIXTURES AND THEIR APPLICATION IN ANTIMICROBIAL TESTING

References

- [1] J. Gmeiner, H.H. Martin, Phospholipid and Lipopolysaccharide in *Proteus mirabilis* and Its Stable Protoplast I-Form, *European J. Biochem.* 67 (1976) 487–494.
- [2] R.S. Conrad, H.E. Gilleland, Lipid Alterations in Cell Envelopes of Polymyxin-Resistant *Pseudomonas aeruginosa* Isolates, *J. Bacteriol.* 148 (1981) 487–497.
- [3] V.W. Rowlett, V.K.P.S. Mallampalli, A. Karlstaedt, W. Dowhan, H. Taegtmeier, W. Margolin, H. Vitrac, Impact of Membrane Phospholipid Alterations in *Escherichia coli* on Cellular Function and Bacterial Stress Adaptation, *J. Bacteriol.* 199 (2017) e00849-16.
- [4] H. Masaaki, O. Akinobu, K. Reiko, A. Masufumi, K. Yasuhiro, Lipid Composition of *Staphylococcus aureus* and Its Derived L-forms, *Microbiol. Immunol.* 23 (1979) 435–442.
- [5] A.D. Crandall, T.J. Montville, Nisin Resistance in *Listeria monocytogenes* ATCC 700302 Is a Complex Phenotype, *Appl. Environ. Microbiol.* 64 (1998) 231–237.
- [6] A. Haque, N.J. Russell, Strains of *Bacillus cereus* vary in the phenotypic adaptation of their membrane lipid composition in response to low water activity, reduced temperature and growth in rice starch, *Microbiology (N Y)*. 150 (2004) 1397–1404.
- [7] S. Clejan, T.A. Krulwich, K.R. Mondrus, D. Seto-Young, Membrane Lipid Composition of Obligately and Facultatively Alkalophilic Strains of *Bacillus* spp, *J. Bacteriol.* 168 (1986) 334–340.

Chapter 8

The most important results of the thesis and future outlook

Throughout this thesis I dedicated my attention to two distinct categories of organisms, endeavoring to replicate the cell membranes found in prokaryotes (both gram-negative and gram-positive bacteria) as well as eukaryotes (specifically mammals). In my pursuit of reconstructing the natural plasma membrane, I employed three biomimetic models: GUVs, SUVs, and SLBs, leveraging their varied and unique properties to enhance the accuracy of the mimicked structures. Equipped with these diverse models I focused on the different internal and external parameters that could impact the structural organization of membranes such as the pH of the aqueous medium, hydration level, or the composition of the membrane itself. To thoroughly describe the membrane heterogeneities and to understand the origin of the membrane structural reorganization I deployed techniques such as AFM, fluorescence microscopy, FRAP, DLS and zeta potential measurements, which all together provided a comprehensive characterization of my model membrane systems. This chapter serves as a synthesis of the most important findings derived from my research, while also delineating the potential future experimental pathways.

8.1 Summary of results

The following thesis is a collection of three thematically related research publications. In each of them, I focused on different factors that may trigger changes in the structural organization of lipid membranes. These different factors may influence parameters such as the size and shape of ordered lipid domains, the hydrophobic mismatch between L_d and L_o phases, membrane charge, curvature, or asymmetry of leaflets. Below I summarized the main conclusions from each publication.

The most important findings of publication 1

"Lateral organization of biomimetic cell membranes in varying pH conditions":

- The average size of L_o domains and area occupied by L_o domains increase with the increase of pH in the range 2.1-9.0. Within pH range 3.7-6.7 the domain size decreases linearly with the lowering of the buffer pH (more acidic character of the

environment). This established relationship between the specific size of domains and pH of the buffer can be used to form SM- and cholesterol-rich membrane heterogeneities with pre-defined and repeatable size for their further application in studying domain-binding molecules.

- L_o domains with a specific size, formed in the buffer of corresponding pH maintain their average size even upon replacement of the aqueous medium with the buffer of neutral pH. This effect sustains for a minimum of 72 hours, providing a unique opportunity to investigate pH-sensitive molecules, particularly proteins. In many instances, maintaining the appropriate conformation of these molecules requires a physiological pH of the surrounding environment.
- The observation of nucleation and growth of domains upon thermal heating of the membrane above phase transition temperature revealed the time-dependent evolution of the domain size, which was different depending on the applied pH of the buffer. Thus, it was concluded that the formation of domains with specific size, characteristic for the corresponding pH, occurs during membrane formation on solid support.
- The dynamics of the L_d phase, characterized by the diffusion coefficient, remains consistent across the pH range of 1.7-9.0. Similarly, the identical effect is observed for the L_o phase within the pH range of 4.2-9.0. At the same time, the MF for the L_d phase was increasing with the pH, showing values in the range $\sim 70-90\%$. Although the membranes prepared at varying pH conditions differed significantly in terms of the structural arrangement, the movement of their constituents was not affected by pH.

The most important findings of publication 2

"Nanoscale structural response of biomimetic cell membranes to controlled dehydration":

- The integrity of lipid membranes can endure complete desiccation even in the absence of stabilizing agents, provided that the dehydration process is performed gradually and with precise control. The gradual dehydration method effectively preserves the overall structural organization of the membrane, ensuring the absence of defects or holes.
- Although in the microscale the membrane remains unaffected by complete desiccation, there is a prominent nanoscale structural reorganization as revealed by AFM. The removal of bulk water and subsequent lowering of the hydration leads to increased migration of lipids from the L_d phase to the L_o phase and formation of fluid L_d nanodomains within more ordered L_o phase. At the same time, the boundary between phases becomes more jagged, an effect attributed to the reduction in the line tension stemming from the absence of water.
- The height mismatch between L_d and L_o phases decreases with the lowering of the membrane's hydration state in a linear manner. This process is fully reversible, as the subsequent increase of the environmental humidity leads to the restoring of the height mismatch to its initial value.

- The line tension at the boundary of L_d and L_o phases decreases 3-fold for a completely desiccated membrane compared with the fully hydrated. The greater is the line tension, the higher is the tendency of the membrane to phase separate in order to avoid the energetically unfavorable exposure of the hydrophobic parts. The decrease in line tension under dehydration conditions explains the increased admixing of the lipids from L_d and L_o phases.

The most important findings of publication 3

"Tunable biomimetic bacterial membranes from binary and ternary lipid mixtures and their application in antimicrobial testing":

- The choice of lipids and their respective ratios exerts a substantial influence on the resultant models, causing notable variations in size, membrane curvature, charge, and lateral organization. Especially, the replacement of the PE lipid, abundantly present in the bacterial cell membranes, with the eukaryotic lipid PC leads to: (i) the asymmetry of the membrane; membranes composed of POPC and POPG or (ii) the formation of bend inward PC-rich domains (membranes containing POPC and POPE).
- The interchangeable use of lipids with analogous chemical structures or limiting the composition to just one or two lipid species can significantly alter the overall characteristics of bacterial membranes, potentially leading to erroneous conclusions about the membrane's behavior.
- The commonly used electroformation method can successfully be applied for the preparation of GUVs containing not only zwitterionic lipids but also those with a substantial amount of negatively charged lipids (e.g. POPE or cardiolipin).
- The efficiency of daptomycin binding to the membrane is strongly dependent on the amount of incorporated negatively charged lipids. Daptomycin does not bind to the membranes composed of zwitterionic POPC lipids but it undergoes a reaction with POPG and cardiolipin.
- The vesicles trapped within the mother vesicle are not affected by daptomycin, leading to the conclusion that this antimicrobial peptide does not internalize in the vesicle lumen and rather binds solely to the outer leaflet of the membrane.

8.2 Outlook

In this thesis, my primary focus was on exploring the influence of environmental conditions on eukaryotic cell membranes. I am particularly intrigued by how water or buffer, its composition, or simply the amount of aqueous solution can influence the structural organization of model membranes. The proposed in this thesis biomimetic prokaryotic membranes are great models for performing further research on the impact of water on bacterial cell membranes. At the same time, the developed in our group method of membrane preservation upon its partial or complete dehydration opened up countless possibilities for follow-up studies on membrane behavior in water scarcity conditions.

Especially noteworthy for me is the mechanism of anhydrobiosis, known as the ability of living organisms to lose all or almost all water and suspend the whole metabolism until the moment when favorable hydration is restored [201]. In general, anhydrobiosis is more common in gram-positive bacteria [202]. *S. aureus*, which is a representative member of this group, can remain stable for months in dehydration conditions. *E. coli*, which belongs to gram-negative bacteria is not resistant to desiccation [203], however, its ability to withstand the absence of water was reported to drastically improve upon the addition of trehalose to the culture medium [204]. On the other hand bacteria from phylum *Deinococcota* (e.g. *D. radiodurans*), which developed remarkable dehydration and ionic radiation resistance, seem to combine the characteristics of both gram-positive and gram-negative bacterial cell walls. Their thick cell walls give them a gram-positive type of staining (violet), while the presence of the second membrane points toward their classification as gram-negative bacteria [205]. It can be therefore concluded that anhydrobiosis in bacteria is strongly related to the properties of their cell envelope.

Intriguingly bacterial adaptation to low hydration conditions goes far beyond the use of saccharides. Gram-positive bacteria for instance accumulate Mn^{2+} and Fe^{2+} divalent cations in their cell walls [206]. The presence of these ions is believed to be connected with the increased desiccation tolerance and at the same time to the ability to survive ionizing radiation. Furthermore, dehydration leads to oxidative stress in the cell, which is the imbalance between free radicals and antioxidants. Oxidative stress and formation of reactive oxygen species lead to lethal double-strand DNA breaks, cleavage, and aggregation of proteins, that result in hampered functioning or complete loss of activity [207]. Bacteria with an outstanding ability to survive dehydration developed mechanism to combat oxidative stress by the production of unique DNA repair-related proteins: DdrB, DdrC, DdrD, PprA, and DdrO [206]. Last but not least, some bacteria created a mechanism of biofilm production. These extracellular matrices form a covering layer that protects them from extensive drying during short periods of time when the level of environmental hydration is not sufficient to sustain metabolic processes.

Clearly, different types and strains of bacteria developed various mechanisms to prevent cell damage due to dehydration or to cope with the consequences of dehydration. It is evident that none of these protection and adaptation processes is universal for all types of bacteria and the exact molecular-level mechanisms driving dehydration survival remain elusive. While all the discovered mechanisms have been apparently working well towards dehydration resistance it remains absolutely unclear what do these mechanisms prevent from on the molecular level. In other words - what happens to the membrane/cell envelope, or its particular part, during dehydration in the absence of the protective mechanism? How specific factors such as membrane composition, cell envelope architecture, lateral organization of the membrane, or lipid dynamics, influence the ability for bacteria to survive under harsh dehydration conditions is not well understood.

The preliminary results obtained for very simple model membranes, composed of POPE mixed with 14:1 PC in a molar ratio 1:1, revealed that the addition of POPE drastically changes the dynamic properties of the membrane upon its dehydration. POPE is abundantly found in gram-negative bacteria, e.g. it comprises even up to 70% of *E. coli* inner cell membrane. As a comparison a single component lipid bilayer composed of 14:1 PC was made, which represented the most basic model of eukaryotic membrane. Membranes were imaged at full hydration, then carefully dehydrated and equilibrated

to room humidity of 30% RH (Fig. 8.1 A). The process of dehydration did not lead to damage in the structure of both model membranes, indicating that structurally both systems behave in a similar manner under desiccation conditions. However, the analysis of the FRAP curves (Fig. 8.1 B) revealed that the dynamics of mammalian membranes is more influenced by dehydration (27-fold slower diffusion) than it was observed for bacterial membranes (4-fold decrease of diffusion coefficient) (Fig. 8.1 C). These preliminary experiments gave me already a strong indication that bacterial membranes respond completely differently to dehydration in terms of lipids mobility and seem to exhibit higher resistance to desiccation.

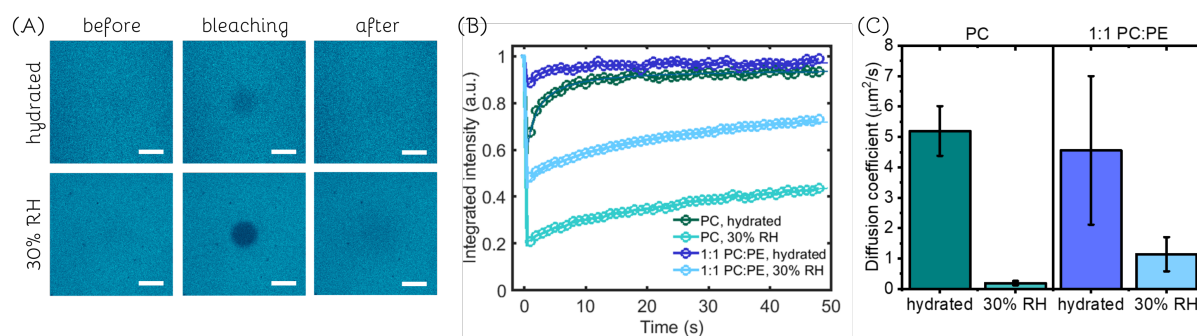


Figure 8.1: (A) Representative confocal images of SLB composed of PC:PE at molar ratio 1:1, recorded during FRAP experiment at full hydration and upon equilibration to 30% RH. Scale bars correspond to $10 \mu\text{m}$. Membranes were labeled with DOPE Atto-633. The collected grayscale images were pseudo-colored in post-processing. (B) FRAP traces for fully hydrated and dehydrated membranes composed of PC (the most basic model of mammalian lipid membrane) and 1:1 PC:PE (resembling very simple bacterial cell membrane). (C) The diffusion coefficient for fully hydrated and dehydrated membranes, obtained from at least 10 FRAP traces.

The understanding of anhydrobiosis in bacterial cell membranes is crucial for revealing the mechanisms of bacterial survival under dehydration, which is inevitably connected to their ability to maintain pathogenicity. Moreover, it has been shown that there is a strong correlation between bacterial resistance to dehydration and UV radiation [206], which is one of the basic antimicrobial techniques applied in public buildings such as hospitals, daycares, or rehabilitation centers [208]. UV light sanitizers are commonly used to easily sterilize the whole room and prevent the transmission of bacteria and viruses to other patients. Because of this inseparability of dehydration and UV resistance, the information about the factors that make bacterial cell membranes resistant to dehydration could help in better understanding their survival under UV light and lead to more effective use of antimicrobial treatment.

Chapter 9

Scientific achievements

9.1 Education

1. **10.2019 – 03.2024** PhD studies, Doctoral School of Poznan University of Technology, discipline: Materials Engineering, Poznań University of Technology, Poland.
2. **10.2017 – 09.2019** Master of Science (M.Sc.), Molecular Bioengineering, Dresden University of Technology, Center for Molecular and Cellular Bioengineering, Germany.
3. **10.2015 – 08.2016** Erasmus Exchange Student, Biological, Chemical and Pharmaceutical Engineering, Technical University of Braunschweig, Germany.
4. **09.2013 – 01.2017** Engineering Studies (B.Eng.), Biomedical Engineering, Poznań University of Technology, Faculty of Mechanical Engineering and Management, Poland.

9.2 Internships

1. **07.2022 – 10.2022** Max Planck Institute of Colloids and Interfaces, Department of Theory and Bio-Systems, Potsdam, Germany, group of Prof. Rumiana Dimova.
Research internship
2. **10.2021 – 11.2021** Max Planck Institute of Biochemistry, Department of Cellular and Molecular Biophysics, Martinsried, Germany, group of Prof. Petra Schwille.
Short-term PhD internship
3. **03.2019 – 08.2019** Fraunhofer Institute for Ceramic Technologies and Systems IKTS, Department of Bio- and Nanotechnology, Dresden, Germany, supervisor: Dr. rer. nat. Jörg Opitz.
Student research assistant (full time)
4. **10.2018 – 02.2019** Fraunhofer Institute for Ceramic Technologies and Systems IKTS, Department of Bio- and Nanotechnology, Dresden, Germany, supervisor: Dr. Sascha Balakin.
Student internship

5. **07.2016 – 08.2016** Helmholtz Centre for Infection Research, Braunschweig, Germany, supervisor: Prof. Rafael Mikolajczyk.
Student internship

9.3 Publications

1. **Emilia Krok***, Henri G. Franquelim, Madhurima Chattopadhyay, Hanna Orlikowska-Rzeznik, Petra Schwille, Lukasz Piatkowski*, *Nanoscale structural response of biomimetic cell membranes to controlled dehydration*, Nanoscale, 2023, volume 16, issue 1, 72-84, doi: 10.1039/D3NR03078D, **IF: 6.7**
2. **Emilia Krok***, Mareike Stephan, Rumiana Dimova*, Lukasz Piatkowski, *Tunable biomimetic bacterial membranes from binary and ternary lipid mixtures and their application in antimicrobial testing*, Biochimica et Biophysica Acta (BBA) - Biomembranes, 2023, volume 1865, issue 7, 184194, doi: 10.1016/j.bbamem.2023.184194, **IF: 3.4**
3. Hanna Orlikowska-Rzeznik*, **Emilia Krok**, Madhurima Chattopadhyay, Agnieszka Lester, Lukasz Piatkowski*, *Laurdan Discerns Lipid Membrane Hydration and Cholesterol Content*, Journal of Physical Chemistry B, 2023, volume 127, issue 15, 3382–3391, doi: 10.1021/acs.jpcc.3c00654, **IF: 3.3**
4. Madhurima Chattopadhyay*, **Emilia Krok**, Hanna Orlikowska-Rzeznik, Lukasz Piatkowski*, *Cooperativity between sodium ions and water molecules facilitates lipid mobility in model cell membranes*, Chemical Science, 2023, volume 14, issue 15, 4002-4011, doi: 10.1039/D2SC06836B, **IF: 8.4**
5. **Emilia Krok***, Agnieszka Batura, Madhurima Chattopadhyay, Hanna Orlikowska, Lukasz Piatkowski*, *Lateral organization of biomimetic cell membranes in varying pH conditions*, Journal of Molecular Liquids, 2022, volume 345, number 117907, doi: 10.1016/j.molliq.2021.117907, **IF: 6.0**
6. Madhurima Chattopadhyay*, **Emilia Krok**, Hanna Orlikowska, Petra Schwille, Henri G. Franquelim, Lukasz Piatkowski*, *Hydration layer of only a few molecules controls lipid mobility in biomimetic membranes*, Journal of the American Chemical Society, 2021, volume 143, issue 36, 14551–14562, doi: 10.1021/jacs.1c04314, **IF: 16.4**
7. Madhurima Chattopadhyay*, Hanna Orlikowska, **Emilia Krok**, Lukasz Piatkowski*, *Sensing hydration of biomimetic cell membranes*, Biosensors, 2021, volume 11, issue 7, doi: 10.3390/bios11070241, **IF: 5.4**
8. **Emilia Krok***, Sascha Balakin, Jonas Jung, Frank Gross, Jörg Opitz*, Gianuario Cunierti, *Modification of titanium implants using biofunctional nanodiamonds for enhanced antimicrobial properties*,

Nanotechnology, 2020, volume 31, number 20, 205603 doi: 10.1088/1361-6528/ab6d9b,
IF: 3.9

*corresponding author(s)

Total impact factor: 53.5, h-index: 4

9.4 Published conference abstracts

1. **Emilia Krok**, Madhurima Chattopadhyay, Hanna Orlikowska-Rzeznik, Henri G. Franquelim, Petra Schwille, Lukasz Piatkowski, *Impact of water scarcity conditions on the nanoscale structural arrangement of biomimetic cell membranes*, European Biophysics Journal, 2023, volume 52, pages 1–220, doi: 10.1007/s00249-023-01668-7, **IF: 2.1**
2. Madhurima Chattopadhyay, **Emilia Krok**, Hanna Orlikowska-Rzeznik, Lukasz Piatkowski, *Cooperative effort of sodium ions and water molecules facilitates lipid mobility in model cell membranes*, European Biophysics Journal, 2023, volume 52, pages 1–220, doi: 10.1007/s00249-023-01668-7, **IF: 2.1**
3. Lukasz Piatkowski, Madhurima Chattopadhyay, **Emilia Krok**, Hanna Orlikowska-Rzeznik, Petra Schwille, Henri Franquelim, *Lipid-water-ion interactions determine cell membrane structure and dynamics*, European Biophysics Journal, 2023, volume 52, pages 1–220, doi: 10.1007/s00249-023-01668-7, **IF: 2.1**
4. **Emilia Krok**, Madhurima Chattopadhyay, Hanna Orlikowska-Rzeznik, Lukasz Piatkowski, *Decreased hydration causes nanoscale structural rearrangement within biomimetic cell membranes*, FEBS Open Bio, 2022, volume 12, issue 1, SShT-04.2-1, doi: 10.1002/2211-5463.13442, **IF: 2.8**
5. Agnieszka Lester, **Emilia Krok**, Madhurima Chattopadhyay, Lukasz Piatkowski, *Engineering cell membranes—the effect of pH on the formation, structure, and mobility of biomimetic cell membranes*, FEBS Open Bio, 2022, volume 12, issue S1, P-04.2-008, doi: 10.1002/2211-5463.13440, **IF: 2.8**
6. Madhurima Chattopadhyay, **Emilia Krok**, Hanna Orlikowska-Rzeznik, Lukasz Piatkowski, *Sodium ions support lipid mobility in dehydrated biomembranes*, FEBS Open Bio, 2022, volume, issue S1, P-04.2-009, doi: 10.1002/2211-5463.13440, **IF: 2.8**
7. Hanna Orlikowska-Rzeznik, **Emilia Krok**, Madhurima Chattopadhyay, Agnieszka Lester, Lukasz Piatkowski, *Direct effect of biomimetic cell membrane hydration on Laurdan fluorescence*,

FEBS Open Bio, 2022, volume, issue S1, P-04.2-007, doi: 10.1002/2211-5463.13440, **IF: 2.8**

8. Lukasz Piatkowski, Madhurima Chattopadhyay, **Emilia Krok**, Hanna Orlikowska-Rzeznik, Agnieszka Lester *How the absence of just a few water molecules affects the structure and dynamics of cell membranes*, FEBS Open Bio, 2022, volume, issue S1, P-04.2-005, doi: 10.1002/2211-5463.13440, **IF: 2.8**

9.5 Participation in conferences

Presented talks:

1. **Emilia Krok**, Mareike Stephan, Rumiana Dimova, Lukasz Piatkowski, *The fascinating world of microbes – the development of model bacterial cell membranes*, XXVIII Warsztaty Biofizyczne/XXVIII Biophysical Workshop, **Kazimierz Dolny, Poland**, 25-26.05.2023.
2. **Emilia Krok**, Madhurima Chattopadhyay, Hanna Orlikowska-Rzeznik, Lukasz Piatkowski, *Decreased hydration causes nanoscale structural rearrangement within biomimetic cell membranes*, The Biochemistry Global Summit – the 25th IUBMB, 46th FEBS and 15th PABMB Congresses, **Lisbon, Portugal**, 09-14.07.2022.
3. **Emilia Krok**, *pH-driven lateral organization of biomimetic cell membranes*, 1st symposium on Molecular Biosensing: From Theory to Practice Horizon 2020 MSCA-ITN LogicLab, **Jena, Germany**, 17-19.11.2021.
4. **Emilia Krok**, Madhurima Chattopadhyay, Hanna Orlikowska, Lukasz Piatkowski, *When the cells get “thirsty” – the impact of the extreme dehydration on the biological cell membranes*, Konferencja Młodych Naukowców nt. Biologia, Chemia i Środowisko – Spojrzenie Młodych Naukowców/Young Scientists’ Conference Biology, Chemistry, Environment – the Perspective of Young Scientists, **Kraków, Poland**, 24-25.04.2021. **Best talk award.**
5. **Emilia Krok**, Sascha Balakin, Jonas Jung, Frank Gross, Jörg Opitz, Gianaurelio Cunberti, *Nanodiamonds are the surgeon’s best friends – how to create orthopedic implants with antimicrobial properties?* Innowacyjne pomysły młodych naukowców: Nauka – Startup – Przemysł, VI edycja konferencji/ Innovative Ideas of Young Scientists: Science-Startup-Industry, 6th edition, **Wrocław, Poland**, 11-13.05.2020.
6. **Emilia Krok**, Sascha Balakin, Jonas Jung, Frank Gross, Jörg Opitz, Gianaurelio Cunberti, *Modification of titanium implants by using nanodiamonds for enhanced antimicrobial properties*, XI Ogólnokrajowa Konferencja Młodzi Naukowcy w Polsce-Badania i Rozwój/ 11th National Conference Young Scientists in Poland – Research and Development, **Poznań, Poland**, 30.03.2020.
7. **Emilia Krok**, Madhurima Chattopadhyay, Hanna Orlikowska, Lukasz Piatkowski, *Membrane anhydrobiosis— the impact of hydration on the structure and dynamics of*

biomimetic cell membranes, 4th EMBO Workshop on Computational and Structural Biology and Chemistry 2020, **Waplewo, Poland**, 28-29.02.2020.

Poster presentations:

1. **Emilia Krok**, Madhurima Chattopadhyay, Hanna Orlikowska-Rzeznik, Petra Schwille, Henri G. Franquelim, Lukasz Piatkowski, *Impact of water scarcity conditions on the nanoscale structural arrangement of biomimetic cell membranes*, 14th European Biophysical Societies' Association (EBSA) Congress 2023, **Stockholm, Sweden**, 31.07-04.08.2023.
2. **Emilia Krok**, Mareike Stephan, Rumiana Dimova, Lukasz Piatkowski, *Reverse microengineering - development of tunable biomimetic bacterial membranes*, #RSC-Poster Twitter Conference, Royal Society of Chemistry, **United Kingdom**, 28.02.-01.03.2023.
3. **Emilia Krok**, Henri G. Franquelim, Hanna Orlikowska-Rzeznik, Madhurima Chattopadhyay, Petra Schwille, Lukasz Piatkowski *Nanoscale structural rearrangement within biomimetic cell membranes under water scarcity conditions*, Biomembrane Days 2022, **Berlin, Germany**, 19-21.09.2022.
4. **Emilia Krok**, Madhurima Chattopadhyay, Hanna Orlikowska, Lukasz Piatkowski, *Water scarcity causes nanoscale structural reorganization of biomimetic cell membranes*, #RSCPoster Twitter Conference, Royal Society of Chemistry, **United Kingdom**, 01-02.04.2022.
5. **Emilia Krok**, *Engineering of biological cell membranes; pH-driven formation of lipid rafts*, Systems Chemistry Virtual Symposium, **Strasbourg, France**, 7-9.07.2021.
6. **Emilia Krok**, Madhurima Chattopadhyay, Hanna Orlikowska, Lukasz Piatkowski, *Water interacting with biomimetic cell membranes – can anhydrobiosis be recreated in the lab?*, International Conference on Time Resolved Vibrational Spectroscopy (TRVS), **Michigan, USA**, 13-18.06.2021.
7. **Emilia Krok**, Agnieszka Batura, Madhurima Chattopadhyay, Hanna Orlikowska, Lukasz Piatkowski, *The fascinating world of lipid rafts— what do we know about their functions, structure and how can we control them for biological purposes?* Konferencja Młodych Naukowców nt. Biologia, Chemia i Środowisko— Spojrzenie Młodych Naukowców/Young Scientists' Conference Biology, Chemistry, Environment – the Perspective of Young Scientists, **Kraków, Poland**, 24-25.04.2021. **Special award for engagement in the research discussion with other participants.**
8. **Emilia Krok**, Madhurima Chattopadhyay, Hanna Orlikowska, Lukasz Piatkowski, *Biomimetic cell membranes that can survive dehydration*, Chemical Systems Meeting, **Valencia, Spain**, 22-23.03.2021.

9. **Emilia Krok**, Madhurima Chattopadhyay, Hanna Orlikowska, Lukasz Piatkowski, *Membrane anhydrobiosis— the impact of hydration on the structure of biomimetic cell membranes*, Chemical Science conference, ChemSci2020: Leaders in the Field Symposium, **IISER Kolkata, India**, 7-10.12.2020.
10. **Emilia Krok**, Sascha Balakin, Jonas Jung, Frank Gross, Jörg Opitz, Gianarelio Cunberti, *Nanodiamonds are the doctors' best friends!*, Systems Chemistry Symposium "Life-like emergent behavior in complex molecules and ensembles", **New York, USA**, 18-20.05.2020.
11. **Emilia Krok**, *Implanty ortopedyczne o właściwościach antybakteryjnych – wykorzystanie nanodiamentów jako nośników antybiotyków w implantologii*, III Ogólnopolskie Sympozjum Chemii Bioorganicznej, Organicznej i Biomateriałów/ 3rd National Symposium on Bioorganic and Organic Chemistry, and Biomaterials, **Poznań, Poland**, 07.12.2019. **The best poster award in the section "Biomaterials"**.

9.6 Patents/Patent applications

1. Patent application, PL438733, Poland, date of registration: 13.08.2021, patent title: *Preparation procedure of lipid membranes with controlled size of laterally separated domains, deposited on a solid substrate/Sposób otrzymywania membran lipidowych o kontrolowanym rozmiarze lateralnie wydzielonych domen, osadzonych na stałym podłożu*, authors: **Emilia Krok**, Agnieszka Batura, Hanna Orlikowska, Madhurima Chattopadhyay, Lukasz Piatkowski, patent registered by Poznan University of Technology.
2. Patent application, PL437600, Poland, date of registration: 16.04.2021, patent title: *Method of measuring the local hydration of lipid layers in biomimetic and biological systems/Sposób pomiaru lokalnego stopnia nawodnienia warstw lipidowych układów biomimetycznych i biologicznych*, authors: Madhurima Chattopadhyay, **Emilia Krok**, Hanna Orlikowska, Łukasz Piątkowski, patent registered by Poznan University of Technology.
3. Patent application, PL437601, Poland, date of registration: 16.04.2021, patent title: *Method of measuring the local hydration of lipid layers in biomimetic and biological systems/Sposób pomiaru lokalnego stopnia nawodnienia warstw lipidowych układów biomimetycznych i biologicznych*, authors: Madhurima Chattopadhyay, **Emilia Krok**, Hanna Orlikowska, Łukasz Piątkowski, patent registered by Poznan University of Technology.

9.7 Scientific grants

Principal investigator in grants:

1. *Dry and Alive – the impact of hydration on the properties of bacterial cell membranes and its role in prokaryotic anhydrobiosis.*

Preludium-22, National Science Center, grant number: 2023/49/N/ST4/02140, years: 2024-2027.

2. *Reverse microengineering - developing functional biomimetic lipid membranes that mimic the biological membranes characteristic of gram-negative and positive bacterial cells./Mikroinżynieria wsteczna - opracowanie funkcjonalnych, biomimetycznych błon lipidowych naśladujących błony biologiczne charakterystyczne dla komórek bakterii gram-ujemnych oraz dodatnich.*

SBAD-MK, Project within the framework of funds allocated from the subvention of the Faculty of Materials Engineering and Technical Physics for the conduct of scientific research or development works and related tasks for the development of young scientists funded in the internal competition procedure in 2023, grant number: 0512/SBAD/6214, year: 2023.

3. *Biomimetic cell membranes under extreme dehydration - analysis of nanoscopic structural changes./Biomimetyczne błony komórkowe w warunkach ekstremalnego odwodnienia - analiza nanoskopowych zmian strukturalnych.*

SBAD-MK, Project within the framework of funds allocated from the subvention of the Faculty of Materials Engineering and Technical Physics for the conduct of scientific research or development works and related tasks for the development of young scientists funded in the internal competition procedure in 2022, grant number: 0512/SBAD/6212, year: 2022.

Co-investigator in grants:

1. *Can female sex hormones heal? Determining the interactions of selected steroid hormones with biomimetic cell membranes./Czy żeńskie hormony płciowe mogą leczyć? Określenie oddziaływań wybranych hormonów steroidowych z biomimetycznymi błonami komórkowymi.*

SBAD-MK, Project within the framework of funds allocated from the subvention of the Faculty of Materials Engineering and Technical Physics for the conduct of scientific research or development works and related tasks for the development of young scientists funded in the internal competition procedure in 2024, principal investigator: M. Eng. Anna Łągowska, year: 2024.

2. *Functionalised polymeric materials for biomedical engineering applications - fabrication and characterisation./Funkcjonalizowane materiały polimerowe do zastosowań w inżynierii biomedycznej - wytwarzanie i charakterystyka.*

Interdisciplinary Rector's Grant, grant number: 0912/SIGR/8058, principal investigator: Prof. Dr habil. Eng. Krystyna Prochaska, years: 2022-2024.

3. *How do transmembrane proteins deal with the hydrophobic mismatch?*

EMBO Young Investigator Small Grant, European Molecular Biology Organization, principal investigator: Dr. habil. Eng. Łukasz Piątkowski, Prof. PUT, years: 2019-2022.

4. *Biological water: the role of hydration in cell membrane organization.*
EMBO Installation Grant, European Molecular Biology Organization, grant number: IG 4147, principal investigator: Dr. habil. Eng. Łukasz Piątkowski, Prof. PUT, years: 2022-2024.
5. *Investigating the influence of water molecules on the formation of lipid bilayers on solid substrates and quantifying their hydration state using quartz crystal microbalance.*/Badanie wpływu cząsteczek wody na formowanie dwuwarstw lipidowych na podłożu stałym oraz określenie ilościowe ich nawodnienia przy pomocy mikrowagi kwarcowej.
SBAD-MK, Project within the framework of funds allocated from the subvention of the Faculty of Materials Engineering and Technical Physics for the conduct of scientific research or development works and related tasks for the development of young scientists funded in the internal competition procedure in 2020, grant number: 0512/SBAD/6209, principal investigator: M. Eng. Hanna-Orlikowska Rzeźnik, year: 2020.
6. *HYDRA – Elucidating the role of hydration heterogeneity and hydrophobic mismatch in biomimetic cell membranes organization.*
First Team, Foundation of Polish Science, grant number: POIR.04.04.00-00-5D32/-18-00, principal investigator: Dr. habil. Eng. Łukasz Piątkowski, Prof. PUT, years: 2019-2022.

9.8 Scholarships/Awards

1. **EBSA Student Bursary 2023**, a bursary for the participation in the 14th European Biophysical Societies' Association (EBSA) Congress 2023 in Stockholm, Sweden, awarded: 25.04.2023.
2. **Rector's award for outstanding scientific achievements in the year 2021**, group award for the best scientific team at Poznan University of Technology, awarded: 05.10.2022.
3. **Project „Towards Internationalization of Poznan University of Technology Doctoral School” (2022-2024)**, under the STER programme co-financed by Polish National Agency for Academic Exchange (NAWA), scholarship duration: 04.07.2022-02.10.2022.
4. **Becas Santander for MIT Leading Digital Transformation**, scholarship financing the course *Leading Digital Transformation* at Massachusetts Institute of Technology (MIT), awarded: 04.2020.
5. **Deutscher Akademischer Austauschdienst**, Study Scholarships for Graduates of All Disciplines, 2017/18 (number 57314016), scholarship for whole Master Studies at Technical University of Dresden, scholarship duration: 01.10.2017-30.09.2019.
6. **Erasmus+** scholarship for Erasmus exchange at Technical University Braunschweig, scholarship duration 01.10.2015 – 20.09.2016.

7. **Rector's Scholarship for top 5% of students at Poznan University of Technology**, the scholarship awarded during the entire Bachelor Studies (2013-2017).

9.9 Courses

1. **Summer School in Protocell Models: Coacervates and Vesicles**, organized by MPI-CBG and ProtoMet-ETN, Dresden, Germany, 5-8.07.2021.
2. **IOP Peer Review Excellence Certification** course for reviewers, organized by IOP Training and Certification, 21.06.2021.
3. **ACS Reviewer Lab**, course for reviewers, organized by American Chemical Society, 15.06.2021.
4. **Knowledge about the functioning of a brain in the didactic work**, course for academic teachers, organized by Poznan University of Technology, 17-20.11.2020.
5. **Good practices in the writing of scientific articles** organized by National Institute of Geriatrics, Rheumatology and Rehabilitation, TERMEDIA Publishing House, Warsaw, 18-19.11.2020.
6. **Leading Digital Transformation** from Massachusetts Institute of Technology (MIT), Cambridge, Massachusetts, US, 05.05.2020 - 09.06.2020.

9.10 Reviewing activity

Reviewer in the following journals:

- eLife, IF 7.7,
- Life Sciences (Elsevier), IF 6.1,
- Progress in Biomedical Engineering, (IOP Publishing), IF 4.7,
- Nanotechnology (IOP Publishing), IF 3.5,
- World Journal of Surgical Oncology (Springer Nature), IF 3.2,
- Journal of Micromechanics and Microengineering (IOP Publishing), IF 2.3,
- Journal of Visualized Experiments (JoVE), IF 1.2.

Awards

Awarded two times for the contributions to the reviewer's community:

1. IOP Trusted Reviewer Award - awarded to 15% of the best reviewers in physical sciences (2021).
2. IOP Outstanding Reviewer Awards 2021 – awarded to the best reviewers of the year based on the quality, quantity, and timeliness of their reviews (2021).

Bibliography

1. Singer, S. J. & Nicolson, G. L. The Fluid Mosaic Model of the Structure of Cell Membranes. *Science* **175**, 720–731 (1972).
2. Nicolson, G. L. Transmembrane control of the receptors on normal and tumor cells. I. Cytoplasmic influence over surface components. *Biochimica et Biophysica Acta* **457**, 57–108 (1976).
3. Sezgin, E., Levental, I., Mayor, S. & Eggeling, C. Transmembrane control of the receptors on normal and tumor cells. I. Cytoplasmic influence over surface components. *Nature Reviews Molecular Cell Biology* **18**, 361–374 (2017).
4. Simons, K. & Vaz, W. L. Model Systems, Lipid Rafts, and Cell Membranes. *Annual Review of Biophysics and Biomolecular Structure* **33**, 269–295 (2004).
5. Kiessling, V., Wan, C. & Tamm, L. K. Domain coupling in asymmetric lipid bilayers. *Biochimica et Biophysica Acta (BBA) - Biomembranes* **1788**, 64–71 (2009).
6. Raghupathy, R. *et al.* Transbilayer Lipid Interactions Mediate Nanoclustering of Lipid-Anchored Proteins. *Cell* **161**, 581–594 (2015).
7. Varma, R. & Mayor, S. GPI-anchored proteins are organized in submicron domains at the cell surface. *Nature* **394**, 798–801 (1998).
8. De Almeida, R. F. M. & Joly, E. Crystallization around solid-like nanosized docks can explain the specificity, diversity, and stability of membrane microdomains. *Frontiers in Plant Science* **5**, 72 (2014).
9. Matsumoto, K., Kusaka, J., Nishibori, A. & Hara, H. Lipid domains in bacterial membranes. *Molecular microbiology* **61**, 1110–1117 (2006).
10. Gohrbandt, M. *et al.* Low membrane fluidity triggers lipid phase separation and protein segregation in living bacteria. *The EMBO Journal* **41**, e109800 (2022).
11. Mileykovskaya, E. & Dowhan, W. Visualization of phospholipid domains in *Escherichia coli* by using the cardiolipin-specific fluorescent dye 10-N-nonyl acridine orange. *Journal of Bacteriology* **182**, 1172–1175 (2000).
12. Bagnat, M., Keränen, S., Shevchenko, A., Shevchenko, A. & Simons, K. Lipid rafts function in biosynthetic delivery of proteins to the cell surface in yeast. *Proceedings of the National Academy of Sciences* **97**, 3254–3259 (2000).
13. Mollinedo, F. Lipid raft involvement in yeast cell growth and death. *Frontiers in oncology* **2**, 140 (2012).

14. Mongrand, S. *et al.* Lipid Rafts in Higher Plant Cells: purification and characterization of Triton X-100-insoluble microdomains from tobacco plasma membrane. *Journal of Biological Chemistry* **279**, 36277–36286 (2004).
15. Borner, G. H. *et al.* Analysis of Detergent-Resistant Membranes in Arabidopsis. Evidence for Plasma Membrane Lipid Rafts. *Plant Physiology* **137**, 104–116 (2005).
16. Mamode Cassim, A. *et al.* Sphingolipids in plants: a guidebook on their function in membrane architecture, cellular processes, and environmental or developmental responses. *FEBS Letters* **594**, 3719–3738 (2020).
17. Suzuki, K. G. N. in *Lipid Signaling Protocols* (ed Waugh, M. G.) 229–238 (Springer New York, 2016).
18. Eggeling, C. *et al.* Direct observation of the nanoscale dynamics of membrane lipids in a living cell. *Nature* **457**, 1159–1162 (2009).
19. Wawrezynieck, L., Rigneault, H., Marguet, D. & Lenne, P.-F. Fluorescence Correlation Spectroscopy Diffusion Laws to Probe the Submicron Cell Membrane Organization. *Biophysical Journal* **89**, 4029–4042 (2005).
20. Laganowsky, A. *et al.* Membrane proteins bind lipids selectively to modulate their structure and function. *Nature* **510**, 172–175 (2014).
21. Yang, S.-T., Kiessling, V., Simmons, J. A., White, J. M. & Tamm, L. K. HIV gp41-mediated membrane fusion occurs at edges of cholesterol-rich lipid domains. *Nature Chemical Biology* **11**, 424–431 (2015).
22. Fujinaga, Y. *et al.* Gangliosides That Associate with Lipid Rafts Mediate Transport of Cholera and Related Toxins from the Plasma Membrane to Endoplasmic Reticulum. *Molecular Biology of the Cell* **14**, 4783–4793 (2003).
23. Li, B., Qin, Y., Yu, X., Xu, X. & Yu, W. Lipid raft involvement in signal transduction in cancer cell survival, cell death and metastasis. *Cell Proliferation* **55**, e13167 (2022).
24. Staubach, S., Razawi, H. & Hanisch, F.-G. Proteomics of MUC1-containing lipid rafts from plasma membranes and exosomes of human breast carcinoma cells MCF-7. *Proteomics* **9**, 2820–2835 (2009).
25. Hari, R. *et al.* Localization of uPAR and MMP-9 in lipid rafts is critical for migration, invasion and angiogenesis in human breast cancer cells. *BMC Cancer* **10**, 647 (2010).
26. Larsen, J. B. *et al.* Membrane curvature enables N-Ras lipid anchor sorting to liquid-ordered membrane phases. *Nature Chemical Biology* **11**, 192–194 (2015).
27. Shuo, Z. *et al.* The lipid rafts in cancer stem cell: a target to eradicate cancer. *Nature Chemical Biology* **11**, 192–194 (2015).
28. Cuesta-Marbán, Á. *et al.* Drug Uptake, Lipid Rafts, and Vesicle Trafficking Modulate Resistance to an Anticancer Lysophosphatidylcholine Analogue in Yeast. *Journal of Biological Chemistry* **288**, 8405–8418 (2013).
29. Pavel, S., Bojan, D. & Klaus, L. Macrophage differentiation to foam cells. *Current Pharmaceutical Design* **11**, 3061–3072 (2005).

30. Rios, F. J. O. *et al.* Uptake of oxLDL and IL-10 Production by Macrophages Requires PAFR and CD36 Recruitment into the Same Lipid Rafts. *PLOS ONE* **8**, e76893 (2013).
31. Barenholz, Y. Sphingomyelin and cholesterol: from membrane biophysics and rafts to potential medical applications. *Sub-cellular Biochemistry* **37**, 167–215 (2004).
32. Bodil, R. & Peter J., S. Interaction of cholesterol with sphingomyelins and acyl-chain-matched phosphatidylcholines: a comparative study of the effect of the chain length. *Biophysical Journal* **76**, 908–915 (1999).
33. Tulodziecka, K. *et al.* Remodeling of the postsynaptic plasma membrane during neural development. *Molecular Biology of the Cell* **27**, 3480–3489 (2016).
34. García-Sáez, A. J., Chiantia, S. & Schwille, P. Effect of line tension on the lateral organization of lipid membranes. *The Journal of biological chemistry* **282**, 33537–33544 (2007).
35. Honigsmann, A. *et al.* A lipid bound actin meshwork organizes liquid phase separation in model membranes. *eLife* **3**, e01671 (2014).
36. Machta, B. B., Papanikolaou, S., Sethna, J. P. & Veatch, S. L. Minimal model of plasma membrane heterogeneity requires coupling cortical actin to criticality. *Biophysical journal* **100**, 1668–1677 (2011).
37. Fritzsche, M. *et al.* Self-organizing actin patterns shape membrane architecture but not cell mechanics. *Nature Communication* **14347**, 1668–1677 (2017).
38. Sandhu, J. *et al.* Aster Proteins Facilitate Nonvesicular Plasma Membrane to ER Cholesterol Transport in Mammalian Cells. *Cell* **175**, 514–529 (2018).
39. Mollinedo, F. & Gajate, C. Lipid rafts as signaling hubs in cancer cell survival/death and invasion: implications in tumor progression and therapy: Thematic Review Series: Biology of Lipid Rafts. *Journal of Lipid Research* **61**, 611–635 (2020).
40. Zhdanov, V. P. & Höök, F. Kinetics of enzymatic reactions in lipid membranes containing domains. *Physical Biology* **12**, 026003 (2015).
41. Parmryd, I., Day, C. A. & Kenworthy, A. K. Functions of cholera toxin B-subunit as a raft cross-linker. *Essays in Biochemistry* **57**, 135–145 (2015).
42. Staubach, S. & Hanisch, F.-G. Lipid rafts: signaling and sorting platforms of cells and their roles in cancer. *Expert Review of Proteomics* **8**, 263–277 (2011).
43. Hanzal-Bayer, M. F. & Hancock, J. F. Lipid rafts and membrane traffic. *FEBS letters* **581**, 2098–2104 (2007).
44. Gómez-Llobregat, J., Buceta, J. & Reigada, R. Interplay of cytoskeletal activity and lipid phase stability in dynamic protein recruitment and clustering. *Scientific Reports* **3**, 2608 (2013).
45. Bukrinsky, M. I., Mukhamedova, N. & Sviridov, D. Lipid rafts and pathogens: the art of deception and exploitation: Thematic Review Series: Biology of Lipid Rafts. *Journal of Lipid Research* **61**, 601–610 (2020).

46. Rosetti, C. M., Mangiarotti, A. & Wilke, N. Sizes of lipid domains: What do we know from artificial lipid membranes? What are the possible shared features with membrane rafts in cells? *Biochimica et Biophysica Acta (BBA) - Biomembranes* **1859**, 789–802 (2017).
47. Yeagle, P. L. in *The Membranes of Cells (Third Edition)* (ed Yeagle, P. L.) 1–25 (Academic Press, 2016).
48. Bondos, S. E., Dunker, A. K. & Uversky, V. N. Intrinsically disordered proteins play diverse roles in cell signaling. *Cell Communication and Signaling* **20**, 20 (2022).
49. Alberts, B. *et al.* in *Molecular Biology of the Cell* (ed Welch, M.) (Garland Science, 2008).
50. Weiss, D. R., Raschke, T. M. & Levitt, M. How hydrophobic buckminsterfullerene affects surrounding water structure. *The Journal of Physical Chemistry B* **112**, 2981–2990 (2008).
51. Meyer, E. E., Rosenberg, K. J. & Israelachvili, J. Recent progress in understanding hydrophobic interactions. *Proceedings of the National Academy of Sciences* **103**, 15739–15746 (2006).
52. Blazek, A. D., Paleo, B. J. & Weisleder, N. Plasma Membrane Repair: A Central Process for Maintaining Cellular Homeostasis. *Physiology* **30**, 438–448 (2015).
53. Contreras, F.-X., Sánchez-Magraner, L., Alonso, A. & Goñi, F. M. Transbilayer (flip-flop) lipid motion and lipid scrambling in membranes. *FEBS Letters* **584**, 1779–1786 (2010).
54. Siontorou, C. G., Nikoleli, G.-P., Nikolelis, D. P. & Karapetis, S. K. Artificial Lipid Membranes: Past, Present, and Future. *Membranes* **7**, 38 (2017).
55. Los, D. A. & Murata, N. Membrane fluidity and its roles in the perception of environmental signals. *Biochimica et Biophysica Acta (BBA) - Biomembranes* **1666**, 142–157 (2004).
56. Chattopadhyay, M. *et al.* Hydration Layer of Only a Few Molecules Controls Lipid Mobility in Biomimetic Membranes. *Journal of the American Chemical Society* **143**, 14551–14562 (2021).
57. Sameni, S., Malacrida, L. & Tan, Z. Alteration in Fluidity of Cell Plasma Membrane in Huntington Disease Revealed by Spectral Phasor Analysis. *Scientific Reports* **8**, 734 (2018).
58. Aozaki, S. Decreased membrane fluidity in erythrocytes from patients with Crohn's disease. *Gastroenterologia Japonica* **24**, 246–254 (1989).
59. Tomohiro, K. *et al.* Decreased membrane fluidity and unsaturated fatty acids in Niemann–Pick disease type C fibroblasts. *Biochimica et Biophysica Acta (BBA) - Molecular Basis of Disease* **1406**, 327–335 (1998).
60. Fabiani, C. & Antollini, S. S. Alzheimer's Disease as a Membrane Disorder: Spatial Cross-Talk Among Beta-Amyloid Peptides, Nicotinic Acetylcholine Receptors and Lipid Rafts. *Frontiers in Cellular Neuroscience* **13**, 309 (2019).
61. Van Meer, G., Voelker, D. & Feigenson, G. Membrane lipids: where they are and how they behave. *Nature Reviews Molecular Cell Biology* **9**, 112–124 (2008).

62. Harayama, T. & Riezman, H. Understanding the diversity of membrane lipid composition. *Nature Reviews Molecular Cell Biology* **19**, 281–296 (2018).
63. Yamashita, A. *et al.* Acyltransferases and transacylases that determine the fatty acid composition of glycerolipids and the metabolism of bioactive lipid mediators in mammalian cells and model organisms. *Progress in lipid research* **53**, 18–81 (2014).
64. Pulkoski-Gross, M. J., Donaldson, J. C. & Obeid, L. M. Sphingosine-1-phosphate metabolism: A structural perspective. *Critical Reviews in Biochemistry and Molecular Biology* **50**, 298–313 (2015).
65. Silva, Y. P., Bernardi, A. & Frozza, R. L. The Role of Short-Chain Fatty Acids From Gut Microbiota in Gut-Brain Communication. *Frontiers in Endocrinology* **11**, 25 (2020).
66. Shepelenko, M. *et al.* Polymorphism, Structure, and Nucleation of Cholesterol·H₂O at Aqueous Interfaces and in Pathological Media: Revisited from a Computational Perspective. *Journal of the American Chemical Society* **144**, 5304–5314 (2022).
67. Dufourc, E. J. Sterols and membrane dynamics. *Journal of Chemical Biology* **1**, 63–77 (2008).
68. Carabeo, R. A., Mead, D. J. & Hackstadt, T. Golgi-dependent transport of cholesterol to the Chlamydia trachomatis inclusion. *Proceedings of the National Academy of Sciences* **100**, 6771–6776 (2003).
69. Smith, P. F. Biosynthesis of Cholesteryl Glucoside by Mycoplasma gallinarum. *Journal of Bacteriology* **108**, 986–991 (1971).
70. Sáenz, J. P. *et al.* Hopanoids as functional analogues of cholesterol in bacterial membranes. *Proceedings of the National Academy of Sciences* **112**, 11971–11976 (2015).
71. Belin, B. J. *et al.* Hopanoid lipids: from membranes to plant-bacteria interactions. *Nature reviews. Microbiology* **16**, 304–315 (2018).
72. Dufourc, E. J. Sterols and membrane dynamics. *Journal of chemical biology* **1**, 63–77 (2008).
73. Vriet, C., Russinova, E. & Reuzeau, C. From squalene to brassinolide: the steroid metabolic and signaling pathways across the plant kingdom. *Infection Control & Hospital Epidemiology* **6**, 1738–1757 (2013).
74. Haque, M. A. & Russell, N. J. Strains of Bacillus cereus vary in the phenotypic adaptation of their membrane lipid composition in response to low water activity, reduced temperature and growth in rice starch. *Microbiology* **150**, 1397–1404 (2004).
75. Op den Kamp J. A. F. and Redai, I. & van Deenen, L. L. M. Phospholipid Composition of Bacillus subtilis. *Journal of Bacteriology* **99**, 298–303 (1969).
76. Crandall, A. D. & Montville, T. J. Nisin Resistance in Listeria monocytogenes ATCC 700302 is a complex phenotype. *Applied and Environmental Microbiology* **64**, 231–237 (1998).

BIBLIOGRAPHY

77. Hayami, M., Okabe, A., Kariyama, R., Abe, M. & Kanemasa, Y. Lipid composition of *Staphylococcus aureus* and its derived L-forms. *Microbiology and immunology* **23**, 435–442 (1979).
78. Trombe, M.-C., Lanéelle, M.-A. & Lanéelle, G. Lipid composition of aminopterin-resistant and sensitive strains of *Streptococcus pneumoniae*. Effect of aminopterin inhibition. *Biochimica et Biophysica Acta (BBA)-Lipids and Lipid Metabolism* **574**, 290–300 (1979).
79. Rowlett Veronica W .and Mallampalli, V. K. *et al.* Impact of membrane phospholipid alterations in *Escherichia coli* on cellular function and bacterial stress adaptation. *Journal of bacteriology* **199**, 10–1128 (2017).
80. Goldfine, H. Bacterial membranes and lipid packing theory. *Journal of lipid research* **25**, 1501–1507 (1984).
81. Gmeinfr, J. & Martin, H. H. Phospholipid and Lipopolysaccharide in *Proteus mirabilis* and Its Stable Protoplast l-Form: Difference in Content and Fatty Acid Composition. *European Journal of Biochemistry* **67**, 487–494 (1976).
82. Conrad, R. S. & Gilleland Jr, H. Lipid alterations in cell envelopes of polymyxin-resistant *Pseudomonas aeruginosa* isolates. *Journal of Bacteriology* **148**, 487–497 (1981).
83. Bartholomew, J. & Mittwer, T. The Gram stain. *Bacteriological reviews* **16**, 1–29 (1952).
84. Miller, S. I. Antibiotic Resistance and Regulation of the Gram-Negative Bacterial Outer Membrane Barrier by Host Innate Immune Molecules. *mBio* **7**, e01541–16 (2016).
85. Beauchamp, S. & Lacroix, M. Resistance of the genome of *Escherichia coli* and *Listeria monocytogenes* to irradiation evaluated by the induction of cyclobutane pyrimidine dimers and 6-4 photoproducts using gamma and UV-C radiations. *Radiation Physics and Chemistry* **81**, 1193–1197 (2012).
86. Harikrishnan, H., Ismail, A. & Banga Singh, K. Temperature-regulated expression of outer membrane proteins in *Shigella flexneri*. *Gut Pathogens* **5**, 38 (2013).
87. García, A. H. Anhydrobiosis in bacteria: from physiology to applications. *Journal of biosciences* **36**, 939–950 (2011).
88. Lopes, S. C., Neves, C. S., Eaton, P. & Gameiro, P. Improved model systems for bacterial membranes from differing species: The importance of varying composition in PE/PG/cardiolipin ternary mixtures. *Molecular Membrane Biology* **29**, 207–217 (2012).
89. Silhavy, T. J., Kahne, D. & Walker, S. The bacterial cell envelope. *Cold Spring Harbor perspectives in biology* **2**, a000414 (2010).
90. Kakimoto, Y. & Tero, R. Supported Lipid Bilayers of *Escherichia coli* Extracted Lipids and Their Calcium Dependence. *Frontiers in Materials* **5**, 48 (2018).
91. Hayami, M., Okabe, A., Kariyama, R., Abe, M. & Kanemasa, Y. Lipid composition of *Staphylococcus aureus* and its derived L-forms. *Microbiology and immunology* **23**, 435–442 (1979).

-
92. Quinn, P. J. & Chapman, D. The dynamics of membrane structure. *Critical Reviews in Biochemistry* **8**, 1–117 (1980).
 93. van de Vossenberg, J. L., Driessen, A. J., da Costa, M. S. & Konings, W. N. Homeostasis of the membrane proton permeability in *Bacillus subtilis* grown at different temperatures. *Biochimica et Biophysica Acta - Biomembranes* **1419**, 97–104 (1999).
 94. Ingram, L. O. Changes in lipid composition of *Escherichia coli* resulting from growth with organic solvents and with food additives. *Applied and Environmental Microbiology* **33**, 1233–1236 (1977).
 95. Heimburg, T. in *Handbook of Molecular Biophysics: Methods and Applications* (ed Bohr, H. G.) 593–616 (Wiley, 2009).
 96. Bangham, A. & Horne, R. Negative staining of phospholipids and their structural modification by surface-active agents as observed in the electron microscope. *Journal of Molecular Biology* **8**, 660–668 (1964).
 97. Reeves, J. P. & Dowben, R. M. Formation and properties of thin-walled phospholipid vesicles. *Journal of Cellular Physiology* **73**, 49–60 (1969).
 98. Dimova, R. *The Giant Vesicle Book* (eds Dimova, R. & Marques, C.) 1–676 (CRC Press, Taylor & Francis Group, 2019).
 99. Dimova, R. *et al.* A practical guide to giant vesicles. Probing the membrane nanoregime via optical microscopy. *Journal of Physics: Condensed Matter* **18**, S1151 (2006).
 100. Bhatia, T. *et al.* Preparing giant unilamellar vesicles (GUVs) of complex lipid mixtures on demand: Mixing small unilamellar vesicles of compositionally heterogeneous mixtures. *Biochimica et Biophysica Acta (BBA) - Biomembranes* **1848**, 3175–3180 (2015).
 101. Przybylo, M. *et al.* Lipid diffusion in Giant Unilamellar Vesicles is more than 2 times faster than in Supported Phospholipid Bilayers under identical conditions. *Langmuir* **22**, 9096–9099 (2006).
 102. Martos, A., Jiménez, M., Rivas, G. & Schwille, P. Towards a bottom-up reconstitution of bacterial cell division. *Trends in Cell Biology* **22**, 634–643 (2012).
 103. Fanalista, F. *et al.* Shape and Size Control of Artificial Cells for Bottom-Up Biology. *ACS Nano* **13**, 5439–5450 (2019).
 104. Haluska, C. K. *et al.* Time scales of membrane fusion revealed by direct imaging of vesicle fusion with high temporal resolution. *Proceedings of the National Academy of Sciences* **103**, 15841–15846 (2006).
 105. Su, L., Peichi, C. H. & Noah, M. Imaging molecular transport across lipid bilayers. *Biophysical Journal* **101**, 700–708 (2011).
 106. Tsumoto, K., Matsuo, H., Tomita, M. & Yoshimura, T. Efficient formation of giant liposomes through the gentle hydration of phosphatidylcholine films doped with sugar. *Colloids and surfaces. B, Biointerfaces* **61**, 98–105 (2009).
 107. Akashi, K.-i., Miyata, H., Itoh, H. & Kinosita, K. Formation of Giant Liposomes Promoted by Divalent Cations: Critical Role of Electrostatic Repulsion. *Biophysical Journal* **74**, 2973–2982 (1998).
-

108. Rodriguez, N., Pincet, F. & Cribier, S. Giant vesicles formed by gentle hydration and electroformation: A comparison by fluorescence microscopy. *Colloids and Surfaces B: Biointerfaces* **42**, 125–130 (2005).
109. Garten, M., Aimon, S., Bassereau, P. & Toombes, G. E. S. Reconstitution of a Transmembrane Protein, the Voltage-gated Ion Channel, KvAP, into Giant Unilamellar Vesicles for Microscopy and Patch Clamp Studies. *Journal of Visualized Experiments* **95**, e52281 (2015).
110. Horger, K. S., Estes, D. J., Capone, R. & Mayer, M. Films of Agarose Enable Rapid Formation of Giant Liposomes in Solutions of Physiologic Ionic Strength. *Journal of the American Chemical Society* **131**, 1810–1819 (2009).
111. Angelova, M. I. & Dimitrov, D. S. Liposome electroformation. *Faraday Discuss. Chem. Soc.* **81**, 303–311 (1986).
112. Zhihua, L., Miao, C., Xin, Y. & Wenpeng, Z. Membrane-tension-dominated growth mechanism and size modulation of giant unilamellar vesicles in electroformation. *Journal of the Mechanics and Physics of Solids* **170**, 105120 (2023).
113. Kumaran, V. Instabilities due to Charge-Density-Curvature Coupling in Charged Membranes. *Phys. Rev. Lett.* **85**, 4996–4999 (2000).
114. Marcos, Yang, C., Ooi, K., Wong, T. & Masliyah, J. Frequency-dependent laminar electroosmotic flow in a closed-end rectangular microchannel. *Journal of Colloid and Interface Science* **275**, 679–698 (2004).
115. Drabik, D., Doskocz, J. & Przybyło, M. Effects of electroformation protocol parameters on quality of homogeneous GUV populations. *Chemistry and Physics of Lipids* **212**, 88–95 (2018).
116. Ghellab, S. E., Mu, W., Li, Q. & Han, X. Prediction of the size of electroformed giant unilamellar vesicle using response surface methodology. *Biophysical Chemistry* **253**, 106217 (2019).
117. Kisak, E. T., Coldren, B., Evans, C. A., Boyer, C. & Zasadzinski, J. A. The Vesosome-A Multicompartment Drug Delivery Vehicle. *Current Medicinal Chemistry* **11**, 1241–1253 (2004).
118. Giuliano, C. B., Cvjetan, N., Ayache, J. & Walde, P. Multivesicular Vesicles: Preparation and Applications. *ChemSystemsChem* **3**, e2000049 (2021).
119. Akbarzadeh, A. *et al.* Liposome: classification, preparation, and applications. *Nanoscale research letters* **8**, 102 (2013).
120. Silva, R., Ferreira, H., Little, C. & Cavaco-Paulo, A. Effect of ultrasound parameters for unilamellar liposome preparation. *Ultrasonics Sonochemistry* **17**, 628–632 (2010).
121. Maulucci, G. *et al.* Particle Size Distribution in DMPC Vesicles Solutions Undergoing Different Sonication Times. *Biophysical Journal* **88**, 3545–3550 (2005).
122. Zhu, T. F., Budin, I. & Szostak, J. W. in *Laboratory Methods in Enzymology: Cell, Lipid and Carbohydrate* (ed Lorsch, J.) 275–282 (Academic Press, 2013).

-
123. Scott, H. L. *et al.* On the Mechanism of Bilayer Separation by Extrusion, or Why Your LUVs Are Not Really Unilamellar. *Biophysical Journal* **117**, 1381–1386 (2019).
 124. Brian, A. A. & McConnell, H. M. Allogeneic stimulation of cytotoxic T cells by supported planar membranes. *Proceedings of the National Academy of Sciences* **81**, 6159–63 (1984).
 125. Richter, R. P., Bérat, R. & Brisson, A. R. Formation of Solid-Supported Lipid Bilayers: An Integrated View. *Langmuir* **22**, 3497–3505 (2006).
 126. Richter, R., Mukhopadhyay, A. & Brisson, A. Pathways of Lipid Vesicle Deposition on Solid Surfaces: A Combined QCM-D and AFM Study. *Biophysical Journal* **85**, 3035–3047 (2003).
 127. Seantier, B. & Kasemo, B. Influence of Mono- And Divalent Ions on the Formation of Supported Phospholipid Bilayers via Vesicle Adsorption. *Langmuir* **25**, 5767–5772 (2009).
 128. Chiantia, S., Kahya, N., Ries, J. & Schwille, P. Effects of ceramide on liquid-ordered domains investigated by simultaneous AFM and FCS. *Biophysical journal* **90**, 4500–4508 (2006).
 129. Thompson, N. L., Pearce, K. H. & Hsieh, H. V. Total internal reflection fluorescence microscopy: application to substrate-supported planar membranes. *European biophysics journal: EBJ* **22**, 367–378 (1993).
 130. Crane, J. M. & Tamm, L. K. in *Methods in Membrane Lipids* (ed Dopico, A. M.) 481–488 (Humana Press, 2007).
 131. Jackman, J. A. & Cho, N.-J. Supported Lipid Bilayer Formation: Beyond Vesicle Fusion. *Langmuir* **36**, 1387–1400 (2020).
 132. Bailey, C. M., Tripathi, A. & Shukla, A. Effects of flow and bulk vesicle concentration on supported lipid bilayer formation. *Langmuir* **33**, 11986–11997 (2017).
 133. Hong, S. *et al.* Interaction of Polycationic Polymers with Supported Lipid Bilayers and Cells: Nanoscale Hole Formation and Enhanced Membrane Permeability. *Bioconjugate Chemistry* **17**, 728–734 (2006).
 134. Ye, Q., Konradi, R., Textor, M. & Reimhult, E. Liposomes Tethered to Omega-Functional PEG Brushes and Induced Formation of PEG Brush Supported Planar Lipid Bilayers. *Langmuir* **25**, 13534–13539 (2009).
 135. Blakeston, A. C. *et al.* New Poly(amino acid methacrylate) Brush Supports the Formation of Well-Defined Lipid Membranes. *Langmuir* **31**, 3668–3677 (2015).
 136. Kibrom, A. *et al.* Hydrogel-supported protein-tethered bilayer lipid membranes: a new approach toward polymer-supported lipid membranes. *Soft Matter* **7**, 237–246 (2011).
 137. Diaz, A. J., Albertorio, F., Daniel, S. & Cremer, P. S. Double cushions preserve transmembrane protein mobility in supported bilayer systems. *Langmuir* **24**, 6820–6826 (2008).
 138. Ul-Hamid, A. in *A Beginners' Guide to Scanning Electron Microscopy* (ed Ul-Hamid, A.) 1–14 (Springer International Publishing, 2018).
-

BIBLIOGRAPHY

139. Kato, K. in *Microbial Diversity in Time and Space* (eds Colwell, R. R., Simidu, U. & Ohwada, K.) 141–147 (Springer US, 1996).
140. Louten, J. in *Essential Human Virology* (ed Louten, J.) 19–29 (Academic Press, 2016).
141. Valeur, B. & Berberan-Santos, M. N. A Brief History of Fluorescence and Phosphorescence before the Emergence of Quantum Theory. *Journal of Chemical Education* **88**, 731–738 (2011).
142. Partington, J. Lignum nephriticum. *Annals of Science* **11**, 1–26 (1955).
143. Muyskens, M. & Vitz, E. The Fluorescence of Lignum nephriticum: A Flash Back to the Past and a Simple Demonstration of Natural Substance Fluorescence. *Journal of Chemical Education* **83**, 765 (2006).
144. Stokes, G. G. On the change of refrangibility of light. *Philosophical Transactions of the Royal Society of London* **142**, 463–562 (1852).
145. Jablonski, A. Efficiency of Anti-Stokes Fluorescence in Dyes. *Nature* **131**, 839–840 (1933).
146. Sugimoto, H., Hasebe, H., Furuyama, T. & Fujii, M. Direct Excitation of Triplet State of Molecule by Enhanced Magnetic Field of Dielectric Metasurfaces. *Small* **17**, 2104458 (2021).
147. Schulman, S. G., Di, Q. Q. & Juchum, J. in *Encyclopedia of Spectroscopy and Spectrometry* (ed Lindon, J. C.) 1718–1725 (Elsevier, 1999).
148. Lewis, G. N. & Kasha, M. Phosphorescence and the Triplet State. *Journal of the American Chemical Society* **62**, 2100–2116 (1944).
149. Minsky, M. Memoir on inventing the confocal scanning microscope. *Scanning* **10**, 128–138 (1988).
150. Alt, P. *RESOLFT nanoscopy with water-soluble synthetic fluorophores* PhD thesis (2018), 1–110.
151. Rayleigh, F. XXXI. Investigations in optics, with special reference to the spectroscope. *The London, Edinburgh, and Dublin Philosophical Magazine and Journal of Science* **8**, 261–274 (1879).
152. Holme, I. Sir William Henry Perkin: a review of his life, work and legacy. *Coloration Technology* **122**, 235–251 (2006).
153. Shimomura, O., Johnson, F. H. & Saiga, Y. Extraction, Purification and Properties of Aequorin, a Bioluminescent Protein from the Luminous Hydromedusan, Aequorea. *Journal of Cellular and Comparative Physiology* **59**, 223–239 (1962).
154. Andrey, S. K. & Kreder, R. Fluorescent Probes for Lipid Rafts: From Model Membranes to Living Cells. *Chemistry & Biology* **21**, 97–113 (2014).
155. Baumgart, T., Hess, S. & Webb, W. Imaging coexisting fluid domains in biomembrane models coupling curvature and line tension. *Nature* **825**, 821–824 (2003).
156. Dietrich, C. *et al.* Lipid rafts reconstituted in model membranes. *Biophysical Journal* **80**, 1417–1428 (2001).

-
157. Sengupta, P., Hammond, A., Holowka, D. & Baird, B. Structural determinants for partitioning of lipids and proteins between coexisting fluid phases in giant plasma membrane vesicles. *Biochimica et Biophysica Acta (BBA) - Biomembranes* **1778**, 20–32 (2008).
 158. Honigsmann, A., Mueller, V., Hell, S. W. & Eggeling, C. STED microscopy detects and quantifies liquid phase separation in lipid membranes using a new far-red emitting fluorescent phosphoglycerolipid analogue. *Faraday Discuss.* **161**, 77–89 (0 2013).
 159. Sezgin, E. *et al.* Partitioning, diffusion, and ligand binding of raft lipid analogs in model and cellular plasma membranes. *Biochimica et Biophysica Acta (BBA) - Biomembranes* **1818**, 1777–1784 (2012).
 160. Baumgart, T., Hunt, G., Farkas, E. R., Webb, W. W. & Feigenson, G. W. Fluorescence probe partitioning between Lo/Ld phases in lipid membranes. *Biochimica et Biophysica Acta (BBA) - Biomembranes* **1768**, 2182–2194 (2007).
 161. Parasassi, T., De Stasio, G., d’Ubaldo, A. & Gratton, E. Phase fluctuation in phospholipid membranes revealed by Laurdan fluorescence. *Journal of Physics D: Applied Physics* **57**, 1179–1186 (1990).
 162. Krasnowska, E. K., Gratton, E. & Parasassi, T. Prodan as a membrane surface fluorescence probe: partitioning between water and phospholipid phases. *Biophysical Journal* **74**, 1984–1993 (1998).
 163. Amaro, M., Reina, F., Hof, M., Eggeling, C. & Sezgin, E. Laurdan and Di-4-ANEPPDHQ probe different properties of the membrane. *Journal of Physics D: Applied Physics* **50**, 134004 (2017).
 164. Sánchez, S. A. & Günther, G. in *Modern research and educational topics in microscopy* (eds Méndez-Vilas, A. & J., D.) (2007).
 165. Scheinpflug, K., Krylova, O. & Strahl, H. in *Antibiotics: Methods and Protocols* (ed Sass, P.) 159–174 (Springer New York, 2017).
 166. Sezgin, E., Sadowski, T. & Simons, K. Measuring Lipid Packing of Model and Cellular Membranes with Environment Sensitive Probes. *Langmuir* **30**, 8160–8166 (2014).
 167. Owen, D., Rentero, C., Magenau, A., Abu-Siniyeh, A. & K., G. Quantitative imaging of membrane lipid order in cells and organisms. *Nature Protocols* **7**, 24–35 (2012).
 168. Barrantes, F. J. in *New Methods and Sensors for Membrane and Cell Volume Research* (eds Model, M. A. & Levitan, I.) 257–314 (Academic Press, 2021).
 169. Parasassi, T., Krasnowska, E. & Bagatolli, L. Laurdan and Prodan as Polarity-Sensitive Fluorescent Membrane Probes. *Journal of Fluorescence* **8**, 365–373 (1998).
 170. Bagatolli, L. A., Parasassi, T., Fidelio, G. D. & Gratton, E. A model for the interaction of 6-lauroyl-2-(N,N-dimethylamino)naphthalene with lipid environments: implications for spectral properties. *Photochemistry and Photobiology* **70**, 557–564 (1999).
-

BIBLIOGRAPHY

171. Weber, G. & Farris, F. J. Synthesis and spectral properties of a hydrophobic fluorescent probe: 6-propionyl-2-(dimethylamino)naphthalene. *Biochemistry* **18**, 3075–3078 (1979).
172. Binnig, G., Quate, C. F. & Gerber, C. Atomic Force Microscope. *Physical Review Letters* **56**, 930–933 (1986).
173. Binnig, G., Rohrer, H., Gerber, C. & Weibel, E. Surface Studies by Scanning Tunneling Microscopy. *Physical Review Letters* **49**, 57–61 (1982).
174. Johnson, D., Hilal, N. & Bowen, W. R. in *Atomic Force Microscopy in Process Engineering* (eds Hilal, N. & Bowen, R. W.) 1–30 (Elsevier, 2009).
175. Hans-Jürgen, B. Measuring electrostatic, van der Waals, and hydration forces in electrolyte solutions with an atomic force microscope. *Biophysical journal* **60**, 1438–1444 (1991).
176. Sang, H. *et al.* Identifying tips for intramolecular NC-AFM imaging via in situ fingerprinting. *Scientific Reports* **4**, 1–12 (2014).
177. Hansma, H. G. *et al.* Recent advances in atomic force microscopy of DNA. *Scanning* **15**, 296–299 (1993).
178. Martin, Y., Williams, C. C. & Wickramasinghe, H. K. Atomic force microscope–force mapping and profiling on a sub 100-Å scale. *Journal of Applied Physics* **61**, 4723–4729 (1987).
179. Pike, L. J. Rafts defined: a report on the Keystone symposium on lipid rafts and cell function. *Journal of Lipid Research* **47**, 1597–1598 (2006).
180. Nickels, J. D. & Katsaras, J. in *Membrane Hydration: The Role of Water in the Structure and Function of Biological Membranes* (ed Disalvo, A. E.) 45–67 (Springer International Publishing, 2015).
181. Kuzmin, P. I., Akimov, S. A., Chizmadzhev, Y. A., Zimmerberg, J. & Cohen, F. S. Line Tension and Interaction Energies of Membrane Rafts Calculated from Lipid Splay and Tilt. *Biophysical Journal* **88**, 1120–1133 (2005).
182. Lee, T. H., Sani, M. A., Overall, S., Separovic, F. & Aguilar, M. I. Effect of phosphatidylcholine bilayer thickness and molecular order on the binding of the antimicrobial peptide maculatin 1.1. *Biochimica et biophysica acta. Biomembranes* **1860**, 300–309 (2018).
183. Kenworthy, A. K. What’s past is prologue: FRAP keeps delivering 50 years later. *Biophysical Journal* **122**, 3577–3586 (2023).
184. Pincet, F. *et al.* FRAP to Characterize Molecular Diffusion and Interaction in Various Membrane Environments. *PLOS ONE* **11**, 1–19 (2016).
185. Ishikawa-Ankerhold, H. C., Ankerhold, R. & Drummen, G. P. Advanced fluorescence microscopy techniques-FRAP, FLIP, FLAP, FRET and FLIM. *Molecules* **17**, 4047–4132 (2012).
186. Soumpasis, D. M. Theoretical analysis of fluorescence photobleaching recovery experiments. *Biophysical Journal* **41**, 95–97 (1983).

-
187. Magidson, V. & Khodjakov, A. in *Digital Microscopy* (eds Sluder, G. & Wolf, D. E.) 545–560 (Academic Press, 2013).
 188. Bigg, C. in *Compendium of Quantum Physics* (eds Greenberger, D., Hentschel, K. & Weinert, F.) 81–84 (Springer Berlin Heidelberg, 2009).
 189. Einstein, A. Zur Theorie der Brownschen Bewegung. *Annalen der Physik* **324**, 371–381 (1906).
 190. Stetefeld, J., McKenna, S. & Patel, T. Dynamic light scattering: a practical guide and applications in biomedical sciences. *Biophysical Reviews* **8**, 409–427 (2016).
 191. Mudalige, T. *et al.* in *Nanomaterials for Food Applications* (eds Rubio, A. L., Rovira, M. J. F., Martínez Sanz, M. & Gómez-Mascaraque, L. G.) 313–353 (Elsevier, 2019).
 192. Enoki, T. A., Henriques, V. B. & Lamy, M. T. Light scattering on the structural characterization of DMPG vesicles along the bilayer anomalous phase transition. *Chemistry and Physics of Lipids* **165**, 826–837 (2012).
 193. Vogel, R. *et al.* High-Resolution Single Particle Zeta Potential Characterisation of Biological Nanoparticles using Tunable Resistive Pulse Sensing. *Scientific Reports* **7**, 17479 (2017).
 194. Henry, D. C. The cataphoresis of suspended particles. Part I.—The equation of cataphoresis, *Proceedings of the Royal Society London A* **133**, 106–129 (1931).
 195. Lowry, G. V. *et al.* Guidance to improve the scientific value of zeta-potential measurements in nanoEHS. *Environmental Science: Nano* **3**, 953–965 (2016).
 196. Smoluchowski, M. v. Handbuch der Elektrizität und des Magnetismus. *Band II, Barth-Verlag, Leipzig*, 366–427 (1921).
 197. Midekessa, G. *et al.* Zeta Potential of Extracellular Vesicles: Toward Understanding the Attributes that Determine Colloidal Stability. *ACS omega* **5**, 16701–16710 (2020).
 198. Sengupta, P. *et al.* Membrane-permeable Calmodulin Inhibitors (e.g. W-7/W-13) Bind to Membranes, Changing the Electrostatic Surface Potential: dual effect of W-13 on epidermal growth factor receptor activation. *Journal of Biological Chemistry* **282**, 8474–8486 (2007).
 199. Freire, J. *et al.* Using zeta-potential measurements to quantify peptide partition to lipid membranes. *European Biophysics Journal* **40**, 481–487 (2011).
 200. Ribeiro, M., Domingues, M., Freire, J., Santos, N. & Castanho, M. Translocating the blood-brain barrier using electrostatics. *Frontiers in Cellular Neuroscience* **6**, 44 (2012).
 201. Crowe, J. H. in *Membrane Hydration: The Role of Water in the Structure and Function of Biological Membranes* (ed Disalvo, E. A.) 263–280 (Springer International Publishing, 2015).
 202. Armando Hernández, G. Anhydrobiosis in bacteria: from physiology to applications. *Journal of Biosciences* **36**, 939–950 (2011).
-

203. Chen, A. I. & Goulian, M. A network of regulators promotes dehydration tolerance in *Escherichia coli*. *Environmental microbiology* **20**, 1283–1295 (2018).
204. Khroustalyova, G., Boudrant, J. & Rapoport, A. Resistance of a recombinant *Escherichia coli* to dehydration. *Cell Biology International* **33**, 1194–1195 (2009).
205. Cox, M. M. & Battista, J. R. *Deinococcus radiodurans* - the consummate survivor. *Nature reviews. Microbiology* **3**, 882–892 (2005).
206. Slade, D. & Radman, M. Oxidative Stress Resistance in *Deinococcus radiodurans*. *Microbiology and Molecular Biology Reviews* **75**, 133–191 (2011).
207. Fasnacht, M. & Polacek, N. Oxidative Stress in Bacteria and the Central Dogma of Molecular Biology. *Frontiers in Molecular Biosciences* **8**, 671037 (2021).
208. Rutala, W. A., Gergen, M. F. & Weber, D. J. Room Decontamination with UV Radiation. *Infection Control & Hospital Epidemiology* **31**, 1025–1029 (2010).

Declarations of the co-authors



POLITECHNIKA POZNAŃSKA

FACULTY OF MATERIALS ENGINEERING AND TECHNICAL PHYSICS

Institute of Physics

Piotrowo 3, 60-965 Poznań

www.put.poznan.pl



Poznań, 26.01.2024

dr hab. inż. Łukasz Piątkowski, prof. PP
Politechnika Poznańska
Wydział Inżynierii Materiałowej i Fizyki Technicznej
Instytut Fizyki
Tel. 61 665 31 80
e-mail: lukasz.j.piatkowski@put.poznan.pl

Declaration of Co-Authorship

I declare that according to the CRediT author statement, in the following publications:

1. *Lateral organization of biomimetic cell membranes in varying pH conditions*
Emilia Krok, Agnieszka Batura, Madhurima Chattopadhyay, Hanna Orlikowska, Lukasz Piatkowski
Journal of Molecular Liquids, volume 345, number 117907, 2022
2. *Nanoscale structural response of biomimetic cell membranes to controlled dehydration*
Emilia Krok, Henri G. Franquelim, Madhurima Chattopadhyay, Hanna Orlikowska, Petra Schuille, Lukasz Piatkowski
Nanoscale, volume 16, issue 1, pages 72-84, 2023
3. *Tunable biomimetic bacterial membranes from binary and ternary lipid mixtures and their application in antimicrobial testing*
Emilia Krok, Mareike Stephan, Rumiana Dimova, Lukasz Piatkowski
Biochimica et Biophysica Acta (BBA) - Biomembranes, volume 1856, issue 7, 184194, 2023

my contribution was: conceptualization (2, 3), formal analysis (1), funding acquisition (1, 2, 3), writing – original draft (2), writing – review & editing (1, 3), validation (2), supervision (1-3).

I agree to submit the above work by **M. Eng. Emilia Krok**, as a part of her PhD dissertation titled: *“Eukaryotic and prokaryotic biomimetic cell membranes: structure and its relation to environmental conditions”* in the form of a collection of published and thematically related scientific articles.

.....
Co-author's signature



POLITECHNIKA POZNAŃSKA

FACULTY OF MATERIALS ENGINEERING AND TECHNICAL PHYSICS

Institute of Physics
Piotrowo 3, 60-965 Poznań
www.put.poznan.pl



Poznań, date: 31.01.2024

M. Eng. Hanna Orlikowska-Rzeźnik
Poznan University of Technology,
Faculty of Materials Engineering and Technical Physics
Institute of Physics
email: hanna.orlikowska@put.poznan.pl

Declaration of Co-Authorship

I declare that according to the CRediT author statement, in the following publications:

1. *Lateral organization of biomimetic cell membranes in varying pH conditions*
Emilia Krok, Agnieszka Batura, Madhurima Chattopadhyay, Hanna Orlikowska, Lukasz Piatkowski
Journal of Molecular Liquids, volume 345, number 117907, 2022
2. *Nanoscale structural response of biomimetic cell membranes to controlled dehydration*
Emilia Krok, Henri G. Franquelim, Madhurima Chattopadhyay, Hanna Orlikowska-Rzeźnik, Petra Schwille, Lukasz Piatkowski
Nanoscale, volume 16, issue 1, pages 72-84, 2023

my contribution was: methodology (1), validation (2) and writing – review and editing (1-2).

I agree to submit the above work by **M. Eng. Emilia Krok**, as a part of her PhD dissertation titled: *“Eukaryotic and prokaryotic biomimetic cell membranes: structure and its relation to environmental conditions”* in the form of a collection of published and thematically related scientific articles.



POLITECHNIKA POZNAŃSKA

FACULTY OF MATERIALS ENGINEERING AND TECHNICAL PHYSICS

Institute of Physics

Piotrowo 3, 60-965 Poznań

www.put.poznan.pl



Poznań, date: 29.01.2024

M. Eng. Agnieszka Lester
Poznań University of Technology,
Faculty of Materials Engineering and Technical Physics
Institute of Physics
email: agnieszka.lester@doctorate.put.poznan.pl

Declaration of Co-Authorship

I declare that according to the CRediT author statement, in the following publication:

1. *Lateral organization of biomimetic cell membranes in varying pH conditions*
Emilia Krok, Agnieszka Batura, Madhurima Chattopadhyay, Hanna Orlikowska, Lukasz Piatkowski
Journal of Molecular Liquids, volume 345, number 117907, 2022

my contribution was: conceptualization, investigation, and writing – original draft.

I agree to submit the above work by **M. Eng. Emilia Krok**, as a part of her PhD dissertation titled: *“Eukaryotic and prokaryotic biomimetic cell membranes: structure and its relation to environmental conditions”* in the form of a collection of published and thematically related scientific articles.

.....
Agnieszka Lester
Co-author's signature



Dallas, Texas, USA
February 8, 2024

Madhurima Chattopadhyay, Ph.D.
Post-doctoral researcher
Department of Biophysics
University of Texas Southwestern Medical Center
email: Madhurima.Chattopadhyay@UTSouthwestern.edu

Declaration of Co-Authorship

I declare that according to the CRediT author statement, in the following publications:

1. *Lateral organization of biomimetic cell membranes in varying pH conditions*
Emilia Krok, Agnieszka Batura, Madhurima Chattopadhyay, Hanna Orlikowska, Lukasz Piatkowski
Journal of Molecular Liquids, volume 345, number 117907, 2022
2. *Nanoscale structural response of biomimetic cell membranes to controlled dehydration*
Emilia Krok, Henri G. Franquelim, Madhurima Chattopadhyay, Hanna Orlikowska, Petra Schwille, Lukasz Piatkowski
Nanoscale, volume 16, issue 1, pages 72-84, 2023

my contribution was: conceptualization (2), methodology (1), software (1), validation (2), writing – review & editing (1-2).

I agree to submit the above work by **M. Eng. Emilia Krok**, as a part of her PhD dissertation titled: *“Eukaryotic and prokaryotic biomimetic cell membranes: structure and its relation to environmental conditions”* in the form of a collection of published and thematically related scientific articles.

Madhurima Chattopadhyay
Madhurima Chattopadhyay

Max-Planck-Institut für Biochemie

Zelluläre und Molekulare Biophysik – Cellular and Molecular Biophysics

MPI für Biochemie • Am Klopferspitz 18 • D-82152 Martinsried



Prof. Dr. Petra Schwille
Tel: +49-(0)89 / 8578-2900
Fax: +49-(0)89 / 8578-2903
schwille@biochem.mpg.de
www.biochem.mpg.de

07.01.2024

Declaration of Co-Authorship

I declare that according to the CRediT author statement, in the following publication:

Nanoscale structural response of biomimetic cell membranes to controlled dehydration
Emilia Krok, Henri G. Franquelim, Madhurima Chattopadhyay, Hanna Orlikowska, Petra Schwille,
Lukasz Piatkowski
Nanoscale, volume 16, issue 1, pages 72-84, 2023

my contribution was: writing – review and editing of the final manuscript, providing resources, and supervision.

I agree to submit the above work by **M. Eng, Emilia Krok**, as a part of her PhD dissertation titled: “*Eukaryotic and prokaryotic biomimetic cell membranes: structure and its relation to environmental conditions*” in the form of a collection of published and thematically related scientific articles.

.....
Co-author's signature

Am Klopferspitz 18
D-82152 Martinsried

Tel.: +49-(0)89 / 8578-1
Fax: +49-(0)89 / 8578-3777

mpib@biochem.mpg.de
www.biochem.mpg.de



MAX-PLANCK-GESELLSCHAFT

Leipzig, 10/01/2024

Dr. Henri Franquelim

Leipzig University,
Research and Transfer Center for Bioactive Matter,
Junior Research Group Biomimetic Nanotechnology
Phone: +49 341 97- 31365
henri.franquelim@uni-leipzig.de

Declaration of Co-Authorship

I declare that according to the CRediT author statement, in the following publication:

Nanoscale structural response of biomimetic cell membranes to controlled dehydration
Emilia Krok, Henri G. Franquelim, Madhurima Chattopadhyay, Hanna Orlikowska, Petra Schwille,
Lukasz Piatkowski
Nanoscale, volume 16, issue 1, pages 72-84, 2023

my contribution was: conceptualization, validation, investigation, resources, and writing – review and editing of the final version of manuscript.

I agree to submit the above work by **M. Eng. Emilia Krok**, as a part of her PhD dissertation titled: *“Eukaryotic and prokaryotic biomimetic cell membranes: structure and its relation to environmental conditions”* in the form of a collection of published and thematically related scientific articles.



.....
Co-author's signature



Dr. habil. PD Rumiana Dimova
Group leader
Department of Biomimetic and Sustainable Systems

Max Planck Institute of Colloids and Interfaces
Science Park Golm, 14424 Potsdam, Germany
Tel.: +49 331 567 9615
Fax: +49 331 567 9612
Email: rumiana.dimova@mpikg.mpg.de
<https://www.dimova.de>

08th January, 2024

Declaration of Co-Authorship

I declare that according to the CRediT author statement, in the following publication:

Tunable biomimetic bacterial membranes from binary and ternary lipid mixtures and their application in antimicrobial testing

Emilia Krok, Mareike Stephan, Rumiana Dimova, Lukasz Piatkowski
Biochimica et Biophysica Acta (BBA) - Biomembranes, volume 1856, issue 7, 184194, 2023

My contribution was: conceptualization, resources, writing – review and editing of the final version of manuscript, supervision.

I agree with the submission of the above work by **M. Eng. Emilia Krok**, as a part of her PhD dissertation titled: *“Eukaryotic and prokaryotic biomimetic cell membranes: structure and its relation to environmental conditions”* in the form of a collection of published and thematically related scientific articles.

Rumiana Dimova

Potsdam, 08th January, 2024

Dr. Mareike Stephan

Biophysics Lab

Max Planck Institute of Colloids and Interfaces

Sustainable and Bio-inspired Materials

mareike.stephan@posteo.de

Declaration of Co-Authorship

I declare that according to the CRediT author statement, in the following publication:

Tunable biomimetic bacterial membranes from binary and ternary lipid mixtures and their application in antimicrobial testing

Emilia Krok, Mareike Stephan, Rumiana Dimova, Lukasz Piatkowski

Biochimica et Biophysica Acta (BBA) - Biomembranes, volume 1856, issue 7, 184194, 2023

my contribution was: methodology, validation, writing – review and editing.

I agree with the submission of the above work by **M. Eng. Emilia Krok**, as a part of her PhD dissertation titled: *“Eukaryotic and prokaryotic biomimetic cell membranes: structure and its relation to environmental conditions”* in the form of a collection of published and thematically related scientific articles.



.....
Co-author's signature

Acknowledgments

Embarking on a Ph.D. journey goes beyond the conventional notion of a four or five-year laborious commitment to laboratory work, writing, publishing, and teaching. To me, it symbolizes a long odyssey that commenced during my secondary school years, where I chose to channel my efforts into scientific research. Along this enduring expedition, I have crossed paths with numerous remarkable people who have not only supported but also inspired my pursuit of a scientific career. I sincerely apologize if I don't mention all of you by name but please remember that each of you shaped me and influenced my life choices, which I am so grateful for.

Upon completing my Master's studies in Dresden, as I left my scientific community, I was afraid that I might not be able to find equally remarkable people and a comparable scientific environment elsewhere in the world. I sought advice from my older friends who have started or completed their PhD about the things that are crucial for finding a good PhD position, they all said one thing – look for a good supervisor, everything else can be solved, improved, and changed when you have a good leader. I think I would have to write another thesis to summarize all the moments when Łukasz helped me and to describe our daily work. Łukasz, I really appreciate your way of doing science; you always want to dig deeper into a problem, pay attention to details, and always encourage me to improve. Thanks to you I had a unique opportunity to take part in creating a new lab, buying equipment and even designing the lab furniture. I could not imagine a better supervisor who is always happy when I succeed, supportive when I fail, teaches with tremendous patience, points out mistakes, and when needed, wipes my tears with a sophisticated dark humor. I know that having a disabled PhD student is a huge challenge but I am glad that you always saw only my potential and never the physical limitations. Here, I would like to thank Prof. Ewa Stachowska for all her good words about me and for recommending me to Łukasz. Without your help, I would never have had enough courage to apply for DAAD, go to Germany and continue my scientific work as a PhD student.

I am so glad for Madhurima, Hania, Agnieszka, and Ania, who are not only my fellow PhD students but also invaluable friends in our PhD journey. Madhurima, you know you have a special place in my heart; you have become my dear sister and a part of my family. Thank you for all the events we spent together with my mom and Zuzia. We were honored to share our Christmas and Easter traditions, stories about Poland and our family, and opinions about important world events or moral dilemmas. Your presence brought a touch of India into our home, evoking the sights, sounds, and flavors of vibrant Kolkata. I am so grateful that I had an opportunity to work with you and see your passion for science, which motivated me to work harder and not give up when the results of our experiments were not as we expected. I am sure that one day you will be a world-famous scientist and when that time comes, I will proudly say: "That's my girl". Hania, you are

ACKNOWLEDGMENTS

my moral compass, gently reminding me when my tongue is too sharp and jokes get too harsh. I had a wonderful time sharing a room with you during conferences in Lisbon and Stockholm, where you calmed me down before my presentation. Even long hours spent in complete darkness, measuring spectra of extremely boring single component membranes, were fun with you. I learned a lot from your work; how to write grant applications, how to use fancy phrases in publications and what proper scientific drawings should look like. Thank you for being my emotional support during the last battle called “thesis writing” and tolerating my endless complaints about this exhausting process. Agnieszka, you were my first Bachelor student and I could not be more glad that I met you at the beginning of my teaching journey. You became my role model of a good student, and you raised my standards really high. Thank you for all the cakes that you baked to celebrate important events and small successes of our group. You brought our youngest team member to the Piatkowski Lab. I am sure that Ula, having such a wonderful mother, will grow up to be an intelligent, beautiful and strong woman. Ania, we had a relatively short time together because you joined our group in October, yet now I cannot imagine our group without you. I am so glad that I have found a companion for talking about dogs, board games, and sharing funny dog reels. Also, thanks to you, I am no longer the only one answering stupid questions like “Where do you get your protein, you crazy grass eater?”.

I want to thank people from our Institute of Physics for their support, jokes, countless talks about students, teaching, grants, and science. Alicja, Ania M., Kamil, and Karol, you made even terrible days a little bit brighter. Special thanks go to Andrzej and Michał. I could always count on your help with the “man-type of work” that I couldn’t do (like transferring huge nitrogen bottles). I was so lost during my first semester of teaching and your advice and knowledge helped me to survive. Andrzej, thank you for letting me join your Physics classes. I hope that one day I will be as fluent in teaching as you are, although I think I might never be able to reach your level of enthusiasm and patience. Marta and Semir, you know that you are the honorary members of the Piatkowski Lab. Thank you for saving us from complete starvation when Lukasz and I were too lazy to cook something for dinner. Denver wanted me to write you that he appreciates your petting and that there is no other treasure chest in the world like your trash can. Ania P., they say that “*an accountant is someone who solves a problem you didn’t know you had in a way you don’t understand*” and this is a quintessence of your work. I have lost track of how many times you saved our group, helping in a completely ridiculous bureaucracy. Your sense of humor made even the most ridiculous problems seem easy. I would like to express my gratitude to Prof. Mirosław Szybowicz, Prof. Arkadiusz Ptak and Prof. Ryszard Czajka for putting faith in me and giving me the opportunity to join our faculty. It is extremely important for a young scientist to have strong support from more experienced researchers.

This thesis would not have been written in its current form without the amazing support of our collaborators in Germany. Prof. Petra Schwillie and Dr. Henri G. Franquelim, everything that we know about the preparation of SLBs is thanks to you. Thank you for sharing your knowledge, protocols and tips that are impossible to find in any publication. Henri, thank you for your patience, support with extremely difficult AFM measurements under dehydration, many video calls and for showing us Lisbon. Prof. Rumiana Dimova – Rummy, I am so grateful that you agreed to host me for 3 months in your group and showed me the secrets of GUVs. I really enjoyed our “lettuce eat” moments with Agu, Mareike,

Matilde, Mina, Nicky, Shahenda and Shreya. Thank you for inviting me to Biomembrane Days - the best conference I have ever attended.

Last but not least, I would like to thank my amazing family. Mom, you were the one who was with me in all the moments that led me to the day of my PhD defense. People have no idea how many obstacles we had to overcome together, how many times you stood by my side when someone said there was no point in saving my life, improving my health and finally finding the best education for me. I am forever indebted to you for your sacrifices, guidance, and unwavering belief in my abilities. Thank you, Mom, for always being my rock. Zuzia, my dear sister, we are like Elsa and Anna, completely different, but still loving each other forever. Thank you for being my little sunshine. Mateusz, thank you for listening to my never-ending stories about work, lab, new equipment, not working equipment, and failed experiments. I know that it requires at least ten Nemesis-size boxes of patience to listen about something that you don't fully understand. Thank you for being there, listening, and embracing all aspects of who I am. Campari, I am grateful that you kept our agreement and waited until the moment when I submitted my last publication. You knew that from that moment on, I would be strong enough to finish my PhD without you by my side. Please keep an eye on Denver from the Rainbow Bridge, you know that he is really trying to be as good as you.